Characterization of novel proteins regulating and remodeling lipid fluxes during the intracellular development of Apicomplexan parasites

Sheena Dass

THÈSE

Pour obtenir le grade de

DOCTEUR DE L'UNIVERSITÉ GRENOBLE ALPES

Spécialité : Biologie cellulaire

Arrêté ministériel : 25 mai 2016

Présentée par

Sheena DASS

Thèse dirigée par **Cyrille BOTTE**
et co-encadrée par **Yoshiki YAMARYO-BOTTE**

préparée au sein du **Laboratoire Apicolipid - Institute for Advanced Biosciences**
dans **l'École Doctorale Chimie et Sciences du Vivant**

Caractérisation de nouvelles protéines régulant et remodelant les flux lipidiques au cours du développement intracellulaire des parasites Apicomplexan

Characterization of novel proteins regulating and remodeling lipid fluxes during the intracellular development of Apicomplexan parasites

Thèse soutenue publiquement le **6 février 2020**,
devant le jury composé de :

Monsieur CYRILLE BOTTE
DIRECTEUR DE RECHERCHE, CNRS DELEGATION ALPES, Directeur de thèse
Monsieur MALCOLM MCCONVILLE
PROFESSEUR, UNIVERSITE DE MELBOURNE - AUSTRALIE, Rapporteur
Madame DOMINIQUE SOLDATI-FAVRE
PROFESSEUR, UNIVERSITE DE GENEVE - SUISSE, Rapporteur
Monsieur JAMES MACRAE
DOCTEUR-CHERCHEUR, INSTITUT FRANCIS CRICK - ROYAUME-UNI, Examinateur
Monsieur PIERRE HAINAUT
PROFESSEUR DES UNIVERSITES, UNIVERSITE GRENOBLE ALPES, Président

ACKNOWLEDGEMENT

Foremost, I would like to express my deepest gratitude to my thesis supervisors Dr. Cyrille Botté and Dr. Yoshiki Yamaryo Botté for their full support, expert guidance, understanding and encouragement throughout the course of this study. I am extremely grateful to both for mentoring me to my thesis completion. I thank Yoshiki for her timely counsel and an eye for detail that trained me rigorously during my PhD and Cyrille for allowing me to work with new ideas and for always having his office door open in case of doubts and discussions.

I would like to thank team Apicolipid- Cyrine, Christophe, Serena, Samuel and Nick for making the work environment cheerful. A special thanks to Annie, my first tutor of *Plasmodium* molecular biology, for the fun times and constant support; and Nick, ParaFrap partner, for being ever ready to help and for answering my unending scientific queries.

I acknowledge ParaFrap for their financial support and coursework during my thesis. I would also like to thank my thesis committee members Dr. Ali Hakimi and Dr. Jose Juan Lopez Rubio and ParaFrap scientific advisory board. Their thoughtful questions and comments are valued greatly.

I also would like to express my gratitude to my thesis jury members Prof. Malcolm McConville, Prof. Dominique Soldati, Dr. James Macrae and Prof. Pierre Hainaut.

I would like to thank my friends and my constant supporters Pratima and Vrushali. It is their unconditional love and patience that helped me ride through this adventurous journey. A special thanks to Keerthi, Dayana and Georgious for all the food binging and fun times. Thank you for your support during both happy and sad times.

This acknowledgement would be incomplete without mentioning my grandfather who showed faith in me and supported me to achieve my goals in life. Finally, I would like to thank my family, my loving parents and brother. Despite being continents apart, their unfailing support, encouragement and love helped me sail through this incredible journey of 3 years.

ABSTRACT

Apicomplexan parasites are responsible for major human infectious diseases such as malaria and toxoplasmosis against which there are no efficient vaccines and rapid emergence of drug resistance. The propagation and survival of these parasites depends on complex metabolic interactions with their human host cells. Lipid synthesis is one such key pathway crucial for parasite survival, which relies on an essential combination or 'patchwork' of fatty acids synthesized *de novo* and scavenged from the host. Additionally, these parasites can modulate their metabolic capacities depending on the different hosts and their nutritional environments. Availability of the appropriate amount of fatty acids is an essential determinant for successful adaptation of the parasite to various host cells. Since, fatty acid uptake is as essential as *de novo* fatty acid synthesis for the parasite growth and pathogenesis, therefore these fatty acid homeostatic pathways hold promise for specific drug targets. The molecular mechanism by which parasites combine and regulate the fatty acid flux through effective remodelling of their lipid metabolism, remains unknown. Therefore, to determine the same my PhD project investigated pivotal role of two families of enzymes in parasite fatty acid metabolism: acyl CoA synthetases (ACS) putatively allowing the activation of fatty acids and phosphatidic acid phosphatases (LIPIN) the gatekeepers for the synthesis of central lipid precursors.

Phosphatidic acid (PA), the simplest glycerophospholipid, acts as the rate limiting central lipid molecule in this process of fatty acid flux-based homeostasis. During my PhD, I investigated the role of a *Toxoplasma* phosphatidic acid phosphatase called *Tg*LIPIN, in metabolising the critical levels of PA through controlled channelling of parasite vs host derived fatty acids. *Toxoplasma* tachyzoites are unable to survive a knockdown of LIPIN due to severe replication defect amongst several other membrane anomalies. This cytosolic enzyme catalyses the synthesis of diacylglycerol from phosphatidic acid, a central lipid precursor and signal transducer, as confirmed by heterologous complementation and lipidomics approaches. The disruption of *Tg*LIPIN induces loss of parasite lipid storage concomitantly with an increase of the total lipid content (fatty acids), leading to rapid parasite death by 'lipotoxicity'. With the help of novel ^{13}C glucose-based fluxometrics approaches using GC-MS, we identified that the enzyme mainly use and controls the use host fatty acids (esp. C18:1), which become a lipotoxic source for the parasite when disrupting *Tg*LIPIN. One of the physiological consequences is a toxic increase of lipids and free fatty acids killing the parasite. On the other hand, the downregulation of *Tg*LIPIN induced a significant reduction of the apicoplast FASII activity indicating its activity regulates the parasite

de novo synthetic capacities in response to its scavenging activity. Electron microscopy reveals that *Tg*LIPIN indirectly regulates nuclear membrane morphology and also the inner membrane complex biogenesis, suggesting the importance of lipid balance during the growth of parasite. Overall, we suggest that *Tg*LIPIN protects parasite against FA-induced toxicity allowing a normal replication cycle within its host by regulating the critical levels of phosphatidic acid.

The second project during my PhD focused on the enzymatic pathway involved in the activation of fatty acids within these parasites. In eukaryotes, the activation of fatty acids to their acyl-coA thioesters is a two-step energy requiring biochemical process that involves key enzymes called Acyl-coA synthetases (ACS). Since, fatty acids are virtually involved all aspects of cellular biochemistry, their activation pathway could be an Achilles heel for the parasite survival within its host. In an attempt to the same, we have identified a novel family of 7 enzymes in *Toxoplasma gondii* as putative acyl-coA synthases (*Tg*ACSs). All the putative *Tg*ACSs, tagged endogenously, localize to non-overlapping sub-cellular compartments of the parasite. Using parasite genetics approaches and GC-MS based lipidomics, *Tg*ACS3 was functionally characterised. Genetic ablation of *Tg*ACS3 affected parasite replication within its host. *Tg*ACS3 depletion reduced the overall fatty acid content within the parasite phospholipids alongside a significant increase in the amount of free fatty acids, further confirming its function as an ACS.

Another major question I addressed in my PhD (including collaborative papers), is the effect of host environmental/nutritional conditions affecting the adaptation of de novo FA synthesis and host FA scavenging capacities of the parasite. Growing these parasites in the presence of growth media supplemented with different amounts of FBS (Fetal bovine serum) mimics different host nutritional environments in vitro. Normally, high nutritional environment (10% FBS) was able to sustain better parasite growth in comparison to low nutritional status, in a concentration dependent manner (10% FBS>1% FBS> 0% FBS). FBS starvation significantly increased the presence of nile red stained lipid droplets within the parasite or the PV in a dose-dependent manner, suggesting adaptive metabolic capacity of the parasite. However, in case of parasites lacking *Tg*LIPIN and *Tg*ACS3, the consequent growth defect was aggravated in the presence of high nutritional environment i.e. 10% FBS supplemented growth media in comparison to low nutrient conditions (1% and 0% FBS). We determined the reason of this opposite trend (parasite growth rate: 10%FBS<1%FBS<0%FBS) as the increase in the amount of free fatty acids which when

supplemented with external rich source resulted in growth defect due to absence of pivotal enzymes involved in FA metabolism.

This thesis presents data that confirm that the intracellular replication and survival of apicomplexan parasites is reliant on effective remodelling of their lipid metabolic capacity by FA flux derived *de novo*, from the host and its nutritional environment.

RESUME

Les parasites apicomplexes sont des pathogènes unicellulaires eucaryotes responsables de maladies infectieuses humaines majeures de l'homme telles que le paludisme et la toxoplasmose. Il n'existe à ce jour pas de vaccin efficace contre ces agents pathogènes. De plus, l'émergence des souches parasitaires résistantes aux traitements actuels, tous deux pointent l'urgence actuelle sur l'identification de nouvelles cibles thérapeutiques. La propagation et la survie de ces parasites dépendent des interactions métaboliques complexes des parasites avec leurs cellules hôtes humaines. La synthèse des lipides est une de ces voies clés cruciale pour la survie du parasite, qui repose sur une combinaison essentielle ou «patchwork» d'acides gras synthétisés de novo et récupérés de l'hôte. De plus, ces parasites peuvent moduler leurs capacités métaboliques en fonction des différents hôtes et de leurs environnements nutritionnels. La disponibilité de la quantité appropriée d'acides gras est un déterminant essentiel pour une adaptation réussie du parasite à diverses cellules hôtes. Étant donné que l'absorption des acides gras est aussi essentielle que la synthèse de novo des acides gras pour la croissance et la pathogenèse des parasites, ces voies permettant le transport et l'homéostasie des acides gras représentent donc des cibles thérapeutiques. Le mécanisme moléculaire par lequel les parasites combinent les acides gras issus des deux voies d'acquisition/synthèse et régulent le flux d'acides gras grâce à un remodelage efficace de leur métabolisme lipidique reste inconnu. Mon projet de doctorat a focalisé sur l'étude du rôle supposé pivot et essentiel de deux familles d'enzymes dans le métabolisme des acides gras parasitaires : les acyl synthétases d'acyl (ACS) permettant l'activation des acides gras et les acide phosphatidique phosphatases, (PAP/LIPIN) à l'origine de la synthèse des précurseurs centraux de tous les lipides majeurs du parasite.

L'acide phosphatidique (PA) est le glycérophospholipide le plus simple structurellement. De plus, il est ke précurseur unique pour la synthèse de novo de toutes les classes de glycérophospholipides. Le PA agit comme une classe lipidique centrale dont la synthèse limite la vitesse dans ce processus de flux et d'homéostasie des acides gras. Au cours de ma thèse, j'ai étudié le rôle d'une acide phosphatidique phosphatase (PAP) appelée *Tg*LIPIN. TgLipin régule les niveaux critiques du PA cellulaires une canalisation contrôlée des acides gras issus soit de la synthèse de novo du parasite soit obtenus par vol des ressources de l'hôte. L'arrêt de l'expression de *Tg*LIPIN entraine la mort intracellulaire du parasite par arrêt de la division du parasite et par d'importantes anomalies membranaires. Cette enzyme cytosolique catalyse la synthèse du diacylglycérol à partir de l'acide phosphatidique, un précurseur lipidique central et un transducteur de signal, comme confirmé par

les approches de complémentation hétérologue et d'analyses lipidomiques. La perturbation de *Tg*LIPIN induit une perte des classes des lipides de stockage parasitaires en même temps qu'une augmentation de la teneur totale en phosphoglycérolipides et des acides gras libres, entraînant une mort rapide des parasites par «lipotoxicité». À l'aide de fluxométrie par marquage au ^{13}C-glucose suivi d'analyse lipidomique en GC-MS, nous avons identifié que la source lipotoxique de ces acides gras toxiques est directement issu l'hôte (en particulier l'acide oléique, C18 :1). D'autre part, l'activité de la voie FASII est fortement réduite lors de la déplétion de *Tg*LIPIN, suggérant que son activité contrôle aussi directement ou indirectement les voies de néosynthèse des acides gras. La microscopie électronique révèle que *Tg*LIPIN régule indirectement la morphologie de la membrane nucléaire et également la biogenèse du complexe membrane interne (IMC), suggérant l'importance de l'équilibre lipidique pendant la croissance du parasite. Nos approches en fluxomique et lipidomique révèlent donc que *Tg*LIPIN régule la balance synthétique du PA et du DAG, controlant ainsi soit la biogénèse membranaire active du parasite soit le stockage des lipides, respectivement. Mes travaux montrent donc que TgLipin est le régulateur métabolique central controllant la synthèse lipidique du parasite et permettant donc sa division intracellulaire controllée et sa survie intracellulaire.

Le second volet de monprojet de ma thèse a porté sur la voie enzymatique impliquée dans l'activation des acides gras au sein de ces parasites. Chez les eucaryotes, l'activation des acides gras en acyl-coA est une réaction active et obligatoire nécessitant des enzymes clés appelées Acyl-coA synthetases (ACS). Étant donné que les acides gras sont pratiquement impliqués dans tous les aspects de la biochimie cellulaire, leur voie d'activation constituerait donc un talon d'Achille pour la survie du parasite au sein de son hôte. J'ai pu identifié une nouvelle famille de 7 acyl-coA putatives (*Tg*ACS) chez *Toxoplasma gondii*. J'ai pu taggé l'ensemble de ces candidats de manie1re endogène et montre que celles-ci localisent dans des compartiments cellulaires indépendants du parasite. En utilisant des approches de d'inactivation moléculaire et d'analyses lipidomiques basées sur la GC-MS, j'ai réalisé la caractérisation moléculaire de candidate ACS majeurs : *Tg*ACS3. L'inactivation génétique de *Tg*ACS3 provoque l'arrêt de la division parasitaire au sein de sa cellule hôte. Le KO de *Tg*ACS3 induit une forte réduction de la teneur en phospholipides parasitaires parallèlement à une augmentation significative de la quantité d'acides gras libres, confirmant sa fonction en tant qu'ACS et indiquant son rôle dans l'activation des acides gras nécessaires à la synthèse en masse des phospholipides membranaires du parasite.

Une autre question importante que j'ai abordée lors ma thèse (incluant 2 articles collaboratifs), est l'effet des conditions environnementales / nutritionnelles de l'hôte affectant l'adaptation de la synthèse de novo des acides gras et les capacités de piégeage des FA de l'hôte par le parasite. K'ai mis en place des conditions de culture cellulaire mimant les fluctuations nutritionnelles de l'hôte en faisant fluctuer les quantités de sérume de veau Fœtal (FBS), utilisé en tant que source de nutriments dans les mileiux de culture in vitro. En conditions nutritionnelle physiologique, la quantité de nutriments est haute (10%FBS) et permet une croissance soutenue du parasite. Dans le cas de restriction nutritive de l'hôte, les nutriments sont plus faiblement disponibles et impacte directment les taux de division parasitaire au sein de leurs cellules hôtes. Ces mêmes conditions de carence nutritives ont pour conséquence l'augmentation significative de la présence des goutelettes lipidiques au sein du parasite et de sa vacuole parasitophore. Leur présence au sein du parasite est inversement proportionnelle à la quantité du nutriment disponible depuis l'hôte, suggérant une plasticité métabolique du parasite en fonction des conditions nutritives. Lors de l'inactivation de la présence de la protéine *Tg*LIPIN ou de *Tg*ACS3, le défaut de croissance qui en résulte fortement aggravé en présence d'un environnement nutritionnel élevé, (10% de FBS). Ceci suggère que la fonction de ces deux protéines est directement liée et impliqué dans l'utilisation des ressources lipidique de l'hôte.

TABLE OF CONTENTS

ABBREVIATIONS

PV	Parasitophorous vacuole
IMC	Inner Membrane Complex
MJ	Moving Junction
RONs	Rhoptry Neck Proteins
ROPs	Rhoptry bulbous body proteins
IPP	Isopentenyl pyrophosphate
MEP	Methylerythritol phosphate
TCA	Tricarboxylic acid cycle
ETC	Electron transport chain
BCKDH	Branched chain ketoacid dehydrogenase
PC	Phosphatidylcholine
SDPM	Serine-decarboxylase-phosphoethanolamine-methyltransferase
PSD	Phosphatidylserine decarboxylase
PMT	Phosphatidylethanolamine methyltransferase
PE	Phosphatidylethanolamine
ER	Endoplasmic reticulum
PSD1mt	Phosphatidylserine decarboxylase1 (mitochondrial)
PSD	Phosphatidylserine decarboxylase1
NO	Nitric oxide
PSS	Phosphatidylserine synthase
PTS	Phosphatidylthreonine synthase
PS	Phosphatidylserine
Pth	Phosphatidylthreonine
PI	Phosphatidylinositol
PI3P	Phosphatidylinositol-3-monophosphate
PI-PLC	Phosphatidylinositide-phospholipase C
PIP2	Phosphatidylinositol 4,5-bisphosphate

DAG	sn-1,2-diacylglycerol
GPI	Glycosylphosphatidylinositol
CDP-DAG	Cytidine diphosphate diacylglycerol
PA	Phosphatidic acid
CL	Cardiolipin
PG	Phosphatidylglycerol
ACBP2	Acyl coA binding protein2
LC-MS	Liquid Chromatography Mass spectrometry
CDS1	CDP-DAG synthase1
CDS2	CDP-DAG synthase2
EPC	Ceramide phosphor ethanolamine
SLS	Sphingolipid synthase
IPC	Inositol phosphorylceramide
dhSM	dihydrosphingomyelin
ACAT1	acyl CoA: cholesterol acytransferase1
ACAT2	acyl CoA: cholesterol acytransferase2
LDL	Low density lipoprotein
PA	Phosphatidic acid
GPAT	Glycerol-3-phosphate acyltransferase
LPAAT	Acyl CoA: lysophosphatidic acid acyltransferase
DHAP	Dihydroxyacetone phosphate
DGK	Diacylglycerol kinase
ATP	Adenosine triphosphate
DAG	Diacylglycerol
AGPAT	Acylglycerol-3-phosphate acyltransferase
G3PDH	Glycerol-3-phosphate dehydrogenase
GAC	Glideosome associated connector
GC	Guanylate cyclase
TAG	Triacylglycerol
PAP	Phosphatidic acid phosphatase

LD	Lipid droplets
ACP	Acyl carrier protein
TPT	Triose phosphate transporter
3-PGA	3- Phosphoglycerate
PEP	Phosphoenol pyruvate
PK	Pyruvate kinase
BCKDH	Branched chain ketoacid dehydrogenase
ACC	Acetyl coA carboxylase
FabD	Malonyl coA:ACP transacylase
FabH	β-Ketoacyl-ACP synthase III
FabG	β-ketoacyl:ACP reductase
FabZ	β-hydroxyacyl-ACP dehydratase
FabB/F	β-Ketoacyl-ACP synthase I/II
FabI	Enoyl-ACP reductase
SAM	S-adenosylmethionine
PDH	Pyruvate dehydrogenase
FA	Fatty acid
DEH	Dehydratase
ECR	Enoyl reductase
ACS	Acetyl coA synthetase
LFCA	Long chain fatty acid
VLFCA	Very long chain fatty acid
SCD	Stearoyl coA desaturase
GC-MS	Gas chromatography coupled mass spectrometry
IVN	Intravacuolar network
ABCG	ATP binding cassette G transporter proteins
SCP	Sterol carrier protein
FABP	Fatty acid binding protein
ACBP	Acyl coA binding protein
MEF	Murine embryonic fibroblasts

RMVs	RBC-derived microvesicles
LPI	Lysophosphatidylinositol
BMP	Bis(Monoacylglycerol)Phosphate
GM3	Monosialodihexosyl-ganglioside
EEF	Exo-erythrocytic form
RBC	Red blood cell
ACT	Artemisinin combination therapy
PH	Pleckstrin homology

CHAPTER I: PHYLUM APICOMPLEXA

An introduction to the phylum 'APICOMPLEXA'

The phylum apicomplexa resides within the eukaryotic super-group (superphylum) called the 'Alveolata'. Alveolata unites three divergent eukaryotic phyla of unicellular organisms, or protists: Dinoflagellata, Ciliophora (Ciliata), and Apicomplexa (Sporozoa) that have successfully colonized most biotopes on earth. A unifying morphological feature linking the evolution of apicomplexans and dinoflagellates with ciliates, thereby forming the infrakingdom alveolate, is the presence of a unique membrane structure formed of flattened vesicles, called 'cortical alveoli', tightly apposed and maintained underneath the plasma membrane through a network of underlying sub-pellicular microtubules (Gould *et al.*, 2008). This triple-membrane structure has evolved to provide a unique platform notably allowing their motility. In apicomplexan parasites the cortical alveoli are dubbed as the inner membrane complex (IMC) located underneath the plasma membrane.

Unlike free-living dinoflagellates and ciliates, apicomplexans have adopted an obligate intracellular parasitic lifestyle. Apicomplexa form five dominant groups of morphologically and ecologically diverse protists including several pathogenic organisms (Vot *et al.*, 2017):

a) Gregarinida
   These include the understudied *Gregarina,* which are known to inhabit invertebrate (marine, freshwater and terrestrial intestines, coeloms and reproductive vesicles posing as potential threats to insect farms or in laboratory colonies (Vot *et al.*, 2017).
b) Piroplasmida
   This sub-group derives its name after the pear-shaped intra-erythrocytic stages of the parasites. These include *Babesia* (*B. bovis*) and *Theileria* (*T. parva* and *T. annulata*) responsible for cattle-inflicting diseases babesiosis and theileriosis, respectively. These intracellular parasites are transmitted by ticks (Ixodidae) (Jalovecka *et al.*, 2018). Piroplasmosis results in low growth, low milk production, death of infected animals and subsequent economic loss (estimated at more than 100 million dollars direct and indirect losses in the USA).
c) Cryptosporidida
   Cryptosporidium has been identified as the second most common cause of infant diarrhea in developing countries (Kotloff *et al.*, 2013). This notorious apicomplexan is also

responsible for gastrointestinal disease and morbidity within HIV-infected patients. These parasites have a unique epicellular parasitic lifestyle, developing their parasitophorous vacuole (i.e. an intracellular niche which allows its development within the host cell) just on the surface of the invaded host cell.

d) Haemosporidia

Plasmodium, one of the members of Haemosporidia is responsible for enormous human suffering and economic loss through the disease caused, malaria.

e) Coccidia

This group includes parasite *Neospora caninum*, found worldwide in dogs, cattle, and other mammals, *Sarcocytis* sp in cattle and *Eimeria* sp in poultry. One of the most successful coccidian pathogens infecting virtually every mammalian host species, causing Toxoplasmosis, is *Toxoplasma gondii.* This parasite can cause serious complications including chorioretinitis (eye damage) and encephalitis in fetuses (congenital toxoplasmosis) and in immunocompromised patients (HIV/AIDS).

This large group of protists encompass up to 6000 described and several other undescribed species. As described above, this diverse phylum includes unicellular eukaryotes of prime importance in medicine and agriculture. Evolutionary phylogeny roots apicomplexa to photosynthetic flagellates (Vot *et al.*, 2017). This direct link of apicomplexan evolution to the photosynthetic lineage has recently been confirmed by the discovery of photosynthetic protists, Chromerids. Corallicolids, living as mutualists in corals are also the closely related to apicomplexans parasites (Janouškovec *et al.*, 2010; Kwong *et al.*, 2019).

Some of the striking characteristic features of the Apicomplexa phylum include:

- Complex parasitic lifestyle alternating between sexual and asexual stages in different host types
- Apical complex central to parasite invasion and for the establishment of infection within the host
- A non-photosynthetic plastid called ‘apicoplast’ responsible for essential metabolic functions
- A highly reduced genome with a respiring mitochondrion or a non-respiring mitosome (e.g. *Cryptosporidium*)

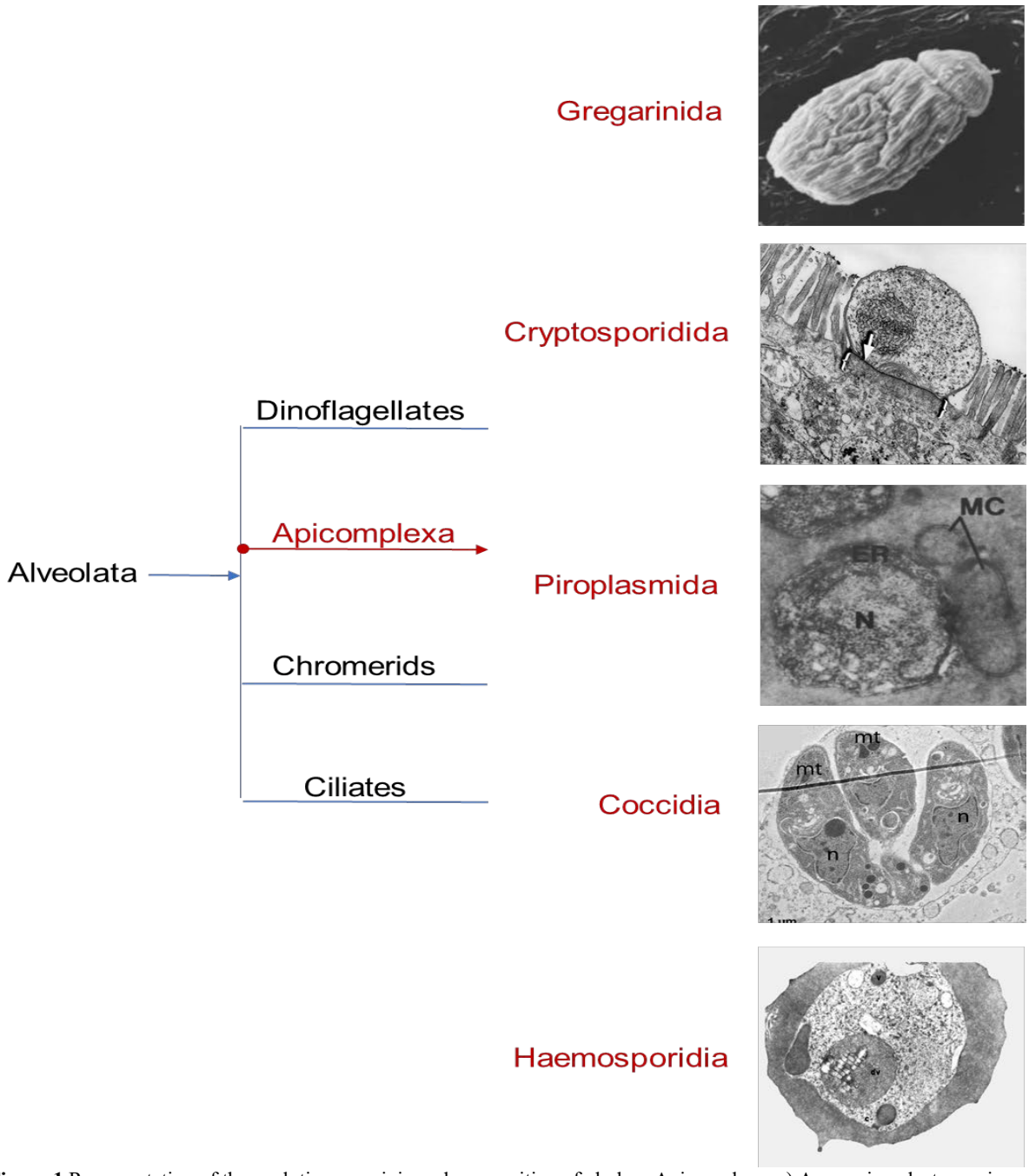

Figure 1 Representation of the evolutionary origin and composition of phylum Apicomplexa. a) A scanning electron microscopic image of *Gregarine* gamonts. (adapted from (Takahashi, Kawaguchi and Toda, 2009). b) Electron microscopic image of Cryptosporidium invading its host (adapted from Elliott and Clark, 2000). c) EM image depicting intra-erythrocyte trophozoite stages of *Babesia bovis* (adapted from (Todorovic, Wagner and Kopf, 1981). d) Transmission EM image of intracellular *Toxoplasma* parasite vacuole (adapted from (Amiar et al., 2016). e) TEM of a *P. falciparum* intra-erythrocytic trophozoite stage (adapted from Francis, Sullivan and Goldberg, 1997).

Apicomplexan parasites with importance in human diseases

a) Plasmodium falciparum

This haemosporidian is responsible for malaria, which is one of the most morbidity-causing disease worldwide. According to the WHO malaria report 2019, no significant gain was attained in terms of curbing malaria between the years 2014-2018. Malaria was responsible for 405,000 deaths between 2010-2018, which unfortunately marked children under 5 years of age as the most vulnerable group (approx. 67% malaria deaths) (World Health Organization, 2019). There are at least 5 different species belonging to the genus *Plasmodium*, including human pathogens *P. vivax*, *P. ovale*, *P. malariae*, *P. knowlesi*, *P. falciparum* and rodent malaria pathogens *P. berghei*, *P. yoelii*. Malaria is treatable if diagnosed promptly. The symptoms of malaria can be mild, which include fever, headache, chills, nausea, vomiting and general fatigue. However, in certain cases the manifestations of the disease can be severe including acute kidney failure, enlargement of spleen, metabolic acidosis, hypoglycemia and severe anemia. Cases where the parasite crosses the blood brain barrier results in cerebral malaria and ultimately death without any known treatment. Existing effective treatment against *P. falciparum* caused malaria is artemisinin combination therapy (ACT), which includes artemisinin-based compounds in combination with companion drugs like lumefantrine, mefloquine, amodiaquine, sulfadoxine/pyrimethamine, piperaquine and chlorproguanil/dapsone. However, its less notorious siblings like *P. vivax* and *P. ovale* are still treated using only chloroquine. The emerging resistance against artemisinin suggests the pressing need of novel drugs (Dondorp *et al.*, 2009).

b) Toxoplasma gondii

T. gondii, responsible for Toxoplasmosis, inhabits approximately one third of the human population worldwide. The seropositivity of this polyxenous parasite amongst humans ranges from 15-70% (Tenter, Heckeroth and Weiss, 2000). Till date, the drugs available for *Toxoplasma* treatment include sulfadiazine and pyrimethamine, mainly targeting parasite's folic acid metabolism. These drugs are active only against the symptomatic acute stage of the parasite known as tachyzoite. The chronic stage bradyzoites of *Toxoplasma* can persist within their hosts for lifetime, as they remain asymptomatic. Immunocompromised individuals like patients with HIV/AIDS or autoimmune disorders and fetuses can face severe consequences of Toxoplasmosis

which results in damage to the brain, eyes, or other organs. Despite being well studied, there are still no vaccines effective against this disease.

Life cycle of apicomplexan parasites

The life cycle of apicomplexans is rather complex and occurs within two different hosts types. This thesis is focused on two apicomplexan parasites responsible for inflicting morbidity in humans, *Toxoplasma gondii* and *Plasmodium falciparum*. The life cycle of coccidians and haemosporidians comprises both asexual division (merogony) and sexual division (gamogony) (Vot *et al.*, 2017).

Life cycle of Plasmodium falciparum

This notorious pathogen has a complex life cycle balancing between female *Anopheles* mosquito and a vertebrate host. The life cycle begins with a blood feed by an infected female *Anopheles* mosquito where it injects sporozoites life stages into the dermis of the vertebrate host. Some of these sporozoites that escape the host immune response within the dermis are successfully able to invade liver cells (i.e. hepatocytes) via bloodstream. This invasion initiates the liver stage of *Plasmodium* life cycle, which is an asymptomatic step, allowing the exponential multiplication of the parasite population. The active invasion of a single sporozoite into a hepatocyte is preceded by the traversal of these sporozoites through various hepatocytes involving formation of a transient vacuole. Once the sporozoite has invaded a hepatocyte, it converts to an exo-erythrocytic form (EEF) over the subsequent 2–10 days after invasion. These EEFs undergo massive asexual replication during which the karyokinesis precedes cytokinesis, called 'schizogony' culminating in the release of up to 40,000 merozoites per hepatocyte into the bloodstream by budding and active egress of parasite-filled vesicles called merosomes (Sturm *et al.*, 2006). The release of merozoites initiates the symptomatic blood stage of the parasite life cycle. These merozoites next encounter and infect red blood cells (RBCs). The RBC invasion by the merozoites is a dynamic multistep process (attachment, apical reorientation and actual invasion) that is complete within 2 min (Cowman *et al.*, 2016). Once erythrocyte infection is established, parasite undergoes another round of schizogony. The invaded parasite then undergoes morphological, cellular and metabolic changes to accomplish the asexual blood stage division cycle, through parasite maturation into stages called ring, trophozoite and schizont over the following 48 h. Such division cycle allows the generation of 16-32 merozoites per erythrocyte. The end of this process is marked by the

destructive release of these merozoites into the blood stream initiated by the active egress of parasites out of the RBC to access new host cells. During the several rounds of schizogony in the bloodstream, few parasites commit to sexual differentiation and develop into gametocytes. After commitment, it takes up to 11 days for the gametocytes to mature into infectious forms ready to be transmitted to mosquitos. Upon ingestion through the *Anopheles* blood feed, these gametocytes develop into female non-motile macrogamete and male exflagellated motile microgametes, within the mosquito mid-gut, likely upon the sensing of environmental signals (like temperature). Furthermore, mating occurs by fusion of micro- and macrogamete resulting in the formation of a zygote, which transforms over next 24 hr into a motile ookinete. The ookinete traverses the mosquito midgut epithelium and encysts to become an oocyst where asexual sporogenic replication occurs (Kuehn and Pradel, 2010). Following oocyst rupture, thousands of motile sporozoites are released into the hemocoel which then pass into salivary glands from where they can be injected into the next human host and restart the deadly life cycle. Illustration of complete life cycle is described in figure.2.

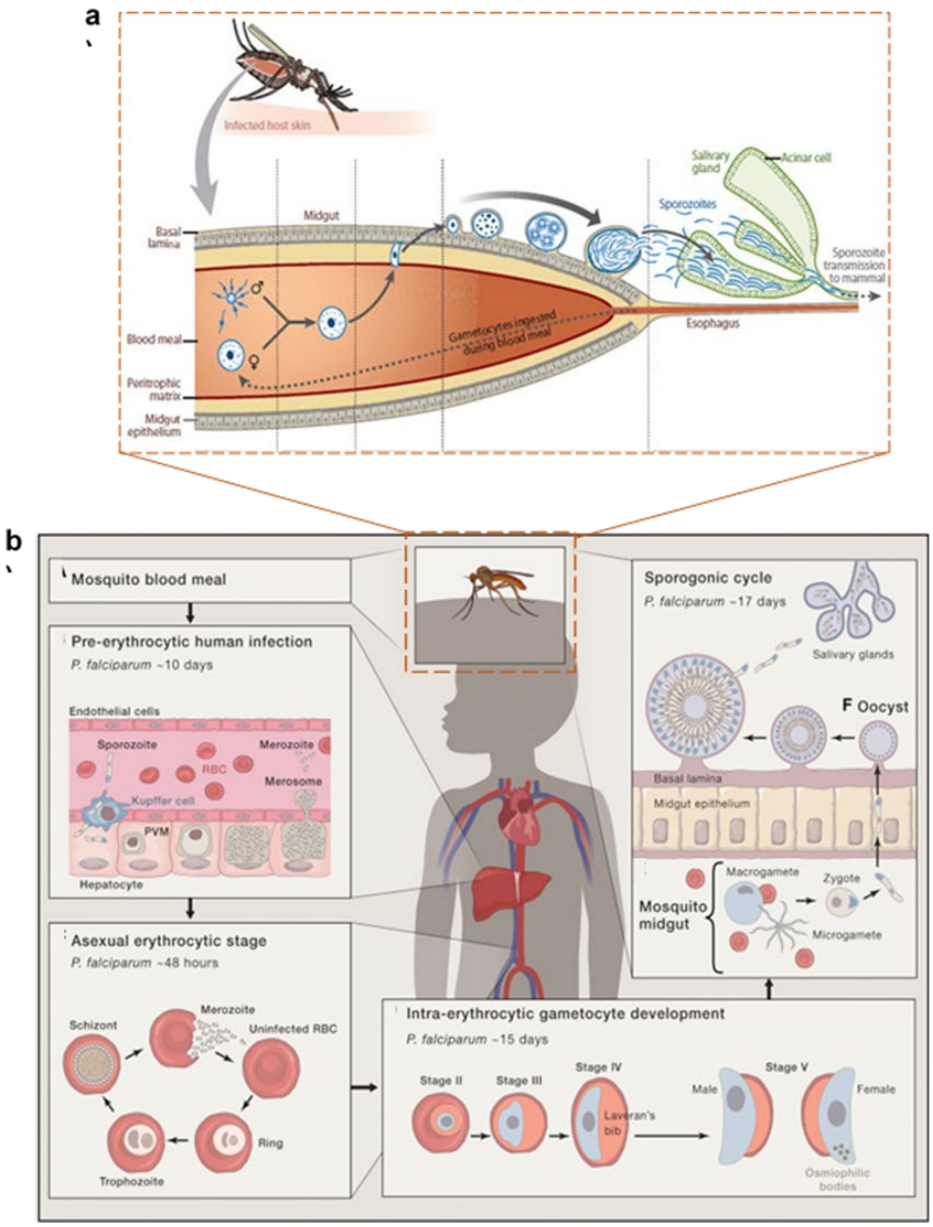

Figure 2 Complete life cycle of *Plasmodium falciparum* with asexual development in human host cells, hepatocytes and erythrocytes (a), adapted from (Cowman et al. 2016) and sexual development involving life stages female/male gametes, ookinetes, oocysts and sporozoites within female *Anopheles* mosquito (b), adapted from (Aly, Vaughan, and Kappe 2009). The initiation of asexual life cycle within human host is initiated by the bite of *Anopheles* injecting sporozoites into the dermis. This is followed by their transport to liver known as the pre-erythrocytic stage where they divide by schizogony (over a period of 10 days) to generate tens of thousands of daughter merozoites are released in packets of merosomes into the bloodstream. Within the bloodstream, these merozoites invade red blood cells carrying out their erythrocytic life stage, a cycle of which lasts for over 48 h. Next, a 15 days period leading to intra-erythrocytic gametocyte development follows which enters the peripheral circulation for ingestion by a mosquito for further transmission. The first part of sexual life cycle occurs in the mosquito midgut where the gametocytes emerge as male and female gametes followed by their fusion into a zygote which transforms into ookinete over a period of 24 h. the ookinete encysts to become oocyst where following sporogony over a period of 10-14 days, thousands of sporozoites are produced. These sporozoites traverse to enter into mosquito salivary gland from where they are transmitted to mammalian host over next blood meal.

Life cycle of Toxoplasma gondii

Toxoplasma gondii was first described in 1908 by Nicolle and Manceaux while working in North Africa, on a semidesert rodent, the common gundi (*Ctenodactylus gundi*) (Black and Boothroyd, 2000). This intracellular parasite replicates within a nucleated host cell with the goal of producing infectious progeny for further survival and dissemination. The complex life cycle of this apicomplexan parasite is split between two host types: an intermediate and a definitive host (illustration: figure. 3).

1) Intermediate host: *Toxoplasma* asexual life stage

The intermediate host covers a wide range of warm-blooded animals, including humans, where *Toxoplasma* undergoes asexual replication and further differentiation into transmissible forms. Within the intermediate host, the parasite is able to fancy two different life forms: fast replicating 'tachyzoites' and slow dividing 'bradyzoites'. The tachyzoite is virtually able to infect any nucleated cell at the advent of *T. gondii* lytic cycle. Although, current data suggest that on top of this large repertoire of host cell type, the parasite can choose and/or use the natural capacities of the host cell to its advantage to improve its dissemination/propagation/dormancy. This asexual life cycle is often called the lytic cycle which proceeds via five cellular steps: attachment, active invasion, vacuole formation notably through the discharge of secretory organelles, replication involving all complex metabolic interactions with the host cell, and active egress (Black and Boothroyd, 2000). After invading the host cell, a tachyzoite surrounds itself with a parasitophorous vacuole (PV) that is the niche and site for interaction between the parasite and its host cell. Replicative tachyzoites undergo several rounds of division, with a generation time of approx. 6-8 h before the final egress out of their inhabitant host cell to further invade its surrounding host cells. The terminology and cellular process used for this replicative process, where daughter progeny is formed within the boundaries of the mother cell that gets consumed at the end of division, is called 'endodyogeny' (Francia and Striepen, 2014; White and Suvorova, 2018). Under immune pressure from the host, the acute phase tachyzoites can commit, convert and differentiate into slow growing bradyzoites, finally forming a structure called tissue cyst, which constitutes a resistant and dormant niche filled with bradyzoites. Normally, the tissue cysts appear 7-10 days post infection, which defines the so-called chronic life stage of this parasite. The dormant cyst forms usually occur within the central nervous system and muscle tissue, where they can survive within host for

lifetime. Congenital infection occurs in case of vertical transmission of these tachyzoites from maternal blood into fetal tissues (Dubey, 2013).

2) Definitive host: *Toxoplasma* Sexual life stage

In *T. gondii* life cycle, the sexual stage is restricted to a feline host, that can acquire *Toxoplasma* through ingestion of contaminated food. The ingested *Toxoplasma* invades the feline intestinal epithelium where it differentiates into five morphologically distinct forms of schizont (Pittman and Knoll, 2015). These schizonts then differentiate into merozoites, which is regarded as the first sexual stage of the parasite life cycle. Merozoites then undergo 2-4 rounds of division to further differentiate into microgametes and macrogametes. This process of division where the nucleus undergoes multiple rounds of division prior to cytokinesis is called 'schizogony'(Ferguson *et al.*, 1974; Francia and Striepen, 2014). These gametes fuse together to form diploid oocyst. These oocysts are shed via cat's feces into the environment, where they can survive moderate conditions due to their possession of a thick impermeable wall. Cats excrete up to 20 million oocysts per day, after approx. 3-10 days of acquiring *Toxoplasma* infection. Under favorable environmental conditions, these oocysts undergo mitotic and meiotic divisions to produce haploid sporozoites encysted by the sturdy oocyst wall.

Toxoplasma transmission between various hosts occurs via:

a) Faeco-oral route, by ingestion of food contaminated with *Toxoplasma* oocysts
b) Congenital acquisition, vertical transmission of parasites from infected mother to fetus

Since, the results of my thesis are majorly focused on *T. gondii*, therefore further description of parasite morphology and establishment of infection within the host is focused on *Toxoplasma.*

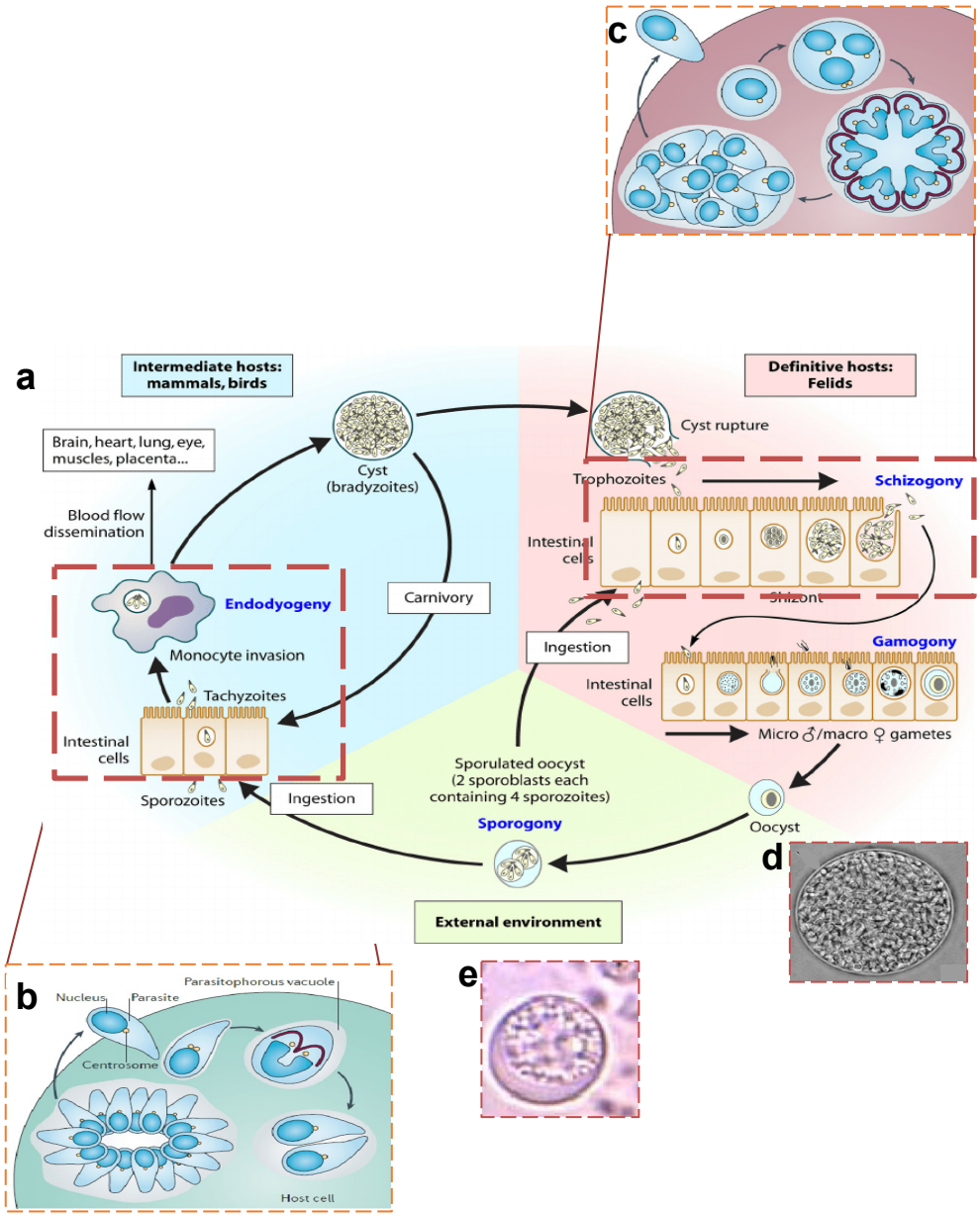

Figure 3. a) Infection of *T. gondii* within the intermediate host (asexual cycle) occurs through ingestion of contaminated food. The transmissible bradyzoites or sporozoites are released into the intestinal lumen where they invade intestinal enterocytes and differentiate into tachyzoites. Tachyzoites divide rapidly by the process of endodyogeny (b) and then egress from the host, infecting neighboring cells to start another cycle. Tachyzoites convert to dormant stage bradyzoites and then finally to tissue cysts that remain persistent within brain or musculature for almost lifetime of the intermediate host(a). The sexual cycle occurs only in cats, initiated by rupture of ingested tissue cyst that releases bradyzoites into enterocytes. These bradyzoites then undergo a self-limiting number of asexual multiplications, characterized by the development of merozoites within schizont, a process called schizogony (c). This is followed by gamogony and fertilization of the gametes forming an unsporulated oocyst (d). These are releases by with cat feces into the external environment where they undergo sporulation generating at least 4 haploid sporozoites per oocyst (e). (a) adapted from (Pittman and Knoll, 2015); (b,c) adapted from (Francia and Striepen, 2014)

Establishment of an infectious niche: active host cell invasion by *T. gondii*

Host cell invasion by *Toxoplasma* is an active process, unlike several other eukaryotic pathogens that embark upon phagocytic engulfment by the host. These parasites employ their actin-myosin machinery for aiding the active entry into their hosts (Carruthers, 2002).

Toxoplasma invasion begins with a reversible attachment of the parasite to the host cell surface, a process called 'gliding motility'. Within *Toxoplasma*, apically located secretory organelles, micronemes and rhoptries act as the main drivers in the process host cell invasion. For instance, the initial binding of the parasite to host cell membrane results in apical release of the micronemal protein MIC2 (Carruthers and Sibley, 1997). The second step is initiated by the discharge of rhoptry proteins in order to form a nascent parasitophorous vacuole. The rhoptries empty their contents apically during the process of host invasion i.e., beginning with the RONs and thereafter ROPs. During the process of invasion, a constriction or tight association, called the moving junction (MJ), is formed between the parasite and host cell membrane (Mordue *et al.*, 1999; Alexander *et al.*, 2005). This MJ associated constriction around an invading parasite migrates from the anterior towards the posterior end. The MJ also serves to exclude all the host cell proteins and parasite secreted micronemes from entering the parasite vacuolar space within its host. The moving junction is formed with a complex of the micronemal protein AMA1 and RONs (RON2,4,5 and 8) within the plasma membrane of the parasite (Besteiro *et al.*, 2009). At the end of the invasion process when the PV formation is complete, the dense granules release their contents called GRA proteins into the PV and beyond to the host cell nucleus (Hakimi and Bougdour, 2015; Mercier and Cesbron-Delauw, 2015). Dense granule proteins (GRA) play important roles in the interaction of the parasite with its host via PVM as well as survival within the host through rewiring of the host cell gene expression.

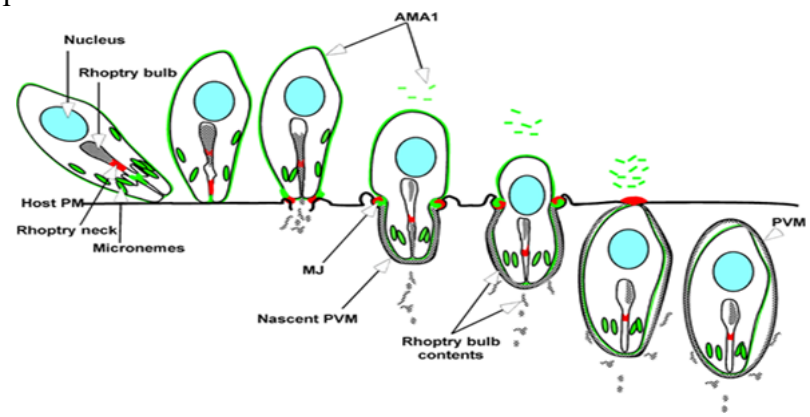

Figure 4 Schematic representation of active invasion process of *T. gondii* inside its host

Ultrastructural morphology of *Toxoplasma* tachyzoite

Toxoplasma derives its name based on its shape, from a Greek work *toxon*, meaning "bow". A typical *Toxoplasma* tachyzoite is crescent-shaped ranging in the size of 2-6 µm (Dubey, Lindsay and Speer, 1998).

1. *The apical complex: machinery guiding the invasion process in T. gondii*

The phylum apicomplexa withholds its name due to the presence of an 'apical complex' which is central to parasite invasion and subsequent proliferation within its host (Hu et al., 2006). The apical complex is a remarkable structure comprising of a) spirally arranged assembly of fibers called conoid, b)polar ring, located at the parasite apex, which serves as the site for origination of subpellicular microtubules, c) two intraconoidal microtubules and d) the preconoidal rings. *Toxoplasma* has several apically located regulated secretory organelles which include micronemes and rhoptries. Micronemes are small rod-shaped electron dense structures. The micronemes released their contents early on during the process of attachment-invasion, following which there is secretion of rhoptries as the invasion process proceeds. The rhoptries appear as club shaped structures in electron micrographs of *T. gondii*. This parasite typically has up to 8-12 rhoptries in total which are composed of a bulbous body structure which tapers into a thin duct-like rhoptry neck extending towards the conoid. The rhoptry neck proteins are referred to as RONs whereas the ones residing in bulbous body area are called ROPs. Rhoptries are known to be rich in proteins as well as lipids which they release alongside their secretion during the time of invasion. There are other cytoplasmic secretory organelles called dense granules that are released towards the end after completion of the process of invasion (Black and Boothroyd, 2000).

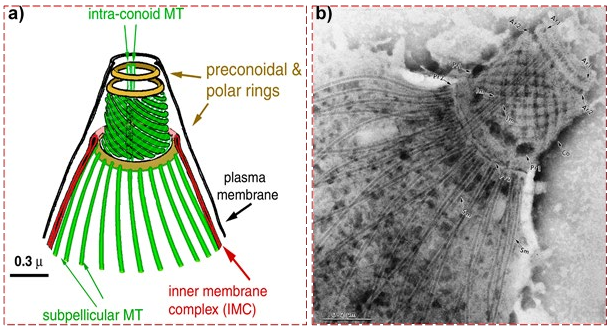

Figure 5 a) Schematic enlarged view of the apical complex cytoskeleton, showing the conoid (green), preconoidal, and polar rings (brown), and two intraconoid MT (green) (adapted from Hu *et al.*, 2006), b) TEM image of the apical complex of *Toxoplasma* tachyzoite (adapted from Dubey, Lindsay and Speer, 1998)

2) *Toxoplasma pellicle: the outer membranes surrounding the parasite*

The parasite pellicle is a trilaminar structure comprising of the outer plasma membrane and an inner membrane complex (IMC) comprising two continuous membranes (Dubey, Lindsay and Speer, 1998). IMC is a unique cytoskeletal organelle which comprises of two distinct elements: a sac of flattened vesicles beneath the parasite plasma membrane called alveoli and a supporting rigid network of intermediate filaments (Mann and Beckers, 2001; Chen et al., 2015). The IMC imbibes a highly dynamic organization crucial for parasite development. The IMC of the mother parasite acts as the scaffold used by daughter cells for undergoing the process of endodyogeny (Ouologuem and Roos, 2014). The daughter IMC elongation is based on the recycling of maternal IMC membranes, after emergence of daughters from the mother cell.

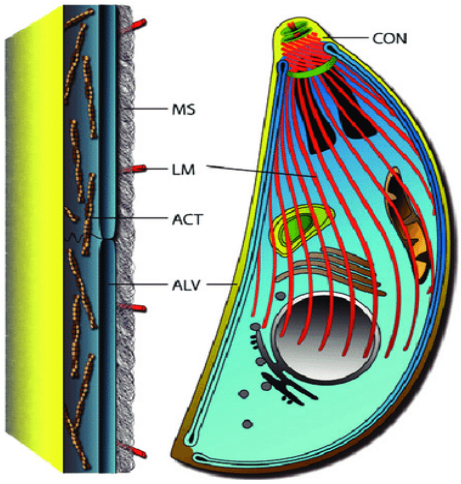

Figure 6 The basic pellicle organization *Toxoplasma* tachyzoite is characterized by alveolar sacs (ALV) associated with the inner membrane complex beneath the plasma membrane (in yellow) supported by a membrane skeleton (MS) and associated with microtubules structures (red) (adapted from Gould *et al.*, 2011)

3) *Metabolically active organelles: Apicoplast and Mitochondria*

Similar to their algal ancestors these parasites also possess a single apicoplast and mitochondrion.

Apicoplast*:*

It is a relict chloroplast present in several apicomplexan parasites, acquired in an event involving secondary endosymbiosis. The primary endosymbiotic event that gave rise to chloroplast in plants and algae arose from engulfment of *Cyanobacterium* by a eukaryotic heterotroph. This was followed by a second endosymbiotic event wherein plastids of chromalveolates were derived from red algae (Lim and McFadden, 2010; van Dooren and Striepen, 2013). Based on its evolutionary

origin apicoplast is surrounded by four membranes enriched with phospholipids instead of galactolipids as their algal ancestors (Botté *et al.*, 2013). Apicoplast has time n again proven itself to be parasites Achilles heel due to its role as parasite's central metabolic hub. This special organelle harbors several metabolic processes crucial for the intracellular development of apicomplexan parasites (van Dooren and Striepen, 2013).

i) Type-II Fatty acid biosynthesis/ FASII pathway: Gene knockout studies of several important enzymes involved in FASII pathway have proven the indispensability of this metabolic pathway for *T. gondii*. The apicoplast FASII contributes to the total cellular pool of short chain fatty acids (myristate, palmitate) which are further used for membrane biogenesis aiding parasite cell division and hence survival within their host (Mazumdar *et al.*, 2006; Ramakrishnan *et al.*, 2012; Amiar *et al.*, 2016).

ii) Isoprenoid precursor assembly pathway: The central precursor required for isoprenoid biosynthesis is isopentenyl pyrophosphate (IPP). Unlike mammalian cells, the IPP within apicomplexans is synthesized via a non- mevalonate pathway, involving methylerythritol phosphate (MEP), localized within parasite apicoplast. Genetic ablation of the last step of the MEP pathway involving enzyme LytB is lethal to the *Toxoplasma* tachyzoites (Nair *et al.*, 2011). Isoprenoids act as components of membrane lipids and mitochondrial electron chain coenzyme Q. These compounds also participate in post-translational modifications of several proteins imparting important functions like protein-protein interactions (van Dooren and Striepen, 2013).

iii) Iron-Sulphur cluster biosynthesis: Iron-Sulphur (Fe-S) clusters act as prosthetic groups for proteins involved in various redox reactions (van Dooren and Striepen, 2013). The apicoplast based Fe-S proteins are involved in IPP and fatty acid biosynthetic pathway, thereby suggesting the importance of this metabolic pathway in *T. gondii.*

iv) Heme biosynthesis pathway: Heme is an essential prosthetic group that functions in many cellular redox reactions including the mitochondrial electron transport chain (Van Dooren, Kennedy and McFadden, 2012). Apicomplexan parasites harbor an unusual pathway of heme biosynthesis spanning three different cellular compartments-cytosol, apicoplast and mitochondria (Kořený, Oborník and Lukeš,

2013; Bergmann *et al.*, 2019). Recent study provides the first evidence for presence of a functional heme biosynthesis pathway within *Toxoplasma* apicoplast (Bergmann *et al.*, 2019).

Mitochondria*:*

This organelle acts as reserve of essential central carbon metabolic pathways like the tricarboxylic acid cycle (TCA) and the electron transport chain (ETC). Chemical inhibition of mitochondrial TCA cycle with sodium fluoroacetate (NaFAc) is lethal to *Toxoplasma* tachyzoites (MacRae *et al.*, 2012). *T. gondii* is able to utilize both glucose and glutamine as substrates via the TCA cycle. The catalytic conversion of glycolytic intermediate pyruvate into acetyl coA for further utilization in mitochondrial TCA cycle is facilitated by a branched chain ketoacid dehydrogenase (BCKDH) complex. BCKDH is a functional replacement of mitochondrial PDH in apicomplexan parasites and essential for their intracellular growth (Oppenheim *et al.*, 2014). Another enzyme succinyl coA synthetase, catalyzing the seventh step of TCA cycle succinyl-CoA to succinate, was found to be dispensable for parasite growth (Fleige *et al.*, 2007). A probable reason for this unexpected dispensability could be the leaky expression of the enzyme under control of the anhydrotetracycline regulatable element.

A potential metabolic link between *Toxoplasma* apicoplast and mitochondria was established by showing that the use of a specific inhibitor of TCA cycle, NaFAc resulted in partial reduction in apicoplast FASII biosynthesis. The reason for the same was justified because of a shunt in which mitochondrial citrate is transported to the apicoplast and converted to a-ketoglutarate with regeneration of NADPH (MacRae *et al.*, 2012)

*4)*Other organelles covering the endomembrane system include the posteriorly located nucleus, the tubular network formed by the endoplasmic reticulum extending from the nuclear envelope and the Golgi complex (Nishi *et al.*, 2008). The ER is predominantly located basal end of the parasite while as the Golgi is adjacent to the apical end of the parasite nucleus (Hager *et al.*, 1999).

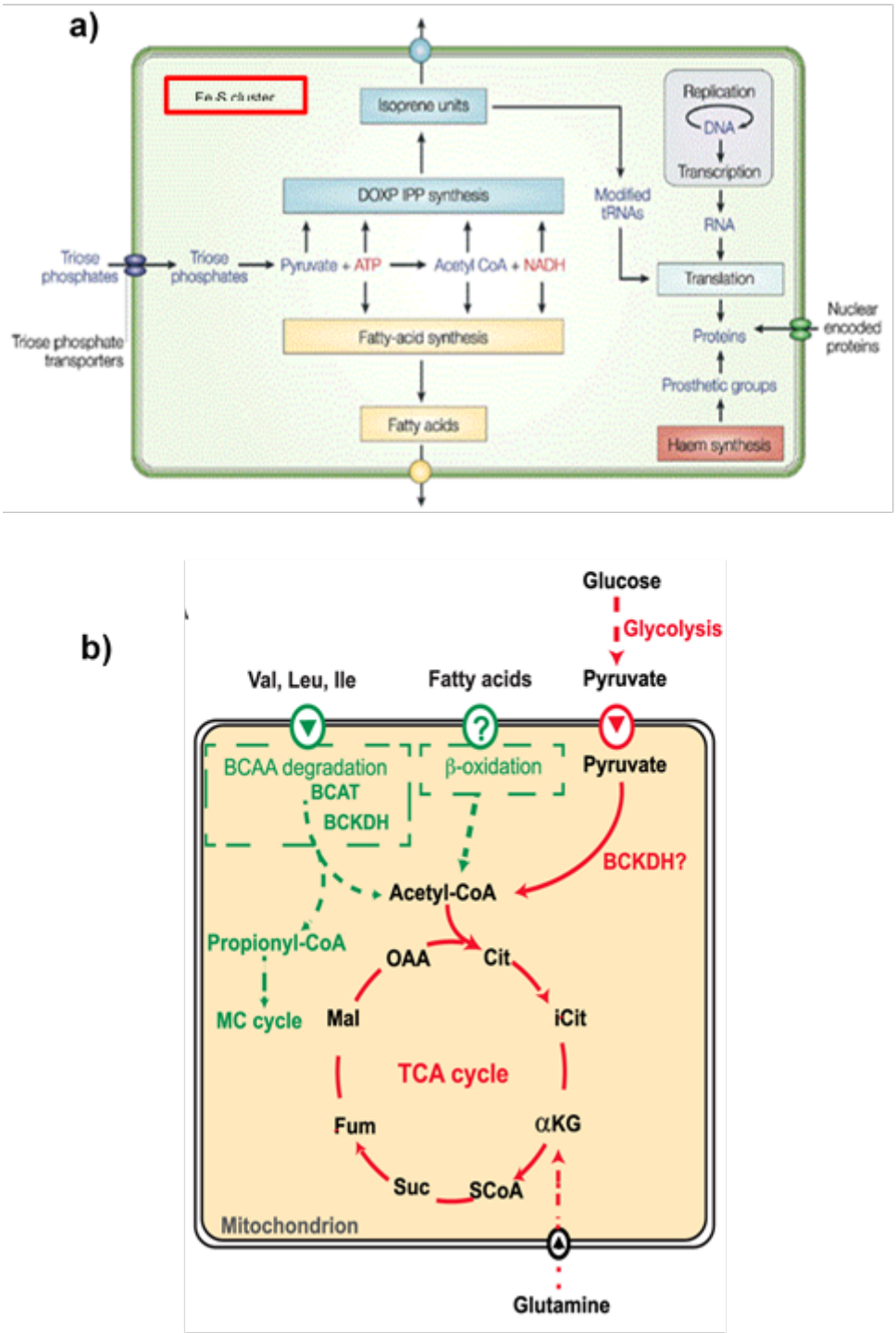

Figure 7 Metabolic pathways present in apicoplast (a) (adapted from Ralph *et al.*, 2004) and mitochondria (b) (adapted from Oppenheim *et al.*, 2014). Apicoplast provides essential metabolites for parasite's intracellular survival: fatty acids via FASII pathway, isoprenoid biosynthesis (IPP), iron-sulfur cluster biosynthesis and haem synthesis. Mitochondria resident tricarboxylic acid cycle contributes to parasite's ATP and anabolic needs

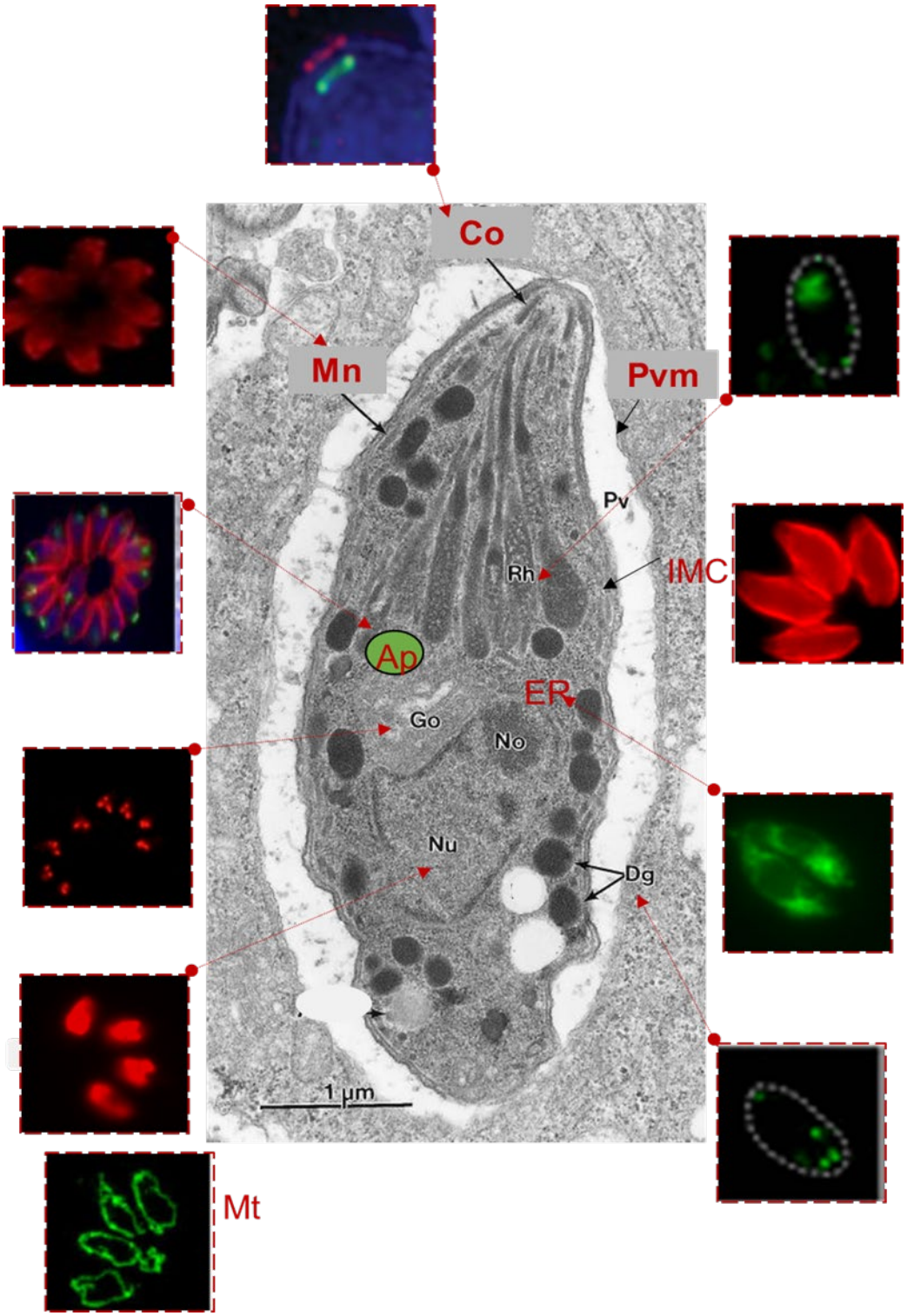

Figure 8. Electron Micrograph showing *Toxoplasma* tachyzoite (adapted from Dubey, Lindsay and Speer, 1998), Co, conoid; Dg, electron-dense granule; Go, Golgi complex; Mn, microneme; Nu, nucleus; Pvm, parasitophorous vacuole membrane; Rh, rhoptry; Ap, apicoplast; IMC, inner mitochondrial membrane; Mt, mitochondria. The immunofluorescence images (IFA) using protein markers of various organelles, IMC1, ER marker Der-1, Nucleus-DAPI (adapted from experiments done in this PhD) ; Rhoptry neck protein ROP1 and dense granule protein GRA7 was (adapted from Wang et al., 2019); conoid (adapted from (Katris et al., 2014) ; Golgi marker GRASP (adapted from (Pfluger et al., 2005); mitochondrial marker TOM40 (adapted from (Van Dooren et al., 2016) ; microneme marker MIC5 (adapted from Huynh, Boulanger and Carruthers, 2014)

CHAPTER II: LIPID METABOLISM IN APICOMPLEXAN PARASITES

LIPID METABOLISM IN APICOMPLEXA: Biosynthesis, Uptake and Recycling

The survival of these parasites within host is predominantly dependent on lipids which play an essential role by regulating metabolic flux, acting as signaling molecules, storage fuels and structural building blocks of membranes. These parasites meet their high demand of lipids through *de novo* synthesis within apicoplast as well as via copious salvage directly from the host and extracellular environment (Coppens, 2006, 2013). This raises the prospect that lipid homeostatic, trafficking and remodeling pathways in the parasite may abound as potential drug targets. For instance, apicoplast resident fatty acid biosynthetic enzymes have been successfully exploited as antimicrobial targets against *Toxoplasma* infections. This section summarizes different lipid species present in two important apicomplexan parasites *T. gondii* and *P. falciparum*:

Phosphatidylcholine

Phosphatidylcholine (PC) is a neutral glycerophospholipid accounting for the major component of total complex lipids. Quantification of total phospholipid profile within apicomplexa reveals high abundance of phosphatidylcholine in *T. gondii* (40%-70%) as well as in *P. falciparum* (40%-50%) (Gupta *et al.*, 2005; Welti *et al.*, 2007; Gulati *et al.*, 2015).

Toxoplasma tachyzoites can synthesize PC via *de novo* Kennedy pathway involving a cytoplasmic choline kinase which utilises choline up taken from external environment (Gupta *et al.*, 2005; Sampels *et al.*, 2012). Selective disruption of PC biosynthesis by supplementation of a choline analog, dimethylethanolamine was able to cause dramatic parasite growth arrest. Dimethylethanolamine interferes with choline uptake and subsequent metabolism to phosphatidylcholine, resulting in inhibition of parasite intracellular replication due to inhibition of PC biosynthesis or massive accumulation of toxic intermediate phosphatidyldimethylethanolamine (Gupta *et al.*, 2005).

Despite the presence of CDP-choline/Kennedy pathway for major PC biosynthesis, *P. falciparum* also employs an alternative pathway called serine-decarboxylase-phosphoethanolamine-methyltransferase (SDPM) pathway which uses host serine and ethanolamine as precursors (Elabbadi, Ancelin and Vial, 1997; Pessi and Mamoun, 2006; Witola *et al.*, 2008). This alternative pathway begins with the decarboxylation of host-derived serine to ethanolamine via serine decarboxylase (*Pf*SD). The next step in catalyzed by a phosphoethanolamine methyltransferase

(*Pf*PMT) in a three-step methylation reaction starting from substrate phosphoethanolamine to phosphocholine which is further incorporated into phosphatidylcholine (PC) (Pessi, Kociubinski and Ben Mamoun, 2004; Pessi and Mamoun, 2006). The loss of *Pf*PMT by gene knockout studies results in strong growth defects alongside abrogation of PC biosynthesis via SDPM pathway within *P. falciparum* (Witola *et al.*, 2008). However, unlike *P. falciparum*, *Toxoplasma* cannot use ethanolamine as a substrate for PC biosynthesis due to the absence of the required methyltransferase enzyme activity (Gupta *et al.*, 2005).

Phosphatidylethanolamine

Phosphatidylethanolamine (PE) is a neutral, second most abundant phospholipid in eukaryotic cells, normally present in the inner bilayer of the plasma membrane. Expectedly, PE is also the second most abundant phospholipid in *T. gondii* (10%-20%) and *P. falciparum* (15%-25%) (Welti *et al.*, 2007; Hartmann *et al.*, 2014; Gulati *et al.*, 2015).

In *T. gondii*, PE biosynthesis occurs differentially at several organellar sites, in the mitochondrion and in the PV by decarboxylation of phosphatidylserine, and in the ER by fusion of CDP-ethanolamine and diacylglycerol (Gupta *et al.*, 2012; Hartmann *et al.*, 2014). Mitochondrial PE biosynthesis is catalyzed by the enzyme phosphatidylserine decarboxylase (*Tg*PSD1mt). The depletion *Tg*PSD1mt impacts parasite's optimal growth, which is rescued by the addition of exogenous ethanolamine. However, despite the simultaneous knockdown of *Tg*PSD1 and ethanolamine-depletion the parasites can still egress and form plaques, albeit reduced in terms of area in comparison to wild type parasites (Hartmann *et al.*, 2014). This suggest that the parasite has employed other routes for PE biosynthesis including the high possibility of direct scavenging from its metabolically enriched host. *Toxoplasma* also secretes a phosphatidylserine decarboxylase (*Tg*PSD1) localizing to the dense granules, into the parasite vacoular space (Gupta *et al.*, 2012). Based on biochemical activity confirmation of *Tg*PSD1, it can be speculated that this enzyme contributes to PE biosynthesis within PV, possibly utilizing host derived precursors.

The PE biosynthesis in *P. falciparum* is also branched into CDP-ethanolamine/Kennedy pathway and the serine decarboxylation pathway (as described above) (Elabbadi, Ancelin and Vial, 1997; Kilian *et al.*, 2018).

Phosphatidylserine

Phosphatidylserine (PS) despite being less than 10% in the total abundance of phospholipids, is still an important anionic lipid. Due to its negative charge, PS is able to impart unique biophysical properties to the membranes and also participates in important biological processes like apoptosis in various eukaryotic cells. In terms of abundance, PS constitutes 5%-10% of the total phospholipid species in both *T. gondii* and *P. falciparum* (Welti *et al.*, 2007; Gulati *et al.*, 2015).

Intriguingly, phosphatidylserine in *T. gondii* has been linked to a mechanism of host immune evasion called apoptotic mimicry (dos Santos *et al.*, 2011). Briefly, during this process *Toxoplasma* expresses PS on the surface thereby decoying itself as an apoptotic cell inside its host macrophages. As a result, the parasite infected macrophages inhibit the synthesis of nitric oxide (NO) via NO synthase degradation, thereby allowing parasite persistence within. Interestingly, *Toxoplasma* utilizes serine as a substrate for PS biosynthesis through two different enzymes functionally behaving as phosphatidylserine synthases, *Tg*PSS (phosphatidylserine synthase) and *Tg*PTS (phosphatidylthreonine synthase) (Arroyo-Olarte *et al.*, 2015). *Tg*PSS, with strict serine-substrate specificity, localizes towards the parasite ER/mitochondrion intersection.

In *P. falciparum* PS acts as an important pathogenicity factor by facilitating erythrocyte cytoadherence (Eda and Sherman, 2002). Micro vesicles derived from the blood sample of *P. falciparum* infected patients been have shown to have elevated levels of phosphatidylserine (Gulati *et al.*, 2015). The malarial parasite synthesizes PS using host derived serine, most of which is obtained from parasite mediated host erythrocyte hemoglobin degradation (Wein *et al.*, 2018). As described above PS also serves as a precursor of PE via serine decarboxylation pathway in both *T. gondii* and *P. falciparum* (Elabbadi, Ancelin and Vial, 1997; Hartmann *et al.*, 2014; Kilian *et al.*, 2018).

Phosphatidylthreonine

Phosphatidylthreonine (PTh) is usually a minor component of the total phospholipid constituent in various eukaryotic cells. Recent study described the existence of Phosphatidylthreonine as a major phospholipid (3-4 times more than phosphatidylserine) in *T. gondii* facilitating a 'lipid-mediated virulence' within its host (Arroyo-Olarte and Gupta, 2016). The parasite employs a novel enzyme phosphatidylthreonine synthase (TgPTS) for generation of PTh within the endoplasmic

reticulum. The *Tg*PTS has evolutionarily evolved from *Tg*PSS as both the enzymes are capable for PS synthesis in the presence of serine as a substrate. Unlike, *Tg*PSS, the presence of threonine induces phosphatidylthreonine biosynthesis by the enzymatic action of *Tg*PTS. Genetic disruption of *Tg*PTS (Δtgpts) impairs the parasite lytic cycle and attenuates its growth within murine model. Lipidomic analysis of parasites lacking *Tg*PTS indicate a significant decline in the PTh levels with a concomitant accumulation of phosphatidylserine. The rescue of strong growth defect and PTh synthesis is attained by complementation of Δtgpts parasites with exogenous copy of *Tg*PTS-HA. The main fatty acid components of the *T. gondii* PTh species included C20:1 and C20:4 (Arroyo-Olarte *et al.*, 2015). The authors of this study further speculate the possible involvement of PTh influencing the calcium flux across the plasma membrane and/or calcium storage organelles (Arroyo-Olarte and Gupta, 2016).

Phosphatidylinositol and related phosphoinositides

Phosphatidylinositol (PI) is a negatively charged important constituent of membrane phospholipids. Phosphate derivatives of phosphatidylinositol, called phosphoinositides have more critical functions within a cell, such as signaling, cell-cell communication, intracellular trafficking.

PI comprises approx. 5% of the total phospholipid abundance in both *T. gondii* and *P. falciparum* (Welti *et al.*, 2007; Gulati *et al.*, 2015). In *Toxoplasma*, phosphatidylinositol-3-monophosphate (PI3P) has been shown to be associated with apicoplast protein-shuttling vesicles. Chemical inhibition of PI3P synthesizing kinase, resulted in aberrant apicoplast morphological development suggesting the role of this phospholipid for apicoplast biogenesis (Tawk *et al.*, 2011). A *Toxoplasma* phosphatidylinositide-phospholipase C (*Tg*PI-PLC), catalyzes the hydrolysis of phosphatidylinositol 4,5-bisphosphate (PIP2) to D-myo-inositol 1,4,5-trisphosphate (IP3) and sn-1,2-diacylglycerol (DAG) at the plasma membrane of the parasite (Fang, Marchesini and Moreno, 2006). Recombinant protein of *Tg*PI-PLC showed a preference for phosphatidylinositol (PI) as a substrate rather than PIP2. Another study showed that this protein was localizing to both plasma membrane and cytoplasm within the parasite, suggesting its multiple roles in lipid regulation (Bullen *et al.*, 2016).

In *P. falciparum*, an enzyme generating 3' phosphorylated phosphoinositides, phosphoinositide-3-kinase (PI3K) is actively transported across the PVM into its erythrocyte host. Using PI3K

inhibitors wortmannin and LY294002, the enzyme and its product were shown to be functionally involved in endocytic trafficking of hemoglobin from the host to the food vacuole within the parasite. This enzymatic function is necessary for the parasite pathogenesis as it allows degradation of the toxic host hemoglobin within the parasite food vacuole to provide amino acid sources for its growth (Vaid *et al.*, 2010). MMV390048, a drug effective against all life stages of malarial parasites specifically targets a phosphatidylinositol 4-kinase within the parasite (Paquet *et al.*, 2017). The sugar-derivates of phosphatidylinositol like glycosylphosphatidylinositol (GPI) have been identified as dominant toxins existing as free or antigen linked molecules on the surface of malaria parasite (Debierre-Grockiego *et al.*, 2006). *Plasmodium falciparum* uses *de novo* synthesized as well as host-scavenged myo-inositol for the synthesis of bulk phosphatidylinositol (Macrae *et al.*, 2014). The scavenged myo-inositol is however directly channeled towards biosynthesis of glycophosphatidylinositol (GPI).

Cardiolipin

Cardiolipin (CL) is basically a diphosphatidyl glcyerolipid bearing four fatty acyl chains and hence double negative charge. The occurrence of cardiolipin is mostly in prokaryotic plasma membrane and eukaryotic mitochondrial membranes (Schlame, 2008). The synthesis of CL within eukaryotes begins with conversion of phosphatidic acid (PA) to cytidine diphosphate-diacylglycerol (CDP-DAG). The final reaction involves an enzyme cardiolipin synthase which catalyzes the transfer of phosphatidyl group from CDP-DAG to another lipid molecule phosphatidylglycerol (PG) resulting in the formation of cardiolipin (Schlame, 2008; Fu *et al.*, 2018).

The presence of a putative cardiolipin synthase candidate gene (TGGT1_309940) is indicative of functional *de novo* cardiolipin biosynthesis pathway in *Toxoplasma* (Fu *et al.*, 2018). A recent study showed that a fatty acid transporter, acyl-coA binding protein-2 (*Tg*ACBP2) actively participates in cardiolipin metabolism and subsequently maintains mitochondrial homeostasis within type-II strain of *T. gondii*. Metabolic analysis of *Tg*ACBP2 depleted type II prugnaid strain using LC-MS showed significant reduction in cardiolipin abundance, esp. with fatty acyl moieties C72:7, C74:9, C74:8, C74:7, C76:9, C78:11, C78:9, C78:8, C82:11, and C82:0. Interestingly, there are reports of increased prevalence of anti-cardiolipin antibodies in patients inflicted with malaria in Asia and Africa (Consigny *et al.*, 2002).

Phosphatidylglycerol

Phosphatidylglycerol (PG) is an anionic phospholipid less abundant in eukaryotes but highly abundant in bacterial membranes. PG in *P. falciparum* makes up almost 2%-3% of the total phospholipids (Gulati *et al.*, 2015). The levels of PG increase in *P. falciparum* infected erythrocytes from undetectable levels to approx. 4% (Tran *et al.*, 2016). The same phospholipid is reduced from 4% to 1% upon maturation of asexual stages to sexual stage gametocytes. There is not much literature available for the functions and biosynthesis of PG in *T. gondii*, however it acts an important precursor for the biosynthesis of another important mitochondrial lipid cardiolipin.

Cytidine diphosphate-diacylglycerol

Cytidine diphosphate-diacylglycerol (CDP-DAG) is a nucleotide of prime importance in lipid metabolism. This high energy intermediary liponucleotide that serves as a precursor for several other phospholipids, however, remains undetectable in lipid composition of various cells. CDP-DAG in *Toxoplasma* is synthesized in two ways, in the ER by a eukaryotic-type CDP-DAG synthase1 (*Tg*CDS1) and in the apicoplast by a prokaryotic-type CDP-DAG synthase2 (*Tg*CDS2) (Kong *et al.*, 2017). Genetic knockdown of *Tg*CDS1 was lethal to *Toxoplasma* tachyzoites and resulted in a significant reduction in the levels of phosphatidylinositol and phosphatidylserine. On contrary, complete knockout of *Tg*CDS2 resulted in selective impairment of phosphatidylglycerol biosynthesis. Overall, a deficit CDP-DAG synthesis pathway within *T. gondii* results in attenuated parasite virulence within mice.

P. falciparum has been reported to have a CDP-DAG synthase with split protein properties (Shastri *et al.*, 2010). The same study demonstrated that a knockout of N-terminal extension of *Pf*CDS was lethal to parasite blood stages, suggesting the importance of this liponucleotide intermediate in the phospholipid metabolism of malaria parasites.

Sphingomyelin

Sphingolipids usually comprise of a long chain or spinghoid bases (e.g. sphingosine or ceramide) which is attached to fatty acyl moiety via amide bond.

In comparison to their host mammalian cells, *T. gondii* has an overall lesser abundance (approx. 1%) of sphingolipids (Welti *et al.*, 2007). Intriguingly, this parasite has a relatively high abundance

of another unusual sphingolipid called ceramide phosphoethanolamine (EPC). EPC comprises approx. 2% of the total polar lipid content in *T. gondii*. Evidence of *de novo* sphingolipid biosynthesis in *T. gondii* was first demonstrated by the bioinformatic identification of a sphingolipid synthase (*Tg*SLS). The enzyme *Tg*SLS was also biochemically validated by its ability to functionally complement a yeast mutant lacking inositol phosphorylceramide (IPC) synthase (Pratt *et al.*, 2013). Metabolic labelling studies also provided experimental evidence of the uptake of tritiated serine and galactose by *T. gondii* for *de novo* glycosphingolipid biosynthesis (Azzouz *et al.*, 2002). Despite the presence of a *de novo* biosynthetic pathway this parasite also relies on host scavenged sphingolipids. *Toxoplasma* accrues sphingolipids from the host in a Golgi dependent manner, with the help of Rab-coated vesicles. Experimental evidence of the same was provided by colocalization of vesicles, marked with Rab14, Rab30, or Rab43, with host derived sphingolipids in the vacuolar space surrounding the parasites (Romano *et al.*, 2013). These parasites replicate slowly in the host cells that are impaired in sphingolipid biosynthesis. For instance, use of myriocin, an inhibitor of serine palmitoyl transferase, in infected host cells was able to decrease the rate of parasite replication in a dose dependent manner, suggesting the importance of sphingolipid uptake in *T. gondii*.

Sphingolipids encompass the second most abundant class of lipids in asexual blood stage *P. falciparum*. The blood stage parasites have a high abundance of the structural sphingolipid, sphingomyelin (approx. 10-15%) and the unexpected presence of dihydrosphingomyelin (dhSM) (approx. 1%) (Gulati *et al.*, 2015). *P. falciparum* is able to induce the formation of an extensive network of tubovesicular membranes (TVM) extending from the PVM to the periphery of the host cell, necessary for nutrient uptake (Lauer *et al.*, 1997). The parasite exports its own sphingomyelin synthase into the host erythrocyte to synthesize sphingomyelin necessary for the development of the tubovesicular membranes (Elmendorf and Haldar, 1994; Haldar, 1996). Other than this, *P. falciparum* has been shown to have sphingomyelin synthase activity in its Golgi apparatus (Lauer, Ghori and Haldar, 1995).

Cholesterol and cholesteryl esters

Cholesterol exists either as a ubiquitous component of membranes or in fatty acid esterified form, cholesteryl ester within lipid storage droplets of the parasites. Apicomplexan parasites are auxotrophic for cholesterol and can compensate via copious salvage of cholesterol directly from

the host (Coppens, 2013). As determined by filipin based staining, cholesterol in *Toxoplasma* tachyzoites is concentrated within plasma membrane, apical organelles and rhoptries (Coppens, Sinai and Joiner, 2000). *Toxoplasma* exploits the host low-density lipoproteins (LDL)for direct uptake of exogenous cholesterol. Consistent with the exogenous cholesterol uptake, impaired *de novo* cholesterol biosynthesis within host cells, does not affect the parasite growth. A membrane bound efflux pump in the host, P-glycoprotein participates in the transport of host-derived cholesterol towards the intracellular parasite (Bottova *et al.*, 2009).

Toxoplasma stores excess fatty acids as palmitate and oleate by their esterification to cholesterol the form of palmitate and oleate containing cholesteryl esters (Coppens, 2013). *Toxoplasma* genome encodes for two enzymes that are involved in cholesteryl ester biosynthesis, acyl CoA: cholesterol acytransferase1 (ACAT1) and acyl CoA acyltransferase2 (ACAT2). Genetic ablation of each the individual ACATs impairs parasite growth due to reduced levels of cholesteryl esters and consequent increase in the amount of membrane cholesterol. The double disruption of ACAT1 an ACAT2 is lethal to *Toxoplasma* tachyzoites (Lige, Sampels and Coppens, 2013).

Liver-stage *P. falciparum* obtains its cholesterol directly from host mevalonate pathway and via LDL and HDL (exogenous sources) (Grellier *et al.*, 1991; Labaied *et al.*, 2011). The proportion of cholesterol fluctuates between 47% in uninfected RBCs to a decrease with 19% in RBCs infected with trophozoites and then increase again to 29% when the infected RBCs mature to sexual stage gametocytes (Tran *et al.*, 2016). Despite an early report on the absence of cholesteryl esters from *P. falciparum* (Nawabi *et al.*, 2003), the parasite does store cholesterol and excess fatty acids in the form of cholesteryl esters (Tran *et al.*, 2014).

Phosphatidic acid

Phosphatidic acid (PA) is the simplest glycerophospholipid bearing a negative charge. This anionic lipid has a phosphomonoester head group. PA acts as a central precursor molecule for the biosynthesis of various other glycerolipids including triglycerides. The cone shaped symmetry of this peculiar phospholipid results in a negative membrane curvature thereby allowing its participation in key membrane remodeling events like fission and fusion (Bullen and Soldati-Favre, 2016; Tanguy *et al.*, 2019). Phosphatidic acid comprises 1% of the total polar lipid composition in *T. gondii* (Welti *et al.*, 2007).

Biogenesis of phosphatidic acid: Reference to apicomplexan enzymes

In various eukaryotes, different species of phosphatidic acid are generated by at least four different pathways. The main pathway contributing to PA synthesis begins with the glycolytic intermediate glycerol-3-phosphate and involves two sequential reactions with acyltransferases-acyl CoA: glycerol-3-phosphate acyltransferase (GPAT) and acyl CoA: lysophosphatidic acid acyltransferase (LPAAT) (Athenstaedt and Daum, 1999). The second pathway also uses acyltransferases however with the involvement of a different substrate i.e. dihydroxyacetone phosphate (DHAP). The third pathway employs the enzyme phospholipase D, which hydrolyses phospholipids like PC to generate phosphatidic acid. Lastly, under certain conditions, diacylglycerol kinases (DGKs) can catalyze the formation of PA in an ATP dependent manner from the substrate diacylglycerol (DAG).

In *T. gondii*, a complete *de novo* pathway of PA biosynthesis localizing to the apicoplast has been identified (Amiar *et al.*, 2016, 2019). Briefly, phosphatidic acid is synthesized within apicoplast by the sequential esterification of fatty acyl-CoA onto a glycerol-3-phosphate backbone by glycerol-3-phosphate acyltransferase (AGPAT/ATS1) forming lysophosphatidic acid (LPA) and then by an acylglycerol-3-phosphate acyltransferase (AGPAT/ATS2) forming PA from LPA. The parasite has also been shown to uptake BODIPY-phosphatidic acid from the extracellular environment and the host (Charron and Sibley, 2002).

Plasmodium on contrary has an incompletely mapped apicoplast PA biosynthetic pathway, with two known enzymes sufficient to catalyze conversion of acyl-ACPs and dihydroxyacetone phosphate (DHAP) into the intermediate lysophosphatidic acid (Lindner *et al.*, 2014; Shears *et al.*, 2017). It is believed that in *Plasmodium*, the apicoplast generates only lysophosphatidic acid which is fully acylated to generate phosphatidic acid within the parasite ER. The table below (Table 1) represents a list of all the enzymes that have been characterized to be involved in phosphatidic acid biosynthetic pathway in apicomplexan parasites *Toxoplasma gondii* and *Plasmodium sp.*

*Tg*ATS1	-apicoplast localized -indispensable for toxoplasma tachyzoites -plant like glycerol-3-phosphate acyltransferase that generates lysophosphatidic acid, the precursor for phosphatidic acid biosynthesis	(Amiar *et al.*, 2016)
*Tg*ATS2	-apicoplast localized -catalyzes the esterification of an activated FA (i.e. acyl-CoA or acyl-ACP) onto LPA to make PA	(Amiar *et al.*, 2019)
*Tg*DGK1	-DGK phosphorylates phosphoinositide phospholipase C (PI-PLC)-derived diacylglycerol (DAG) to form PA, at the parasite plasma membrane	(Bullen *et al.*, 2016)
*Tg*DGK2	-secreted into parasite parasitophorous vacuolar space -produces PA in the parasitophorous vacuolar space which further acts as an intrinsic signal for natural parasite egress	(Bisio *et al.*, 2019)
Pf apiG3PAT	-dispensable during the blood stage of *P. falciparum* -an apicoplast localized glycerol-3-phosphate acyltransferase (G3PAT) -likely catalyzes the second step in apicoplast localized lysophosphatidic acid biosynthesis	(Shears *et al.*, 2017)
*Py*apiG3PDH	-essential for the late liver stage development of *Plasmodium yoelii* -a glycerol-3-phosphate dehydrogenase (G3PDH) that likely catalyzes the first step of PA biosynthesis via conversion of glycolytic intermediate	(Lindner *et al.*, 2014)

	dihydroxyacetone phosphate (DHAP) into glycerol-3-phosphate using NADPH as an electron donor	
*Py*apiG3PAT	-essential for late liver stage development of *P. yoelii* -this glycerol-3-phosphate acyltransferase localizes to the parasite apicoplast -likely catalyzes the formation of lysophosphatidic acid, the immediate precursor of PA	(Lindner *et al.*, 2014)

Table 1: Apicomplexan enzymes involved in phosphatidic acid biosynthesis

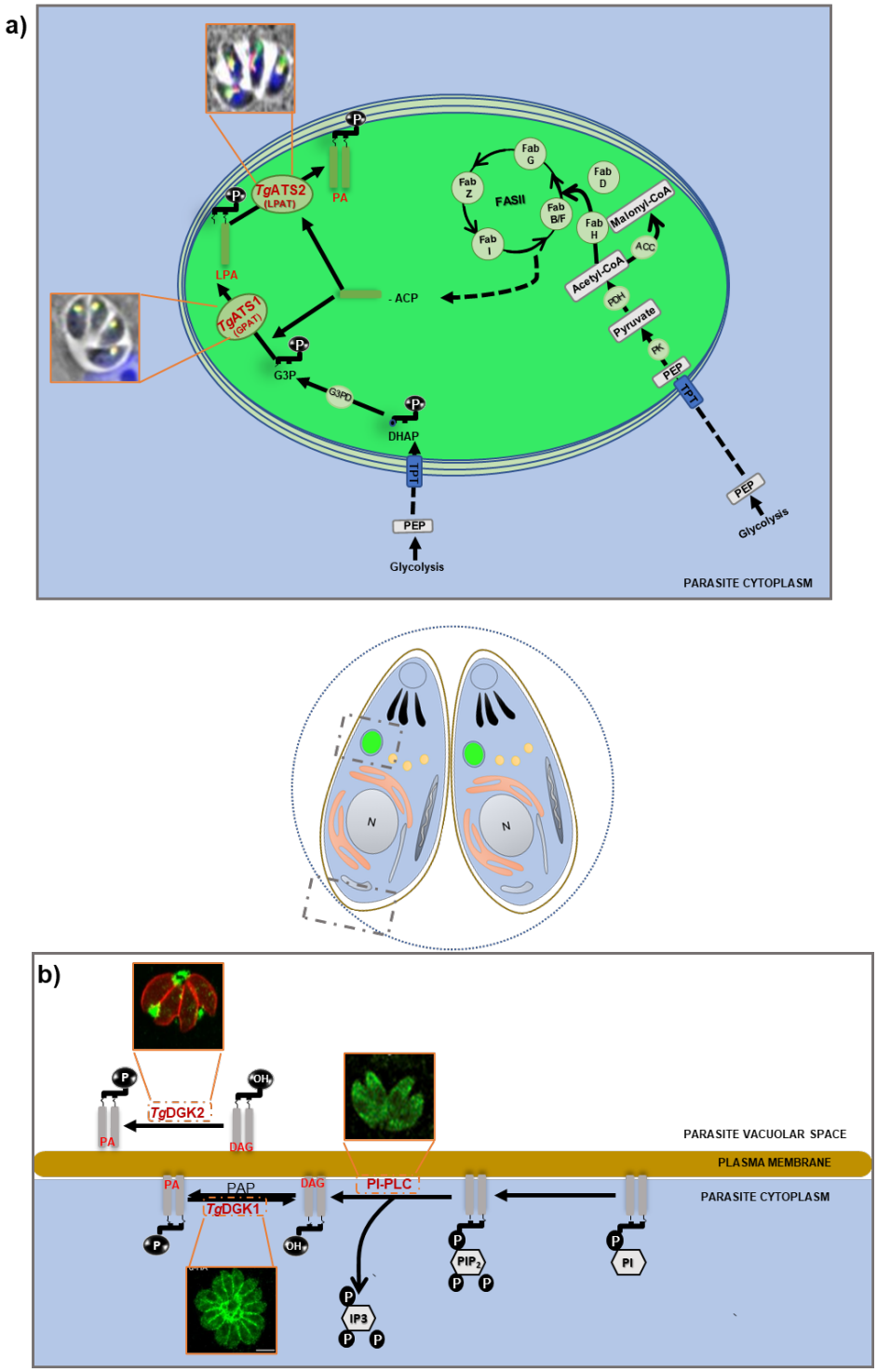

Figure 10 Phosphatidic acid biosynthetic pathways in *T. gondii*. a) Apicoplast-localized pathway of PA generation involving acyltransferases *Tg*ATS1 and *Tg*ATS2 (adapted from Amiar *et al.*, 2016, 2019). b) Generation of signaling species of PA at the parasite plasma membrane and vacuolar space by the action of diacylglycerol kinases *Tg*DGK1 and *Tg*DGK2 (adapted from Bullen *et al.*, 2016; Bisio *et al.*, 2019). Other abbreviations used, PAP, phosphatidic acid phosphatase; PKG, protein kinase G; PI-PLC (adapted from Fang, Marchesini and Moreno, 2006);phosphoinositide phospholipase C; PI, phosphatidylinositol; PIP2, phosphatidylinositol-4,5-bisphosphate; IP3, inositol 1,4,5-trisphosphate; DAG, diacylglycerol.

Phosphatidic acid at the forefront of the biological armor of parasites: Key roles in parasite biology and lipid metabolism

a) Membrane biogenesis: In eukaryotes, phosphatidic acid can be dephosphorylated by an enzyme phosphatidate phosphatase (PAP) in order to yield diacylglycerol (DAG), which serves as a precursor for the formation of major membrane phospholipids, phosphatidylcholine and phosphatidylethanolamine via Kennedy pathway (Athenstaedt and Daum, 1999). *Toxoplasma* apicoplast expresses a plant like acyltransferase called ATS1. *Tg*ATS1 has been shown to catalyze the incorporation of FASII derived fatty acids into lysophosphatidic acid (LPA), an immediate precursor of PA (Amiar *et al.*, 2016). Genetic disruption of *Tg*ATS1 resulted in reduced incorporation of FASII-synthesized fatty acids, specifically myristate (C14:0) and palmitate (C16:0) into PA and downstream phospholipids (PC, PE and PI) and consequently a severe defect in intracellular parasite replication and survival.

b) Lipid signaling modulating parasite invasion, motility and egress: Phosphatidic acid (PA) and diacylglycerol (DAG) have been implicated as important lipid mediators involved in key signaling events in mammalian cells (Bullen and Soldati-Favre, 2016). Several studies in the field of apicomplexa support the involvement of PA in establishment of infection inside the host cells.

In *P. falciparum* liver stage, CelTOS, a protein involved in the traversal of sporozoites across hepatocytes, has been shown to do so by binding and disruption of PA-enriched membranes (Jimah *et al.*, 2016). Glideosome associated connector (GAC) is an actin binding protein which controls the gliding motility and invasion in *Toxoplasma*. GAC links adhesin-MIC2 to parasite actomyosin system while interacting with phosphatidic acid in the parasite plasma membrane via its PH domain (pleckstrin homology-PH) (Jacot *et al.*, 2016).

The maintenance of parasite's intra cellular lifestyle is dependent on coordinated invasion and egress events relying on spatially controlled secretion of apical organelles called micronemes (Bullen *et al.*, 2016). Bullen et al, showed that a delicate balance between PA and DAG governed by a *Toxoplasma* diacylglycerol kinase-1 (DGK1) is the basis for regulated event of microneme secretion. Genetic disruption of *Tg*DGK-1 localized at the parasite periphery resulted in parasite cell death. The impact of PA generated by *Tg*DGK-1in microneme secretion is mediated by contact with a microneme surface protein bearing pleckstrin homology domain-APH1. Thus, in

Toxoplasma PA acts as the lipid mediator of key signaling event involving regulated exocytosis by the recruitment of micronemes via specific effector proteins.

Phosphatidic acid generated by the action of a second diacylglycerol kinase DGK2, is involved in the egress event of parasite infectivity within its host. This enzyme is secreted into the parasitophorous vacuole where it likely generates PA which in turn acts as an intrinsic signal facilitating parasite egress upstream of an atypical guanylate cyclase (GC) (Bisio *et al.*, 2019).

c) Cytokinesis and parasite cell division

Phosphatidic acid and its immediate precursor lysophosphatidic acid balance effectively allowing normal parasite division. A dynamin related protein *Tg*DrpC participates during *T. gondii* endodyogeny which in turn relies on the local LPA/PA balance generating appropriate membrane curvature, thereby assisting in cytokinesis of daughter cells (Amiar *et al.*, 2019).

d) Lipid storage

The unprecedented role of PA in storage is yet to be assessed in apicomplexan parasites. One of the branches of PA metabolism leads to synthesis of triglycerides in various eukaryotic cells (Athenstaedt and Daum, 1999). The hydrolysis of PA generating DAG molecules acts as the substrate for acyltransferases resulting in the generation of triacylglycerols which are major constituents of lipid storage bodies.

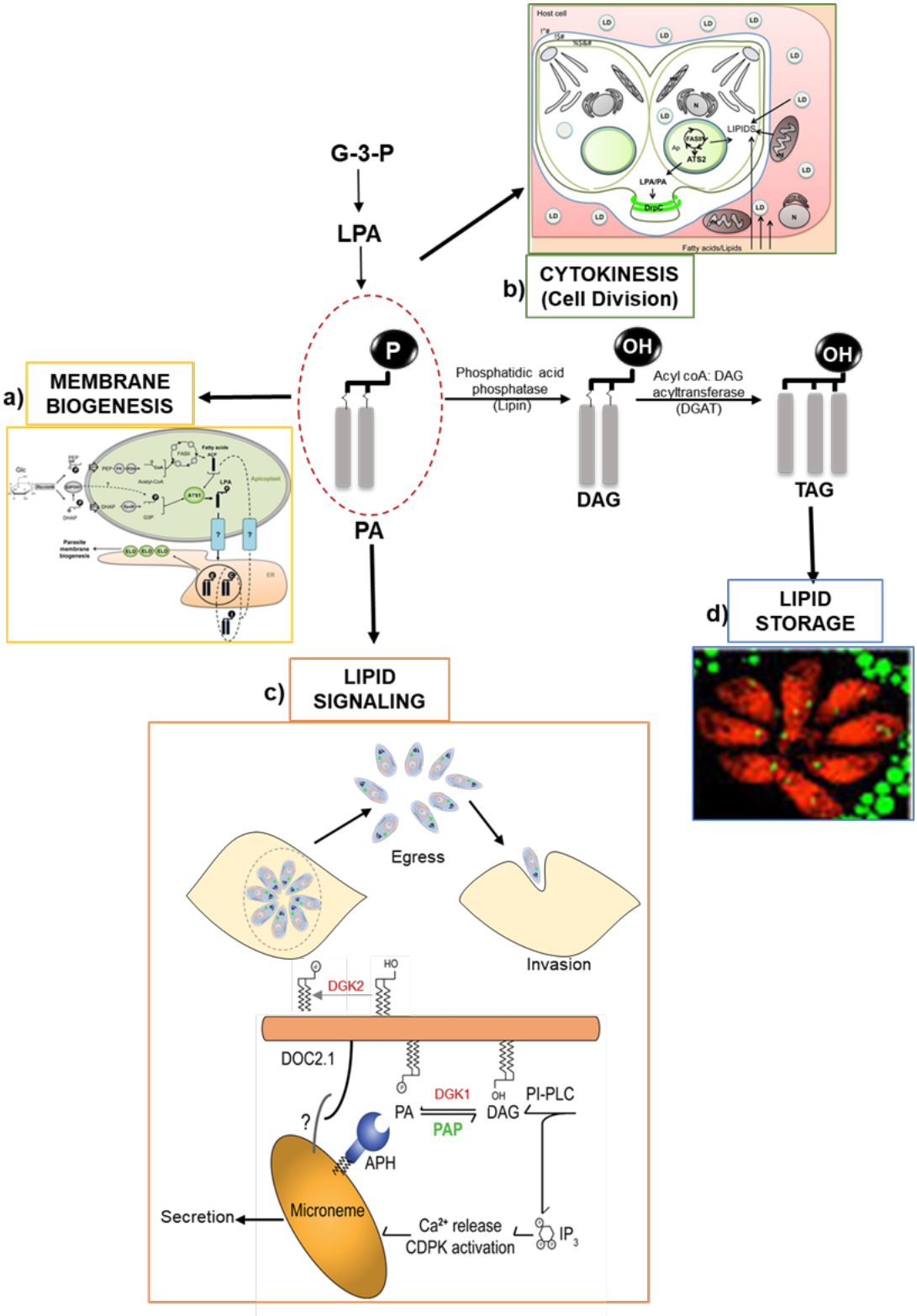

Figure 11 Schematic representation of various known functions of phosphatidic acid (PA) in apicomplexa. PA acts as the central precursor molecule aiding in generation of membrane phospholipids (a) (Amiar *et al*., 2016) and cell division process by maintaining a balance with its own precursor (LPA) (Amiar *et al*., 2019) (b). This dynamic lipid also acts as signaling molecule participating in keys parasite pathogenicity events like invasion and egress (Bullen *et al*., 2016; Bisio *et al*., 2019). PA is also channeled towards lipid storage pathway ((Nolan *et al*., 2018; this thesis).

Triacylglycerols

Biochemically, triacyclglycerols (TAGs) are highly hydrophobic, inert and energetically dense glycerolipid molecules. The TAGs are stored within the distinct cytoplasmic organelles called lipid droplets surrounded by a monolayer of phospholipids. The fatty acids released via TAG hydrolysis serve either for structural purpose in phospholipid biosynthesis or are channeled towards energy metabolism via β-oxidation.

Initial studies on lipid species of *P. falciparum* infected RBCs suggested that the asexual blood stages were able to accumulate a high amount of DAG and TAG (Nawabi *et al.*, 2003). Metabolic labelling studies using palmitic acid (C16:0) and oleic acid (C18:1) revealed a striking accumulation of TAGs from trophozoite to schizonts in *P. falciparum* asexual life cycle (Palacpac *et al.*, 2004). TAGs have also been reported to be involved in the maturation of asexual stage parasites. The use of orlistat, an inhibitor of TAG hydrolysis, on *P. falciparum* asexual life cycle arrested the parasites soon after the onset of merozoite formation (Gulati *et al.*, 2015).

In various eukaryotes, PA and DAG are two main substrates involved in glycerolipid biosynthesis pathway contributing to TAG biosynthesis. The apicomplexan enzymes involved in this pathway are discussed below:

a) Phosphatidic acid phosphatase: The phosphatidic acid species committed to TAG pathway is first dephosphorylated to generate DAG via a phosphatidic acid phosphatase. The genome of *Toxoplasma* and *P. falciparum* have been annotated to encode three and two phosphatidic acid phosphatases respectively (Bullen *et al.*, 2016). One of the PAPs, called PAP2-like protein, localizes to the cytoplasm of *Toxoplasma* in the form of vesicular sutures. This PAP2-like protein was shown to be indispensable for parasite growth probably due to this is its less significant contribution to PA/DAG balance. The *Plasmodium* homologue, *Pf*PAP2 has been shown to contribute to delicate PA and DAG balance necessary for maintaining complete lytic cycle via parasite egress (Kumar Sah *et al.*, 2019). Another PAP studied, has been shown to localizes towards the IMC sutures of *T. gondii* (Chen *et al.*, 2015). In various other eukaryotic cells, most of the phosphatase activity leading to TAG biosynthesis resides in cytoplasmic proteins called ‘lipins’ (Reue and Wang, 2019). Lipins are evolutionarily conserved proteins regulating lipid metabolism

in different cell types (Csaki *et al.*, 2013). These phosphatidic acid phosphatases catalyze the penultimate step of the glycerol-3-phosphate pathway via a Mg^{2+} dependent dephosphorylation of PA to DAG, implicating further in triglyceride and phospholipid biosynthesis. Sometimes these key regulator proteins have also been shown to have transcriptional co activator activity monitoring the expression of various genes involved in lipid metabolism. Both *Toxoplasma* and *Plasmodium* have one genome-annotated lipin which are yet to be characterized. In *Toxoplasma*, lipin has been localized towards parasite cytoplasm, without any further characterization with respect to the glycerolipid biosynthesis pathways (Bullen *et al.*, 2016).

b) Acyl CoA: diacylglycerol acyltransferase (DGAT): In the final step of the glycerolipid biosynthesis pathway, the DAG species are acylated to fatty acids with the help of enzymes called acyl: coA diacylglycerol acyltransferase. The biosynthetic machinery for TAG formation has not been characterized completely in apicomplexa. However, there are evidence for existence of DGAT homolog named *Tg*DGAT. *Tg*DGAT, localizing towards the parasite cortical and perinuclear endoplasmic reticulum preferentially incorporates palmitic acid (C16:0) into TAGs (Quittnat *et al.*, 2004). This suggests that TAG biosynthesis in apicomplexa mirrors other eukaryotes, involving the substrates PA and then DAG. Oleic acid (C18:1) appears to be one of the major constituents of TAGs in *Toxoplasma*. Feeding the parasites with exogenous oleic acid in a concentration dependent manner (0.2 and 0.4 mM) increases the transcriptional activity of *Tg*DGAT (by up to 1.5-fold) allowing the influx of oleate to be channeled towards acylglycerols (Nolan, Romano and Coppens, 2017). However, in case of excess oleic acid (0.5mM and above), the increased *Tg*DGAT activity is unable to protect the parasite from lipotoxic response, resulting in an irreversible replication arrest (Nolan *et al.*, 2018). The vulnerability of *Toxoplasma* tachyzoites and bradyzoites to a chemical inhibitor (T863) of DGAT highlighted the importance of neutral lipid synthesis and storage for avoiding lipotoxicity within parasites. T863-treated tachyzoites show abnormal ER-derived membranous structures that are stockpiled in the cytoplasm, likely impeding normal endodyogeny. Dual addition of oleic acid (0.5 mM) and T863 synergistically deteorates parasite growth. The excess fatty acids unable to be transformed towards storage TAGs due to *Tg*DGAT inactivity are likely channeled towards phospholipid biosynthesis leading to excess

membrane phenotype in the presence of T863. The treatment of *Toxoplasma* bradyzoites with T863 lead to misshapen cysts and reduced lipid droplets (LD) in bradyzoites, although sensitivity occurs at concentrations higher than those observed for tachyzoites.

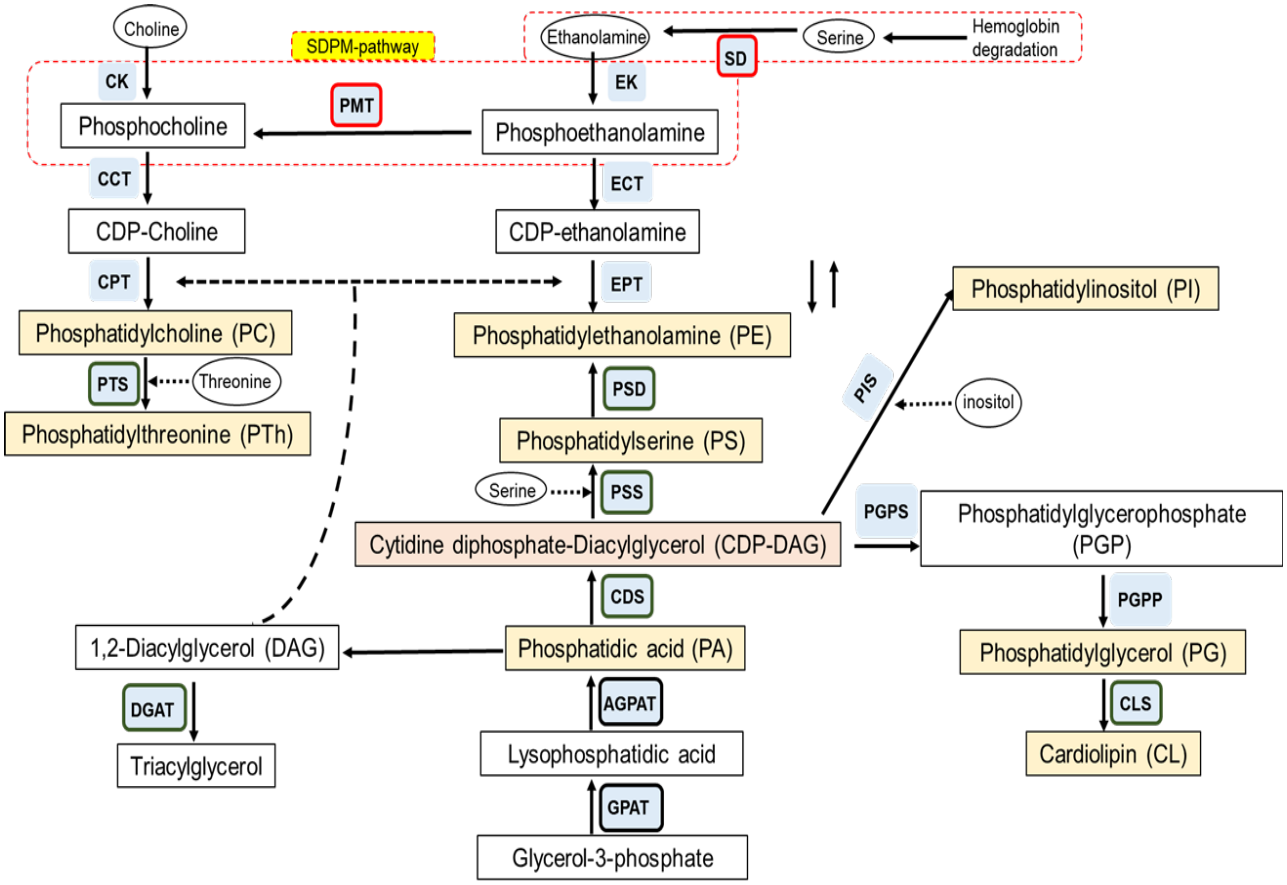

Figure 9 Schematic representation of overall phospholipid biosynthetic pathways within eukaryotes. Enzymes outlines with dark green and red have been characterized in *T. gondii* and *P. falciparum*, respectively. Abbreviations used: CK, choline kinase; CCT, choline phosphate: cytidyltransferase; CPT, diacylglycerol choline phosphotransferase; PTS, phosphatidylthreonine synthase; PMT, phosphatidylethanolamine methyltransferase; SD, serine decarboxylase; EK, ethanolamine kinase; ECT, ethanolamine phosphate: cytidyltransferase; EPT, diacylglycerol ethanolamine phosphotransferase; PSS, phosphatidylserine synthase; PIS, phosphatidylinositol synthase; PGPS, CDP-DAG-glycerol-3-phosphate-3-phosphatidytransferase; PGPP, Phosphatidylglycerophosphatase; CLS, cardiolipin synthase; CDS, cytidine dinucleotide-diacylglycerol synthase; AGPAT, 1-acylglycerol-3-phosphate-o-acyltransferase; GPAT, glycerol-3-phosphate acyltransferase; DGAT, acyl-CoA: diacylglycerol acyltransferase

FATTY ACID METBOLISM IN APICOMPLEXA

Fatty acids are the glycerolipid structural building blocks, which can also serve as energy storage molecules and moieties for the post-translational modification of specific groups of proteins (Watkins *et al.*, 2007)**.** Amongst apicomplexan parasites, *T. gondii* employs three major *de novo* metabolic pathways for coping the pressure of continuous need of fatty acid biosynthesis. These

include the apicoplast-resident prokaryotic type-II fatty acid biosynthesis pathway, the ER-based fatty acid elongation pathway and the cytosolic eukaryotic type-I fatty acid synthase (Mazumdar and Striepen, 2007). Despite such a complex *de novo* FA synthesis network, the parasites also undertake copious salvage of fatty acids directly from the host.

De novo type II fatty acid biosynthesis pathway

The fundamental process of fatty acid biosynthesis is based on of sequential extension of an alkanoic chain, two carbons at a time, by a series of decarboxylative condensation reactions (Chirala and Wakil, 2004). In general, the process of FA biosynthesis begins with carboxylation of acetyl-coA to malonyl-coA. This process is generally initiated with the carboxylation of acetyl-CoA to yield malonyl-CoA (Smith, Witkowski and Joshi, 2003). Next, initiation of condensation reactions begins with translocation of acetyl and malonyl moieties to the malonate group of malonyl-com, which is further is transferred to the phosphopantetheine prosthetic group of a small, acidic protein, called the acyl carrier protein (ACP). This is followed by a series of reactions involving reduction, dehydration and reduction again yielding an acyl-ACP. The elongation of the chain occurs by condensing another malonyl-ACP with the acyl-ACP and repeating the reaction cycle.

In apicomplexan parasites, *T. gondii* and *P. falciparum,* the fundamental FASII pathway occurs within apicoplast. The apicoplast FASII initiation is reliant on glycolytic intermediate phosphoenol pyruvate (PEP). Transport of these glycolytic intermediates into apicoplast is dependent on antiporters that move phosphorylated carbon compounds across membranes in exchange for inorganic phosphate. *Plasmodium* is known to have two triose phosphate transporters each one in the outer (*Pf*oTPT) and inner (*Pf*iTPT) membrane of the apicoplast (Mullin *et al.*, 2006). *Toxoplasma* on the other hand has a single phosphate transporter *Tg*APT, which although localized to apicoplast membranes has not been delineated to a specific membrane of the organelle. *Tg*APT is essential for parasite growth and development (Brooks *et al.*, 2010). Heterologous complementation of yeast with *Tg*APT functionally validated it as a transporter specific for triose phosphates (ATP, NADPH), 3-phosphoglycerate (3-PGA), and phosphoenolpyruvate (PEP).

Pyruvate kinase (PK) embarks the second step and the beginning of preparation phase of FASII by catalytically converting PEP to pyruvate and releasing ATP as a by-product. The genomes of

both *P. falciparum* and *T. gondii* encode two pyruvate kinases PYKI and PYKII, out of which PKI shares strong homology cytoplasmic glycolytic enzyme. The PYKII, localizes to apicoplast in *P. falciparum* (Maeda *et al.*, 2009) whereas its *Toxoplasma* homolog localizes to both mitochondria and apicoplast. In *Toxoplasma* PYKI is refractory to genetic deletion because of its important role in the incorporation of glucose- or glutamine-derived carbon into glycolysis, TCA cycle, amino acids, and fatty acid synthesis pathways (Xia *et al.*, 2019). *Tg*PYKII shows unusual substrate specificity of GDP over ADP and is not essential for parasite growth (Saito *et al.*, 2008; Xia *et al.*, 2019). Double disruption of both the pyruvate kinases was lethal to *Toxoplasma* tachyzoites.

The next step is conversion of pyruvate to acetyl coA, a reaction releasing carbon dioxide, catalyzed by enzyme complex called pyruvate dehydrogenase (PDH). Both *P. falciparum* and *T. gondii* genomes encode a PDH localizing towards the apicoplast (Foth *et al.*, 2005; Fleige *et al.*, 2007). The mitochondrial PDH activity is bypassed by the presence of branched chain ketoacid dehydrogenase (BCKDH) complex in *T. gondii* as well as *P. berghei* (Oppenheim *et al.*, 2014).

The acetyl coA and bicarbonate are condensed to yield malonyl coA using ATP and biotin as a co-factor. This reaction is catalyzed by enzyme called acetyl coA carboxylase (ACC) which exists as a single multi-functional enzyme in *P. falciparum* and two isoforms *T. gondii*. *Tg*ACC1 is localized to the apicoplast functioning for FASII whereas the second ACC is present in the cytosol possibly fueling initial step of FASI pathway (Jelenska *et al.*, 2001).

The next step involves catalytic transfer of Malonyl coA to ACP, aided by malonyl coA: ACP transacylase (FabD), resulting in formation of malonyl-ACP (Shears, Botté and McFadden, 2015). Acyl carrier protein (ACP) is the central carrier protein that binds to fatty acids and their precursors via a phosphopantetheine prosthetic group. ACP essentially participates in transferring substrates between different enzymes of the FASII pathway. With no genetic studies done on *Pf*ACP, the *Tg*ACP has been shown to be refractory to deletion. Conditional knockdown studies on *Tg*ACP show loss of apicoplast which finally leads to arrest of growth of tachyzoites (Mazumdar *et al.*, 2006). Studies using the conditional null mutant of *Tg*ACP determined for the first time that the sole carbon source for apicoplast FASII was glucose rather than acetate and the apicoplast derived fatty acids are usually of the chain length of 12-16 carbon atoms (Mazumdar *et al.*, 2006; Ramakrishnan *et al.*, 2012). This research therefore affirmed the use of labelled glucose to track the direct fatty acid derivatives of FASII pathway.

Catalyzing the last reaction of the FASII initiation phase is β-Ketoacyl-ACP synthase III (FabH). The last condensation reaction involves two 2-carbon substrates acetyl coA and malonyl-ACP, generating a 4-carbon product acetoacetyl-ACP (β-Ketoacyl-ACP) which is further used as a scaffold for the elongation phase of FASII. This reaction is catalyzed by β-Ketoacyl-ACP synthaseI/II , also known as FabB/F. FabH is also a β-Ketoacyl-ACP synthase III that is able to bypass the reaction catalyzed by FabB/F (Shears, Botté and McFadden, 2015).This reaction releases CO_2 and coA, as by-products.

The elongation phase of FASII pathway involves a series of three sequential enzymatic reactions increasing the length of carbon skeleton by 2-carbons at one time. β-Ketoacyl-ACP is reduced by β-ketoacyl: ACP reductase (FabG) to form β-hydroxyacyl-ACP using NADPH as an electron donor. This product is then dehydrated by β-hydroxyacyl-ACP dehydratase (FabZ) to form α, β-*trans* enoyl-ACP. FabZ and FabB/F KO studies revealed the dispensability of FASII for *Plasmodium* blood stages. FabZ however has been shown to be essential for the parasite's transition from the liver to blood due to its indispensability for late stage liver development (Vaughan *et al.*, 2009). This is further reduced to butyryl-ACP by the action of enoyl-ACP reductase (FabI). Genetic depletion studies of FabI provided the first evidence of FASII indispensability for only liver stages of the parasite development. This piece of data also created the barrier between metabolic requirements for different stages of *Plasmodium* development. The dispensability of blood stage FASII suggested the parasite's dependence on the host for its metabolic needs rather than complete reliance on apicoplast FASII (Yu *et al.*, 2008). Further studies on FabI during the mosquito stage parasite life cycle that the *P. falciparum* FAS-II pathway is essential for sporozoite development within the midgut oocyst (van Schaijk *et al.*, 2014).

Morphological analysis using combined light and electron microscopy techniques confirmed the essentially of FASII pathway within *Toxoplasma* tachyzoites (Ramakrishnan *et al.*, 2012; Amiar *et al.*, 2016). *Toxoplasma* tachyzoites lacking FASII activity were unable to complete the process of cytokinesis and eventually gave rise to daughter cells tethered to one another at their basal ends (Martins-Duarte *et al.*, 2016). The phenotype arose due to inability of the parasite to supply fatty acids essential for membrane biogenesis. At the basal ends of these parasites the pellicle formation was incomplete due to the incomplete biogenesis of the IMC and the plasma membrane of the parasite. Exogenous fatty acids were able to only partially revert the tethered phenotype of

daughter cells, thereby confirming the essential contribution of FASII derived fatty acids towards membrane biogenesis.

Another functional pathway belonging to the apicoplast is biosynthesis of short chain fatty acid called 'lipoic acid'. Lipoic acid is an organosulfur-derivative of octanoic acid which acts as an essential cofactor for several multi-subunit enzymes esp. the a-keto acid dehydrogenase complexes (Wrenger and Müller, 2004). One of the short chain fatty acid products of FASII, octanoyl-ACP, is channeled towards lipoic acid biosynthesis pathway. The lipoic acid is formed by catalytic ligation of S-adenosylmethionine (SAM) with octanoyl-ACP. Lipoic acid biosynthesis in the malarial parasites has been differentially compartmentalized. The enzymes involved in this pathway include lipoic acid synthase, lipoyl-ACP: protein N-lipoyl transferase both localizing to apicoplast and lipoic acid protein ligase localizing to the mitochondrion of the parasite. ACP-knockdown parasites are impaired in lipoylation of the apicoplast PDH. Basically, the apicoplast produces lipoic acid to continue the essential FASII via a functional PDH acting as the only source of acetyl coA in the organelle.

Fatty acid elongation pathway

The second pathway contributing to FA biosynthesis in apicomplexa is the elongation machinery localized to the endoplasmic reticulum of the parasite. The FASII and elongation pathway are non-redundant in terms of their functional capacities of maintaining FA bulk synthesis within the apicomplexan parasites (Ramakrishnan *et al.*, 2012).

T. gondii acetyl coA synthetase enzyme provides acetyl coA for the initial step of the fatty acid elongation pathway (Dubois *et al.*, 2018). However, disruption of *Tg*ACS has a minor effect on the global fatty acid composition and subsequently parasite intracellular replication, likely due to the metabolic flux changes induced to compensate for its loss.

The ER -based elongation machinery in *T. gondii* comprises of three elongases, two reductases, and a dehydratase (Ramakrishnan *et al.*, 2012). The loss of three elongases ELO-A, ELO-B and ELO-C did not impede parasite growth suggesting their redundant function. This could also mean that intracellular parasites were able to compensate for the loss of the elongases by scavenging FAs directly from the host cell. On contrary, the parasite mutants deficient in the dehydratase (DEH) and enoyl reductase (ECR) enzymes of the fatty acid elongation pathway exhibited severe

growth defect (Ramakrishnan *et al.*, 2015). The incorporation of ^{14}C-acetate into fatty acids was dramatically decreased in iΔDEH parasites. The loss of DEH activity resulted in depletion of synthesis of unsaturated long (LFCA) and very long chain fatty acids (VLFCA) (C18:1 to C26:1) in phosphatidylethanolamine and phosphatidylinositol species. The growth defect of iΔDEH parasites in the presence of ATc was rescued by supplementation of the medium with a mixture of saturated- and monounsaturated LCFA and VLCFA.

During the FA elongation pathway, the parasites are first desaturated and then further elongated with the help of elongase complexes present in the parasite (Ramakrishnan *et al.*, 2012). The existence of monounsaturated and polyunsaturated FAs in the parasites can be owed to the existence of enzyme desaturases and also the fatty acids scavenged directly from the host (Ramakrishnan *et al.*, 2013). Stearoyl coA desaturases (SCD) are enzymes catalyzing the introduction of a single double bond in a saturated FA backbone thereby generating a monounsaturated FA. There is both genetic and biochemical evidence for the presence of a Δ9-desaturase domain containing SCD in apicomplexan parasites *P. falciparum* and *T. gondii* (Gratraud *et al.*, 2009). In *P. falciparum,* the SCD localizes towards the parasite ER and is necessary for maintaining the intra-erythrocytic developmental cycle by catalyzing the conversion of stearic acid to oleic acid. The *Toxoplasma* cell line over expressing the desaturase *Tg*SCD is able to increase the levels of palmitoleic acid and oleic acid consistent with its function of a desaturase (Hao *et al.*, 2019).

The concept of 'Patchwork lipids' in Toxoplasma gondii: FAs derived from host and de novo synthesis

The survival of *Toxoplasma* within its host is predominantly dependent on lipids, which play an essential role by regulating metabolic flux. The demand for lipids in these parasites relies on an essential combination or 'patchwork' of fatty acids (FA) synthesized *de novo* by the apicoplast FASII pathway and/or by directly salvaging from the host (Mazumdar *et al.*, 2006; Ramakrishnan *et al.*, 2012; Amiar *et al.*, 2016; Fu *et al.*, 2018; Pernas *et al.*, 2018). Mechanisms allowing the parasite to strike a balance between two different sources of fatty acids remain largely unknown. However, the advent of stable isotope labelling using precursors like U-^{13}C-glucose or U-^{13}C-acetate has allowed determination of source of these fatty acid fluxes. Fatty acids showing label incorporation with U-^{13}C-glucose are *de novo* synthesized fatty acids via FASII in apicoplast

whereas the incorporation of U-^{13}C-acetate to fatty acids determines the elongation of fatty acids in cytosol (Ramakrishnan *et al.*, 2012, 2015; Amiar *et al.*, 2016). The FA label incorporation is technically distinguished by the shift of mass using gas-chromatography coupled mass spectrometry (GC-MS).

FA synthesis and flux from within the parasite: Experimental evidences

Metabolic labelling studies with U-^{13}C-glucose have shown that intracellular tachyzoites are capable of synthesizing a range of long and very long chain fatty acids (C14:0–26:1) (Ramakrishnan *et al.*, 2012).^{13}C-Glc based labelling of the ACP knockdown parasites showed a reduction in the FASII activity marked by 80% reduction of the label incorporation into myristic (C14:0) and palmitic acid (C16:0). Genetic ablation of three independent elongases provided insights into the FA fluxes dealt by the FA elongation pathway of the parasite. ELO-A is required for efficient elongation of C16:0 or C16:1 to longer species. ELO-B is largely responsible for the elongation of C18:1/C20:1 to C22:1, whereas the primary role of ELO-C is to elongate fatty acids from C22:1 to C26:1.

FASII derived fatty acids are directly incorporated into lipids used for building membranes during the intracellular development of parasites. Use of a FASII inhibitor, Triclosan on *Toxoplasma* tachyzoites resulted in development of a cytokinesis defect due to insufficient membrane biogenesis. The consequent tethered daughter cell phenotype of these parasites was partially rescued by addition of exogenous fatty acids C14:0, C16:0, C18:1, C22:1. Supplementation of C14:0 alone and in the combination with C16:0 was most successfully able to revert the tethered phenotype, suggesting the importance of these FASII derived fatty acids in parasite membrane biogenesis (Martins-Duarte *et al.*, 2016).

Disruption of ATS1 is lethal to *Toxoplasma* and results in major significant decrease in incorporation of the FASII-generated fatty acid C14:0 (myristate) into bulk synthesis of major phospholipid classes found throughout the parasite membranes. This adverts the importance of apicoplast derived fatty acid flux within the parasite, which cannot always be bypassed by scavenging from the host (Amiar *et al.*, 2016).

Stable isotope labeling using ^{13}C-acetate combined with mass spectrometry-based lipidomic analyses, showed that *Tg*ACS is involved in providing acetyl-CoA for the fatty elongation

pathway in the ER to generate very long fatty acids C18:0, C18:1, C20:0, C20:1, C22:0, C24:0 (Dubois *et al.*, 2018).

FA flux from the host: Experimental evidences

The apicomplexan parasites are auxotrophic for certain metabolites and compensate their demand by scavenging directly from the host and their environment. One of the important metabolites scavenged directly from the host include lipids and fatty acids (Coppens, 2013). The intraerythrocytic malarial parasite blood stages are dependent mostly on the host for their fatty acid demand whereas the sexual life cycle of the malarial parasite within mosquito midgut relies mostly on the *de novo* FA biosynthetic pathway (van Schaijk *et al.*, 2014).

Extracellular fatty acids myristic acid (C14:0) and palmitic acid (C16:0) get incorporated to glycosylphosphatidylinositol (GPI) anchors on the surface antigens of *T. gondii* (Tomavo, Schwarz and Dubremetz, 1989). A remarkable study from Charron and Sibley, provided insights into mobilization of host lipids from various cellular compartments into lipid body and selective endomembrane compartments within the parasite (Charron and Sibley, 2002). This study involved the use using radioisotope and fluorescently labelled lipid precursors for host and parasite labelling and its subsequent detection and analysis by confocal microscopy. NBD-cholesterol was mobilized from pre-labelled host perinuclear compartments to distinct punctate localizations within intracellular parasites. BODIPY-PtdCho (Phosphatidylcholine)was able to move to plasma membrane and distinct punctate localizations within the host and their infected parasites. However, parasites infected after pre-labelling the host were not able to accrue BODIPY-PtdCho, thereby suggesting that direct uptake of PtdCho from the host was unlikely. The uptake of BODIPY-PA (Phosphatidic acid) and fatty acid C4- BODIPY-C9 was concentrated towards large puncta in parasites as well as in a membrane separating the parasite from pre labelled host. The same study also showed that parasites are able to metabolize host-derived neutral lipids including NBD-cholesterol and the BODIPY-conjugated C12 fatty acid. These parasites are also able to uptake lipids in the form of neutral lipid stores directly from the host (Nolan, Romano and Coppens, 2017).

Alongside, acquisition of fatty acids and potentially direct phospholipids from the host, *T. gondii* is also able to scavenge the lipid precursors serine, ethanolamine, and choline from its environment. These polar headgroups are used by the parasite for the synthesis of its major lipids including phosphatidylserine (PtdSer), phosphatidylethanolamine (PtdEtn), and phosphatidylcholine (PtdCho) (Gupta *et al.*, 2005).

Toxoplasma is auxotrophic for cholesterol biosynthesis and is completely reliant for the same on its host. The parasite exploits host cholesterol complexed to low density lipoproteins for cholesteryl ester (CE) synthesis and storage within lipid bodies (Nishikawa *et al.*, 2005). The CE biosynthesis is aided by endoplasmic-reticulum localized acyl CoA: cholesterol acyltransferase (ACAT). Amongst the various radiolabeled fatty acid sources fed to extracellular parasites, palmitic acid (C16:0) was most readily incorporated into CE. Similarly, excess oleate (C18:1) and palmitate (C16:1) in the extracellular medium resulted in 3-4-fold increase in CE biosynthesis within the parasite, which further corroborated with the increased mRNA ACAT expression.

Lipoic acid, an essential co-factor of α-keto dehydrogenases in apicoplast (PDH) and mitochondria (BCKDH) is scavenged from external host environment despite its *de novo* synthesis within apicoplast. This scavenged lipoic acid is specifically channeled towards mitochondria thereby probating a potential link between mitochondria and parasitophorous vacuole membrane for scavenging from the host directly (Crawford *et al.*, 2006).

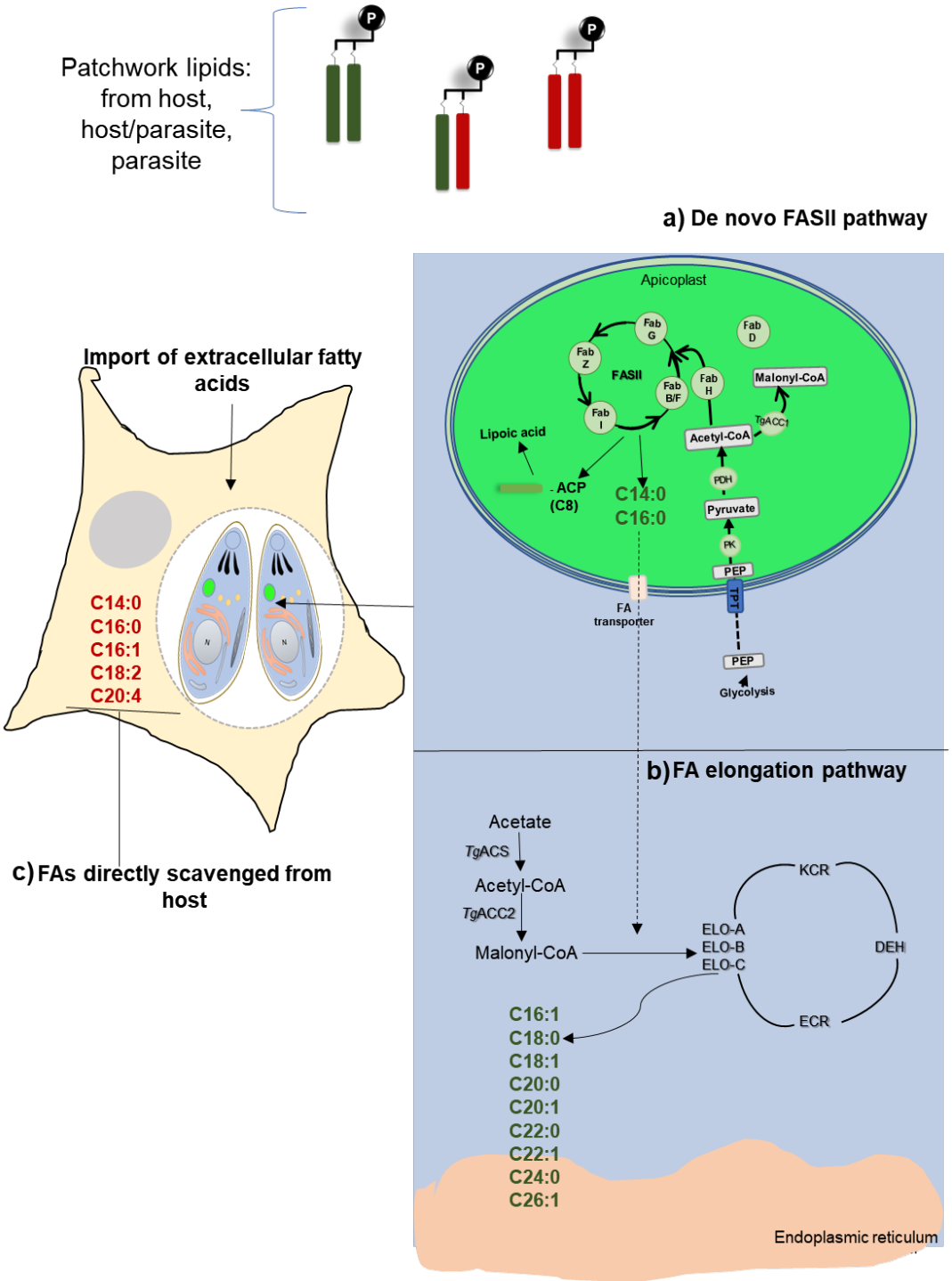

Figure 12 Representation of fatty acid salvage and biosynthetic pathways in *Toxoplasma***.** The parasite lipids are a patchwork of fatty acids derived from the host and de novo biosynthesis. *T. gondii* can synthesize fatty acid *de novo* via FASII (a) and elongate their chain lengths via elongation machinery (b). Apicoplast-localized FASII produces myristic (C14:0), palmitic acid (C16:0) in addition to lipoic acid (a). b) ER-associated elongase system synthesizes long chain monounsaturated fatty acids using the activity of elongases (ELO), ketoacyl-CoA reductase (KCR), hydroxyacyl-CoA dehydratase (DEH) and enoyl-CoA reductase enzymes (ECR) from substrates derived from FASII and acetate metabolism (*Tg*ACS, acetyl CoA synthetase; *Tg*ACC2, acetyl CoA carboxylase 2). c) *T.gondii* is also able to scavenge fatty acids directly from the host, including C14:0, C16:0, C16:1, C18:2, C20:4. Other abbreviations used: TgACC1, acetyl CoA carboxylase 1; ACP, acyl carrier protein; PDH, pyruvate dehydrogenase; PK, pyruvate kinase; TPT, triose phosphate transporter; PEP, phosphoenol pyruvate (adapted from Ramakrishnan *et al.*, 2015).

Acquiring the fats: Potential methods of lipid scavenging by Toxoplasma

The parasite mediates the essential lipid uptake via several routes depending upon the substrate of interest:

a) via the intravacuolar network

   Intravacuolar network (IVN) comprises an extensive network of thin tubules and vesicles that fill the lumen of parasitophorous vacuole (Caffaro and Boothroyd, 2011). Interestingly, a *Toxoplasma* mutant lacking the capacity to form IVN (Δgra2Δgra6) was unable to embark the process of lipid uptake from the host (Nolan, Romano and Coppens, 2017). Also, parasites lacking an IVN localized phospholipase exhibit reduced host lipid scavenging capacity. The involvement of a lipid hydrolyzing enzyme in the parasite vacuolar space suggests that the host lipids are recycled right at the point of entry into the parasites.

b) via physical association of the PVM and host cell organelles allowing mobilization of lipids.

   Host cell mitochondria and endocytic machinery arising from Golgi complex are actively shown to be around PVM post *Toxoplasma* infection, participating in lipid metabolic homeostasis within the parasite (Coppens, Sinai and Joiner, 2000; Pernas *et al.*, 2014, 2018). In *T. gondii* type I and type III strains a parasite protein, MAF1 (mitochondrion associated factor), is necessary for host mitochondrial association with the parasite vacuole (Pernas *et al.*, 2014).

c) uptake of host lipids in an ATP-dependent process

   Toxoplasma has a family of ATP-binding cassette (ABC) G family transporter proteins that participate in the uptake of host lipids and the expulsion of major lipids from the parasite (Ehrenman *et al.*, 2010). One of these ACBGs, *Tg*ACBG$_{107}$ is associated with the vesicles in the PV and plasma membrane participating in the cholesterol import from the host. Four out of the several ABCGs, *Tg*ABCG$_{77}$, *Tg*ABCG$_{84}$, *Tg*ABCG$_{89}$ and *Tg*ABCG$_{87}$ are selectively involved in cholesterol and phosphatidylcholine export.

d) carrier proteins mediated transfer

Fatty acyl-coA esters are amphipathic molecules that can disrupt the membranes they traverse through. These detergent-like molecules need carrier proteins for transport across various endomembrane compartments. Acyl coA binding protein (ACBP) is one such carrier protein that binds fatty acyl coA esters and transports them across various cellular compartments (Neess *et al.*, 2015). *Toxoplasma* genome encodes for two ACBPs- cytosolic ACBP1 and mitochondrial ACBP2 (Fu *et al.*, 2018, 2019). *Tg*ACBP2 binds long chain fatty acids to be transported towards mitochondrial lipid synthesis. This protein is required for the intracellular replication of Type II strain of *T. gondii* (Prugnaid). In terms of lipid metabolism, the mutant strain PruΔacbp2 has a defect in cardiolipin biosynthesis. The overall abundance of cardiolipin and its potential precursor lipids phosphatidic acid (PA) and phosphatidyl glycerol (PG), was significantly reduced in the PruΔacbp2 parasites. The expression of an N-terminally HA-tagged MAF1RHb in PruΔacbp2 tachyzoites was able to complement the defect in cardiolipin metabolism (Fu *et al.*, 2018). The rescue of lipid metabolism defects caused due to loss of *Tg*ACBP2, by exogenous MAF1 expression suggests that the host scavenged lipids were able to rescue the loss of *de novo* biosynthesis. *Toxoplasma* has a sterol carrier protein (SCP) called *Tg*HAD-2SCP2, which unlike its other eukaryotic counterparts is expressed in fusion with the enzyme d-3-hydroxyacyl-CoA dehydrogenase and a second SCP-2 (Lige, Sampels and Coppens, 2013). A *T.gondii* line overexpressing the protein *Tg*HAD-2SCP-2 is able to transport cholesterol and oleate to be incorporated into neutral lipids towards the posterior end of the parasite. Genetic ablation of another FA transporter, *Tg*ACBP1 and *Tg*SCP2 together affects parasite replication and attenuates parasite virulence in mice (Fu *et al.*, 2019). The experimental demonstration of *Tg*ACBP1 dealing mostly with the fatty acids taken up from the host was monitored by uptake of NDB-C16:0. Loss of *Tg*ACBP1 from parasites dramatically promoted the uptake of NBD-C16:0-CoA from external environment to compensate for loss of uptake of other FA species from the host. Results obtained by analyzing *Tg*ACBP1 mutant using gas-chromatography coupled mass spectrometry suggested that there was a specific decline in C18:1 species. Oleic acid is one of the most abundant fatty acid species and it is most likely salvaged from the host (Ramakrishnan *et al.*, 2012; Amiar *et al.*, 2019). *Tg*ACBP1 and

*Tg*SCP2 collectively provide fatty acyl chains of varying length and saturation for glycerides including triacylglycerols (TAG), diacylglycerol (DAG) and monoacylglycerol (MAG).

e) acquisition of lipids via secretory endocytic pathway

In a study linking *T.gondii* gliding motility to endocytic-secretory cycle it was shown that lysophosphatidic acid-LPA accumulates in vesicles that are trafficked through the secretory pathway, with a certain accumulation in the VAC, a plant-like parasite organelle and RAB18, a marker of endoplasmic reticulum. This suggests that lipid uptake in these parasites converges with the endocytic secretory pathway. The study also proposed that LPA acts as a physiological stimulator for endocytosis in *T. gondii* (Gras *et al.*, 2019). Nolan et al 2017, also found that the host-lipid droplets enriched with neutral lipids endocytosed via the parasite PVM intravacuolar network had Rab7 coating onto their membranes. This also proposes a probable interaction between Rab effectors and proteins present on PVM in order to promote this event of scavenging (Nolan, Romano and Coppens, 2017).

f) Via a molecular sieve between host cell cytoplasm and the parasite, the PVM

The non fusogenic parasite niche that supports intracellular replication of *Toxoplasma* tachyzoites within its host, called parasitophorous vacoular membrane (PVM) is heavily modified by parasite proteins in order to facilitate import and export of lipidic and polar metabolites. The PVM allows passage of molecules up to 1300-1900 Da between the host cell cytoplasm and the parasite (Schwab, Beckers and Joiner, 1994). The molecular basis of this porosity is believed to be provided by parasite secreted proteins GRA17 and GRA24 (Gold *et al.*, 2015).

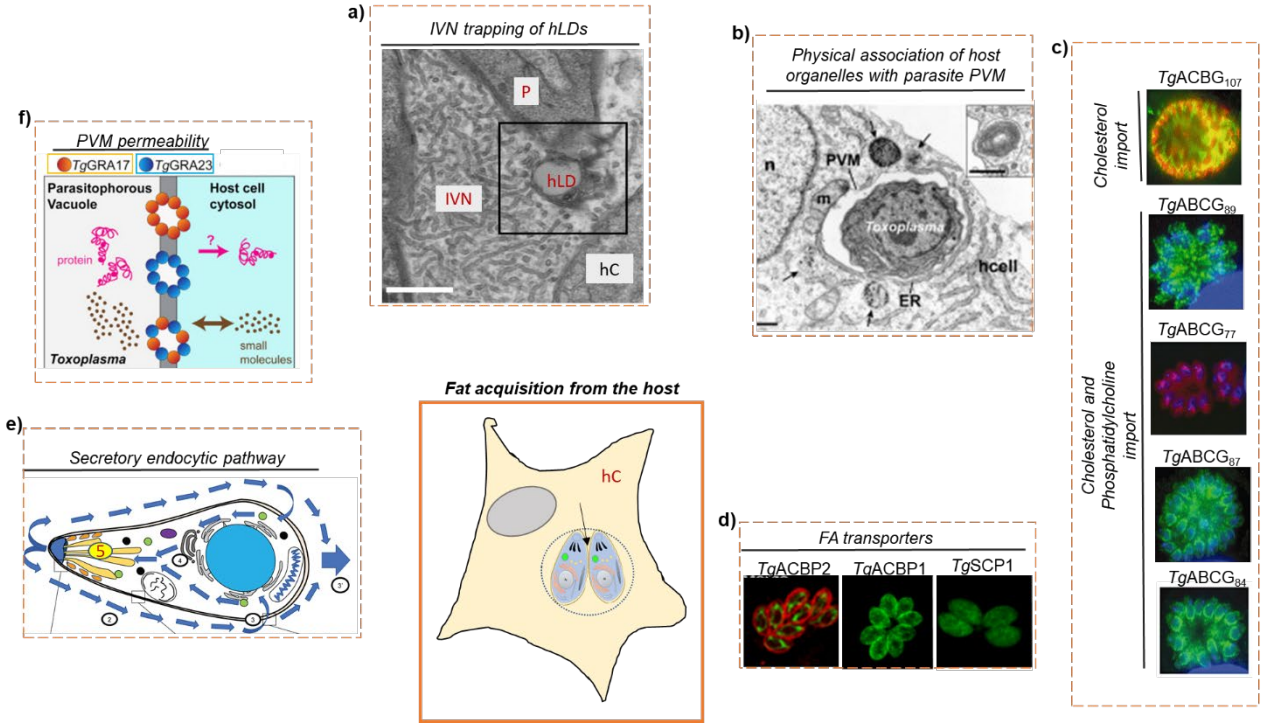

Figure13 Schematic representation of known methods by which parasite scavenge fatty acids from the host. a),b) TEM showing entrapped host derived lipid droplets (hLDs) into the intravacuolar tubular network within the parasitophorous vacuole (a) (adapted from Nolan, Romano and Coppens, 2017)and recruitment of host organelles, mitochondria (m), endoplasmic reticulum (ER) (b) towards the parasitophorous vacuolar membrane (PVM) (adapted from Coppens et al., 2006). c) IFA image localizations of various ATP-binding cassette transporters, *Tg*ACBG$_{107}$, *Tg*ABCG$_{89}$, *Tg*ABCG$_{77}$,*Tg*ABCG$_{87}$.*Tg*ABCG$_{87}$,*Tg*ABCG$_{84}$ involved in import and export of specific lipid between host and parasite (adapted from Ehrenman et al., 2010). d) IFA showing mitochondrial (*Tg*ACBP2, (adapted from Fu et al., 2018) and cytoplasmic localizations (*Tg*ACBP1, *Tg*SCP1, (adapted from Fu et al., 2019) of FA transporters present within the parasite. e) Overview of T. gondii secretory endocytic pathway also assisting in the incorporation of lipids from the external environment (5) (adapted from Gras et al., 2019). f) PVM allows passage of small molecules including lipids, with the help of dense granule proteins *Tg*GRA17 and *Tg*GRA23 (adapted from Gold et al., 2015).

CHAPTER III: METABOLIC REWIRING OF THE HOST TO FACILITATE PARASITE GROWTH

The ability of *Toxoplasma gondii* to infect any nucleated cell resides in the orchestration of its metabolic interaction with the host. These intracellular parasites are in constant competition with their host for nutrient dependencies, which is indirectly dependent on the environmental nutritional conditions (Blume and Seeber, 2018; Amiar *et al.*, 2019).

The host environment, which encompasses lipid metabolites, is one key to unlocking the mystery of species specificity in *T. gondii*. A recent striking work from Di Genova et al, provides evidence of host metabolic reprogramming allowing parasite co-evolution with its host (Di Genova *et al.*, 2019). This study identified the first metabolic factor responsible for the restricted sexual development of *T. gondii* solely within feline intestines. Data from this study shows that the accumulation of systemic linoleic acid (18:2) (25%-46% in cat serum) due to the unusual absence of a Δ6 desaturase within feline intestines, allows parasite oocyst propagation. Such a lipid environment therefore provides a unique platform for the development of sexual stages otherwise absent in intermediate hosts. The species barrier was lifted with this key identarian, C18:2 using mice models: wherein by removal of the Δ6 desaturase enzyme from the murine intestine, alongside linoleic acid feeding allowed development of sexual cycle in mice. Δ6 desaturase usually catalyzes the conversion of linoleic acid (C18:2) to arachidonic acid (C20:4) which in turn can participate in formation of immune mediators like eicosanoids. Therefore, absence of this enzyme in feline intestines would also rescue the parasite from of strong immune response from the host. Another “advantage” of linoleic acid is its ability to perform lipid signaling due to its high susceptibility to oxygenase enzymes thereby generating oxylipins. On the other hand, linoleic acid is toxic for *Toxoplasma* asexual stage tachyzoites, thus favoring sexual stages in the cat intestine environment.

We recently uncovered that when the parasite is facing adverse host environmental/nutritional conditions, it is capable of sensing the host nutritional status to induce a major metabolic response at two levels : (i) by upregulation of its own *de novo* lipid synthesis capacities at the level of the apicoplast FASII to boost fatty acid/lipid production, and (ii) concomitant induction of massive changes within the infected host cellular structure by generation of multi-vesicular bodies arising from host organelles via parasite effectors that are then imported to obtain more membrane material (Amiar *et al.*, 2019). In this work, we put *T. gondii* tachyzoites under nutrient/lipid starvation by growing them under fluctuating levels of fetal bovine serum (FBS) in their culture

medium. Lipidomic analysis revealed that the ^{13}C incorporation into all FASII-generated (C14:0, C16:0) and further ER-elongated FA products (C18:0, C18:1 and C20:1) was significantly increased up to 15% in the absence of FBS in the growth culture medium of the parasites. Importantly, the FASII which is otherwise known to be dispensable for asexual blood stage *P. falciparum* parasites is activated in the presence of lipid deprivation (Botté *et al.*, 2013; Amiar *et al.*, 2019). In these conditions the *P. falciparum* FASII pathway becomes essential during blood stages as confirmed in *P. falciparum* parasites lacking a functional FASII i.e. FabI knockout. Together, this data this challenges the current dogma on IPP (isoprenoid precursor) pathway being the sole function of the apicoplast during blood stages. Instead, our findings put the parasite back into its physiological context where nutrient availability and environmental conditions drive the requirement and regulation for a given metabolic pathway.

Toxoplasma tachyzoites, likely for their own benefit, increase the synthesis and overall levels of triacylglycerols (TAGs) in the host thereby resulting in increased host lipid droplet biogenesis (Hu, Binns and Reese, 2017). Parasites can hi-jack the host LD biogenesis via the modulation of transcription of proteins involved in neutral lipid biosynthesis and lipid transport. These included transcriptional upregulation of key enzymes involved in TAG biosynthesis like acylglycerol-3-phosphate acyltransferase (AGPAT2), acyl CoA: diacylglycerol acyltransferase (DGAT2), and fatty acid binding transport proteins like FABP3, FABP5. The process is also marked by concordant decrease in the mRNA levels of enzymes involved in TAG lipolysis like ATGL within the host. The parasites require assistance from host mTOR and JNK signaling for the upregulation of LD biogenesis. The HFFs infected with RHΔmyr1 parasites and treated with oleic acid showed no change in neutral lipid storage within the host (Hu, Binns and Reese, 2017). MYR1 is a critical parasite secreted protein shown to be involved delivery of effector proteins into the host cells (Franco *et al.*, 2016). Thus, the parasite induced changes in the host neutral lipid metabolism are facilitated by effectors secreted across the PVM into the host as we observed in the case of adaptation to nutrient starvation.

In another interesting study, the authors showed that *Toxoplasma* replication is reduced in host cells that are depleted of LD, or impaired in TAG lipolysis (Nolan, Romano and Coppens, 2017). In fact, the host lipid droplets accrued to a perivacuolar localization around the parasite vacuolar membrane until the parasite egresses. Experimental proof of direct uptake of lipids from host LD

towards parasites was provided by tracking the trafficking of C4-BODIPY-C9 from host LD to the parasite interior by 24 h post infection. The parasite is are able to manipulate the host endocytic machinery for the uptake of various lipids including diversion of host Rab-labelled vesicles from their Golgi apparatus towards parasite PV lumen for allowing uptake of sphingolipids (Romano *et al.*, 2013). Host Rab7-coated lipid droplets are taken up by the parasite via passage through PV lumen including intravacuolar network (Nolan, Romano and Coppens, 2017).

The mechanism of acquiring the lipids and fatty acids directly from the host can also be induced through host LD-lipophagy. Indeed, Pernas et al. found that Atg-/- murine embryonic fibroblasts (MEF) deficient in macro autophagy were able to accumulate 50% less $RC_{12,}$ a 12-carbon chain saturated FA and BODIPY-FL-C_{12} (FL C_{12}) (Pernas *et al.*, 2018). This host autophagy-assisted acquisition of FAs is an essential process for the growth of *Toxoplasma* within its host. *Toxoplasma* proliferation was also reduced in LD-deficient Dgat1-/-,2-/- and LD-lipophagy defective Atg-/- MEFs. The parasite growth defect during its infection in Dgat1-/-,2-/- deficient MEFs was rescued by exogenous addition of cholesterol and fatty acids. This could well mean that the exogenously supplied lipid sources are first metabolized by the host prior to uptake by the parasites as the lipophagy deficient line infected with *T. gondii* was able to restore the growth defect only partially upon addition of oleate and linoleate.

Toxoplasma type I and type III strains are capable of recruiting host mitochondria in close association with the parasitophorous vacuole, a fascinating process regulated by parasite secreted protein, mitochondria associated factor 1 (MAF1) (Pernas *et al.*, 2014). The parasite MAF1 protein interacts with host cell mitochondrial intermembrane space bridging (MIB) complex (Kelly *et al.*, 2017). Later, it was established that the host mitochondrial association was necessary to restrict the intracellular growth of *Toxoplasma* by limiting its access to fatty acids (Pernas *et al.*, 2018). *Toxoplasma* type II strains, on the other hand, lack MAF1 and are much less capable of recruiting host mitochondria to their PV. According to this postulate between type I and Type II strains, the knockdown of the mitochondrial acyl-CoA binding protein *Tg*ACBP2 was detrimental to type II but did not affect the growth of type I *T. gondii* strains. This fatty acid transporter protein was shown to be directly involved in cardiolipin metabolism in type II Prugnaid tachyzoites. Lipidomic analysis of strain lacking ACBP2, PruΔ*acbp2* complemented with an exogenous copy of MAF1RHb1 showed that MAF1RHb1 expression was able to rescue the reduced abundances of

CL and its precursor phospholipids PA and PG (Fu *et al.*, 2018). This observational study provides a strong link between direct scavenging of lipids from the host organelles, in this case mitochondria, recruited towards the parasite vacuole.

Toxoplasma infection accompanying host organellar remodeling events include the intriguing association of host mitochondria with the parasitophorous vacoular membrane through protein mitochondrial associated factor-1 (MAF-1). Use of Etomoxir, an inhibitor of carnitine-palmitoyl coA transferase and hence β-oxidation within host mitochondria, resulted in better uptake of fatty acids by *Toxoplasma* (Pernas *et al.*, 2018). This suggested that the parasites were able to scavenge fatty acids better in the absence of host mitochondrial fatty acid oxidation. By elongation and fusion around the PVM of *Toxoplasma* vacuole, host mitochondria add another layer of innate immune response by restricting the growth of intracellular parasites via limiting the uptake of FAs. This embarks a competitive streak between host and the parasite for several metabolites including lipids and fatty acids.

In *P. falciparum* asexual life cycle the transition from ring to metabolically more active trophozoites boosts major changes in the lipidic composition with an increase in the molar concentration of several phospholipids (Gulati *et al.*, 2015). *P. falciparum* infected RBCs are able to secrete micro vesicles that have been shown to be involved in intracellular signaling and gametocytogenesis (Nantakomol *et al.*, 2011; P.-Y. *et al.*, 2013; Regev-Rudzki *et al.*, 2013). These *P. falciparum* infected RBC-derived micro vesicles (RMVs) were enriched in PS, PI and sphingolipids including ceramide, lactosylceramide (LacCer), dihydroceramide (dhCer) and ganglioside-GM3 (Gulati et al 2015). It is safe to say that despite being non-proliferative blood stage sexual forms, gametocytes do exhibit high variation in their lipidic relative abundance, suggesting active lipid metabolism. Amongst the lipid species that were increased in the gametocytes included PS, sphingolipids including ceramide. More interestingly the ceramide precursor dihydroceramide was increased by 4-fold in the early and late stages of gametocytes. Lysophospholipids specifically lysophosphatidylcholine is decreased in the gametocytes. TAGs and TAG stores called lipid droplets were undetectable in the early and late stage gametocytes (Gulati *et al.*, 2015).

P. falciparum life cycle is dependent on a number of lipid dependent processes including protein trafficking, cell signaling, membrane biogenesis and hemoglobin degradation. The intra

erythrocytic blood stage parasite were examined to have at least 2–fold higher levels of phosphatidylglycerol (PG), acyl PG, Lysophosphatidylinositol (LPI), Bis(Monoacylglycerol)Phosphate (BMP), monosialodihexosyl-ganglioside (GM3), diacylglycerol (DAG) and triacylglycerol (TAG) in comparison to uninfected RBC (Gulati *et al.*, 2015). In the same study the lipids that were enriched in the uninfected RBCs in comparison to the infected ones included phosphatidylserine (PS), phosphatidic acid (PA) and ceramide. These lipids could therefore be serving as a reservoir for the scavenging pathway of the parasite. The sexual stage gametocytes are enriched in sphingomyelin, cholesterol and neutral triglycerides (TAGs). Amongst the phospholipid species that showed a high increase during gametocyte development included PC 34:0, PC 34:2, and PE36:4 (Tran *et al.*, 2016). Supplementing the growth media of *P. falciparum* with polyunsaturated fatty acids is able to induce gametocytogenesis (Tanaka *et al.*, 2019). Another important finding showing the metabolic rewiring during the *Plasmodium* life cycle is that as the parasite matures, it reduces the incorporation of anapleurotic carbon from glucose and increases incorporation via glutamine (Cobbold *et al.*, 2013).

REFERENCES (Chapter I, II and III)

Alexander, D. L. *et al.* (2005) 'Identification of the moving junction complex of Toxoplasma gondii: A collaboration between distinct secretory organelles', *PLoS Pathogens*, 1(2), pp. 0137–0149. doi: 10.1371/journal.ppat.0010017.

Aly, A. S. I., Vaughan, A. M. and Kappe, S. H. I. (2009) 'Malaria Parasite Development in the Mosquito and Infection of the Mammalian Host', *Annual Review of Microbiology*. doi: 10.1146/annurev.micro.091208.073403.

Amiar, S. *et al.* (2016) 'Apicoplast-Localized Lysophosphatidic Acid Precursor Assembly Is Required for Bulk Phospholipid Synthesis in Toxoplasma gondii and Relies on an Algal/Plant-Like Glycerol 3-Phosphate Acyltransferase.', *PLoS pathogens*, 12(8), p. e1005765. doi: 10.1371/journal.ppat.1005765.

Amiar, S. *et al.* (2019) 'Division and adaptation to host nutritional environment of apicomplexan parasites depend on apicoplast lipid metabolic plasticity and host organelles remodelling', *bioRxiv*, p. 585737. doi: 10.1101/585737.

Arroyo-Olarte, R. D. *et al.* (2015) 'Phosphatidylthreonine and Lipid-Mediated Control of Parasite Virulence', *PLoS Biology*, 13(11). doi: 10.1371/journal.pbio.1002288.

Arroyo-Olarte, R. D. and Gupta, N. (2016) 'Phosphatidylthreonine: An exclusive phospholipid regulating calcium homeostasis and virulence in a parasitic protist', *Microbial Cell*, 3(5), pp. 189–190. doi: 10.15698/mic2016.05.496.

Athenstaedt, K. and Daum, G. (1999) 'Phosphatidic acid, a key intermediate in lipid metabolism', *European Journal of Biochemistry*, 266(1), pp. 1–16. doi: 10.1046/j.1432-1327.1999.00822.x.

Azzouz, N. *et al.* (2002) 'Evidence for de novo sphingolipid biosynthesis in Toxoplasma gondii', *International Journal for Parasitology*, 32(6), pp. 677–684. doi: 10.1016/S0020-7519(02)00009-7.

Bergmann, A. *et al.* (2019) 'Toxoplasma gondii'.

Besteiro, S. *et al.* (2009) 'Export of a Toxoplasma gondii rhoptry neck protein complex at the host cell membrane to form the moving junction during invasion', *PLoS Pathogens*, 5(2). doi: 10.1371/journal.ppat.1000309.

Bisio, H. *et al.* (2019) 'Phosphatidic acid governs natural egress in Toxoplasma gondii via a guanylate cyclase receptor platform', *Nature Microbiology*. doi: 10.1038/s41564-018-0339-8.

Black, M. W. and Boothroyd, J. C. (2000) 'Lytic Cycle of Toxoplasma gondii', *Microbiology and Molecular Biology Reviews*, 64(3), pp. 607–623. doi: 10.1128/mmbr.64.3.607-623.2000.

Blume, M. and Seeber, F. (2018) 'Metabolic interactions between Toxoplasma gondii and its host', *F1000Research*, 7(May), pp. 1–10. doi: 10.12688/f1000research.16021.1.

Botté, C. Y. *et al.* (2013) 'Atypical lipid composition in the purified relict plastid (apicoplast) of malaria parasites.', *Proceedings of the National Academy of Sciences of the United States of America*, 110(18), pp. 7506–11. doi:

10.1073/pnas.1301251110.

Bottova, I. *et al.* (2009) 'Host cell P-glycoprotein is essential for cholesterol uptake and replication of Toxoplasma gondii', *Journal of Biological Chemistry*, 284(26), pp. 17438–17448. doi: 10.1074/jbc.M809420200.

Brooks, C. F. *et al.* (2010) 'The Toxoplasma Apicoplast Phosphate Translocator Links Cytosolic and Apicoplast Metabolism and Is Essential for Parasite Survival', *Cell Host and Microbe*. Elsevier Ltd, 7(1), pp. 62–73. doi: 10.1016/j.chom.2009.12.002.

Bullen, Hayley E *et al.* (2016) 'Phosphatidic Acid-Mediated Signaling Regulates Microneme Secretion in Toxoplasma.', *Cell host & microbe*, 19(3), pp. 349–60. doi: 10.1016/j.chom.2016.02.006.

Bullen, Hayley E. *et al.* (2016) 'Phosphatidic Acid-Mediated Signaling Regulates Microneme Secretion in Toxoplasma', *Cell Host and Microbe*, 19(3), pp. 349–360. doi: 10.1016/j.chom.2016.02.006.

Bullen, H. E. and Soldati-Favre, D. (2016) 'A central role for phosphatidic acid as a lipid mediator of regulated exocytosis in apicomplexa', *FEBS Letters*, 590, pp. 2469–2481. doi: 10.1002/1873-3468.12296.

Caffaro, C. E. and Boothroyd, J. C. (2011) 'Evidence for host cells as the major contributor of lipids in the intravacuolar network of toxoplasma-infected cells', *Eukaryotic Cell*, 10(8), pp. 1095–1099. doi: 10.1128/EC.00002-11.

Carruthers, V. B. (2002) 'Host cell invasion by the opportunistic pathogen Toxoplasma gondii', *Acta Tropica*, 81(2), pp. 111–122. doi: 10.1016/S0001-706X(01)00201-7.

Carruthers, V. B. and Sibley, L. D. (1997) 'Sequential protein secretion front three distinct organelles of Toxoplasma gondii accompanies invasion of human fibroblasts', *European Journal of Cell Biology*.

Charron, A. J. and Sibley, L. D. (2002) 'Host cells: Mobilizable lipid resources for the intracellular parasite Toxoplasma gondii', *Journal of Cell Science*, 115(15), pp. 3049–3059.

Chen, A. L. *et al.* (2015) 'Novel components of the toxoplasma inner membrane complex revealed by BioID', *mBio*, 6(1), pp. 1–12. doi: 10.1128/mBio.02357-14.

Chirala, S. S. and Wakil, S. J. (2004) 'Structure and function of animal fatty acid synthase', *Lipids*, 39(11), pp. 1045–1053. doi: 10.1007/s11745-004-1329-9.

Cobbold, S. A. *et al.* (2013) 'Kinetic flux profiling elucidates two independent acetyl-coa biosynthetic pathways in plasmodium falciparum', *Journal of Biological Chemistry*, 288(51), pp. 36338–36350. doi: 10.1074/jbc.M113.503557.

Consigny, P. H. *et al.* (2002) 'High prevalence of co-factor independent anticardiolipin antibodies in malaria exposed individuals', *Clinical and Experimental Immunology*. doi: 10.1046/j.1365-2249.2002.01722.x.

Coppens, I. (2006) 'Contribution of host lipids to Toxoplasma pathogenesis', *Cellular Microbiology*, 8(1), pp. 1–9. doi: 10.1111/j.1462-5822.2005.00647.x.

Coppens, I. *et al.* (2006) 'Toxoplasma gondii Sequesters Lysosomes from Mammalian Hosts in the Vacuolar Space', *Cell*, 125(2), pp. 261–274. doi: 10.1016/j.cell.2006.01.056.

Coppens, I. (2013) 'Targeting lipid biosynthesis and salvage in apicomplexan parasites for improved chemotherapies', *Nature Reviews Microbiology*. Nature Publishing Group, 11(12), pp. 823–835. doi: 10.1038/nrmicro3139.

Coppens, I., Sinai, A. P. and Joiner, K. A. (2000) 'Toxoplasma gondii exploits host low-density lipoprotein receptor-mediated endocytosis for cholesterol acquisition', *Journal of Cell Biology*, 149(1), pp. 167–180. doi: 10.1083/jcb.149.1.167.

Cowman, A. F. *et al.* (2016) 'Malaria: Biology and Disease', *Cell*. Elsevier Inc., 167(3), pp. 610–624. doi: 10.1016/j.cell.2016.07.055.

Crawford, M. J. *et al.* (2006) 'Toxoplasma gondii scavenges host-derived lipoic acid despite its de novo synthesis in the apicoplast', *EMBO Journal*, 25(13), pp. 3214–3222. doi: 10.1038/sj.emboj.7601189.

Csaki, L. S. *et al.* (2013) 'Lipins, lipinopathies, and the modulation of cellular lipid storage and signaling', *Progress in Lipid Research*. Elsevier Ltd, 52(3), pp. 305–316. doi: 10.1016/j.plipres.2013.04.001.

Debierre-Grockiego, F. *et al.* (2006) 'Fatty acids from Plasmodium falciparum down-regulate the toxic activity of malaria glycosylphosphatidylinositols', *Infection and Immunity*, 74(10), pp. 5487–5496. doi: 10.1128/IAI.01934-05.

Dondorp, A. M. *et al.* (2009) 'Artemisinin Resistance in', *Drug Therapy*, 361(5), pp. 455–467. doi: 10.1086/657120.

Van Dooren, G. G. *et al.* (2016) 'The import of proteins into the mitochondrion of toxoplasma gondii', *Journal of Biological Chemistry*. doi: 10.1074/jbc.M116.725069.

Van Dooren, G. G., Kennedy, A. T. and McFadden, G. I. (2012) 'The use and abuse of heme in apicomplexan parasites', *Antioxidants and Redox Signaling*, 17(4), pp. 634–656. doi: 10.1089/ars.2012.4539.

van Dooren, G. G. and Striepen, B. (2013) 'The Algal Past and Parasite Present of the Apicoplast', *Annual Review of Microbiology*, 67(1), pp. 271–289. doi: 10.1146/annurev-micro-092412-155741.

Dubey, J. P. (2013) *The History and Life Cycle of Toxoplasma gondii*. Second Edi, *Toxoplasma Gondii: The Model Apicomplexan - Perspectives and Methods: Second Edition*. Second Edi. Elsevier. doi: 10.1016/B978-0-12-396481-6.00001-5.

Dubey, J. P., Lindsay, D. S. and Speer, C. A. (1998) 'Structures of Toxoplasma gondii tachyzoites, bradyzoites, and sporozoites and biology and development of tissue cysts', *Clinical Microbiology Reviews*. doi: 10.1128/cmr.11.2.267.

Dubois, D. *et al.* (2018) 'Toxoplasma gondii acetyl-CoA synthetase is involved in fatty acid elongation (of long fatty acid chains) during tachyzoite life stages.', *Journal of lipid research*, 59(6), pp. 994–1004. doi: 10.1194/jlr.M082891.

Eda, S. and Sherman, I. W. (2002) ‘Cytoadherence of malaria-infected red blood cells involves exposure of phosphatidylserine’, *Cellular Physiology and Biochemistry*, 12(5–6), pp. 373–384. doi: 10.1159/000067908.

Ehrenman, K. *et al.* (2010) ‘Novel roles for ATP-binding cassette G transporters in lipid redistribution in Toxoplasma’, *Molecular Microbiology*. doi: 10.1111/j.1365-2958.2010.07169.x.

Elabbadi, N., Ancelin, M. L. and Vial, H. J. (1997) ‘Phospholipid metabolism of serine in Plasmodium-infected erythrocytes involves phosphatidylserine and direct serine decarboxylation’, *Biochemical Journal*, 324(2), pp. 435–445. doi: 10.1042/bj3240435.

Elliott, D. A. and Clark, D. P. (2000) ‘Cryptosporidium parvum induces host cell actin accumulation at the host-parasite interface’, *Infection and Immunity*. doi: 10.1128/IAI.68.4.2315-2322.2000.

Elmendorf, H. G. and Haldar, K. (1994) ‘Plasmodium falciparum exports the Golgi marker sphingomyelin synthase into a tubovesicular network in the cytoplasm of mature erythrocytes’, *Journal of Cell Biology*. doi: 10.1083/jcb.124.4.449.

Fang, J., Marchesini, N. and Moreno, S. N. J. (2006) ‘A Toxoplasma gondii phosphoinositide phospholipase C (TgPI-PLC) with high affinity for phosphatidylinositol’, *Biochemical Journal*, 394(2), pp. 417–425. doi: 10.1042/BJ20051393.

Ferguson, D. J. P. *et al.* (1974) ‘Ultrastructural Study of Early Stages of Asexual Multiplication and Microgametogony of Toxoplasma Gondii in the Small Intestine of the Cat’, *Acta Pathologica Microbiologica Scandinavica Section B Microbiology and Immunology*, 82 B(2), pp. 167–181. doi: 10.1111/j.1699-0463.1974.tb02309.x.

Fleige, T. *et al.* (2007) ‘Carbohydrate metabolism in the Toxoplasma gondii apicoplast: Localization of three glycolytic isoenzymes, the single pyruvate dehydrogenase complex, and a plastid phosphate translocator’, *Eukaryotic Cell*, 6(6), pp. 984–996. doi: 10.1128/EC.00061-07.

Foth, B. J. *et al.* (2005) ‘The malaria parasite Plasmodium falciparum has only one pyruvate dehydrogenase complex, which is located in the apicoplast’, *Molecular Microbiology*, 55(1), pp. 39–53. doi: 10.1111/j.1365-2958.2004.04407.x.

Francia, M. E. and Striepen, B. (2014) ‘Cell division in apicomplexan parasites’, *Nature Reviews Microbiology*. Nature Publishing Group, 12(2), pp. 125–136. doi: 10.1038/nrmicro3184.

Francis, S. E., Sullivan, D. J. and Goldberg, and D. E. (1997) ‘ HEMOGLOBIN METABOLISM IN THE MALARIA PARASITE PLASMODIUM FALCIPARUM ’, *Annual Review of Microbiology*. doi: 10.1146/annurev.micro.51.1.97.

Franco, M. *et al.* (2016) ‘proteina MYR1’, 7(1), pp. 1–16. doi: 10.1128/mBio.02231-15.Editor.

Fu, Y. *et al.* (2018) ‘Comprehensive Characterization of Toxoplasma Acyl Coenzyme A-Binding Protein TgACBP2 and Its Critical Role in Parasite Cardiolipin Metabolism’, *mBio*, 9(5), pp. 1–20. doi: 10.1128/mBio.01597-18.

Fu, Y. *et al.* (2019) ‘Synergistic roles of acyl-CoA binding protein (ACBP1) and sterol carrier protein 2 (SCP2) in

Toxoplasma lipid metabolism', *Cellular Microbiology*, 21(3). doi: 10.1111/cmi.12970.

Di Genova, B. M. *et al.* (2019) 'Intestinal delta-6-desaturase activity determines host range for Toxoplasma sexual reproduction', *PLoS Biology*, 17(8), pp. 1–19. doi: 10.1371/journal.pbio.3000364.

Gold, D. A. *et al.* (2015) 'The Toxoplasma dense granule proteins GRA17 and GRA23 mediate the movement of small molecules between the host and the parasitophorous vacuole', *Cell Host and Microbe*. Elsevier Inc., 17(5), pp. 642–652. doi: 10.1016/j.chom.2015.04.003.

Gould, S. B. *et al.* (2008) 'Alveolins, a new family of cortical proteins that define the protist infrakingdom Alveolata', *Molecular Biology and Evolution*, 25(6), pp. 1219–1230. doi: 10.1093/molbev/msn070.

Gould, S. B. *et al.* (2011) 'Ciliate pellicular proteome identifies novel protein families with characteristic repeat motifs that are common to alveolates', *Molecular Biology and Evolution*. doi: 10.1093/molbev/msq321.

Gras, S. *et al.* (2019) 'An endocytic-secretory cycle participates in Toxoplasma gondii in motility', *PLoS Biology*, 17(6), pp. 1–29. doi: 10.1371/journal.pbio.3000060.

Gratraud, P. *et al.* (2009) 'Oleic acid biosynthesis in Plasmodium falciparum: Characterization of the stearoyl-CoA desaturase and investigation as a potential therapeutic target', *PLoS ONE*, 4(9). doi: 10.1371/journal.pone.0006889.

Grellier, P. *et al.* (1991) 'Lipid traffic between high density lipoproteins and Plasmodium falciparum-infected red blood cells', *Journal of Cell Biology*, 112(2), pp. 267–277. doi: 10.1083/jcb.112.2.267.

Gulati, S. *et al.* (2015) 'Profiling the Essential Nature of Lipid Metabolism in Asexual Blood and Gametocyte Stages of Plasmodium falciparum', *Cell Host and Microbe*. Elsevier Inc., 18(3), pp. 371–381. doi: 10.1016/j.chom.2015.08.003.

Gupta, N. *et al.* (2005) 'Selective disruption of phosphatidylcholine metabolism of the intracellular parasite Toxoplasma gondii arrests its growth', *Journal of Biological Chemistry*, 280(16), pp. 16345–16353. doi: 10.1074/jbc.M501523200.

Gupta, N. *et al.* (2012) 'The obligate intracellular parasite Toxoplasma gondii secretes a soluble phosphatidylserine decarboxylase', *Journal of Biological Chemistry*, 287(27), pp. 22938–22947. doi: 10.1074/jbc.M112.373639.

Hager, K. M. *et al.* (1999) 'The nuclear envelope serves as an intermediary between the ER and Golgi complex in the intracellular parasite Toxoplasma gondii', *Journal of Cell Science*, 112(16), pp. 2631–2638.

Hakimi, M. A. and Bougdour, A. (2015) 'Toxoplasma's ways of manipulating the host transcriptome via secreted effectors', *Current Opinion in Microbiology*. Elsevier Ltd, 26, pp. 24–31. doi: 10.1016/j.mib.2015.04.003.

Haldar, K. (1996) 'Sphingolipid synthesis and membrane formation by Plasmodium', *Trends in Cell Biology*, 6(10), pp. 398–405. doi: 10.1016/0962-8924(96)10032-5.

Hao, P. *et al.* (2019) 'Identification and characterization of stearoyl-CoA desaturase in Toxoplasma gondii', *Acta*

Biochimica et Biophysica Sinica, 51(6), pp. 615–626. doi: 10.1093/abbs/gmz040.

Hartmann, A. *et al.* (2014) 'Phosphatidylethanolamine synthesis in the parasite mitochondrion is required for efficient growth but dispensable for survival of toxoplasma gondii', *Journal of Biological Chemistry*, 289(10), pp. 6809–6824. doi: 10.1074/jbc.M113.509406.

Hu, K. *et al.* (2006) 'Cytoskeletal components of an invasion machine - The apical complex of Toxoplasma gondii', *PLoS Pathogens*, 2(2), pp. 0121–0138. doi: 10.1371/journal.ppat.0020013.

Hu, X., Binns, D. and Reese, M. L. (2017) 'The coccidian parasites Toxoplasma and Neospora dysregulate mammalian lipid droplet biogenesis', *Journal of Biological Chemistry*, 292(26), pp. 11009–11020. doi: 10.1074/jbc.M116.768176.

Huynh, M. H., Boulanger, M. J. and Carruthers, V. B. (2014) 'A conserved apicomplexan microneme protein contributes to Toxoplasma gondii invasion and virulence', *Infection and Immunity*. doi: 10.1128/IAI.01877-14.

Jacot, D. *et al.* (2016) 'An Apicomplexan Actin-Binding Protein Serves as a Connector and Lipid Sensor to Coordinate Motility and Invasion', *Cell Host and Microbe*, 20(6), pp. 731–743. doi: 10.1016/j.chom.2016.10.020.

Jalovecka, M. *et al.* (2018) 'The complexity of piroplasms life cycles', *Frontiers in Cellular and Infection Microbiology*. doi: 10.3389/fcimb.2018.00248.

Janouškovec, J. *et al.* (2010) 'A common red algal origin of the apicomplexan, dinoflagellate, and heterokont plastids', *Proceedings of the National Academy of Sciences of the United States of America*. doi: 10.1073/pnas.1003335107.

Jelenska, J. *et al.* (2001) 'Subcellular localization of acetyl-CoA carboxylase in the apicomplexan parasite Toxoplasma gondii', *Proceedings of the National Academy of Sciences of the United States of America*, 98(5), pp. 2723–2728. doi: 10.1073/pnas.051629998.

Jimah, J. R. *et al.* (2016) 'Malaria parasite CelTOS targets the inner leaflet of cell membranes for pore- dependent disruption', *eLife*. doi: 10.7554/eLife.20621.

Katris, N. J. *et al.* (2014) 'The apical complex provides a regulated gateway for secretion of invasion factors in Toxoplasma.', *PLoS pathogens*, 10(4), p. e1004074. doi: 10.1371/journal.ppat.1004074.

Kelly, F. D. *et al.* (2017) ' Toxoplasma gondii MAF1b Binds the Host Cell MIB Complex To Mediate Mitochondrial Association ', *mSphere*. doi: 10.1128/msphere.00183-17.

Kilian, N. *et al.* (2018) 'Role of phospholipid synthesis in the development and differentiation of malaria parasites in the blood', *The Journal of biological chemistry*, 293(45), pp. 17308–17316. doi: 10.1074/jbc.R118.003213.

Kong, P. *et al.* (2017) 'Two phylogenetically and compartmentally distinct CDP-diacylglycerol synthases cooperate for lipid biogenesis in Toxoplasma gondii', *Journal of Biological Chemistry*. doi: 10.1074/jbc.M116.765487.

Kořený, L., Oborník, M. and Lukeš, J. (2013) 'Make It, Take It, or Leave It: Heme Metabolism of Parasites', *PLoS*

Pathogens, 9(1). doi: 10.1371/journal.ppat.1003088.

Kotloff, K. L. *et al.* (2013) 'Burden and aetiology of diarrhoeal disease in infants and young children in developing countries (the Global Enteric Multicenter Study, GEMS): A prospective, case-control study', *The Lancet*. Elsevier Ltd, 382(9888), pp. 209–222. doi: 10.1016/S0140-6736(13)60844-2.

Kuehn, A. and Pradel, G. (2010) 'The coming-out of malaria gametocytes', *Journal of Biomedicine and Biotechnology*, 2010. doi: 10.1155/2010/976827.

Kumar Sah, R. *et al.* (2019) 'Phosphatidic acid homeostasis regulated by a type-2 phosphatidic acid phosphatase represents a novel druggable target in malaria intervention', *Cell Death Discovery*. Springer US, 5(1), pp. 1–16. doi: 10.1038/s41420-019-0187-1.

Kwong, W. K. *et al.* (2019) 'A widespread coral-infecting apicomplexan with chlorophyll biosynthesis genes', *Nature*. doi: 10.1038/s41586-019-1072-z.

Labaied, M. *et al.* (2011) 'Plasmodium salvages cholesterol internalized by LDL and synthesized de novo in the liver', *Cellular Microbiology*, 13(4), pp. 569–586. doi: 10.1111/j.1462-5822.2010.01555.x.

Lauer, S. A., Ghori, N. and Haldar, K. (1995) 'Sphingolipid synthesis as a target for chemotherapy against malaria parasites', *Proceedings of the National Academy of Sciences of the United States of America*, 92(20), pp. 9181–9185. doi: 10.1073/pnas.92.20.9181.

Lige, B., Sampels, V. and Coppens, I. (2013) 'Characterization of a second sterol-esterifying enzyme in Toxoplasma highlights the importance of cholesterol storage pathways for the parasite', *Molecular Microbiology*, 87(5), pp. 951–967. doi: 10.1111/mmi.12142.

Lim, L. and McFadden, G. I. (2010) 'The evolution, metabolism and functions of the apicoplast', *Philosophical Transactions of the Royal Society B: Biological Sciences*, 365(1541), pp. 749–763. doi: 10.1098/rstb.2009.0273.

Lindner, S. E. *et al.* (2014) 'Enzymes involved in plastid-targeted phosphatidic acid synthesis are essential for Plasmodium yoelii liver-stage development', *Molecular Microbiology*, 91(4), pp. 679–693. doi: 10.1111/mmi.12485.

Macrae, J. I. *et al.* (2014) 'Plasmodium falciparum is dependent on de novo myo-inositol biosynthesis for assembly of GPI glycolipids and infectivity', *Molecular Microbiology*, 91(4), pp. 762–776. doi: 10.1111/mmi.12496.

MacRae, J. I. *et al.* (2012) 'Mitochondrial metabolism of glucose and glutamine is required for intracellular growth of toxoplasma gondii', *Cell Host and Microbe*. Elsevier Inc., 12(5), pp. 682–692. doi: 10.1016/j.chom.2012.09.013.

Maeda, T. *et al.* (2009) 'Pyruvate kinase type-II isozyme in Plasmodium falciparum localizes to the apicoplast', *Parasitology International*. doi: 10.1016/j.parint.2008.10.005.

Mann, T. and Beckers, C. (2001) 'Characterization of the subpellicular network, a filamentous.pdf', *Molecular & Biochemical Parasitology*, 115, pp. 257–268.

Martins-Duarte, érica S. *et al.* (2016) 'Apicoplast fatty acid synthesis is essential for pellicle formation at the end of cytokinesis in Toxoplasma gondii', *Journal of Cell Science*, 129(17), pp. 3320–3331. doi: 10.1242/jcs.185223.

Mazumdar, J. *et al.* (2006) 'Apicoplast fatty acid synthesis is essential for organelle biogenesis and parasite survival in Toxoplasma gondii', *Proceedings of the National Academy of Sciences of the United States of America*, 103(35), pp. 13192–13197. doi: 10.1073/pnas.0603391103.

Mazumdar, J. and Striepen, B. (2007) 'Make it or take it: Fatty acid metabolism of apicomplexan parasites', *Eukaryotic Cell*, 6(10), pp. 1727–1735. doi: 10.1128/EC.00255-07.

Mercier, C. and Cesbron-Delauw, M. F. (2015) 'Toxoplasma secretory granules: One population or more?', *Trends in Parasitology*. Elsevier Ltd, 31(2), pp. 60–71. doi: 10.1016/j.pt.2014.12.002.

Mordue, D. G. *et al.* (1999) 'Proteins on the Basis of Their Membrane Anchoring', *J. Exp. Med*, 190(12), pp. 1783–1792.

Mullin, K. A. *et al.* (2006) 'Membrane transporters in the relict plastid of malaria parasites', *Proceedings of the National Academy of Sciences of the United States of America*, 103(25), pp. 9572–9577. doi: 10.1073/pnas.0602293103.

Nair, S. C. *et al.* (2011) 'Apicoplast isoprenoid precursor synthesis and the molecular basis of fosmidomycin resistance in Toxoplasma gondii', *Journal of Experimental Medicine*, 208(7), pp. 1547–1559. doi: 10.1084/jem.20110039.

Nantakomol, D. *et al.* (2011) 'Circulating red cell-derived microparticles in human malaria', *Journal of Infectious Diseases*. doi: 10.1093/infdis/jiq104.

Nawabi, P. *et al.* (2003) 'Neutral-lipid analysis reveals elevation of acylglycerols and lack of cholesterol esters in Plasmodium falciparum-infected erythrocytes', *Eukaryotic Cell*. doi: 10.1128/EC.2.5.1128-1131.2003.

Neess, D. *et al.* (2015) 'Long-chain acyl-CoA esters in metabolism and signaling: Role of acyl-CoA binding proteins', *Progress in Lipid Research*. Elsevier Ltd, 59(April), pp. 1–25. doi: 10.1016/j.plipres.2015.04.001.

Nishi, M. *et al.* (2008) 'Organellar dynamics during the cell cycle of Toxoplasma gondii', *Journal of Cell Science*, 121(9), pp. 1559–1568. doi: 10.1242/jcs.021089.

Nishikawa, Y. *et al.* (2005) 'Host cell lipids control cholesteryl ester synthesis and storage in intracellular Toxoplasma', *Cellular Microbiology*, 7(6), pp. 849–867. doi: 10.1111/j.1462-5822.2005.00518.x.

Nolan, S. J. *et al.* (2018) 'Novel approaches to kill toxoplasma gondii by exploiting the uncontrolled uptake of unsaturated fatty acids and vulnerability to lipid storage inhibition of the parasite', *Antimicrobial Agents and Chemotherapy*, 62(10), pp. 1–34. doi: 10.1128/AAC.00347-18.

Nolan, S. J., Romano, J. D. and Coppens, I. (2017) *Host lipid droplets: An important source of lipids salvaged by the intracellular parasite Toxoplasma gondii*, *PLoS Pathogens*. doi: 10.1371/journal.ppat.1006362.

Oppenheim, R. D. *et al.* (2014) 'BCKDH: The Missing Link in Apicomplexan Mitochondrial Metabolism Is Required

for Full Virulence of Toxoplasma gondii and Plasmodium berghei', *PLoS Pathogens*, 10(7). doi: 10.1371/journal.ppat.1004263.

Ouologuem, D. T. and Roos, D. S. (2014) 'Dynamics of the Toxoplasma gondii inner membrane complex', *Journal of Cell Science*, 127(15), pp. 3320–3330. doi: 10.1242/jcs.147736.

P.-Y., M. *et al.* (2013) 'Malaria-infected erythrocyte-derived microvesicles mediate cellular communication within the parasite population and with the host immune system', *Cell Host and Microbe*. doi: 10.1016/j.chom.2013.04.009 LK -

Palacpac, N. M. Q. *et al.* (2004) 'Developmental-stage-specific triacylglycerol biosynthesis, degradation and trafficking as lipid bodies in Plasmodium falciparum-infected erythrocytes', *Journal of Cell Science*, 117(8), pp. 1469–1480. doi: 10.1242/jcs.00988.

Paquet, T. *et al.* (2017) 'Antimalarial efficacy of MMV390048, an inhibitor of Plasmodium phosphatidylinositol 4-kinase', *Science Translational Medicine*, 9(387). doi: 10.1126/scitranslmed.aad9735.

Pernas, L. *et al.* (2014) 'Toxoplasma Effector MAF1 Mediates Recruitment of Host Mitochondria and Impacts the Host Response', *PLoS Biology*, 12(4). doi: 10.1371/journal.pbio.1001845.

Pernas, L. *et al.* (2018) 'Mitochondria Restrict Growth of the Intracellular Parasite Toxoplasma gondii by Limiting Its Uptake of Fatty Acids', *Cell Metabolism*. Elsevier Inc., 27(4), pp. 886-897.e4. doi: 10.1016/j.cmet.2018.02.018.

Pessi, G., Kociubinski, G. and Ben Mamoun, C. (2004) 'A pathway for phosphatidylcholine biosynthesis in Plasmodium falciparum involving phosphoethanolamine methylation', *Proceedings of the National Academy of Sciences of the United States of America*, 101(16), pp. 6206–6211. doi: 10.1073/pnas.0307742101.

Pessi, G. and Mamoun, C. Ben (2006) 'Pathways for phosphatidylcholine biosynthesis: targets and strategies for antimalarial drugs', *Future Lipidology*, 1(2), pp. 173–180. doi: 10.2217/17460875.1.2.173.

Pfluger, S. L. *et al.* (2005) 'Receptor for retrograde transport in the apicomplexan parasite Toxoplasma gondii', *Eukaryotic Cell*. doi: 10.1128/EC.4.2.432-442.2005.

Pittman, K. J. and Knoll, L. J. (2015) 'Long-Term Relationships: the Complicated Interplay between the Host and the Developmental Stages of Toxoplasma gondii during Acute and Chronic Infections', *Microbiology and Molecular Biology Reviews*, 79(4), pp. 387–401. doi: 10.1128/mmbr.00027-15.

Pratt, S. *et al.* (2013) 'Sphingolipid synthesis and scavenging in the intracellular apicomplexan parasite, Toxoplasma gondii', *Molecular and Biochemical Parasitology*. Elsevier B.V., 187(1), pp. 43–51. doi: 10.1016/j.molbiopara.2012.11.007.

Quittnat, F. *et al.* (2004) 'On the biogenesis of lipid bodies in ancient eukaryotes: Synthesis of triacylglycerols by a Toxoplasma DGAT1-related enzyme', *Molecular and Biochemical Parasitology*, 138(1), pp. 107–122. doi: 10.1016/j.molbiopara.2004.08.004.

Ralph, S. A. *et al.* (2004) 'Metabolic maps and functions of the Plasmodium falciparum apicoplast', *Nature Reviews Microbiology*, 2(3), pp. 203–216. doi: 10.1038/nrmicro843.

Ramakrishnan, S. *et al.* (2012) 'Apicoplast and endoplasmic reticulum cooperate in fatty acid biosynthesis in apicomplexan parasite Toxoplasma gondii', *Journal of Biological Chemistry*, 287(7), pp. 4957–4971. doi: 10.1074/jbc.M111.310144.

Ramakrishnan, S. *et al.* (2013) 'Lipid synthesis in protozoan parasites: A comparison between kinetoplastids and apicomplexans', *Progress in Lipid Research*. doi: 10.1016/j.plipres.2013.06.003.

Ramakrishnan, S. *et al.* (2015) 'The intracellular parasite Toxoplasma gondii depends on the synthesis of long-chain and very long-chain unsaturated fatty acids not supplied by the host cell', *Molecular Microbiology*, 97(1), pp. 64–76. doi: 10.1111/mmi.13010.

Regev-Rudzki, N. *et al.* (2013) 'Cell-cell communication between malaria-infected red blood cells via exosome-like vesicles', *Cell*. doi: 10.1016/j.cell.2013.04.029.

Reue, K. and Wang, H. (2019) 'Mammalian lipin phosphatidic acid phosphatases in lipid synthesis and beyond: Metabolic and inflammatory disorders', *Journal of Lipid Research*. doi: 10.1194/jlr.S091769.

Romano, J. D. *et al.* (2013) 'Toxoplasma gondii salvages sphingolipids from the host Golgi through the rerouting of selected Rab vesicles to the parasitophorous vacuole', *Molecular Biology of the Cell*, 24(12), pp. 1974–1995. doi: 10.1091/mbc.E12-11-0827.

Saito, T. *et al.* (2008) 'A novel GDP-dependent pyruvate kinase isozyme from Toxoplasma gondii localizes to both the apicoplast and the mitochondrion', *Journal of Biological Chemistry*, 283(20), pp. 14041–14052. doi: 10.1074/jbc.M709015200.

Sampels, V. *et al.* (2012) 'Conditional mutagenesis of a novel choline kinase demonstrates plasticity of phosphatidylcholine biogenesis and gene expression in Toxoplasma gondii', *Journal of Biological Chemistry*, 287(20), pp. 16289–16299. doi: 10.1074/jbc.M112.347138.

dos Santos, T. A. T. *et al.* (2011) 'Phosphatidylserine exposure by Toxoplasma gondii is fundamental to balance the immune response granting survival of the parasite and of the host', *PLoS ONE*. doi: 10.1371/journal.pone.0027867.

van Schaijk, B. C. L. *et al.* (2014) 'Type II fatty acid biosynthesis is essential for Plasmodium falciparum sporozoite development in the midgut of anopheles mosquitoes', *Eukaryotic Cell*, 13(5), pp. 550–559. doi: 10.1128/EC.00264-13.

Schlame, M. (2008) 'Cardiolipin synthesis for the assembly of bacterial and mitochondrial membranes', *Journal of Lipid Research*, 49(8), pp. 1607–1620. doi: 10.1194/jlr.R700018-JLR200.

Schwab, J. C., Beckers, C. J. M. and Joiner, K. A. (1994) 'The parasitophorous vacuole membrane surrounding intracellular Toxoplasma gondii functions as a molecular sieve', *Proceedings of the National Academy of*

Sciences of the United States of America, 91(2), pp. 509–513. doi: 10.1073/pnas.91.2.509.

Shastri, S. *et al.* (2010) 'Plasmodium CDP-DAG synthase: An atypical gene with an essential N-terminal extension', *International Journal for Parasitology*, 40(11), pp. 1257–1268. doi: 10.1016/j.ijpara.2010.03.006.

Shears, M. J. *et al.* (2017) 'Characterization of the Plasmodium falciparum and P. berghei glycerol 3-phosphate acyltransferase involved in FASII fatty acid utilization in the malaria parasite apicoplast', *Cellular Microbiology*, 19(1). doi: 10.1111/cmi.12633.

Shears, M. J., Botté, C. Y. and McFadden, G. I. (2015) 'Fatty acid metabolism in the Plasmodium apicoplast: Drugs, doubts and knockouts', *Molecular and Biochemical Parasitology*. Elsevier B.V., 199(1–2), pp. 34–50. doi: 10.1016/j.molbiopara.2015.03.004.

Smith, S., Witkowski, A. and Joshi, A. K. (2003) 'Structural and functional organization of the animal fatty acid synthase', *Progress in Lipid Research*, 42(4), pp. 289–317. doi: 10.1016/S0163-7827(02)00067-X.

Sturm, A. *et al.* (2006) 'Manipulation of host hepatocytes by the malaria parasite for delivery into liver sinusoids', *Science*, 313(5791), pp. 1287–1290. doi: 10.1126/science.1129720.

Takahashi, K. T., Kawaguchi, S. and Toda, T. (2009) 'Observation by electron microscopy of a gregarine parasite of Antarctic krill: Its histological aspects and ecological explanations', *Polar Biology*. doi: 10.1007/s00300-008-0563-4.

Tanaka, T. Q. *et al.* (2019) ' Polyunsaturated fatty acids promote Plasmodium falciparum gametocytogenesis ', *Biology Open*, 8(7), p. bio042259. doi: 10.1242/bio.042259.

Tanguy, E. *et al.* (2019) 'Phosphatidic acid: From pleiotropic functions to neuronal pathology', *Frontiers in Cellular Neuroscience*, 13(January), pp. 1–8. doi: 10.3389/fncel.2019.00002.

Tawk, L. *et al.* (2011) 'Phosphatidylinositol 3-monophosphate is involved in Toxoplasma apicoplast biogenesis', *PLoS Pathogens*, 7(2), pp. 1–16. doi: 10.1371/journal.ppat.1001286.

Tenter, A. M., Heckeroth, A. R. and Weiss, L. M. (2000) 'Toxoplasma gondii: From animals to humans', *International Journal for Parasitology*, 30(12–13), pp. 1217–1258. doi: 10.1016/S0020-7519(00)00124-7.

Todorovic, R. A., Wagner, G. G. and Kopf, M. (1981) 'Ultrastructure of Babesai bovis (Babes, 1888)', *Veterinary Parasitology*. doi: 10.1016/0304-4017(81)90060-1.

Tomavo, S., Schwarz, R. T. and Dubremetz, J. F. (1989) 'Evidence for glycosyl-phosphatidylinositol anchoring of Toxoplasma gondii major surface antigens.', *Molecular and Cellular Biology*, 9(10), pp. 4576–4580. doi: 10.1128/mcb.9.10.4576.

Tran, P. N. *et al.* (2014) 'A female gametocyte-specific ABC transporter plays a role in lipid metabolism in the malaria parasite', *Nature Communications*. Nature Publishing Group, 5. doi: 10.1038/ncomms5773.

Tran, P. N. *et al.* (2016) 'Changes in lipid composition during sexual development of the malaria parasite Plasmodium

falciparum', *Malaria Journal*. BioMed Central, 15(1), pp. 1–13. doi: 10.1186/s12936-016-1130-z.

Vaid, A. *et al.* (2010) 'PfPI3K, a phosphatidylinositol-3 kinase from Plasmodium falciparum, is exported to the host erythrocyte and is involved in hemoglobin trafficking', *Blood*, 115(12), pp. 2500–2507. doi: 10.1182/blood-2009-08-238972.

Vaughan, A. M. *et al.* (2009) 'Type II fatty acid synthesis is essential only for malaria parasite late liver stage development', *Cellular Microbiology*, 11(3), pp. 506–520. doi: 10.1111/j.1462-5822.2008.01270.x.

Vot, J. *et al.* (2017) *Handbook of the Protists*, *Handbook of the Protists*. doi: 10.1007/978-3-319-32669-6.

Wang, Y. *et al.* (2019) 'Three toxoplasma gondii dense granule proteins are required for induction of lewis rat macrophage pyroptosis', *mBio*. doi: 10.1128/mBio.02388-18.

Watkins, P. A. *et al.* (2007) 'Evidence for 26 distinct acyl-coenzyme A synthetase genes in the human genome', *Journal of Lipid Research*, 48(12), pp. 2736–2750. doi: 10.1194/jlr.M700378-JLR200.

Wein, S. *et al.* (2018) 'Contribution of the precursors and interplay of the pathways in the phospholipid metabolism of the malaria parasite', *Journal of Lipid Research*. doi: 10.1194/jlr.M085589.

Welti, R. *et al.* (2007) 'Lipidomic analysis of Toxoplasma gondii reveals unusual polar lipids', *Biochemistry*, 46(48), pp. 13882–13890. doi: 10.1021/bi7011993.

White, M. W. and Suvorova, E. S. (2018) 'Apicomplexa Cell Cycles: Something Old, Borrowed, Lost, and New', *Trends in Parasitology*. Elsevier Ltd, 34(9), pp. 759–771. doi: 10.1016/j.pt.2018.07.006.

Witola, W. H. *et al.* (2008) 'Disruption of the Plasmodium falciparum PfPMT gene results in a complete loss of phosphatidylcholine biosynthesis via the serine-decarboxylase- phosphoethanolamine-methyltransferase pathway and severe growth and survival defects', *Journal of Biological Chemistry*, 283(41), pp. 27636–27643. doi: 10.1074/jbc.M804360200.

World Health Organization (2019) *WHO | This year's World malaria report at a glance*, *Who*.

Wrenger, C. and Müller, S. (2004) 'The human malaria parasite Plasmodium falciparum has distinct organelle-specific lipoylation pathways', *Molecular Microbiology*, 53(1), pp. 103–113. doi: 10.1111/j.1365-2958.2004.04112.x.

Xia, N. *et al.* (2019) 'Pyruvate homeostasis as a determinant of parasite growth and metabolic plasticity in toxoplasma gondii', *mBio*, 10(3), pp. 1–16. doi: 10.1128/mBio.00898-19.

Yu, M. *et al.* (2008) 'The Fatty Acid Biosynthesis Enzyme FabI Plays a Key Role in the Development of Liver-Stage Malarial Parasites', *Cell Host and Microbe*. Elsevier Inc., 4(6), pp. 567–578. doi: 10.1016/j.chom.2008.11.001.

HYPOTHESIS AND AIMS OF THE THESIS

Lipid metabolism in apicomplexan parasites has been proven to be essential for the generation of infectious progeny and persistence within their hosts. The production of fatty acids (FA) is central to parasite lipid metabolism as they constitute essential hydrophobic building blocks required for membrane lipid synthesis. Apicomplexa was long thought to suffice their fatty acid needs solely by scavenging from the host cell but this hypothesis was challenged by the discovery of a prokaryotic fatty acid synthesis pathway: FASII within a non-photosynthetic plastid called apicoplast. Thus, we propose that parasite lipids are a patchwork of fatty acids synthesized de novo and/or scavenged from the host. These parasites infect various kinds of hosts and therefore encounter different nutritional challenges/host environments. Recent work (including ours) in the field of apicomplexa biology showed that the lipid synthesis and intracellular parasite development are also dependent on the host environment/nutritional conditions (Blume and Seeber 2018; Amiar et al. 2019). However, the molecular mechanism by which these parasites combine and regulate the fatty acid flux from these two sources in context of the host nutritional status to sustain their intracellular survival, remains unknown.

My PhD project focused on understanding how and why the parasite utilizes both FA sources to form a 'patchwork lipid'. In quest for the same, I investigated two important metabolic pathways and their enzymes: a) for the activation of the FA building blocks by acyl coA synthetases (ACS) and b) use of FA to generate central lipid precursor, phosphatidic acid (PA) and diacylglycerol (DAG) by phosphatidic acid phosphatase. We hypothesized that lipin and ACSs act at the crossroads of utilization of FA from the two sources-de novo machinery and scavenging from host for building of central precursor lipid molecules within the parasite.

In pursuit of the same, my thesis projects aimed for the following objectives:

i. Functional characterisation of lipin proteins in *T. gondii* and *P. falciparum* by generation of genetic knockouts and core lipidomics using GC-MS.
ii. Identification of putative candidate genes encoding acyl-CoA synthetases in *T. gondii* and their subsequent functional characterisation by lipidomics to determine their expected roles as fatty acid activators allowing their further trafficking and utilisation by the parasite

iii. Elucidating the role of host nutritional status on the parasites to ascertain adept metabolic capacity of the parasite.

iv. Developing novel fluxomic approaches using different stable isotope substrates (^{13}C-U-Glucose, ^{31}d-C16:0) to determine the different sources and flux of FAs from synthetic organelles and/or from host and its environment contributing to the formation of parasite lipids.

CHAPTER IV: LIPIN, A PIVOTAL NEXUS IN *TOXOPLASMA* LIPID METABOLISM, CHANNELING HOST FATTY ACID FLUX TO STORAGE AND MEMBRANE BIOGENESIS

CHAPTER IV SUMMARY

Lipid biosynthesis and metabolism in apicomplexan parasites is reliant on an essential combination of fatty acid flux derived from de novo synthesis and scavenging from the host. The survival of these parasites within their hosts requires a balance between the different sources of FA flux directed towards lipid synthesis for generation of membranes, signaling events and storage. In this study we characterized a key phosphatidic acid phosphatase *Tg*LIPIN participating in the parasite FA homeostasis by regulating the critical levels of central precursor lipid molecules phosphatidic acid (PA) and diacylglycerol (DAG).

Major findings of this study are summarized below:

i. *Tg*LIPIN is a functional phosphatidic acid phosphatase, essential for *Toxoplasma* tachyzoite replication and survival within the host.
ii. Parasites lacking *Tg*LIPIN face growth arrest due to severe membrane anomalies mainly affecting inner membrane complex and nuclear envelope.
iii. *Tg*LIPIN, regulates phospholipid biosynthesis feeding parasite membranes by maintaining a balance between its precursor PA and product DAG.
iv. *Tg*LIPIN metabolizes PA to DAG, which is turn serves as precursor for parasite lipid storage pathway.
v. Most importantly, this key protein channels host scavenged FAs towards membrane biogenesis and storage, preventing their accumulation and thus protecting the parasite from lipotoxicity.

TITLE: LIPIN, a pivotal nexus in *Toxoplasma* lipid metabolism, channeling host fatty acid flux to storage and membrane biogenesis (in submission)

Sheena Dass[1], Laurence Berry[2], Christophe-Sebastien Arnold[1], Nicholas J. Katris[1], Marie-France Cesbron-Delauw[1], Yoshiki Yamaryo-Botté[1]*, Cyrille Y. Botté[1]*

1 Apicolipid Team, Institute for Advanced Biosciences, CNRS UMR5309, Université Grenoble Alpes, INSERM U1209, Grenoble, France,

2 Dynamique des interactions Membranaires normales et pathologiques, UMR5235, Université Montpellier II, France.

* Equal senior and corresponding authors. To whom correspondence should be sent, cyrille.botte@univ-grenoble-alpes.fr/cyrille.botte@gmail.com; yoshiki.botte-yamaryo@univ-grenoble-alpes.fr

ABSTRACT

Apicomplexans are obligate intracellular parasites responsible for major human diseases worldwide. Their intracellular survival relies on intense lipid synthesis feeding membrane biogenesis. Parasite lipids are generated as an essential combination of fatty acids scavenged from the host and *de novo* synthesized within the parasite apicoplast. The molecular and metabolic mechanisms allowing regulation and channeling of these fatty acid fluxes for intracellular parasite survival are currently unknown. Here, we identified an essential phosphatidic acid phosphatase in *Toxoplasma gondii*, *Tg*LIPIN, as the central metabolic nexus responsible for controlled lipid synthesis sustaining parasite development. Lipidomics reveals that *Tg*LIPIN controls the synthesis of diacylglycerol and levels of phosphatidic acid that regulates the fine balance of lipids between storage and membrane biogenesis. Using novel fluxomics approaches, we uncovered the first parasite host-scavenged lipidome and showed that *Tg*LIPIN prevents parasite 'lipotoxicity' through effective channeling of host-scavenged fatty acids to storage triglycerides and membrane phospholipids.

INTRODUCTION

Apicomplexa includes several pathogenic protists that are responsible for major chronic and infectious diseases with massive human and economic burden. Two prominent examples are *Toxoplasma gondii* and *Plasmodium falciparum*, the respective causative agents of toxoplasmosis, which affects about 1/3 of the world population, and human malaria, which affects ~200 million people/year killing about 450,000 of the global population (WHO Report 2018). Apicomplexans are obligate intracellular parasites, which have an enormous demand for lipids for sustaining their survival within their human host cells. The utilization of fatty acids (FA) to synthesize the complex lipids is an essential determinant for the successful host adaptation by these parasites. These parasites meet their high demand of lipids through *de novo* synthesis via type II fatty acid synthesis within apicoplast as well as via copious salvage directly from the host and extracellular environment (Ramakrishnan *et al.*, 2012, 2015; Coppens, 2013; Amiar *et al.*, 2019; Di Genova *et al.*, 2019). Recent data suggests that the tight regulation of FA flux between host, parasite and its pivotal metabolic organelles, potentially through key lipid intermediates, is particularly vital for intracellular development of these apicomplexan pathogens (Nolan *et al.*, 2018; Amiar *et al.*, 2019). For instance, the exposure of *Toxoplasma* to high concentrations of unsaturated FAs results in irreversible growth arrest due to 'lipotoxicity' (Nolan *et al.*, 2018). However, the molecular and metabolic pathways controlling the FA flux towards parasite membrane biogenesis and storage remain largely unknown.

Phosphatidic acid (PA), the simplest glycerophospholipid, could contribute to the regulation of FA flux in apicomplexans, as it is the key precursor and intermediate balancing the biosynthesis of both glycerophospholipids and triacylglycerols (TAGs) towards membrane biogenesis and lipid storage in eukaryotes (Csaki and Reue, 2010). Apicomplexan parasites can generate PA either (i) *de novo* from FA and glycerol-3-phosphate in a two-step acylation reaction catalyzed by glycerol-3-phosphate acyltransferases (GPAT/ATS1) and acylglycerol acyltransferases (AGPAT/LPAAT/ATS2), respectively (Lindner *et al.*, 2014; Amiar *et al.*, 2016, 2019; Shears *et al.*, 2017), and (ii) from existing glycerolipids by diacylglycerol kinases (DGK1 and DGK2) or phospholipase D (Bullen *et al.*, 2016; Bisio *et al.*, 2019). PA has pleiotropic roles depending on its biosynthetic source and the site of production within the parasite, (i) as a signal transducer modulating parasite invasion, motility and egress (Bullen *et al.*, 2016; Jacot *et al.*, 2016; Jimah *et*

al., 2016; Bisio *et al.*, 2019), (ii) as a regulator of lysoPA (LPA)/PA levels for modulating membrane curvature for cytokinesis and endocytosis (Amiar *et al.*, 2019), and (iii) as the central precursor of phospholipid synthesis in the apicoplast/ER pathway formed by ATS1 and ATS2 (Amiar *et al.*, 2016, 2019).

Since, PA appears at the forefront of parasite biological armor, therefore, the enzymes involved in its metabolism are critical for our understanding of parasite pathogenesis. PA can be catabolized to another key signaling lipid diacylglycerol (DAG), by phosphatidic acid phosphatases (PAP), which play key metabolic functions in eukaryotes (Carman and Han, 2019). Apicomplexan parasites possess three putative PAPs although none of them has been characterized to date.

Here, we determined that *Toxoplasma* lipin, *Tg*LIPIN, is a phosphatidic acid phosphatase that localizes at the cytosolic-ER interface and is essential for the intracellular survival of tachyzoites. Its inducible disruption immediately leads to gross membrane anomalies at the parasite IMC and nucleus. Lipidomics of the inducible knockdown mutant reveals a time-dependent accumulation of PA concomitant with the reduction of DAG, lipid droplets and storage lipid triacylglycerol (TAG). Consequently, the mutant dies from a lipotoxic accumulation of free FA and membrane phospholipids. Further, we conducted novel fluxomics experiments using U-^{13}C glucose-labelled host cells to monitor which FA are being salvaged by the parasite, providing the first host scavenged lipidome of *Toxoplasma.* This allowed to determine that *Tg*LIPIN acts as the central metabolic point that tightly controls the flux of host-derived FA for the synthesis and regulation of phospholipids vs TAG towards membrane biogenesis and storage, necessary for intracellular parasite development. We therefore unravel the molecular mechanism by which the parasite uses both host and *de novo* synthesized lipid resources to generate the lipids required for its survival.

RESULTS

Toxoplasma genome encodes a single lipin, TgLIPIN, which has functional phosphatidate phosphatase activity

Bioinformatics analysis of *Tg*LIPIN (TGGT1_230690) revealed that the protein has an unusually large size compared to other phosphatidate phosphatases encoded by the genome of *T. gondii*. *Tg*LIPIN possesses the two typical and highly conserved domains of eukaryotic lipins, the amino

terminal N-LIP domain, and the carboxy terminal C-LIP domain harboring its functional PA phosphatase catalytic motif DXDXT/V (HAD-like domain) (Fig. 1a**)** (Carman and Han, 2009). Phylogenetic analysis confirms that the enzyme is highly conserved as a single lipin within phylum apicomplexa, cladding specifically within a coccidian subgroup. (Sup Fig.1a).

To confirm the predicted phosphatidic acid phosphatase activity of *Tg*LIPIN, we performed heterologous complementation of a *Saccharomyces cerevisiae* Δ*dpp1*Δ*lpp1*Δ*pah1* triple mutant deficient in PAP activity with a temperature sensitive phenotype not allowing growth at 37ºC (Nakamura *et al.*, 2009; Chae, Han and Carman, 2012). The C-LIP domain of *Tg*LIPIN was able to rescue the temperature sensitive phenotype in the yeast mutant (Fig. 1b) thereby confirming presence of PAP enzymatic activity.

Next, *Tg*LIPIN was endogenously tagged with 3×HA at its C-terminal end (Huynh and Carruthers, 2009). Immunofluorescence assay (IFA) revealed a broad cytosolic and perinuclear localization. (Fig. 1c). Interestingly *Tg*LIPIN lacks an apparent nuclear localization signal (NLS) that most of eukaryotic lipin usually possess (Csaki and Reue, 2010; Zhang and Reue, 2017). To further resolve its localization, we conducted IFAs of *Tg*LIPIN-HA with a known *Toxoplasma* ER marker, Der1-GFP (Agrawal *et al.*, 2009), which confirmed proximity to the endomembrane system with partial ER co-localization (Fig. S1b, c). We then sought to assess the localization of the putative *P. falciparum* lipin, *Pf*LIPIN via endogenous tagging. Unlike *Tg*LIPIN, the *Plasmodium* lipin is predicted to have a nuclear localization (NLS) sequence. IFAs confirmed that *Pf*LIPIN was specifically expressed during the schizont stage of the parasite erythrocytic life cycle, as punctate vesicles in close vicinity to, or at the parasite nucleus (Fig. S3d).

TgLIPIN disruption induces rapid division defects leading to replication arrest and parasite death

To understand the importance of *Tg*LIPIN for parasite growth, we generated an N-terminal HA-tagged inducible knockdown parasite line based on Tet-off system, *Tg*LIPIN-iKD (Meissner, Schlüter and Soldati, 2002; Sheiner *et al.*, 2011) (Fig. S2a,b). Downregulation of *Tg*LIPIN-iKD showed no detectable protein by western blot after 48h of anhydrotetracycline (ATc) treatment (Fig. 2a). Cytoplasmic localization of the protein and its downregulation were both confirmed by IFA, which also revealed gross parasite malformation after 48h of ATc treatment (Fig. 2b). This result suggests that *Tg*LIPIN disruption dramatically impacts parasite development within its host.

To further delineate the morphological phenotype of *Tg*LIPIN downregulation, IFAs were performed prior to complete protein loss, at 24 h of ATc treatment (Fig. 2c). Severe membrane anomalies and division defects were observed at this early time point of ATc treatment, suggesting *Tg*LIPIN levels are crucial to maintain parasite intracellular growth. Co-localization with known parasite inner membrane complex marker GAP45, suggested a gross defect in IMC biogenesis (Fig. 2c, enlarged image). This irregular membrane biogenesis caused a severe intracellular replication defect in *Tg*LIPIN-ikD with a significant increase of small vacuoles containing 1-2 parasite vacuoles (15-20%) and vacuoles containing morphologically abnormal parasites (10-15%), alongside with a concomitant significant decrease (25-80%) of larger vacuoles containing 3-10 parasites (Fig. 2d). To further assess the effect of *Tg*LIPIN on parasite intracellular growth, plaque assays were performed investigating the mutant capacity to maintain proper growth with fluctuating levels of host nutrients. When cultured in regular growth conditions with 1% FBS, *Tg*LIPIN-ikD (+ATc) exhibited a severe growth defect with few plaques (Fig. 2e) as expected from IFA results (Fig. 2b,c). In an attempt to rescue this defect, the parasites were grown in the presence of 10% FBS (Amiar *et al.*, 2019). However, surprisingly, *Tg*LIPIN-ikD (+ATc) showed a significant decline in growth in 10% than with 1% FBS containing culture medium, as marked by complete absence of plaques (Fig. 2e,f). In contrast, a decrease in host nutritional environment with 0% FBS slightly and significantly enhanced the growth of *Tg*LIPIN-ikD (+ATc) (Fig. 2e,f) suggesting that the exogenous lipidic nutrient source such as free FA or phospholipids are somehow toxic to the parasites lacking *Tg*LIPIN. This data is an example of robust adaptation of parasite to its host nutritional environment.

Electron microscopy reveals gross membrane anomalies as an early impact of TgLIPIN downregulation

In order to further resolve the cellular phenotype marked by the *Tg*LIPIN down regulation, *Tg*LIPIN-iKD (+ATc) parasites were examined by transmission electron microscopy (TEM). Interestingly, as early as 24 h treatment with ATc , when *Tg*LIPIN levels are only slightly reduced, both parasite inner membrane complex (IMC) and plasma membrane displayed gross abnormalities in forming evaginations or lateral interruptions, without affecting the parasite size (Fig. 3 b). Concordantly, IFA data of *Tg*LIPIN-ikD (+ATc) also hinted at aberrant IMC (Fig. 3c). The nuclear envelope membranes also imbibed a grave effect early in the process of

*Tg*LIPIN down regulation (24 h +ATc). The nuclear membrane appeared multi-lobed marked by abnormal extensions into the cytoplasm (Fig. 3d**)**. Interestingly, this nuclear envelope phenotype is also observed in the yeast lipin mutant coupling phospholipid biosynthesis to nuclear membrane (Santos-Rosa *et al.*, 2005; Siniossoglou, 2009).

Furthermore, observations of *Tg*LIPIN-iKD at 24 h +ATc showed daughter cells abnormally attached through IMC (Fig. 3c, right). In agreement with the replication assay data (Fig. 2d), TEM images showed that the process of parasite endodyogeny was affected by the absence of appropriate levels of *Tg*LIPIN (24 h +ATc), marked by arrest of multiple daughter cells within a single mother cell (Fig. 3e). This suggests that indispensability of *Tg*LIPIN for parasite growth is based on its direct involvement in endomembrane biogenesis (i.e. plasma membrane, IMC, nucleus), in turn affecting the process of parasite replication within host cell.

TgLIPIN regulates the synthesis of glycerophospholipids by controlling the bulk synthesis of PA and DAG

To determine the functional role of *Tg*LIPIN in parasite PA synthesis and membrane biogenesis, we conducted comprehensive lipidomic analysis. To precisely assess the timely impact of *Tg*LIPIN-ikD disruption on lipid synthesis, parasites were grown for 24 to 48 h with and without ATc. Total lipids were separated by high performance thin layer chromatography (HPTLC) and quantified by gas chromatography-mass spectrometry (GC-MS).

PA levels were significantly increased to almost three times early on at 24 h + ATc in *Tg*LIPIN-ikD in comparison to the control (-ATc) (Fig. 4b). Such an increase was maintained after 48 h of *Tg*LIPIN downregulation (Fig. 4b). Analysis of the FA composition of PA molecular species revealed that the disruption of *Tg*LIPIN showed a significant increase in the level of unsaturated fatty acid oleate (C18:1) besides decline in levels of various saturated fatty acids, significantly stearate (C18:0) (Fig. 4c). The amount of DAG, the product of *Tg*LIPIN, was significantly reduced to almost half in the *Tg*LIPIN-ikD (+ATc), beginning from 24 h up to 48 h treatment with ATc (Fig. 4d). The concomitant increase in PA and decrease in DAG indicated that *Tg*LIPIN is an active phosphatidic acid phosphatase, controlling the bulk levels of PA and DAG. Despite a strong replication defect and reduction in parasite number, the total amount of phospholipids was increased to almost twice in the *Tg*LIPIN-ikD (+ATc) in comparison to the control (-ATc) (Fig. 4e**)**. Accordingly, the phospholipid classes directly made from PA via the CDP-DAG pathway

(Kong *et al.*, 2017) were found significantly increased, i.e. cardiolipin (CL) and phosphatidylserine (PS) and indirectly phosphatidylcholine (PC) likely formed from PS and phosphatidylethanolamine (PE) (Fig. S4a).

TgLIPIN controls critical levels of DAG and free fatty acids towards parasite storage lipids, triacylglycerols

In eukaryotes TAG biosynthesis occurs at the last step of the glycerol-3-phosphate pathway through the *sn-3* acylation of DAG catalysed by a diacylglycerol-acyltransferase (DGAT) that uses FFA (Cases *et al.*, 1998; Nolan, Romano and Coppens, 2017; Nolan *et al.*, 2018). However, the key and limiting step of TAG synthesis is the formation of its precursor, DAG, the production of which in turn is dependent on a phosphatidate phosphatase (lipin). We tested the role of *Tg*LIPIN in this key process by comparing the levels of neutral lipid majorly comprising TAGs and cholesteryl esters within reserve organelles called lipid droplets by nile red staining (Greenspan, Mayer and Fowler, 1985) in the *Tg*LIPIN ikD parasites (+ATc/-ATc). Nile red staining showed that the number of lipid droplets per parasite vacuole in the presence of ATc was reduced to almost 60% in comparison to the control (Fig. 5a, b), suggesting that *Tg*LIPIN is involved in the synthesis of storage lipids. Accordingly, relative abundance of TAGs was significantly reduced after 48 h of ATc treatment, with a 24 h time lag compared to DAG levels (Fig. 5c). Other neutral lipids making the bulk of lipid droplets, cholesteryl esters (CE), were also significantly decreased (Fig. S4c).

TAGs and CEs are neutral storage lipids potentially implied in the parasite's ability to cope with the excess FA (Nolan *et al.*, 2018). The synthesis of TAG via enzyme DGAT requires two substrates, DAG and free fatty acids (FFA). We therefore determined the FFA content of the *Tg*LIPIN-ikD. Lipidomics revealed a significant accumulation of FFA in the *Tg*LIPIN-iKD (+ATc/-ATc), increasing with time points 24 to 48 h (Fig. 5d). Interestingly, similar to PA, C18:1 (oleate) was the only FA found significantly increased in the parasite free FA (FFA) pool (**Fig. S3**), suggesting this FA is an important intermediate in the pathways regulated by *Tg*LIPIN, as previously hinted (Hu, Binns and Reese, 2017; Nolan *et al.*, 2018; Pernas *et al.*, 2018).

Therefore, this key result suggests cell death in parasites lacking *Tg*LIPIN is caused due to 'lipotoxicity' or toxic effect of FFAs, arising because of impaired TAG biosynthesis. This is consistent with the reduced viability of parasite in high FBS content (Fig. 2e, f).

TgLIPIN regulates the flux of host fatty acids to control parasite lipid synthesis and prevent accumulation of toxic free fatty acids levels

Previous results from this study suggest that *Tg*LIPIN is involved in DAG synthesis and regulation of PA levels, further channeling fatty acids towards TAG and/or phospholipid biosynthesis. Fatty acids required for lipid synthesis in *T.gondii* are either obtained from the host (Ramakrishnan *et al.*, 2012, 2015; Nolan, Romano and Coppens, 2017; Pernas *et al.*, 2018; Amiar *et al.*, 2019) and/or synthesized *de novo* via the apicoplast FASII (Mazumdar and Striepen, 2007; Amiar *et al.*, 2016). In order to identify the source of increased phospholipids and toxic FA observed upon *Tg*LIPIN depletion, we set up fluxomics approaches where we grew parasites and/or host cells using different stable isotope substrates-containing media (^{13}C-U-Glucose, ^{31}d-C16:0) and performed lipidomic analyses for each experimental setup (Fig. 6a,b,c) .

First, parasites were labelled with ^{13}C-U-Glucose, which was added to a glucose free medium, to confluent host cells together with parasites with or without ATc to monitor *de novo* FASII activity (Fig. 6a**)**. Total lipid content, including both FFA and FA originating from glycerolipids, was extracted to determine the ratio of ^{13}C incorporation to each FA as a measure of FASII activity. In *Tg*LIPIN-ikD (+ATc), the amount of labelled FA made by FASII was overall similar to the control (-ATc) in terms of both total lipid content (Fig. 6d) and the FFA pool (Fig. 6e). This suggested that both phospholipid and FFA increase in *Tg*LIPIN deficient strain does not rely on the *de novo* fatty acid synthesis. We then assessed the FASII activity in both normal and *Tg*LIPIN depleted parasites. In the *Tg*LIPIN-ikD (+ATc), there was a significant reduction in percentage of ^{13}C labelling in C14:0, the major FASII product (Fig. 6f)**.** Distribution of ^{13}C incorporation to each isotopologue of FASII FA product confirmed that the pathway was nevertheless functional (Fig S5a, b). This suggests that although the *Tg*LIPIN depleted parasites do not source FA from FASII, its activity is slightly reduced in the mutant.

In order to monitor the FAs sourced from the external environment/culture medium, we grew parasites and confluent host cells in a medium supplemented with deuterated palmitic acid (^{31}d-C16:0) (Fig. 6c**.** Parasites were harvested and total lipids were extracted to determine the incorporation of ^{31}d-C16:0 in parasite lipids. In the total lipid content, ^{31}d-C16:0 and its elongation/desaturation product ^{29}d-C18:1 were detected in a similar amount in the *Tg*LIPIN-ikD parasites with or without ATc (Fig. 6g). However, a reduction in the d31-C16:0 incorporation to

FFA species within *Tg*LIPIN-ikD (+ATc) in comparison to the control (-ATc), further abolished host external environment as the source of increased lipids within the mutant (Fig. 6h).

To monitor the fatty acids directly scavenged from the host, we designed a novel assay using U-^{13}C-Glc to label host lipids (Fig. 6b). Non confluent host cells were grown in the presence of medium containing U-^{13}C-Glc which would theoretically fuel any of the active FA synthesis pathways within the host (FASI, elongases) via the synthesis of their substrates, acetyl-CoA, thereby generating ^{13}C-pre-labelled host metabolites including lipids and fatty acids (Mashima, Seimiya and Tsuruo, 2009). These ^{13}C-pre-labelled host cells were then infected with parasites in the presence of normal culture medium, which contains regular ^{12}C-Glc. Then total lipid was extracted from the parasites to determine the ratio of ^{13}C incorporation to each fatty acids to determine the origin from the host or not. Using this novel approach, we were able to determine (i) the FA biosynthetic capacities of the host cells (Fig. 6i), and more importantly (ii) the first scavenged FA lipidome of the parasite (Fig. 6j). Host, human foreskin fibroblast (HFF), are capable of synthesizing FA ranging from C14:0 to C20:1, with the most abundant FA species being C18:1 (Fig. 6i). The wild type (*Tg*LIPIN-ikD -ATc) parasites are capable of scavenging all these FA species made by the host cell with a major preference again for C18:1 (Fig. 6j**)**. Importantly, in *Tg*LIPIN-ikD +ATc parasites, both total lipid and FFA exhibited significantly increased ^{13}C incorporation from host FA in comparison to the control strain (-ATc) (Fig. 6j). This strongly supports that the origin of FA source for the excess phospholipids and FFA in *Tg*LIPIN-iKD+ATc is the host (Fig. 4e,5d). In terms of individual FA species, C16:0 and C18:0 were significantly increased in the FFAs derived from the *Tg*LIPIN mutant (+ATc) (Fig 6k). Furthermore, analysis of the molecular species in the most abundant phospholipid, PC, showed a significant increase of host derived C18:1 in *Tg*LIPIN mutant (+ATc) (Fig 6l). Together, this data correlating with our previous results also suggests that the *Tg*LIPIN specifically fuels PA enriched in oleic acid (C18:1) towards phospholipid synthesis and simultaneously channels DAG and FFAs-C16:0/18:0 for TAG synthesis.

DISCUSSION

Our data here shows that *Tg*LIPIN is a phosphatidate phosphatase controlling the flux of FAs towards either phospholipid synthesis or storage, disruption of which has multiple phenotypic consequences within the parasite (Fig. 7).

In *Saccharomyces cerevisiae*, lipin acts as a Mg2+ dependent phosphatidate phosphatase catalyzing the biochemical conversion of PA to DAG in the route of glycerol-3-phosphate (Carman and Han, 2009). In mammalian cells, lipin is encoded by three independent genes lipin1, lipin2 and lipin3, all of which have PA phosphatase activity modulating the levels of TAGs and phospholipids (Zhang and Reue, 2017). Genetic mutation within these lipins causes severe metabolic disorders including rhabdomyolysis (lipin1), obesity (lipin1), autoinflammatory disease (lipin2) and impaired lipoprotein assembly in the intestines (lipin2 and 3) (Reue and Wang, 2019). The essentiality of lipin for *T. gondii* growth also suggests distinct function from the two other parasite PAPs. Neither *Toxoplasma* PAPs (TGGT1_247360 and TGGT1_246490) appeared to compensate for the loss of *Tg*LIPIN, which is in contrast to yeast in which deletion of gene encoding lipin was compensated, at least in part, by other PA phosphatases (Chae, Han and Carman, 2012).*Tg*LIPIN was localized widely to parasite cytosol overlapping endomembrane compartments. In other eukaryotic systems, the cytosolic lipin proteins are able to translocate to various membrane depending on the availability of their substrate PA and/or in response to stimuli such as fatty acids (Zhang and Reue, 2017). These phosphatidate phosphatases also translocate to the nuclear compartment and act as transcriptional regulators, e.g. lipin1 acts as an inducible amplifier of PGC1 alpha/PPAR alpha pathway in hepatocytes (Finck *et al.*, 2006). Like its human counterpart, yeast Pah1 has implications in UASINO-containing genes, and the growth of the nuclear/ER membrane (Carman and Han, 2009). Therefore, it is conceivable that *Tg*LIPIN might be quite dynamic and the perinuclear localization we see in part might be more prominent if it is activated more so to embed it into the ER, nuclear membrane. The *Tg*LIPIN mutant hints at an probable link between metabolism and the nucleus of the parasite.

Metabolic regulation of TgLIPIN

Of note, unlike other enzymes of the TAG biosynthetic pathway, Pah1 and lipins lack transmembrane domains and therefore must first translocate onto membranes in order to generate DAG. This step is inhibited by multisite phosphorylation, mediated by Pho85, Cdc28, and protein

kinase A in yeast (Choi *et al.*, 2012; Su *et al.*, 2012) and target of rapamycin (TOR) and mitotic kinases in mammals (Harris *et al.*, 2007; Grimsey *et al.*, 2008). In continuation with this, we observed a hypophosphorylation at a serine residue (amino acid position-1019) of *Tg*LIPIN protein in a phospho-proteomic screen of a cyclin-dependent protein kinase-*Tg*CDPK7 knockout strain (unpublished data). This suggests the possibility of *Tg*CDPK7 as the kinase regulating *Tg*LIPIN via phosphorylation.

In contrast, dephosphorylation of Pah1 in yeast is catalysed by the highly conserved transmembrane Nem1-Spo7 complex (Siniossoglou, 1998; Santos-Rosa *et al.*, 2005), which is also required for Pah1 membrane recruitment and activation (O'Hara *et al.*, 2006; Karanasios *et al.*, 2010; Choi *et al.*, 2012). Dullard, a homolog of Nem1p in mammalian cells is involved in dephosphorylation of phosphatidate phosphatase, which further generates a phosphate cascade consequently regulating nuclear membrane biogenesis (Kim *et al.*, 2007). Using bioinformatic screen, we identified the *T. gondii* Nem1p/Dullard homolog and named it *Tg*DULL. *Tg*DULL is a predicted protein phosphatase harboring a HAD domain and upon endogenous tagging with 3xHA, the protein localized to the endoplasmic reticulum of the parasite (Fig. S7). The protein functional domain and localization of *Tg*DULL present it as a strong candidate as the master regulator of *Tg*LIPIN. This however needs further experimental proof showing an effect on the phosphorylation status and localization of *Tg*LIPIN upon genetic disruption of *Tg*DULL.

Implications of lipid changes on phenotype of TgLIPIN mutant: Phospholipid and TAG biosynthesis

One of the early phenotypic stress evoked in *Tg*LIPIN mutant was its impact on major membranes including the nuclear envelope complexed with the ER and the parasite inner membrane complex. Downregulation of lipin and its homologs in other eukaryotes impacts nuclear membrane biogenesis. In addition to their critical role in yeast lipid metabolism, mutant strains lacking pah1 gene display a striking expansion of the ER and the nuclear membrane. (Santos-Rosa *et al.*, 2005; Siniossoglou, 2009). Fission yeast cells lacking the Pah1 orthologue Ned1 also display the peculiar nuclear defect (Tange, Hirata and Niwa, 2002). There are evidences that suggest that the nuclear membrane biogenesis is directly linked to PA metabolism. In Δpah1 yeast, mutations in upstream biosynthetic steps of the glycerolipid pathway that lower PA levels also reduced the aberrant expansion of nuclear membrane (Han *et al.*, 2008). Effects of pah1 deletion could be phenocopied

by overexpression of Dgk1p, a novel nuclear/ER membrane DAG kinase that generates PA(Han *et al.*, 2008). Catalytically inactive Pah1 retains its nuclear membrane capability, but lipid precursors are redirected toward phospholipids instead of storage TAGs, thereby resulting in deformation of nuclear membrane (Barbosa *et al.*, 2015). Another hypothesis for the same could be increased phospholipid biosynthesis due to PA accumulation via the CDP-DAG pathway (Fig. S4a), as has also been shown in Δpah1 yeast (Han *et al.*, 2008).

In apicomplexa biology, a recent study demonstrated that use of DGAT inhibitor-T863 to inhibit lipid storage capacity in *T. gondii* resulted in rapid accumulation of membranous structure accompanied by rapid parasite death due to strong replication defect (Nolan *et al.*, 2018). This cytopathy was restricted mainly to the endomembrane system, i.e. ER and the associated nuclear envelope, during the early time points of treatment, similarly as in case of *Tg*LIPIN depletion. The electron micrographs of the *Tg*LIPIN mutant (+ATc) clearly suggest that the replication arrest was due to accumulation of excessive membranes within the parasite. The replication arrest within the parasite is possibly directly linked to aberrant IMC biogenesis. The IMC is one of the first membranes recycled directly from the mother cell into progeny, thus playing key role in the process of parasite endodyogeny (Ouologuem and Roos, 2014).

Phosphatidic acid is the central precursor for all glycerophospholipids as well as triglycerides thereby residing at a pivotal metabolic bifurcation point. In the *Tg*LIPIN mutant an accumulation of PA redirects the pathway towards increase in phospholipids via the liponucleotide cytidine diphosphate-diacylglycerol (CDP-DAG). This is complemented by the utilization of excess free fatty acids into phospholipids, partially circumventing their inability to be sequestered into storage triglycerides. We observed an overall increase in the major membrane phospholipids including cardiolipin (CL) and phosphatidylserine (PS) which are indeed derivatives of the CDP-DAG pathway in other eukaryotes (Fakas, Konstantinou and Carman, 2011). Other than this we also observed an increase in the major membrane phospholipid PC, which could be channeled via increased PS through Kennedy pathway. Based on existing literature another plausible explanation of lipids excess could be the involvement of increased PA levels in de-repression of phospholipid biosynthesis genes expression, as has been reported in eukaryotic model yeast. The yeast lipin mutant pah1Δ is characterized by accumulation of PA which contributes to increased phospholipid biosynthesis by sequestering transcriptional oppressor Opi1acting against transcriptional

activators Ino2p/Ino4p (Han, Wu and Carman, 2006; Han, Siniossoglou and Carman, 2007). Additionally, Pah1 has also been reported to be a part of the protein complex that binds DNA to block transcription from promoters of genes transcriptionally controlled by INO1 and OPI1 (Santos-Rosa *et al.*, 2005). In *Toxoplasma*, an immunoprecipitation with the HA-tagged *Tg*LIPIN could provide major insights into its possible role in transcriptional regulation of genes involved in phospholipid biosynthesis. By defining the protein-interacting partners of *Tg*LIPIN, several regulatory mechanisms can also be elucidated.

The triacylglycerol content in *Tg*LIPIN mutant decreases only 48 h post protein downregulation with ATc suggesting that due to decrease in the substrate-specific DAG species because of *Tg*LIPIN unavailability, the parasite is unable to acylate the free fatty acids to generate its subsequent product TAG. We did not detect any significant changes between the cholesteryl ester species (Fig. S4c) in the mutant vs wild type strain, further strengthening the reaction specificity of *Tg*LIPIN towards TAG biosynthesis.

In mammalian cells the inhibition of triglyceride synthesis leads to oleic acid (C18:1) induced lipotoxicity (Listenberger *et al.*, 2003). Thus, lipid droplets act as more than just cellular energy reserves by protecting the cells from deleterious effects of toxic excess free fatty acids by their incorporation into TAGs.

Nutrient sensing and host mediated remodeling of parasite lipids

By pre-labelling the host fibroblast cells with U-^{13}C-Glucose, we were able to track the source of excess fatty acid and phospholipid content in the *Tg*LIPIN mutant. In keeping with previously reported data, using ^{13}C-fluxomics we observed that the parasite has a specific preference for scavenging oleic acid (C18:1) directly from host (Pernas *et al.*, 2018). Existing literature provides a strong evidence of involvement of C18:1 is TAG biosynthesis and subsequent LD formation in mammals (Listenberger *et al.*, 2003) as well as parasites (Nolan *et al.*, 2018). Thus, the excess oleate within the parasite sourced directly from the host has a strong correlation to the lipid storage defect in *Tg*LIPIN mutant. In *T. gondii* the salvage of C18:1 from host environment is in part utilized for phospholipid synthesis resulting in extra membranous structures, further impeding the process of endodyogeny (Nolan *et al.*, 2018). With the model of *Tg*LIPIN parasite mutant we propose that the host participates in active remodeling of parasite phospholipids as well as neutral lipids. This is directly rooted to our observation of the difference between phosphatidic acid FA

molecular species in the mutant in comparison to the wild type, with a significant rise in the levels of C18:1 specifically in the mutant. Such phospholipid remodeling has also been reported in the yeast mutant where deletion of Pah1 results in an increase (22–27%) in palmitoleic acid and a decrease (17–21%) in oleic acid (Fakas, Konstantinou and Carman, 2011). We were able to detect an increase in the host-derived (^{13}C labelled) oleic acid within the parasite phosphatidylcholine. However, we could not detect any ^{13}C labelling in the parasite PA. The plausible explanation behind this is the dynamic nature of PA that is rapidly utilized for membrane phospholipids and other signaling derived events.

Meanwhile, the reduction in prokaryotic type-FASII activity in response to increased amount of fatty acids within the parasite suggests adaptation of parasite to nutrient sensing. In the case of *Tg*LIPIN mutant an increase of fatty acids derived from host signals the parasite to stagnate its FASII activity. Similar observations on metabolic plasticity show that there is a reduction in growth of *P. falciparum* FASII KO mutant in the presence of nutrient-deprived culture conditions (Amiar *et al.*, 2019). Another study in bacteria shows that the FASII pathway is repressed in a negative feedback loop mediated by acyl-CoA (Fujita, Matsuoka and Hirooka, 2007). Taken together, it can be concluded that *Tg*LIPIN is one of key proteins regulating major fatty acid fluxes from the host as well as apicoplast into parasite membrane and storage lipids. Furthermore, indispensability of *Tg*LIPIN suggests the importance of maintaining the lipid homeostasis by control of critical levels of PA.

METHODS AND MATERIALS

Sequence analysis and structure generation

*Tg*LIPIN (TGGT1_230690) and *Pf*LIPIN (Pf3D7_0302300) were identified using EuPathDB web sources ToxoDB (http://toxodb.org/toxo/) and PlasmoDB (http://plasmodb.org/plasmo/) respectively. A phylogenetic tree of lipin proteins in several eukaryotes was created using the online platform Phylogeny.fr. The organisms used for lipin protein sequences for generation of the phylogenetic tree include: *Toxoplasma gondii* (TGGT1_230690), *Plasmodium falciparum* (PF3D7_0303200), *P. berghei* (PBANKA_040180) , *Homo sapiens* (NX_Q14693), *H. sapiens* (NX_Q92539), *H. sapiens* **(**NX_Q9BQK8), *Saccharomyces cerevisiae* _PAH1 (PAP1, SMP2, YMR165C, YM8520.14C), *Cyrptosporidium parvum* (cgd3_3210), *Cyanidioschzyon merolae*

(CYME_CMN061C), *Neospora caninum* (BN1204), *Hammondia hammondi* (HHA_230690), *Chlamydomonas reindhartii* (CHLRE_12g506600v5), *Arabiodopsis thaliana*_AtPAH1 (At3g09560), *Arabidopsis thaliana*_AtPAH2 (At5g42870), *Leishmania major* (LMJF_06_0830), *Trypanosoma brucei* (Tb927.7.5450), *Chromera velia* (Cvel_24403). First step involved the curation of these protein sequences. The protein sequences were aligned (ClustalW) and then gaps were removed from the alignment. Finally, the phylogenetic tree was constructed using the maximum likelihood method in the PhyML program. The default substitution model (WAG) was selected. Graphical representation and edition of the phylogenetic tree were performed with Cladogram.

T. gondii strains and cultures

The parasite host cells human foreskin fibroblasts (HFF) were cultured using Dulbecco's Modified Eagle's Medium (DMEM, Gibco) supplemented with 10% fetal bovine serum (FBS, Gibco), 2 mM glutamine (Gibco) and 25 µg/mL gentamicin (Gibco) at 37°C and 5% CO2.

T.gondii tachyzoite parental strains RH-ΔKu80 TATi, RH-ΔKu80 as well as mutant strains *Tg*LIPIN-iKD, *Tg*LIPIN-3*HA were propagated by serial passage within their host HFF using DMEM supplemented with 1% fetal bovine serum (FBS, Gibco), 2 mM glutamine (Gibco) and 25 µg/mL gentamicin (Gibco) at 37°C and 5% CO2.

Generation of HA-tagged and inducible knockdown line for TgLIPIN

A C-terminally tagged HA line was generated expressing from the gene's endogenous locus using the classical pLIC strategy using homologous recombination in a RH-ΔKu80 strain. For the same, a 1677 bp homology region of *Tg*LIPIN located towards to C-terminus excluding the stop codon, was amplified from the parasite genomic DNA using the primers forward 5'-TACTTCCAATCCAATTTAATGCACGGCAGATTTCTCTTACTGG-3' and reverse 5'-TCCTCCACTTCCAATTTTAGCCAAATTACTGCATTTGCGTTCAC-3'. The homology region was assembled into *PacI* digested pLIC-HA-DHFR plasmid using ligation independent cloning protocol (Huynh and Carruthers, 2009). The assembled plasmid with linearized with single enzyme site specific to the parasite DNA sequence within the plasmid-*NsiI* just before transfection. Parasites were selected with the drug pyrimethamine and cloned by limiting dilution.

For generation of inducible knockdown plasmid pPR2-DHFR (Katris *et al.*, 2014), two separate homology flanks were chosen. The 5' flank was amplified 1637 bp upstream of the *Tg*LIPIN start codon using the primers forward 5′-GGGCGCGCCGGATCCTTAATTAATCGAGAATTCCAAACATCGATGCG-3' and reverse 5′- TGGATCCGGCGCGCCATGCATCCTGGACCAGAGAGGAAAAGAG-3'. The pcr product was ligated to *PacI* and *NdeI* digested vector pPR2 using NEB assembly reaction. Next, the 3' flank was amplified as a 1739 bp fragment beginning at the start codon of *Tg*LIPIN with the primers forward 5′-TGTTCCAGATTATGCCTTACCCGGGATGTGGGGGAAGATTGTCTCGAGC-3' and reverse 5′- GCACTGACTGGCATGAATGGCCAGGCGCTGCCTTCTTTCCATTC-3'. The 3' homology flank was annealed to *XmaI* and *NotI* digested pPR-HA3-DHFR vector that already contained the *Tg*LIPIN 5' flank. The final cloned vector positions the start codon of *Tg*LIPIN downstream of the ATc-regulatable t7s4 promoter and a 3xHA tag. The resulting vector with *Not*I and transfected this into TATiΔku80 parasites. Parasites were selected with the drug pyrimethamine and cloned by limiting dilution.

Screening of parasite clones where the t7s4 promoter had successfully replaced the native *Tg*LIPIN promoter, was done using the primers P1 5'- CGATGACCTGTGTCGACCTGT-3' P2 5′-TCTTCTTTGAGGGAAGAGGAAACG-3', P3 5'- GGTACCGAGCTCGACTTTCAC-3', P4 5'- CAGCTGATCGGAGGTTGGTCT-3' and P5 5'- CTCCACCGTTTCCGGTTCCGT-3' in the combinations described in supplementary fig S2. All PCRs were performed with TaKara primestar max polymerase. The knockdown of *Tg*LIPIN was induced with 0.5 μg ml^{-1} of anhydrotetracycline (ATc).

Generation of HA-tagged and inducible knockdown line for PfLIPIN

A transgenic *P. falciparum* line was generated using riboswitch based glmS system in which *Pf*LIPIN was tagged at the C-terminus with 3×HA. The construct used for transfection, ptex-HAglmS, contained 867 bp of homology sequence (3' homology region) immediately upstream of the stop codon of *Pf*LIPIN (Pf3D7_0303200). The 3' homology flank was PCR amplified from *P. falciparum* 3D7 genomic DNA (gDNA) with the primers forward ACGTAACAGACTTAGGAGGAGATCTGTGAAATAACAGAGCATATGTTTCC and reverse GGACGTCGTACGGGTAAGCTGCAGGTATATGAATGTTAGTGACAGTAGC and

cloned into the *Bgl*II and *Pst*I sites of ptex-HAglmS using neb assembly reaction mix (Counihan *et al.*, 2017). Asexual ring stage 3D7 parasites were transfected with the final construct *Pf*LIPIN-ptex-HAglmS. Transgenic parasites were selected with 2.5 nM WR99210 (Jacobus).

The positive parasite population was screened using the primers, P1 5'-GATAGAATCCGAGTAAGATATCG-3', P2 5'- CATCGTACGGATACGCATAAT-3', P3 5'-CTTGGTTTGAAGAAATCCTTACG-3', P4 5'- CGAACATTAAGCTGCCATATC-3', P5 5'-GATGCAGTTTAGCGAACCA-3' in the combinations described in Fig S2. All PCRs were performed using TaKara primestar GXL polymerase.

Immunofluorescence assay

Primary antibodies anti-HA (Rat, Roche) , anti-IMC1 (Mouse), anti-GAP45 (Mouse) were used at dilutions 1:500, 1:1000 and 1:1000 respectively. Secondary AlexaFluor 488- and 546-conjugated anti-mouse, anti-rat and anti-rabbit antibodies (Life Technologies) were used at 1/2500. For the immunofluorescence assay (IFA) parasites were grown on confluent HFF on coverslips and fixed in PBS containing 2.5% paraformaldehyde (PFA) for 15 min at room temperature (RT). Samples were permeabilized with 0.25% Triton X-100 in PBS for 10 min at RT prior to blocking in PBS containing 3% BSA and subsequent incubation with primary antibodies then secondary antibodies diluted in the blocking solution. Labelled parasites were stained with Hoechst (1/10000, Life technologies) for 20 min and then washed three times in PBS before final mounting of the coverslips on a glass slide using fluorogel. The IFA slides were visualized using fluorescence microscope (Axio Imager 2_apotome; ZEISS).

Western blot analysis

Parasites were harvested for western blot after complete egress from their host. In order to remove any host cell debris, the parasites were passed through a 3 µm filter, then counted by hemocytometer and solubilized in SDS buffer at equivalent cell densities. Equal amount of protein was separated on a 4-12% gradient SDS-polyacrylamide (Life Technologies) and transferred to Nitrocellulose membrane (check this) using the XCellII Blot Module (Invitrogen). Primary antibodies anti-HA (Rat, Roche) and anti-TOM40 (Rabbit, Geil G Van Dooren et al 2016 JBC) were used at a dilution of 1:500 and 1:1000, respectively. Secondary goat anti-mouse and anti-rabbit horse radish peroxidase (HRP) conjugated antibodies (Thermo Scientific) were used at 1:2000. Protein signal was detected by chemiluminescence after membrane staining with luminata

crescendo western HRP detection kit (Millipore). The signal strength of protein was quantified using a BioRad chemidoc imager (BioRad).

Phenotypic analysis

Plaque assay- The extracellular parasites were harvested after filtration and counted by hemocytometer. Then approx. 500 parasites were inoculated to confluent HFF flask (25 cm^2). *Tg*ACS3-ikD was grown for plaque assay in the presence or absence of ATc (0.5 μg ml^{-1}) for 7-10 days. Plaque sizes were visualized by crystal violet staining (30-60 min) after aspiration of culture media, and cells fixation with 100% ethanol (5 min) followed by phosphate-buffered saline (PBS) wash.

Replication assay- The parasites were grown for two days with or without ATc (0.5 μg ml^{-1}), harvested and filtered. Equal number of parasites were allowed to invade confluent HFF grown on coverslips. Following 2 h of invasion, the coverslips were washed thrice with ED1 (1% FBS containing DMEM), in order to remove any uninvaded parasites and promote synchronized replication. Anhydrotetracycline (ATc) (0.5 μg ml^{-1}) was added at the outset of the experiment, allowing the treatment for 24 h, alongside control parasites without ATc. These coverslips were then fixed and processed for IFA using anti-HA, anti-SAG1 antibodies wherein the parasite number per parasitophorous vacuole was analyzed.

Electron microscopy

*T*he *Tg*LIPIN-ikD parasites were grown from 12 h and 24 h in the presence and absence of ATc, in labteks (Nunk, Thermofisher). The labteks containing parasite infected HFF were fixed in 0.1 M cacodylate buffer with 2.5% glutaraldehyde for 2 h and kept at 4°C until further processing. During processing, the sample were fixed again for 1 h with 1% osmium tetroxide in cacodylate buffer followed by overnight treatment in 2% uranyl acetate in distilled water. After dehydration in graded series of acetonitrile, samples were progressively impregnated in Epon812, the wells were then filled with fresh resin and allowed to polymerize 48 h at 60°C. Ultrathin 70 nm section were obtained with a Leica UCT Ultramicrotome and collected on copper grids. Grids were post-stained with uranyl acetate and lead citrate before their observation on a Jeol1200EXII Transmission Electron Microscope. All chemicals were from Electron Microscopy Sciences.

Nile red staining of lipid droplets

The *Tg*LIPIN-ikD parasites were allowed to infect and grow in confluent monolayer HFF grown on coverslips, in the +/- ATc conditions for 24 h and 48 h. Similar to IFA, these coverslips were fixed using 2.5% PFA, permeabilized with 0.25% triton X-100 and then stained with primary rat anti-HA antibody followed by detection with secondary AlexaFluor 488- conjugated goat anti-rat antibody. Thereafter, the sample coverslips were incubated for 1 h with nile red in 1X PBS before proceeding to DNA staining with Hoechst. The coverslips were mounted onto a glass slide in fluorogel prior to imaging using fluorescence microscope (Axio Imager 2_apotome; ZEISS). For visualizing nile red stained droplets yellow-gold fluorescence (excitation, 450-500 nm; emission, greater than 528 nm) (Greenspan *et al.,* 1985) was used on the axio-imager. Quantification in +/- ATc condition was done by counting the no. of lipid droplets per parasite vacuole.

Heterologous complementation

Codon-optimized carboxy terminal lipin sequence (548-765 a.a) harboring the catalytic HAD domain (DVDGT), obtained from GenScript was ligated to *NotI/MluI* digested pD0170 yeast expression vector (obtained from Carman's lab). Cloned vector CLIP *Tg*LIPIN-pD0170 was transformed into yeast strain Δ*dpp1*Δ*lpp1*Δ*pah1* (kind gift from Dr. George Carman's lab, Rutgers Center for Lipid Research, New Jersey) and the transformants were screened on solid SD medium containing YNB agar lacking histidine, tryptophan, leucine, and uracil. Positive transformants were then proceeded for temperature sensitivity assay using drop-test. Briefly, the WT yeast strain, untransformed yeast strain Δ*dpp1*Δ*lpp1*Δ*pah1* positive transformants from the plate were grown respectively in YPD and SD medium (Ura-, His-, Trp-and Leu-) to reach to $O.D_{600}$ value 1. This culture was then diluted ten-fold, up to 5 times in a 96-well plate (first well is undiluted, 2^{nd} 10^{-1} dilution, 3^{rd} 10^{-2} dilution etc) and 5ul of each dilution was drop plated onto YPD agar plate. The plate was allowed to soak the yeast drop culture for up to 10-15 min prior to further incubation. The experiment was performed in duplicate to be tested for growth at 30°C and 37°C separately for at least 48 h post inoculation.

Lipidomic analysis

The parasites were grown for 24 h ad 48 h in +/- ATc conditions within a confluent monolayer of HFF in flasks (175 cm^2). At each time point, parasites were harvested as intracellular tachyzoites (1×10^7 cell equivalents per replicate) after syringe filtration with 3-µm pore size membrane.

These parasites were metabolically quenched by rapid chilling in a dry ice-ethanol slurry bath and then centrifuged down at 4˚C. The parasite pellet thus obtained was washed with ice-cold PBS thrice, before transferring the final pellet to a microcentrifuge tube. Then total lipids were extracted in chloroform/methanol/water (1:3:1, v/v/v) containing PC (C13:0/C13:0), 10 nmol and C21:0 (10 nmol) as internal standards for extraction. Next, the polar and apolar metabolites were separated by phase partitioning by adding chloroform and water to give the ratio of chloroform/methanol/water as 2:1:0.8 (v/v/v). For lipid analysis, the organic phase was dried under N_2 gas and dissolved in 1-butanol to obtain 1µl butanol/10^7 parasites.

Total lipid analysis – The extracted total lipid sample was then added with 1 nmol pentadecanoic acid (C15:0) as internal standard and online derivatized to give fatty acid methyl ester (FAME) using trimethylsulfonium hydroxide (TMSH, Machenery Nagel) for total glycerolipid content. Resultant FAMEs were then analyzed by GC-MS as previously described (Dubois et al. 2016). All FAMEs were identified by comparison of retention time and mass spectra from GC-MS with authentic chemical standards. The concentration of FAMEs was quantified after initial normalization to different internal standards and finally to parasite number.

Free fatty acid and cholesterol analysis - Total lipid was dried and derivatized with BSTFA+TMCS, 99:1 (Sigma) to generate trimethylsilyl (TMS-) fatty acids and TMS-cholesterol. These TMS derivatives were analyzed by GCMS as described above.

Phospholipid and neutral lipid analysis- For phospholipid analysis, the extracted **t**otal lipid extracted (as above) was separated with 1 nmol PA(C17:0/C17:0) (Avanti Polar lipids) by two-dimensional silica gel high-performance thin layer chromatography (HPTLC, Merck). The solvent system used for the 1st and 2nd dimension was chloroform/methanol/28% ammonium hydroxide,12:7:1.6 (v/v) and chloroform/acetone/methanol/acetic acid/water, 10:4:2:2.6:1 (v/v/v/v/v), respectively. For DAG, TAG, Free fatty acids (FFA) and cholesteryl ester (CE) analysis, total lipid fraction was separated by 1D-HPTLC using hexane/diethyl ether/formic acid, 80:20:2 (v/v/v) as solvent system. Then each lipid spot on the HPTLC plate was scrapped off and lipids were methanolized with 200 µl 0.5 M methanolic HCl in the presence of 1 nmol pentadecanoic acid (C15:0) as internal standard at 85ºC for 3 h. The resulting FAMEs were extracted with hexane and analyzed by GC-MS (Agilent).

Stable isotope metabolic labelling experiment

Tracking FASII origin fatty acids - The *Tg*LIPIN parasites were infected to confluent monolayer of HFF in glucose free-DMEM (1% FBS) supplemented with U-^{13}C-glucose or U-^{12}C-glucose at a final concentration of 800 µM, with or without ATc (0.5 µg ml^{-1}). The parasites were harvested up to 48 h post depletion of *Tg*LIPIN and metabolically quenched as described previously (Amiar et al 2016). Lipid were extracted, derivatized using TMSH (Macherey-Nagel) and analyzed by GC-MS as described above. ^{13}C incorporation to each fatty acid was calculated as the percent of the metabolite pool containing one or more ^{13}C atoms after correction for natural abundance and the amount of ^{13}C-carbon source in the culture medium. The degree of the incorporation of ^{13}C into fatty acids (%carbon incorporation) was determined by the mass isotopomer distribution (MID) of each FAMEs. MID was obtained from the shift in isotopic mass dependent on the amount of ^{12}C carbons compared to the integration of ^{13}C carbon atoms. The total abundance of ^{13}C-labelled fatty acids was obtained by calculating the concentration of all isotopomers of ^{13}C-labelled FAMEs and finally normalizing to authentic internal standards and parasite number.

Tracking host-derived fatty acids -

The HFF cells were grown (1×10^8 cell equivalents per replicate) to confluency in the presence of stable isotope U-^{13}C-glucose at a final concentration of 800 µM added to a glucose-free DMEM. These ^{13}C-pre labelled HFF were then infected with *Tg*LIPIN-iKD parasites in the presence of normal-glucose containing DMEM under +/-ATc (0.5 µg/ml). The host HFF and parasites were metabolically quenched separately, and their lipid content was quantified by GC-MS as described above. As described previously, the degree of the incorporation of ^{13}C into fatty acids (%carbon incorporation) is determined by the mass isotopomer distribution (MID) of each FAMEs. The total abundance of ^{13}C-labelled fatty acids was analyzed initially for HFF to check labelling of the metabolites (described previously). Later, the same was calculated for parasites to confirm direct uptake of ^{13}C-labelled fatty acids from the host.

Tracking uptake of deuterated fatty acid from medium (host environment)-

Deuterated palmitic acid (^{31}d-C16:0) was dissolved in 10 mM in fatty acid-free bovine serum albumin/PBS solution by sonication in water bath for 30 min followed by incubation at 55ºC for 30 min. Freshly egressed *Tg*LIPIN parasites were allowed to invade a confluent monolayer of HFF for at least 2 h under conditions of +/- ATc. Following invasion, the uninvaded parasites were

washed off with DMEM and further allowed to grow in the normal culture medium-DMEM (1% FBS) containing ^{31}d-C16:0 at a final concentration of 0.1 mM in +/- ATc until 24 and 48 h of growth. The parasites were harvested by metabolic quenching as described previously. Lipid were extracted, derivatized using TMSH as well as TMS and further analyzed by GC-MS (described previously)

Statistical analysis for all experiments

Entire graphical data for this study was generated using GraphPad prism software. Three biological replicates were used per experiment (n=3). The error bars are representative of standard error of mean (SEM) for each study. Statistical significance was determined for each experiment by t-test using GraphPad Prism. Range of statistical significance was signified as per the p value, wherein 0.01-0.05=*, 0.01-0.001=** and <0.001=***.

FIGURES

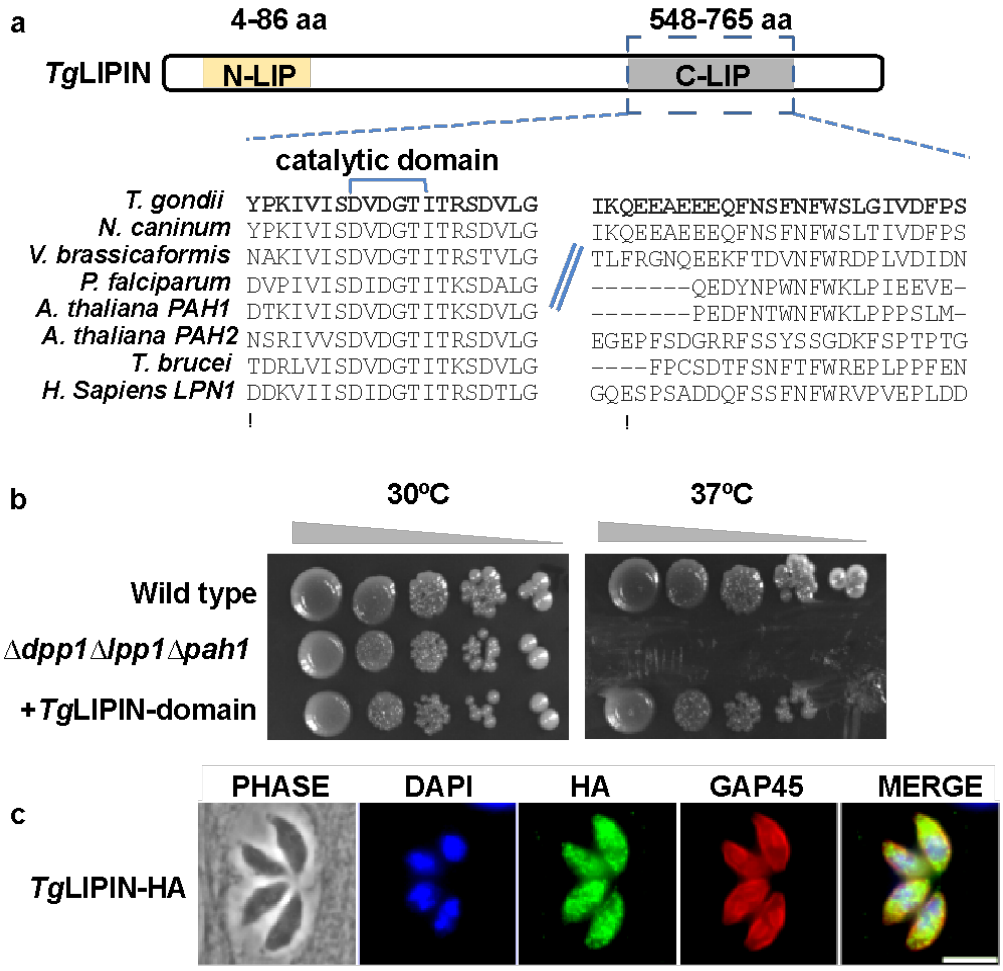

Fig. 1 T. gondii LIPIN (TgLIPIN) is a phosphatidate phosphatase localized to parasite cytoplasm

a) The C-LIP domain of *Tg*LIPIN is evolutionarily conserved amongst eukaryotic orthologs and harbors the catalytic motif DVDGT known to be central to PA phosphatase activity. b) Yeast drop-test shows the rescue of temperature sensitive phenotype of Δ*dpp1*Δ*lpp1*Δ*pah1* (PA-deficient strain) through heterologous complementation with *Tg*LIPIN C-LIP domain (panels 2 and 3 from top). c) IFA of *Tg*LIPIN-HA (endogenous C-terminal tag) with anti-HA and anti-GAP45 antibodies, shows disperse cytoplasmic localization of the enzyme. Scale bar: 2.0 µm.

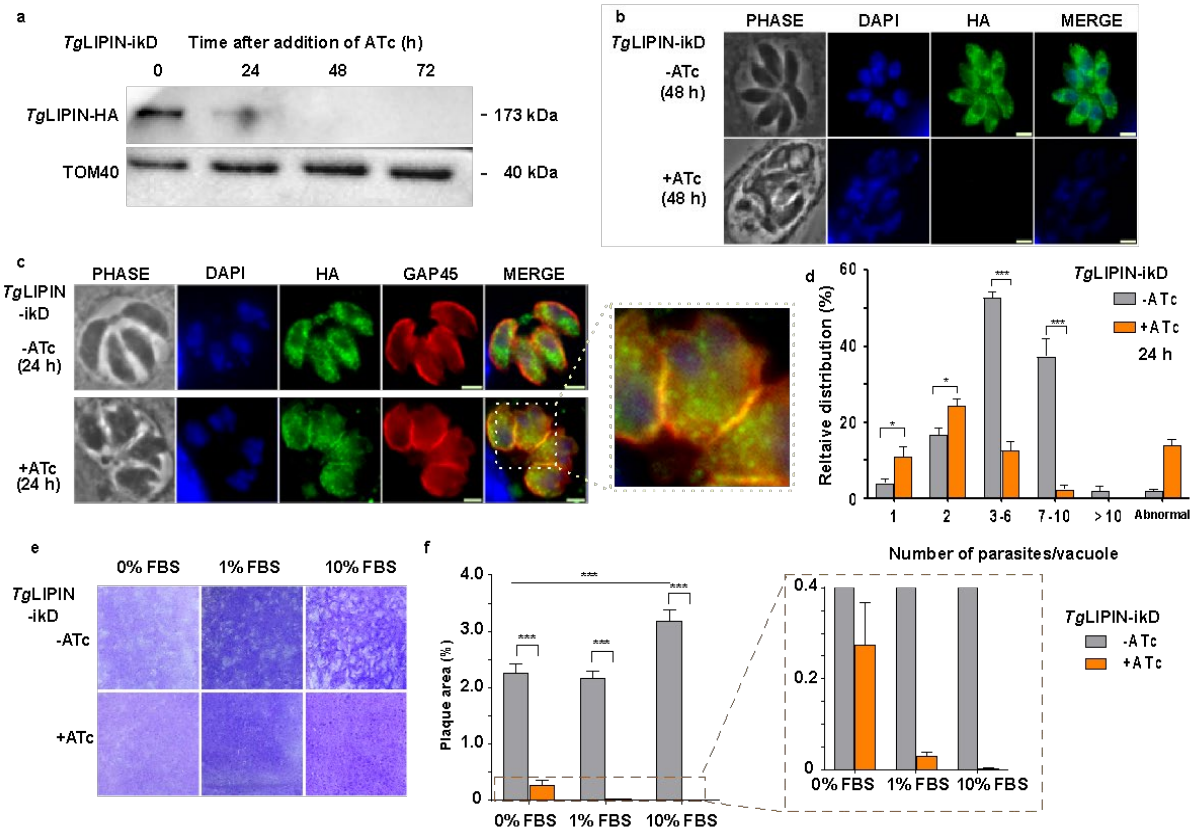

Fig. 2 TgLIPIN is indispensable for parasite replication and growth within its host

a) Western blot shows *Tg*LIPIN downregulation in *Tg*LIPIN-ikD parasite line, 48 h + ATc (0.5 µg/mL). *Tg*LIPIN (173 kDa) was probed with anti-HA antibody and TOM40 (40 kDa) was used as the loading control. b) IFA of *Tg*LIPIN-ikD, indicating loss of protein using anti-HA antibodies (panel 3: +ATc) at 48 h +ATc. Phase panel of *Tg*LIPIN+ATc (48 h) illustrates gross morphological anomalies arising because of *Tg*LIPIN depletion. c) IFA illustrating early phenotypic effects of *Tg*LIPIN depletion (24 h+ ATc). Panel 3 with HA (-/+ATc) shows presence of residual protein. DNA staining with hoechst (panel 2) and inner membrane complex staining (IMC) with anti-GAP45 antibody (panel 4,5) clearly shows aberrant nuclear and IMC membrane biogenesis. d) Replication rate of *Tg*LIPIN parasites grown with (+) or without (−) ATc measured by parasite number per parasitophorous vacuole after 24 h of growth post infection. >100 vacuoles were counted per biological replicate, error bars=standard error of the mean. Strong replication defect in represented in the form of increase in vacuoles having 1 and 2 parasites in the +ATc (orange bar) vs –ATc (grey bar). Scale bar=2.0 µm e) *Tg*LIPIN-ikD plaque assays measuring parasite growth over 8-10 days (+/-ATc) in different FBS conditions (0%,1% and 10%). f) Comparison between the growth rates was done by calculation of mean plaque area per sample using ImageJ software, between different FBS conditions in the presence or absence of ATc in *Tg*LIPIN-iKD.

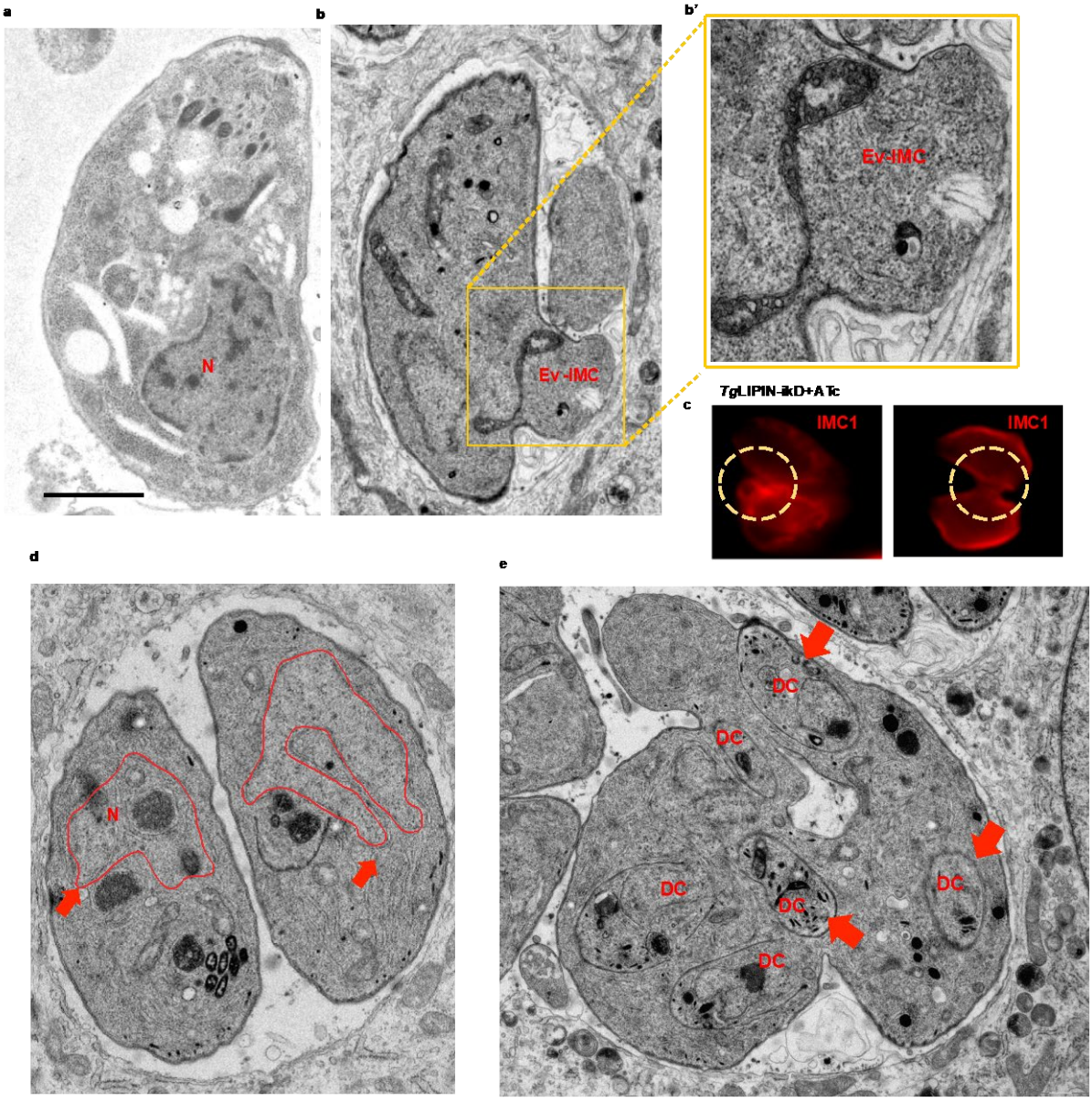

Fig.3 TgLIPIN depletion results in gross membrane anomalies early on during the process of ATc downregulation

a) Transmission electron micrograph representing a normal parasite with regular nucleus and other endomembrane organelles. b) TEM image showing evaginated IMC (encircled and zoomed in image b'), in *Tg*LIPIN-ikD + ATc (12 h). c) IFA representation of aberrant IMC biogenesis s in the *Tg*LIPIN-ikD (24 h +ATc) parasites by probing with anti-IMC1 antibody (red). d) The nuclei in *Tg*LIPIN-ikD (24 h +ATc) parasites appear multi-lobed characterized by membranous extensions into the cytoplasm, marked with red overlay on the electron micrograph. e) *Tg*LIPIN-ikD (24 h + ATc): Intracellular replication defect represented as multiple daughter cells (DC) arrested within two parasite mother cells.

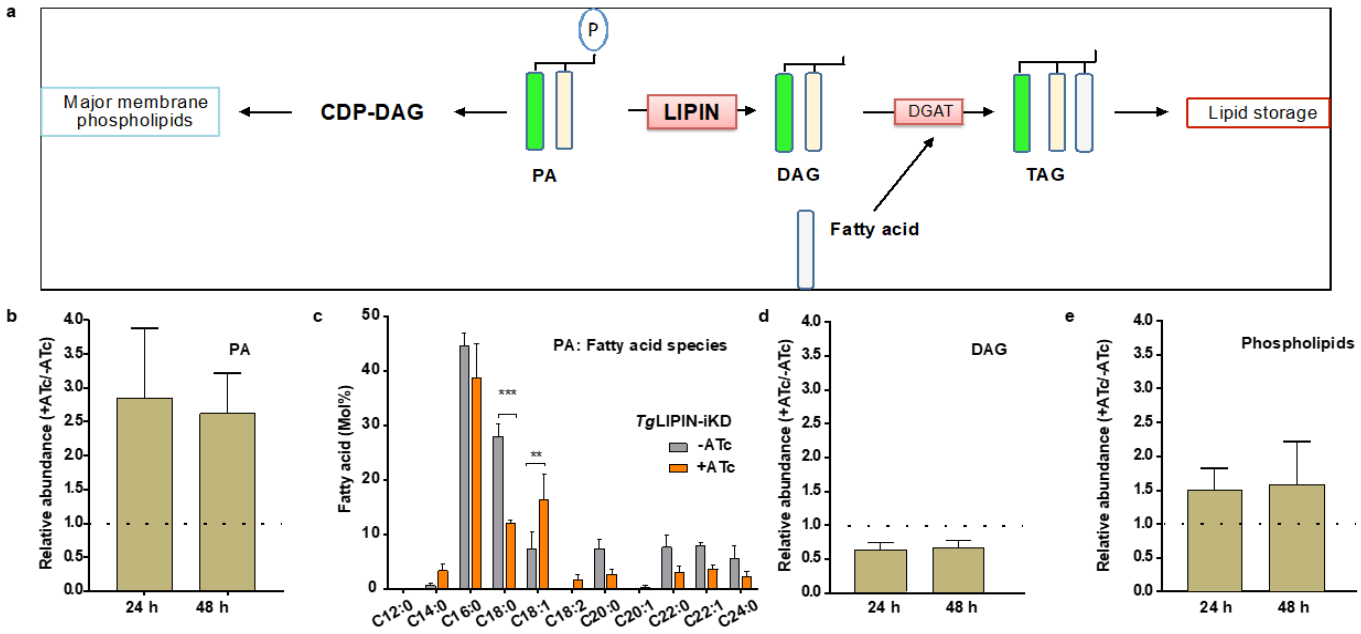

Fig. 4 TgLIPIN regulates critical levels of PA and other major phospholipids

a) Representative glycerolipid biosynthesis pathway in eukaryotes. *Tg*LIPIN catalyzes the biochemical conversion of PA to DAG. PA, can be channeled into major membrane phospholipids through CDP-DAG pathway. On the other hand, DAG generated by catalytic action of *Tg*LIPIN is specifically channeled towards triglyceride biosynthesis (TAGs) b) Relative abundance of PA in *Tg*LIPIN-iKD (24 h and 48 h +ATc) is represented as ratio of nmol/parasite no. in +ATc and –ATc. *Tg*LIPIN depletion induces approx. 3-fold rise PA relative abundance in the +ATc vs –ATc conditions. c) Fatty acid composition of PA in *Tg*LIPIN-ikD (+/-ATc) in Mol%. d) Relative abundance of DAG (+ATc/-ATc) is reduced almost to 0.5 by *Tg*LIPIN depletion (24 h and 48 h + ATc).e) Relative phospholipid abundance (+ATc/-ATc) is increased by *Tg*LIPIN depletion using +ATc for 24 and 48 h. Error bars=standard error of the mean, n=3. p values are indicated as follows: 0.01-0.05=*, 0.01-0.001=** and <0.001=***

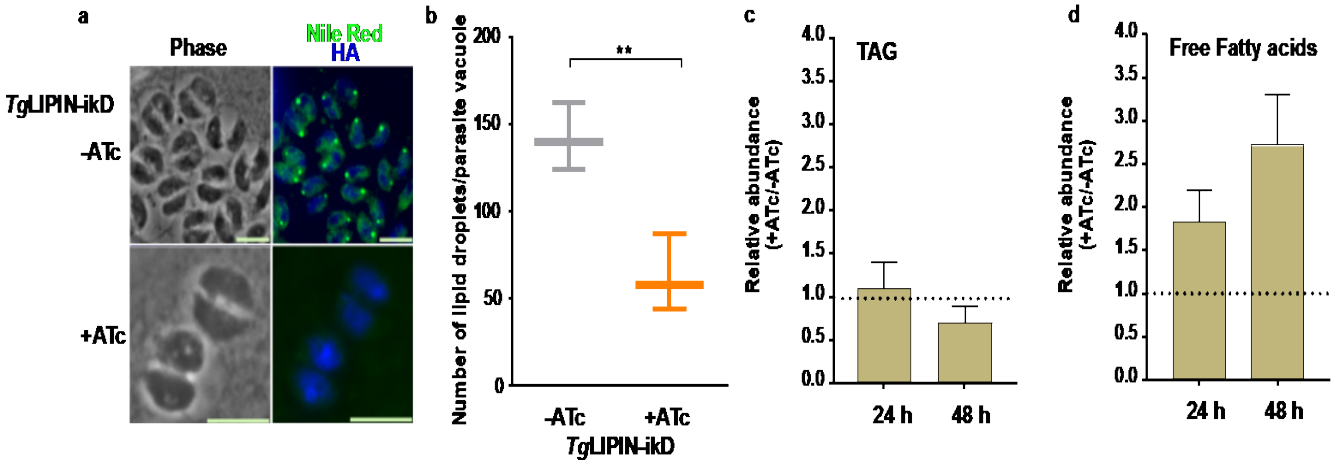

Fig. 5 TgLIPIN generated DAG is directed towards neutral lipid storage

a) Nile red staining, which is seen as green dots within *Tg*LIPIN-ikD -ATc parasites (panel 2 –ATc) is absent in the +ATc conditions (panel 2 +ATc). Presence and absence of *Tg*LIPIN due to ATc induction is visualized by anti-HA antibody (panel 2 -/+ATc) b) Graphical representation of reduction of nile red droplets/parasite vacuole in *Tg*LIPIN-ikD +Atc by up to 60%. c) Relative abundance of TAGs in *Tg*LIPIN-ikD (+ATc/-ATc). Corroborating with nile red IFA data, the TAG levels were relatively reduced by up to 0.6 (+ATc/-ATc) in the *Tg*LIPIN-ikD (48 h + ATc). d) In keeping with TAG reduction, a 2-3-fold increase in the relative abundance of free fatty acids (+ATc/-ATc), was recorded in the *Tg*LIPIN-ikD. Error bars=standard error of the mean, n=3. p values are indicated as follows: 0.01-0.05=*, 0.01-0.001=** and <0.001=***

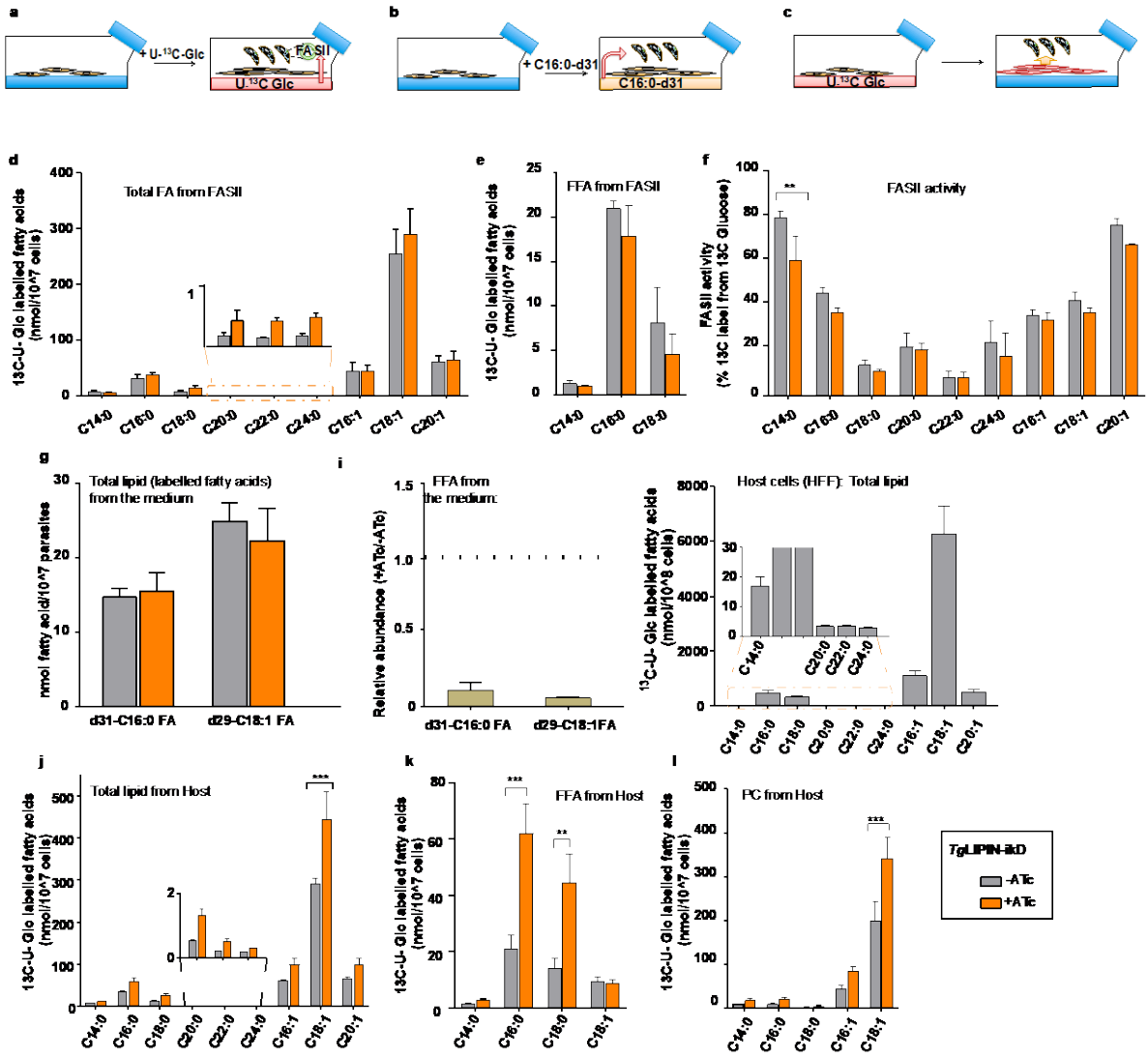

Fig. 6. Monitoring the source of excess fatty acids in TgLIPIN-iKD

a)b)c) Schematic for experimental procedure of stable isotope labelling to determine the origin of fatty acids in *Tg*LIPIN-ikD a) Parasite FASII derived fatty acids were determined by the addition of U-^{13}C-glucose to the culture medium (1% FBS, low glucose, +/-ATc) at the time of parasite infection to the host. b) Fatty acids scavenged from the extracellular host environment was determined by the addition of ^{31}d-palmitic acid (^{31}d-C16:0) into the parasite culture medium (high glucose, 1% FBS). c) Host cell derived fatty acids were determined by growing host cells in the presence of U-^{13}C-glucose (low glucose, 10% FBS) till confluency prior to the infection parasites with normal medium (high glucose, 1% FBS, +/-ATc). d) Abundance of apicoplast FASII derived ^{13}C labelled total fatty acids in the *Tg*LIPIN-iKD. ATc (grey bars) and +ATc (orange bars). e) Abundance of apicoplast FASII derived ^{13}C labelled free fatty acids f) FASII activity in *Tg*LIPIN-ikD as measured as % ^{13}C-incorporation. g) Relative abundance of medium

derived free fatty acid in *Tg*LIPIN-ikD (+ATc/-ATc). h) Abundance of medium derived fatty acids (C16:0 and C18:1) in total lipid from *Tg*LIPIN-iKD+ATc or -ATc. i) ^{13}C-U-Glucose labelled fatty acids in the host cells. j) Significant increase in the oleic acid (C18:1) in the host derived ^{13}C labelled total fatty acids in the *Tg*LIPIN-ikD+/-ATc. k) Significant increase in host-derived ^{13}C labelled C16:0 and stearic acid (C18:0) in the free fatty acid pool in *Tg*LIPIN-iKD+ATc. l) Excess ^{13}C-labelled C18:1 from the host was directly channeled to major membrane phospholipid within *Tg*LIPIN-ikD parasite upon ATc induction. Error bars=standard error of the mean, n=3 (no. of biological replicates). Statistical significance was calculated by t-test performed in GraphPad Prism software p value 0.01-0.05=*, 0.01-0.001=** and <0.001=***

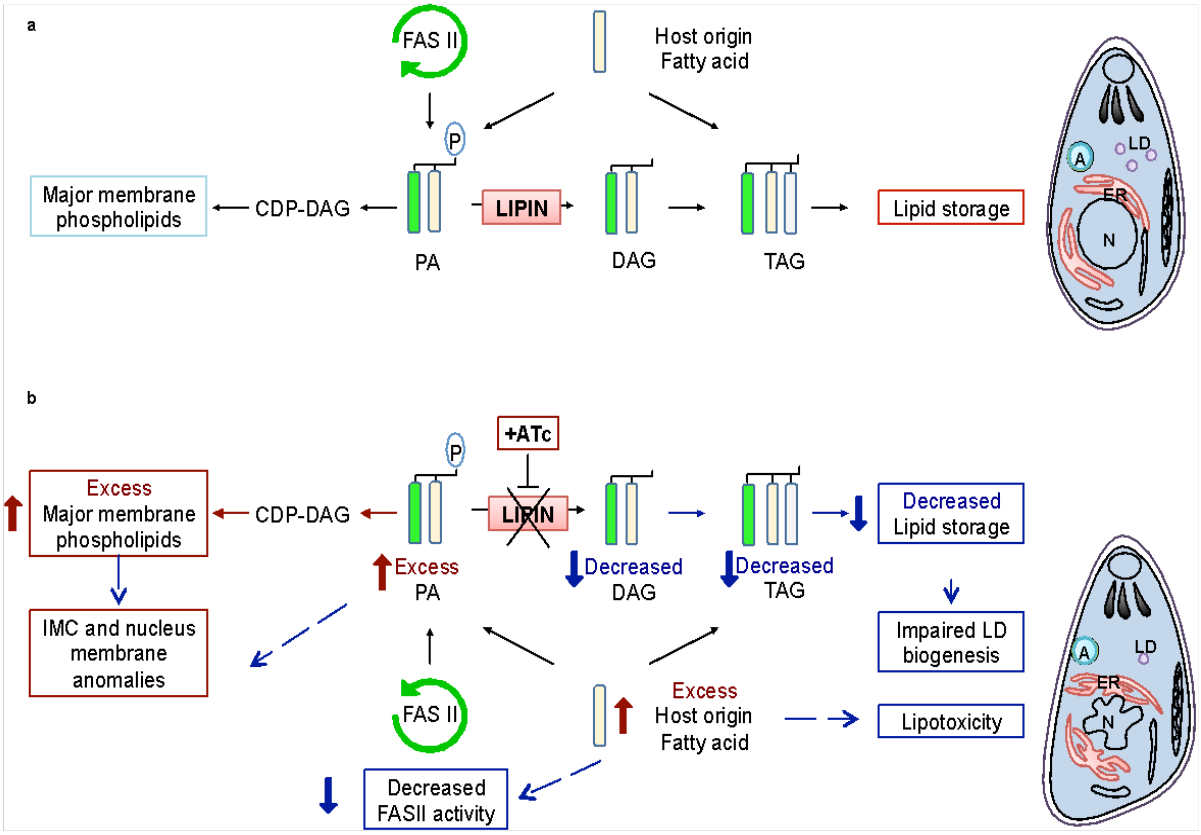

Fig. 7 Proposed role of LIPIN in Toxoplasma lipid metabolism

Schematic representation of the dual essential role of *Tg*LIPIN in parasite lipid metabolism including, membrane biogenesis and lipid storage. a) The parasite utilizes fatty acids derived from both apicoplast FASII and host to synthesize major lipids, beginning with phosphatidic acid (PA). PA is hydrolyzed to diacylglycerol (DAG), which is further acylated to generate triacylglycerol (TAG). The other branch of this pathway redirects PA towards generation of major membrane phospholipids via CDP-DAG pathway. The FA homeostasis between membrane biogenesis and storage essential for normal parasite development within its host is maintained by the PA phosphatase *Tg*LIPIN. (b) Genetic ablation of *Tg*LIPIN in the presence of anhydrotetracycline (ATc) results in PA/DAG imbalance. The increased PA is channeled towards CDP-DAG pathway resulting in excess phospholipids and consequent gross membrane anomalies within the parasite IMC and nucleus. Simultaneously, the reduction in DAG affected TAG biogenesis and hence the lipid storage capacity, marked by decreased lipid droplets, within the parasite lacking *Tg*LIPIN. The impairment of TAG biosynthesis, resulted in excess fatty acids derived from the host, within *Tg*LIPIN mutant, causing lipotoxicity.

Supplementary Figures

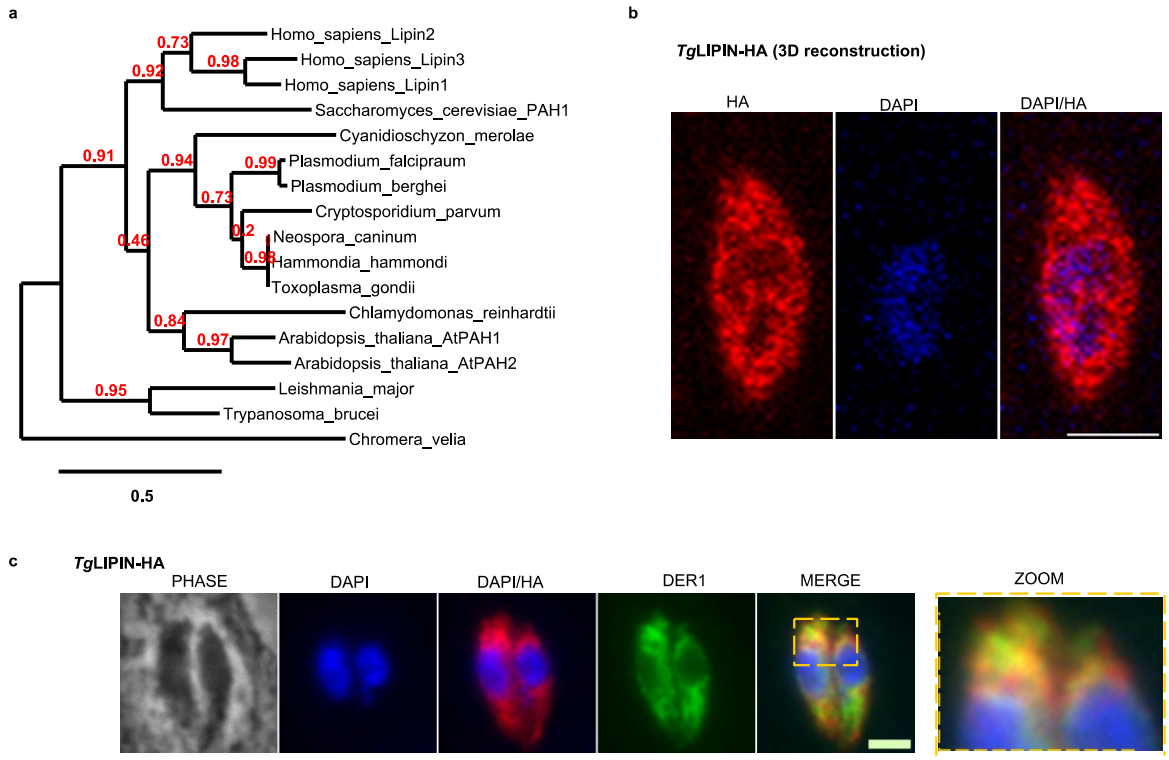

Fig. S1 a) Phylogenetic tree of the eukaryotic lipin homologs of *Tg*LIPIN. Entire protein sequence was used to create the tree using web server Phlogeny.fr. b) 3D reconstruction of confocal images of *Tg*LIPIN-HA localization, generated using ICY software, confirmed the perinuclear localization of the protein. c) IFA showing *Tg*LIPIN-HA (in red) in close vicinity of the endoplasmic reticulum marker Der-1 (in green).

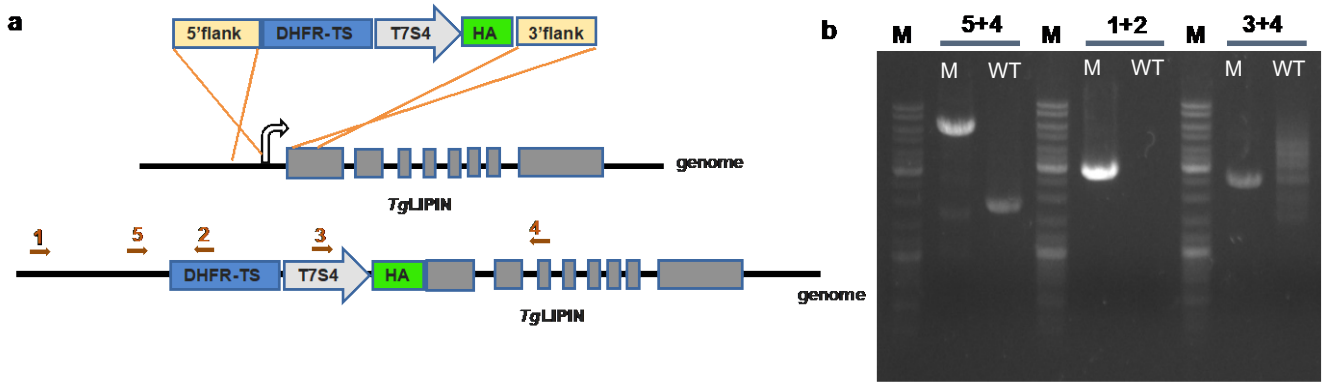

Fig. S2 a) Schematic of molecular strategy for generation of *Tg*LIPIN-ikD tagged with 3*HA at its N-terminus. b) Confirmation of correct promoter replacement in the *Tg*LIPIN-ikD line. Primers combinations during the screening PCR yielded products of expected amplicon size validating the mutant. The template genomic DNA was extracted from *Tg*LIPIN-ikD line (M) and RHΔ Ku80 TATi strain (WT) (control). Primers 5+4 generated 1890 bp amplicon with RHΔ Ku80 TATi strain (WT) and approx. 4800 bp using *Tg*LIPIN-ikD gDNA (M), suggesting incorporation of tetracycline inducible elements along with DHFR cassette at the genome locus of *Tg*LIPIN. Expectedly, primers combinations specific to Tet-regulatable elements (1+2, 3+4) generated an amplicon approx. 3000 bp in size only using *Tg*LIPIN (M) as the gDNA template.

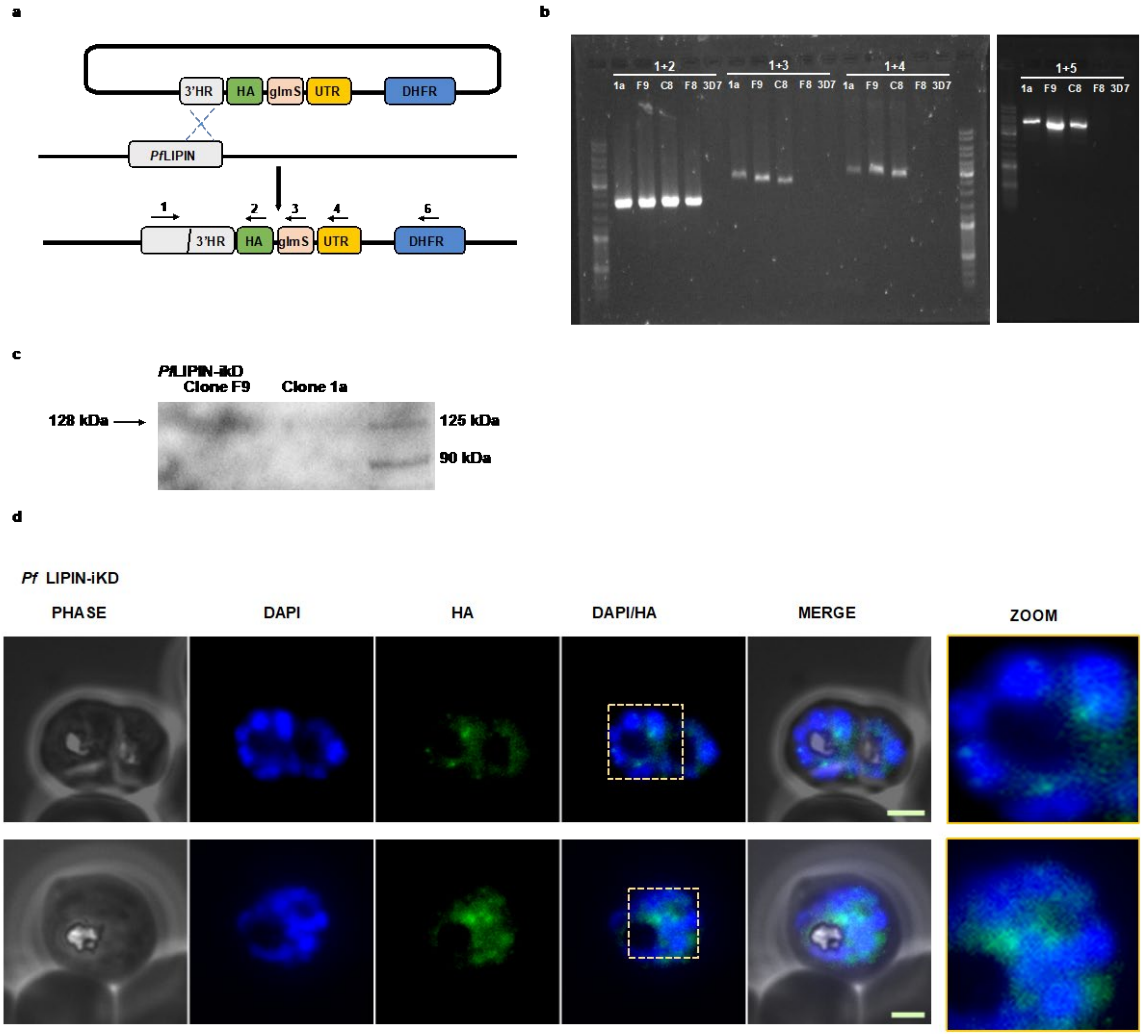

Fig. S3 a) Schematic representation of glmS-riboswitch based molecular strategy used for generation of *Pf*LIPIN-ikD tagged with 3×HA at its C-terminus. b) PCR validation of *P. falciparum* transgenic clones, *Pf*LIPIN-ikD line. Primers combinations during the screening PCR yielded products of expected amplicon size validating the mutant. The template genomic DNA (gDNA) was extracted from *Pf*LIPIN-ikD clonal lines 1a, F9,C8,F8 and wild type 3D7. Primers specific for coding region of *Pf*lipin upstream of 3'HR (P1), HA-tag (P2), glmS ribozyme sequence (P3), ribozyme-associated UTR (P4) and DHFR cassette (P5) generated PCR products expected size only using gDNA from *Pf*LIPIN-ikD: 1+2=1840 bp, 1+3=2053 bp,1+4=2097 bp,1+5=3811 bp. c) Western blot analysis using anti-HA antibodies, showed expression of the protein at its correct size (128 kDa) in *Pf*LIPIN-ikD clones F9 and 1a d) IFA of *Pf*LIPIN-HA (endogenous C-terminal tag) with anti-HA antibody, shows vesicular localization coinciding with the DNA stain-hoechst, specifically during the schizont stage of *P. falciparum* erythrocytic life cycle. Scale bar: 2.0 µm

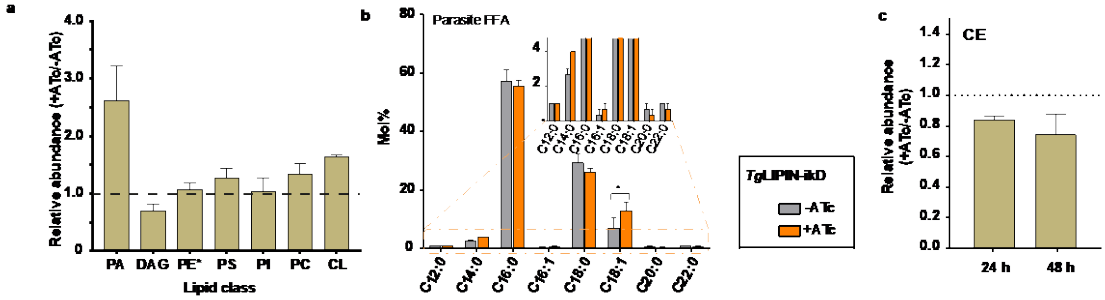

Fig. S4 a) Relative abundance of major phospholipid species, PA, PS, PC and CL, showed a significant increase in the *Tg*LIPIN-ikD mutant (+ATc, orange) in comparison to the control (-ATc, grey). The biochemical product of *Tg*LIPIN, DAG was reduced in the *Tg*LIPIN-ikD mutant (+ATc) whereas, phospholipids PE, PI remained unchanged. b) Composition of the molecular species within free fatty acid (FFA) content of *Tg*LIPIN-ikD (+ATc/-ATc), showing a significant increase of oleate upon *Tg*LIPIN depletion. c) The relative abundance (+ATc/-ATc) of cholesteryl esters remained unaffected upon depletion of *Tg*LIPIN. Experiments were conducted in triplicates. Statistical significance was determined by t-test using GraphPad Prism. Range of statistical significance was signified as per the p value, wherein 0.01-0.05=*, 0.01-0.001=** and <0.001=***

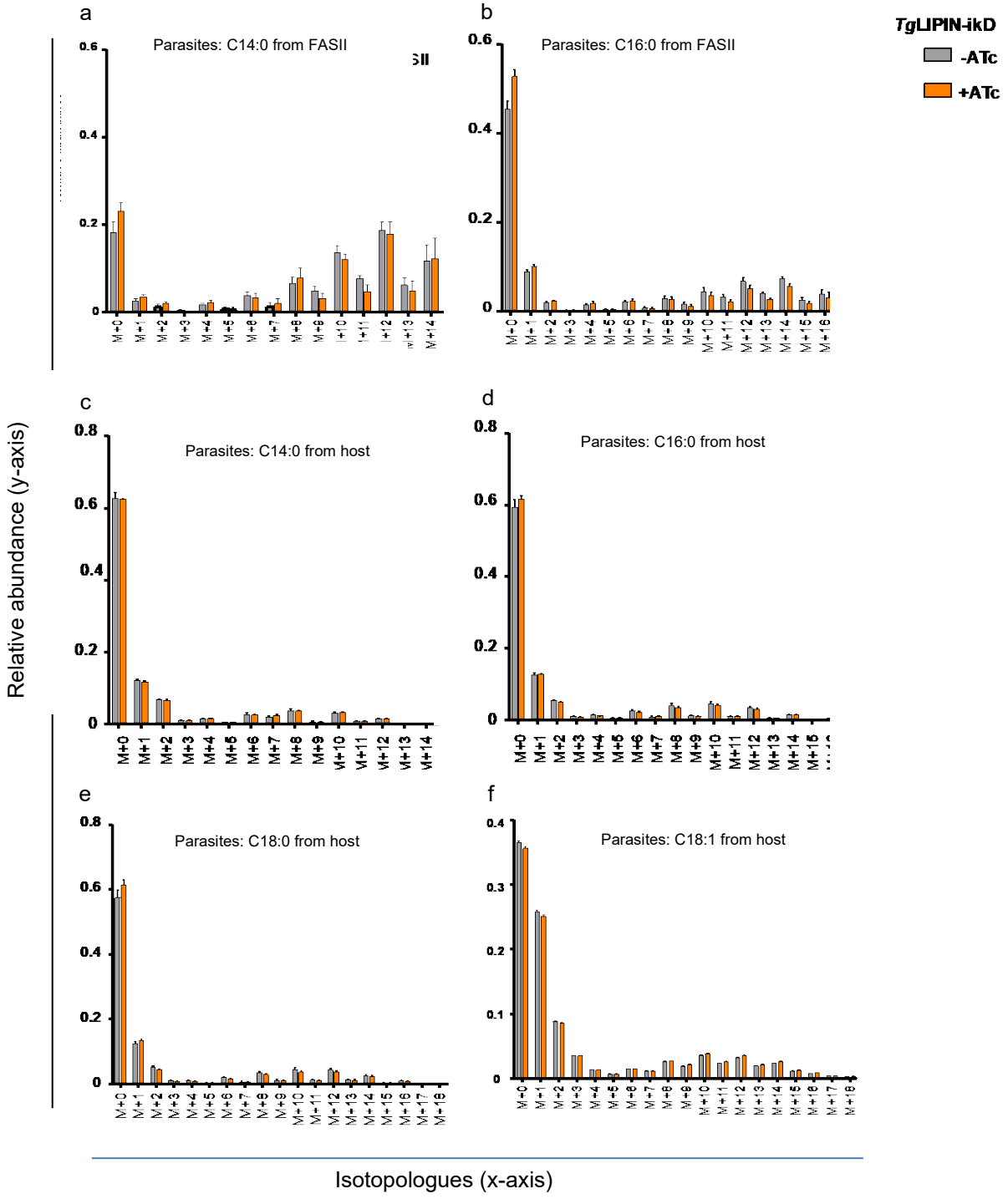

Fig. S5 Graphical representation of mass isotopologue distribution of ^{13}C into C14:0 (a), C16:0 (b) derived from FASII activity of *Tg*LIPIN-ikD (+ATc-orange, -ATc-grey). Mass isotopologue distribution of C14:0 (c), C16:0 (d), C18:0 (e) and C18:1 (f) fatty acids scavenged directly from the host. Experiments were conducted in triplicates.

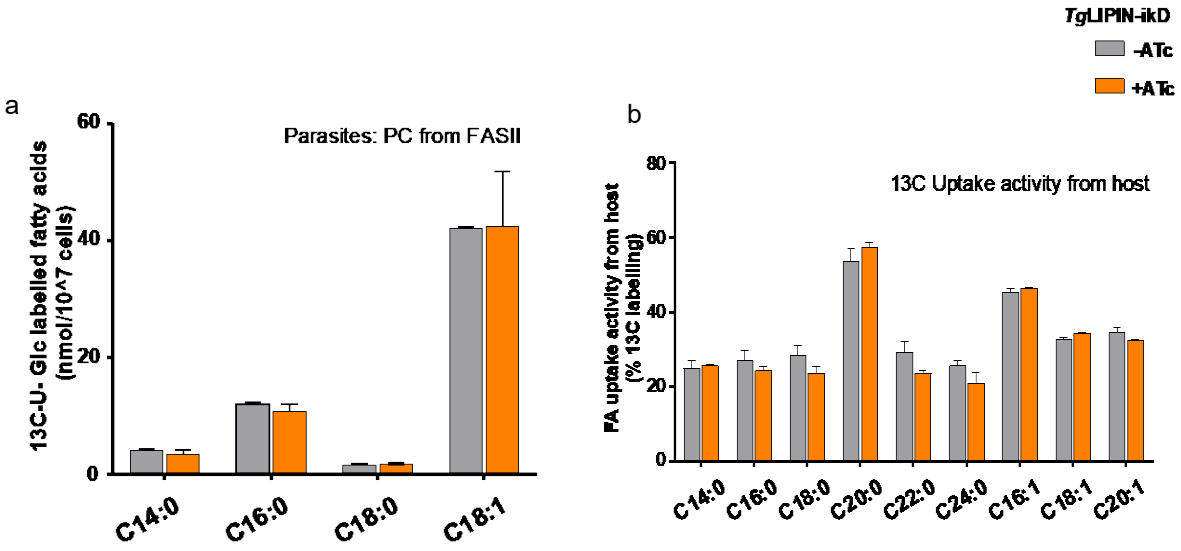

Fig. S6 a) The graph represents ^{13}C-labelled fatty acid species derived fatty acid species within phosphatidylcholine of *Tg*LIPIN-ikD (+ATc-orange, -ATc-grey). b) The degree of incorporation of ^{13}C-labelled host-derived fatty acids within *Tg*LIPIN-ikD parasites (+ATc-orange, -ATc-grey) determined their FA uptake activity from the host. Experiments were conducted in triplicates. Statistical significance was determined by t-test using GraphPad Prism. Range of statistical significance was signified as per the p value, wherein 0.01-0.05=*, 0.01-0.001=** and <0.001=***

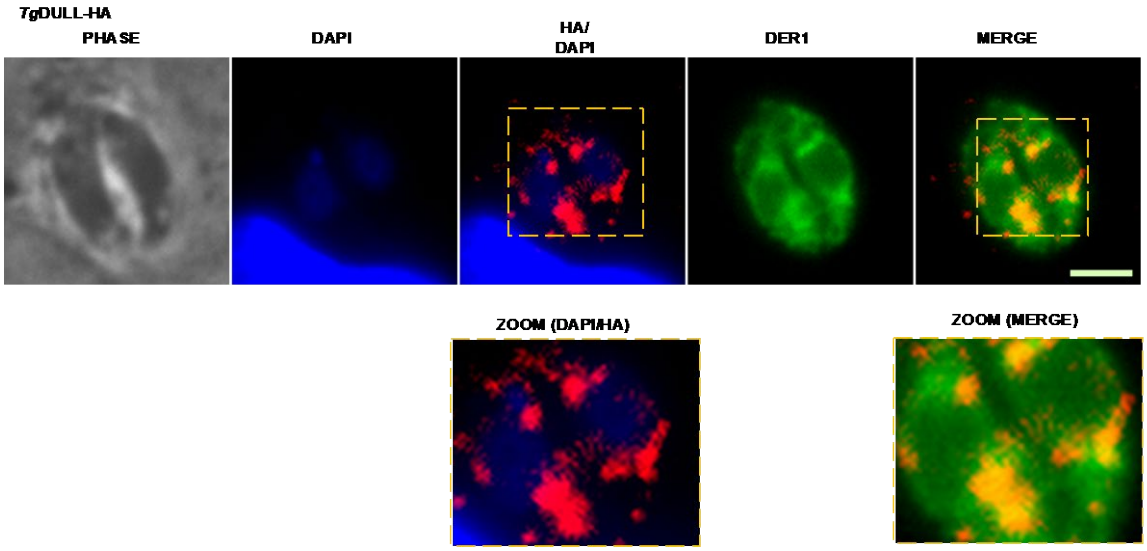

Fig. S7 Immunofluorescence assay-based images showing localization of *Tg*DULL-HA (red) around the nucleus (Zoom, DAPI/HA). Co-localization studies with endoplasmic reticulum (ER) marker Der-1 confirms the localization of *Tg*DULL at parasite ER.

REFERENCES (Chapter IV)

Agrawal, S. *et al.* (2009) 'Genetic evidence that an endosymbiont-derived endoplasmic reticulum-associated protein degradation (ERAD) system functions in import of apicoplast proteins', *Journal of Biological Chemistry*. doi: 10.1074/jbc.M109.044024.

Amiar, S. *et al.* (2016) 'Apicoplast-Localized Lysophosphatidic Acid Precursor Assembly Is Required for Bulk Phospholipid Synthesis in Toxoplasma gondii and Relies on an Algal/Plant-Like Glycerol 3-Phosphate Acyltransferase.', *PLoS pathogens*, 12(8), p. e1005765. doi: 10.1371/journal.ppat.1005765.

Amiar, S. *et al.* (2019) 'Division and adaptation to host nutritional environment of apicomplexan parasites depend on apicoplast lipid metabolic plasticity and host organelles remodelling', *bioRxiv*, p. 585737. doi: 10.1101/585737.

Barbosa, A. D. *et al.* (2015) 'Lipid partitioning at the nuclear envelope controls membrane biogenesis', *Molecular Biology of the Cell*. doi: 10.1091/mbc.E15-03-0173.

Bisio, H. *et al.* (2019) 'Phosphatidic acid governs natural egress in Toxoplasma gondii via a guanylate cyclase receptor platform', *Nature Microbiology*. doi: 10.1038/s41564-018-0339-8.

Bullen, H. E. *et al.* (2016) 'Phosphatidic Acid-Mediated Signaling Regulates Microneme Secretion in Toxoplasma', *Cell Host and Microbe*, 19(3), pp. 349–360. doi: 10.1016/j.chom.2016.02.006.

Carman, G. M. and Han, G. S. (2009) 'Phosphatidic acid phosphatase, a key enzyme in the regulation of lipid synthesis', *Journal of Biological Chemistry*. doi: 10.1074/jbc.R800059200.

Carman, G. M. and Han, G. S. (2019) 'Fat-regulating phosphatidic acid phosphatase: A review of its roles and regulation in lipid homeostasis', *Journal of Lipid Research*, 60(1), pp. 2–6. doi: 10.1194/jlr.S087452.

Cases, S. *et al.* (1998) 'Identification of a gene encoding an acyl CoA:diacylglycerol acyltransferase, a key enzyme in triacylglycerol synthesis', *Proceedings of the National Academy of Sciences of the United States of America*. doi: 10.1073/pnas.95.22.13018.

Chae, M., Han, G. S. and Carman, G. M. (2012) 'The Saccharomyces cerevisiae actin patch protein app1p is a phosphatidate phosphatase enzyme', *Journal of Biological Chemistry*. doi: 10.1074/jbc.M112.421776.

Choi, H. S. *et al.* (2012) 'Pho85p-Pho80p phosphorylation of yeast pah1p phosphatidate phosphatase regulates its activity, location, abundance, and function in lipid metabolism', *Journal of Biological Chemistry*. doi: 10.1074/jbc.M112.346023.

Coppens, I. (2013) 'Targeting lipid biosynthesis and salvage in apicomplexan parasites for improved chemotherapies', *Nature Reviews Microbiology*. Nature Publishing Group, 11(12), pp. 823–835. doi: 10.1038/nrmicro3139.

Counihan, N. A. *et al.* (2017) 'Plasmodium falciparum parasites deploy RhopH2 into the host erythrocyte to obtain nutrients, grow and replicate.', *eLife*, 6. doi: 10.7554/eLife.23217.

Csaki, L. S. and Reue, K. (2010) 'Lipins: Multifunctional Lipid Metabolism Proteins', *Annual Review of Nutrition*, 30(1), pp. 257–272. doi: 10.1146/annurev.nutr.012809.104729.

Fakas, S., Konstantinou, C. and Carman, G. M. (2011) 'DGK1-encoded diacylglycerol kinase activity is required for phospholipid synthesis during growth resumption from stationary phase in Saccharomyces cerevisiae', *Journal of Biological Chemistry*. doi: 10.1074/jbc.M110.194308.

Finck, B. N. *et al.* (2006) 'Lipin 1 is an inducible amplifier of the hepatic PGC-1α/PPARα regulatory pathway', *Cell Metabolism*. doi: 10.1016/j.cmet.2006.08.005.

Fujita, Y., Matsuoka, H. and Hirooka, K. (2007) 'Regulation of fatty acid metabolism in bacteria', *Molecular Microbiology*. doi: 10.1111/j.1365-2958.2007.05947.x.

Di Genova, B. M. *et al.* (2019) 'Intestinal delta-6-desaturase activity determines host range for Toxoplasma sexual reproduction', *PLoS Biology*, 17(8), pp. 1–19. doi: 10.1371/journal.pbio.3000364.

Greenspan, P., Mayer, E. P. and Fowler, S. D. (1985) 'Nile red: A selective fluorescent stain for intracellular lipid droplets', *Journal of Cell Biology*. doi: 10.1083/jcb.100.3.965.

Grimsey, N. *et al.* (2008) 'Temporal and spatial regulation of the phosphatidate phosphatases lipin 1 and 2', *Journal of Biological Chemistry*. doi: 10.1074/jbc.M804278200.

Han, G. S. *et al.* (2008) 'An unconventional diacylglycerol kinase that regulates phospholipid synthesis and nuclear membrane growth', *Journal of Biological Chemistry*, 283(29), pp. 20433–20442. doi: 10.1074/jbc.M802903200.

Han, G. S., Siniossoglou, S. and Carman, G. M. (2007) 'The cellular functions of the yeast lipin homolog Pah1p are dependent on its phosphatidate phosphatase activity', *Journal of Biological Chemistry*. doi: 10.1074/jbc.M705777200.

Han, G. S., Wu, W. I. and Carman, G. M. (2006) 'The Saccharomyces cerevisiae lipin homolog is a Mg2+-dependent phosphatidate phosphatase enzyme', *Journal of Biological Chemistry*. doi: 10.1074/jbc.M600425200.

Harris, T. E. *et al.* (2007) 'Insulin controls subcellular localization and multisite phosphorylation of the phosphatidic acid phosphatase, lipin 1', *Journal of Biological Chemistry*. doi: 10.1074/jbc.M609537200.

Hu, X., Binns, D. and Reese, M. L. (2017) 'The coccidian parasites Toxoplasma and Neospora dysregulate mammalian lipid droplet biogenesis', *Journal of Biological Chemistry*, 292(26), pp. 11009–11020. doi: 10.1074/jbc.M116.768176.

Huynh, M. H. and Carruthers, V. B. (2009) 'Tagging of endogenous genes in a Toxoplasma gondii strain lacking Ku80', *Eukaryotic Cell*, 8(4), pp. 530–539. doi: 10.1128/EC.00358-08.

Jacot, D. *et al.* (2016) 'An Apicomplexan Actin-Binding Protein Serves as a Connector and Lipid Sensor to Coordinate Motility and Invasion', *Cell Host and Microbe*, 20(6), pp. 731–743. doi: 10.1016/j.chom.2016.10.020.

Jimah, J. R. *et al.* (2016) 'Malaria parasite CelTOS targets the inner leaflet of cell membranes for pore- dependent

disruption', *eLife*. doi: 10.7554/eLife.20621.

Karanasios, E. *et al.* (2010) 'A phosphorylation-regulated amphipathic helix controls the membrane translocation and function of the yeast phosphatidate phosphatase', *Proceedings of the National Academy of Sciences of the United States of America*. doi: 10.1073/pnas.1007974107.

Kim, Y. *et al.* (2007) 'A conserved phosphatase cascade that regulates nuclear membrane biogenesis', *Proceedings of the National Academy of Sciences of the United States of America*. doi: 10.1073/pnas.0702099104.

Kong, P. *et al.* (2017) 'Two phylogenetically and compartmentally distinct CDP-diacylglycerol synthases cooperate for lipid biogenesis in Toxoplasma gondii', *Journal of Biological Chemistry*. doi: 10.1074/jbc.M116.765487.

Lindner, S. E. *et al.* (2014) 'Enzymes involved in plastid-targeted phosphatidic acid synthesis are essential for Plasmodium yoelii liver-stage development', *Molecular Microbiology*, 91(4), pp. 679–693. doi: 10.1111/mmi.12485.

Listenberger, L. L. *et al.* (2003) 'Triglyceride accumulation protects against fatty acid-induced lipotoxicity', *Proceedings of the National Academy of Sciences of the United States of America*. doi: 10.1073/pnas.0630588100.

Mashima, T., Seimiya, H. and Tsuruo, T. (2009) 'De novo fatty-acid synthesis and related pathways as molecular targets for cancer therapy', *British Journal of Cancer*. doi: 10.1038/sj.bjc.6605007.

Mazumdar, J. and Striepen, B. (2007) 'Make it or take it: Fatty acid metabolism of apicomplexan parasites', *Eukaryotic Cell*, 6(10), pp. 1727–1735. doi: 10.1128/EC.00255-07.

Meissner, M., Schlüter, D. and Soldati, D. (2002) 'Role of Toxoplasma gondii myosin a in powering parasite gliding and host cell invasion', *Science*, 298(5594), pp. 837–840. doi: 10.1126/science.1074553.

Nakamura, Y. *et al.* (2009) 'Arabidopsis lipins mediate eukaryotic pathway of lipid metabolism and cope critically with phosphate starvation', *Proceedings of the National Academy of Sciences of the United States of America*. doi: 10.1073/pnas.0907173106.

Nolan, S. J. *et al.* (2018) 'Novel approaches to kill toxoplasma gondii by exploiting the uncontrolled uptake of unsaturated fatty acids and vulnerability to lipid storage inhibition of the parasite', *Antimicrobial Agents and Chemotherapy*, 62(10), pp. 1–34. doi: 10.1128/AAC.00347-18.

Nolan, S. J., Romano, J. D. and Coppens, I. (2017) *Host lipid droplets: An important source of lipids salvaged by the intracellular parasite Toxoplasma gondii*, *PLoS Pathogens*. doi: 10.1371/journal.ppat.1006362.

O'Hara, L. *et al.* (2006) 'Control of phospholipid synthesis by phosphorylation of the yeast lipin Pah1p/Smp2p Mg2+-dependent phosphatidate phosphatase', *Journal of Biological Chemistry*. doi: 10.1074/jbc.M606654200.

Ouologuem, D. T. and Roos, D. S. (2014) 'Dynamics of the Toxoplasma gondii inner membrane complex', *Journal of Cell Science*, 127(15), pp. 3320–3330. doi: 10.1242/jcs.147736.

Pernas, L. *et al.* (2018) 'Mitochondria Restrict Growth of the Intracellular Parasite Toxoplasma gondii by Limiting

Its Uptake of Fatty Acids', *Cell Metabolism*. Elsevier Inc., 27(4), pp. 886-897.e4. doi: 10.1016/j.cmet.2018.02.018.

Ramakrishnan, S. *et al.* (2012) 'Apicoplast and endoplasmic reticulum cooperate in fatty acid biosynthesis in apicomplexan parasite Toxoplasma gondii', *Journal of Biological Chemistry*, 287(7), pp. 4957–4971. doi: 10.1074/jbc.M111.310144.

Ramakrishnan, S. *et al.* (2015) 'The intracellular parasite Toxoplasma gondii depends on the synthesis of long-chain and very long-chain unsaturated fatty acids not supplied by the host cell', *Molecular Microbiology*, 97(1), pp. 64–76. doi: 10.1111/mmi.13010.

Reue, K. and Wang, H. (2019) 'Mammalian lipin phosphatidic acid phosphatases in lipid synthesis and beyond: Metabolic and inflammatory disorders', *Journal of Lipid Research*. doi: 10.1194/jlr.S091769.

Santos-Rosa, H. *et al.* (2005) 'The yeast lipin Smp2 couples phospholipid biosynthesis to nuclear membrane growth', *EMBO Journal*. doi: 10.1038/sj.emboj.7600672.

Shears, M. J. *et al.* (2017) 'Characterization of the Plasmodium falciparum and P. berghei glycerol 3-phosphate acyltransferase involved in FASII fatty acid utilization in the malaria parasite apicoplast', *Cellular Microbiology*, 19(1). doi: 10.1111/cmi.12633.

Sheiner, L. *et al.* (2011) 'A systematic screen to discover and analyze apicoplast proteins identifies a conserved and essential protein import factor.', *PLoS pathogens*, 7(12), p. e1002392. doi: 10.1371/journal.ppat.1002392.

Siniossoglou, S. (1998) 'A novel complex of membrane proteins required for formation of a spherical nucleus', *The EMBO Journal*. doi: 10.1093/emboj/17.22.6449.

Siniossoglou, S. (2009) 'Lipins, lipids and nuclear envelope structure', *Traffic*. doi: 10.1111/j.1600-0854.2009.00923.x.

Su, W. M. *et al.* (2012) 'Protein kinase A-mediated phosphorylation of Pah1p phosphatidate phosphatase functions in conjunction with the Pho85p-Pho80p and Cdc28p-Cyclin B kinases to regulate lipid synthesis in yeast', *Journal of Biological Chemistry*. doi: 10.1074/jbc.M112.402339.

Tange, Y., Hirata, A. and Niwa, O. (2002) 'An evolutionarily conserved fission yeast protein, Ned1, implicated in normal nuclear morphology and chromosome stability, interacts with Dis3, Pim1/RCC1 and an essential nucleoporin', *Journal of Cell Science*. doi: 10.1242/jcs.00135.

Zhang, P. and Reue, K. (2017) 'Lipin proteins and glycerolipid metabolism: Roles at the ER membrane and beyond', *Biochimica et Biophysica Acta - Biomembranes*. doi: 10.1016/j.bbamem.2017.04.007.

CHAPTER V: CHARACTERIZATION OF *TOXOPLASMA GONDII* ACYL-COA SYNTHETASES REVEAL THE CRITICAL ROLE OF *TG*ACS3 IN PROVIDING ACYL-COA FOR PHOSPHOLIPID SYNTHESIS DURING TACHYZOITE DIVISION

CHAPTER V: SUMMARY

Fatty acid (FA) biosynthesis is an essential anabolic pathway required for the synthesis of lipids required for the growth and division of apicomplexan parasites within their host. Ongoing research in the field of parasite lipid metabolism suggests that major phospholipid classes making the bulk of *T. gondii* lipid composition are obligate patchwork molecules composed of FAs made *de novo* and derived from the host. Other than acting as structural building blocks for lipids, FAs also are important energy storage molecules and their fatty acyl derivatives involved in post-translational modification of various proteins. Therefore, the acquisition and utilization of FAs are pivotal pathways for parasite survival. One of the key steps involved in FA metabolism is their activation via thioesterification to coenzyme A (CoA) by enzymes called acyl-CoA synthetases (ACS). Based on their FA metabolism, these ACSs in apicomplexan parasites can be required for activation of FAs derived from *de novo* FASII and the host. In phylum apicomplexa, ACSs have been annotated and defined in *P. falciparum* (13 in total) and *C. parvum* (3 in total). In the following study, we identified a family of putative ACSs in *T. gondii* and characterized the role of an essential ACS (*Tg*ACS3) in parasite replication and growth.

The major findings of this study are enlisted below:

i. *T. gondii* genome encodes for 7 putative ACSs. These *Tg*ACSs possess canonical eukaryotic ACS motifs within their characteristic AMP-binding domain.
ii. The identified *Tg*ACSs localize to different sub-cellular compartments of the parasite, thereby suggesting their non-redundant roles in FA metabolism.
iii. *Tg*ACS3, is essential for parasite intracellular development and adaptation to different host nutritional conditions.
iv. Lipidomic data suggest that *Tg*ACS3 is potentially required for metabolic utilization of FAs for phospholipid biosynthesis within the parasite.

TITLE: Characterization of *Toxoplasma gondii* acyl-CoA synthetases reveal the critical role of *Tg*ACS3 in providing acyl-CoA for phospholipid synthesis during tachyzoite division (in preparation)

Sheena Dass, Laurence Berry[2], Nicholas J. Katris1, Yoshiki Yamaryo-Botté[1]*, Cyrille Y. Botté[1]*

1 Apicolipid Team, Institute for Advanced Biosciences, CNRS UMR5309, Université Grenoble Alpes, INSERM U1209, Grenoble, France,

2 Dynamique des interactions Membranaires normales et pathologiques, UMR5235, Université Montpellier II, France. * Equal senior and corresponding authors. To whom correspondence should be sent, cyrille.botte@univ-grenoble-alpes.fr / cyrille.botte@gmail.com; yoshiki.botte-yamaryo@univ-grenoble-alpes.fr

ABSTRACT

Apicomplexa comprise several pathogenic protists, that heavily depend on lipid metabolism for the survival within their hosts. The lipid synthesis within these parasites relies on an essential combination of fatty acids obtained from *de novo* synthesis and scavenging from the host. The metabolic utilization of these fatty acids is mediated by acyl-activating enzymes. These include acyl CoA synthases (ACS) that catalyze the activation of fatty acids, primarily through the formation of a thioester bond. The role of these enzymes in FA utilization in *T. gondii* has been unforeseen. Here, we identified 7 putative ACSs encoded by the genome of *T. gondii* (*Tg*ACS). Interestingly, the *Tg*ACSs localize to different sub-cellular compartments of the parasite, suggesting their exclusive functions. The perinuclear/cytoplasmic *Tg*ACS3 regulates replication and growth of *Toxoplasma* tachyzoites. Lipidomic analysis of parasites lacking *Tg*ACS3, suggests its role in activation of FAs directed towards parasite phospholipid synthesis. Altogether, the results presented here describe a putative ACS family of enzymes in *T. gondii* potentially involved in FA activation and metabolism.

INTRODUCTION

Apicomplexan parasites are a group of unicellular eukaryotes that include pathogens responsible for various morbidity causing diseases. These include *Toxoplasma gondii*, *Plasmodium sp*. and *Cryptosporidium parvum* causing the infectious diseases toxoplasmosis, malaria and cryptosporidiosis respectively. Eradicating these pathogens is a worldwide priority and the renewal of our therapeutic arsenal relies on understanding of the host-parasite interactions. Metabolic pathways that sustain parasite intracellular development and therefore host-parasite interactions represent ideal targets for drug development. One of the key determinants impacting the pathogenicity of these parasites within their host is lipid metabolism.

Toxoplasma gondii is capable of infecting virtually any nucleated cell, thereby displaying its metabolic strength in adapting to different nutritional environments. During the intracellular development of *T. gondii*, lipids play an essential role by providing structural building blocks for membrane biogenesis (Ramakrishnan et al. 2012; Amiar et al. 2016), as signaling molecules participating in key events like active invasion and egress through microneme secretion (Bullen et al. 2016; Bisio et al. 2019) and also as storage fuels, which plays critical role to maintain proper intracellular development (Nolan et al. 2018). To cope with the continuous need for lipids with the different host cells environments, *T. gondii* has evolved so it harbors three *de novo* synthetic pathways to generate fatty acids (FA), central lipid building blocks: (i) the apicoplast resident prokaryotic type-II fatty acid biosynthesis pathway (FASII) (Mazumdar and Striepen 2007; Amiar et al. 2016), (ii) the ER-based FA elongation pathway (Ramakrishnan et al. 2012) and (iii) the eukaryotic type-I fatty acid synthase present in the cytosol (Mazumdar and Striepen 2007). Additionally, the parasite is also heavily reliant on acquiring FA directly from their hosts (Ramakrishnan et al. 2012; Fu et al. 2019; Pernas et al. 2018; Amiar et al. 2019; Nolan et al. 2018). Ongoing research on parasite lipid metabolism suggests that the FA flux derived from both apicoplast FASII (Mazumdar et al. 2006; Amiar et al. 2016) as well as from direct scavenging from the host (Ramakrishnan et al. 2012; Fu et al. 2018; Pernas et al. 2018; Amiar et al. 2019) are both essential for intracellular parasite viability. Furthermore, major phospholipid classes making the bulk of *T. gondii* lipid composition are obligate “patchwork molecules” composed of FA from the host and made de novo (Amiar et al. 2016). Taken together, FA, and most importantly their acquisition and utilization are pivotal pathways for parasite survival.

One of the key biochemical steps required for general FA utilization and trafficking is its activation by thioesterification to a Co-Enzyme A (CoA) that is catalyzed by the essential acyl-CoA synthetase (or acyl-CoA ligase) family (Watkins et al. 2007). Biochemically, ACS catalyzes a two-step reaction to form fatty acyl-CoA. The initial step involves the formation of an adenylated intermediate through the hydrolysis of an ATP molecule, thus releasing pyrophosphate (Black et al. 1992). The ATP-activated enzyme then binds to the carboxyl group of incoming a free FA (FFA) moiety through an acyl bond to the phosphoryl group of AMP. Final fatty acyl-CoA product is formed after the transfer of the fatty acyl group to the sulfhydryl group of coenzyme A, thereby releasing AMP (Black et al. 1992).

Acyl-CoA synthases (ACS) exist as different isoforms in eukaryotes depending upon FA substrate specificity, which is based on FA chain length and degree of unsaturation. Humans have 26 enzymes that comprise the large ACS family activating short-chain, medium chain, long chain and very long chain fatty acid substrates (Watkins et al. 2007). There are 9 long chain ACSs (LACS) that have been well characterized in *Arabidopsis thaliana* (Shockey, Fulda, and Browse 2002). This family of AMP-binding domain containing enzymes to a larger extend are indispensable for fatty acid metabolism in various eukaryotes. ACSs have been shown to be predominantly involved in glycerolipid biosynthesis as well as catabolic β-oxidation pathway and transport of fatty acids across organellar membranes (Watkins et al. 2007; Zhao et al. 2019).

The phylum apicomplexa is engaged actively in fatty acid metabolism and hence the role of the ACSs in parasite survival within its host cannot be undermined. ACSs in apicomplexa potentially activate fatty acids derived from both *de novo* synthetic machinery and from the host. This can be supported with the existence of ACS encoding genes in the genome of *Cryptosporidium* and *Theileria* which lack the *de novo* fatty acid biosynthetic machinery (Mazumdar and Striepen 2007). *Cryptosporidium parvum* has been reported to have three AMP-binding domain containing long-chain fatty acid CoA ligases out of which two *Cp*ACS1 and *Cp*ACS2 have been biochemically characterized as functional ACSs (Guo et al. 2016). *Plasmodium falciparum* on the other hand has a large family of ACSs encoded by 13 genes (PfACS1a-PfACS12) (Bethke et al. 2006). Bethke et al also describes ACSs as the only family of metabolic enzymes that are encoded by genes expanded into the sub telomeric region which usually harbors parasite virulence genes (Bethke et al. 2006). Drugs specific to ACSs in *C. parvum* have shown potent parasite killing activity, thereby

hinting that this enzymatic reaction is a potential Achilles heel for apicomplexans (Guo et al. 2014).

Here, we identified 7 enzymes in *Toxoplasma gondii* which we classify as putative acyl-CoA synthases (*Tg*ACS). All the putative *Tg*ACSs were endogenously tagged and localize to non-overlapping sub-cellular compartments of the parasite, including vesicular, mitochondrial, perinuclear-ER and basal end/cap of the tachyzoites. We further characterized two most interesting candidates, the mitochondrial *Tg*ACS2 and the cytosolic-perinuclear *Tg*ACS3 by generating inducible knockdown parasite lines using the classical Tet-off system. Downregulation of these shows that *Tg*ACS2 has a minor role in maintaining parasite survival whereas *Tg*ACS3 is critical for tachyzoite intracellular development. *Tg*ACS3 is especially required for maintaining the division of large parasite vacuoles, with a marked role under high nutrient host environments. Lipidomic analyses further show that the disruption of *Tg*ACS3 significantly reduces phospholipid content along with a concomitant and significant increase of free FA content within the parasite. Our analysis therefore suggests that *Tg*ACS3 is the major source of FAs most likely obtained through host scavenging, which are then fueled to generate bulk phospholipid content for maintaining tachyzoite division.

RESULTS

Identification of seven genes encoding putative acyl-CoA synthetase (ACS) enzymes within the Toxoplasma genome

In order to identify putative members of ACS gene family in *Toxoplasma gondii*, we searched for genes with AMP binding domain in the ToxoDB database (http://toxodb.org/toxo/), and identified several candidate genes. Within these candidates bearing the AMP-binding domain, seven proteins were identified to have highly conserved ACS motifs: Motif I- {Y,F} TSG {T,S} TGXPK; Motif II- TGDX (7) GX hX (2) RX (4) Hx (3,4) GX (2) hX (4) hE ; Motif III- YGXTE (WWQTE); Motif IV-LPLXH; Motif V- LPLSH, V-PKTX{S,T} GKIX {R,K} (KXX {R,K}) (Watkins et al. 2007) (Fig.ure 1a,b). We then named the 7 putative *T. gondii* ACS (*Tg*ACS) candidates as *Tg*ACS1 (TGGT1_297220), *Tg*ACS2 (TGGT1_310150), *Tg*ACS3 (TGGT1_310080), *Tg*ACS4 (TGGT1_243800), *Tg*ACS5 (TGGT1_247760), *Tg*ACS6 (TGGT1_ 232580), *Tg*ACS7

(TGGT1_276155) (Fig.1a). These 7 *Tg*ACS candidates were further validated by bioinformatic analysis including sequence alignment and phylogeny (Fig. 1b, Fig. 2, Fig. S1). Multiple sequence alignment using Clustal Omega online tool (https://www.ebi.ac.uk/Tools/msa/clustalo) showed that the all of 7 putative *Tg*ACS candidates possess consensus amino acid sequences of canonical ACS motifs 1-IV and partly of motif V (Fig. 1b, Sup 1). Phylogenetic analysis clustered the different *Tg*ACSs to specific clusters based on their homology to other eukaryotic counterparts (Fig. 2). Of note, *Tg*ACS1 cladded together with the human ACSs belonging to the bubble-gum gene family (ACSBG), also known to be involved in β-oxidation (Pei et al. 2003). *Tg*ACS2, *Tg*ACS3, *Tg*ACS4 and *Tg*ACS5 clustered in the long chain acyl-CoA synthetase (or acyl-CoA ligases) group within a coccidian/chromerida super-clade (Fig. 2). *Tg*ACS6 clustered with the human ACSS family, more specific to short acyl chains like propionyl-CoA (Watkins et al. 2007) (Fig. 2) Interestingly, *Tg*ACS7 clustered away from all known ACSs from humans, *A. thaliana* and *P. falciparum*. Further sequence and phylogenetic analyses showed no direct homology/conservation of *Tg*ACS7 with the sequences of known homologs from humans, *A. thaliana*, or *P. falciparum*. However, unique conserved homologs of *Tg*ACS7 were identified within the coccidians and the chromerids (close photosynthetic relatives of apicomplexans), *Hammondia hammondi*, *Cryptosporidium parvum, Neospora_caninum*, and *Chromera velia* using EuPathDB (https://eupatdb.org). These homologs clustered together with *Tg*ACS7 with confident bootstrap scores forming a previously unidentified novel group of ACSs within apicomplexa (Guo et al. 2016) (Fig. 2).

Putative TgACSs localize to non-overlapping intracellular compartments of T. gondii tachyzoites

To determine the physiological localization of the 7 putative *Tg*ACS, we generated *T. gondii* tachyzoite parasite lines expressing each protein fused to a C-terminal triple haemagglutinin (3×HA) epitope-tag under control of their endogenous promoter (Huynh and Carruthers 2009). Immunofluorescence assays (IFA) using anti-HA antibody revealed that the 7 TgACSs localize to distinct sub-cellular compartments of the parasite (Fig. 3a). *Tg*ACS1, *Tg*ACS6 and *Tg*ACS7 were localized widely within the parasite cytoplasm, mostly as vesicular patterns (Fig.3a). Interestingly, *Tg*ACS2 localized in a compartment reminiscent of the parasite mitochondria (Fig. 3a). Confocal microscopy and 3D reconstruction with the *T. gondii* mitochondrial outer membrane marker

TOM40 (Van Dooren et al. 2016) confirmed the close vicinity and the co-localization of *Tg*ACS2 with the parasite mitochondria (Fig. 4a, b)**.** *Tg*ACS3 was localized broadly at the cytosol, accumulating around and yet avoiding the nuclear area of the parasite (Fig. 3a). *Tg*ACS4 showed a distinct and interesting peri-nuclear/ER-like localization (Fig. 3a). Finally, *Tg*ACS5 displayed an interesting cytoplasmic localization, particularly enriched at the basal end of the parasite. (Fig. 3a). These localizations suggest non-redundant functions of ACSs within the different endomembrane compartments and cytoplasm of *T. gondii*. The ACSs in other eukaryotes have different fatty acid substrate specificities and functions depending upon their differential localizations (Watkins et al. 2007; Fulda et al. 2002; Schnurr et al. 2002).

The endogenously tagged parasite lines were further confirmed by western blot analysis using anti-HA antibody (Fig. 3b). The migration of all the *Tg*ACS-HA was in accordance to their annotated protein sizes on ToxoDB (Fig. 3b). *Tg*ACS2-HA, however, showed a size shift of approximately 10 kDa below the predicted protein size (103 kDa), appearing at ~95 kDa (Fig. 4c).

To assess the importance of *Tg*ACSs, we probed their crispr based phenotype scores (Sidik et al. 2016) together with their endogenous localizations (Fig. 3a). Among all *Tg*ACSs only *Tg*ACS1 and *Tg*ACS3 displayed negative score of -1.88 and -2.53, respectively (Fig. 3a), suggesting their important/essential role for the intracellular development of *T. gondii* tachyzoites.

TgACS3 is critical for tachyzoite intracellular development especially in high host nutrient environments

Based on negative phenotype scores and an interesting mitochondrial localization putatively linked to adaptive metabolic function, we generated inducible knockdown tachyzoite strains for *Tg*ACS1, *Tg*ACS2, and *Tg*ACS3. The inducible knockdown lines (ikD) were generated by promoter replacement using the Tet-off system in TATi_Δ*Ku80* background (Meissner, Schlüter, and Soldati 2002; Sheiner et al. 2011) with an additional N-terminal HA-tagging (i.e. *Tg*ACS1/2/3-ikD-HA). Promoter replacement and insertion of the HA tag were confirmed by PCR (Fig. S2). Intriguingly, although we obtained and recovered several polyclonal cell lines expressing *Tg*ACS1-iKD-HA but we were never able to obtain its monoclonal cell line, unlike *Tg*ACS2 and *Tg*ACS3.

Interestingly, the N-terminally tagged *Tg*ACS2-iKD-HA migrated approximately 10 kDa higher than the endogenously C-terminally tagged *Tg*ACS2-HA, with an apparent size of ~103kDa, correlating its predicted size on ToxoDB (Fig. 4c). Based on our dual tagging approach, we can assume that the C-*Tg*ACS2-HA is representative of correct protein size (~ 95 kDa) most likely due to its expression from endogenous promoter. It further suggests the existence of a probable different start codon for *Tg*ACS2 than the one annotated on ToxoDB.

Western blot and IFA analyses both confirmed the downregulation of respective proteins within *Tg*ACS2-iKD-HA (Fig 4d, e) and *Tg*ACS3-iKD-HA (Fig. 5a,b) parasite lines by anhydrotetracycline (ATc) treatment. Complete protein depletion was observed at 24 h and 48 h after ATc treatment, respectively for *Tg*ACS2 (Fig. 4c) and *Tg*ACS3 (Fig. 5a). IFA confirmed the respective localization of *Tg*ACS2 at the parasite mitochondria (Fig. 4d, upper panel), and *Tg*ACS3 at the cytosol/perinuclear compartment (Fig5b, upper panel). IFA also revealed that the ATc treatment leading to *Tg*ACS2 depletion did not affect the overall morphology of intracellular tachyzoites. On the other hand, the disruption of *Tg*ACS3 had a direct deleterious effect on tachyzoite intracellular morphology, especially on large vacuoles (>10parasites) where parasites appeared round and unhealthy (Fig. 5b, lower panel, phase).

We further performed plaque assays in the presence of different host nutritional environments (0,1 and 10% FBS containing growth media/DMEM) to probe the mutant's capacity to maintain normal growth under these conditions. We previously showed that wild type parasites sense host nutritional status and grow better with higher levels of host nutrient (10% FBS) (Amiar et al. 2019). The disruption of *Tg*ACS2 had no effect on the intracellular development of tachyzoites at any levels of host nutrient (0%, 1% or 10% FBS) as shown by the absence of difference in plaque area also represented graphically (Fig. 4e, f). However, the disruption of *Tg*ACS3 had a negative impact on the parasite growth, which escalated with increasing levels of FBS in the growth culture medium. When grown in regular culture conditions with 1% FBS, parasites lacking *Tg*ACS3 had significantly smaller and lesser plaques, although it was only mildly reduced compared to the control (Fig. 5c, d). Importantly, when grown in high nutrient environment, at 10% FBS, parasites lacking *Tg*ACS3 displayed a much stronger growth phenotype than at 0 and 1% FBS, with significantly lesser and smaller plaques than in the control (Fig. 5c, d). Reduction of host nutrient to 0% FBS had no effect on growth of *Tg*ACS3-iKD in the +/- ATc (Fig. 5c, d). The growth

phenotype was confirmed by a replication assay where *Tg*ACS3 depleted parasites had significantly fewer large vacuoles (7-10 parasites) and more smaller vacuoles (3-6 parasites) (Fig. 5e). *Tg*ACS3-iKD parasites displayed a mild egress defect in the presence of ATc (Fig. 5f). The egress assay was performed using calcium ionophore A23187 to chemically induce parasite egress.

Disruption of TgACS3 leads to reduction of parasite phospholipids and concomitant increase of free fatty acid content

Our results suggest that *Tg*ACS3 has an important role for the division, overall intracellular tachyzoite development and potential metabolic adaptation of the parasite to different host nutritional environments. To determine its precise function, we performed lipidomics analysis on *Tg*ACS3-iKD +/-ATc (48 h time point) using gas chromatography-mass spectrometry (GC-MS) approaches. We first determined the overall fatty acid (FA) abundance and composition of total lipid fraction (including FAs from all glycerolipids, neutral lipids and free FA). Overall, we did not observe any significant difference in the total lipid abundance of *Tg*ACS3-iKD (+ATc and -ATc) (Fig. 6a). However, the detailed profile of the total FA composition showed a slight yet significant increase in oleic acid (C18:1) content in the mutant (*Tg*ACS3-iKD +ATc) (Fig. 6b), possibly suggesting a substrate specificity of the enzyme for C18:1. To assess this and determine the precise function of *Tg*ACS3, total lipid was separated by high performance thin layer chromatography (HPTLC), and the composition and content of phospholipids (PL), free fatty acid (FFA), and storage lipid triacylglycerol (TAG) were quantified by GC-MS. Interestingly, this detailed lipidomic analysis revealed that the overall PL content was significantly reduced in the *Tg*ACS3-iKD +ATc mutant (Fig. 6c). Furthermore, FFA were significantly increased in the mutant (*Tg*ACS3-iKD +ATc) (Fig. 6d). This suggested that due to absence of ACS activity (*Tg*ACS3) within the parasite, inactivated FA could not be used for PL synthesis and thus accumulated as toxic FFA. The FFA excess in *Tg*ACS3-iKD mutant (+ATc) corroborated with the increased growth defect phenotype in the presence of 10% FBS (Fig. 5c). However, disruption of *Tg*ACS3 resulted in a slight increase (insignificant) the levels of TAGs (Fig. 6e). Quantification of the FA composition of the FFA fraction revealed significant decrease in palmitic acid (C16:0) and increase of stearic acid (C18:0) in parasite lacking *Tg*ACS3 (*Tg*ACS3-iKD +ATc) (Fig. 6g). Analysis of the FA composition from TAG in the *Tg*ACS-iKD mutant (+ATc), showed a similar trend in the variation of FA species, i.e. decrease in C16:0 increase C18:0 (Fig. 6h).

DISCUSSION

Acyl CoA synthetases catalyze a fundamental and limiting reaction in FA metabolism: the activation of free FA via thioesterification to coenzyme A (CoA). This key reaction allows the fatty acyl CoA intermediates to participate further in trafficking, assembly into complex lipids, post-translational modification of membrane proteins, and/or the catabolism of FAs via β-oxidation (Watkins et al. 2007).

A unifying feature of acyl-CoA synthetase (ACS) enzymes and the ANL super-family that comprises **A**CS, **N**on-ribosomal peptide synthase adenylation domain and **L**uciferase enzymes (Gulick 2009, Ellis et al. 2010), is the presence of AMP-binding domain as their catalytic domain (Babbitt et al. 1992). All the 7 proteins that we identified as putative *Tg*ACSs possess the consensus amino acid sequences mostly as a part of their annotated AMP-binding domains (Fig. 1a, 1b). The multiple sequence alignment of entire protein sequence of the *Tg*ACSs with other eukaryotic counterparts suggested an overall identity of up to 30-40% with high conservation in the AMP-binding domain (Fig. S1). Phylogenetic analysis of the identified *Tg*ACSs with known ACS from other eukaryotes clustered them to various clades, potentially based on their enzymatic substrate-specificity and function (Fig. 2). The interesting separate sub-grouping of *Tg*ACS7 alongside its homologs from coccidia and chromerida may indicate a coccidian-photosynthetic origin of *Tg*ACS7 potentially lost during the evolution of haemosporidians (*P. falciparum*).

The existence of several ACSs in the *Plasmodium* and *Toxoplasma* genome are indicative of their unique and central functions for maintaining parasite survival. These parasites harbor extensively diverse range of FA varying in chain lengths and degree of saturation/unsaturation. Thus, it is not surprising that the parasites have a long list of ACS encoding genes. Similarly, there are 26 ACSs in humans, 11 of which are long-chain (ACSL) and very long chain acyl-CoA synthetases (ACSVL) (Watkins et al. 2007). These ACSL and ACSVL have the specificity to activate fatty acid up to 16-22 carbons in length (Watkins et al. 2007). The ACSLs, however typically activate the highly abundant fatty acids in nature including palmitate (C16:0) and oleate (C18:1). Others include, short-chain ACSs (ACSSs) that typically activate acetate, propionate, or butyrate and medium-chain ACSs (ACSMs) that activate fatty acids ranging in chain lengths from C6 to C10 (Watkins et al. 2007). Lastly, the bubble gum-ACSs called ACSBG gene family (also known as lipidosin) that are capable of activating FAs of chain length 16-24 (Lopes-Marques et al. 2018).

The *Toxoplasma* candidates *Tg*ACS2,3,4 and 5 clustered within the long chain ACS group alongside the human long chain ACSLs and ACSVLs (Fig. 2) whereas *Tg*ACS6 was found with short FA chain specific ACSS, corroborating with its annotated function of propionyl CoA ligase (C3).

The diverse sub compartmental localization of putative *Toxoplasma* ACSs indicates non-redundancy and their highly specific roles in fatty acid activation. The correlation between protein localization and its function has been established with extended family of ACSs in humans (Watkins et al. 2007). For example, the role of endogenous ACSL1 in liver in neutral lipid synthesis and FA oxidation could correspond to its dual localization at the endoplasmic reticulum (ER) and mitochondria (Li et al. 2009). Similarly, cardiac ACSL1 localized at mitochondria, has a significant contribution to FA β-oxidation (Ellis et al. 2010). ACSL3, which has been found on lipid droplets and ER, participates in FA uptake and glycerolipid biosynthesis (Poppelreuther et al. 2012). The localization of *Cryptosporidium parvum Cp*ACS1 at the apical end of cell-free sporozoites has been linked to FA biosynthesis required during process of invasion, and/or early stage development (Guo et al. 2016). Similar polarization of *Tg*ACS5 at the basal end of the *Toxoplasma* tachyzoites could suggest its potential role in parasite cell division and cytokinesis (Hu 2008).

Additionally, the localization of the ACS could also direct the fate of the acyl-CoAs by allowing the ACSs to interact with different proteins involved in the direct downstream processing. For example, human ACSL1 coimmunoprecipitates with mitochondrial outer membrane proteins carnitine palmitoyl transferase 1a (CPT1a) and voltage-dependent anionic channel (VDAC) (Lee et al. 2011). This proximity of ACSL1 to CPT1a functionally places it in the aspect of mitochondrial FA β-oxidation as CPT1a converts acyl-CoAs to mitochondria activated forms called acyl-carnitines (Lee et al. 2011). Recent data including ours, provide evidence for the presence of an active acyl-CoA binding protein-2 (ACBP) that localizes to the mitochondria of the parasite (Amiar et al. 2019; Fu et al. 2018). We suggest that *Tg*ACS2 (mitochondrial vicinity) and *Tg*ACBP2 are potentially coherently involved in FA activation and transport within the parasite mitochondria. However, whether they participate in mitochondrial membrane biogenesis and/or rather β-oxidation is yet to be determined.

Amongst several functions of the ACSs includes channeling of FA towards energy yielding process of β-oxidation (Grevengoed et al. 2014; Watkins et al. 2007, Shockey et al 2002). The mouse ortholog of human hsACSBG1, called mBG1 localizing in the form of vesicles in close proximity to mitochondria of neuronal cells was shown to be involved in mitochondrial β-oxidation of the long chain fatty acid palmitate (Pei et al. 2003). Interestingly, based on phylogenetic analysis *Tg*ACS1 clusters together with the hsACSBG-gene family known to be involved in β-oxidation (Watkins et al. 2007). The presence of FA β-oxidation in apicomplexa has been a relatively unexplored. In eukaryotes, this energy yielding process compartmentalizes to mitochondria and vesicular organelles called peroxisomes. There is genomic and bioinformatic evidence for the presence of peroxisomes in *T. gondii* (Kaasch and Joiner 2000; Ding et al. 2000; Moog et al. 2017). Proteins imported into the peroxisomal lumen bear two canonical targeting sequences- peroxisomal targeting sequence type 1 (PTS1), a C-terminal tripeptide with the consensus sequence [SAC]-[KRH]-[LM] and peroxisomal targeting sequence type 2 (PTS2), an N-terminal peptide comprised of the amino acids [RK]-[LVIQ]-X-X-[LVIHQ]-[LSGAK]-X-[HQ]-[LAF] (Moog et al. 2017). In *A. thaliana* LACS6 is targeted by a type 2 (PTS2) peroxisomal targeting sequence whereas LACS7 inhabits both functional PTS1 as well as a PTS2 (Fulda et al. 2002). This peroxisomal LACS activity has been shown to be essential for seedling growth (Fulda et al. 2004). Moog et al. provides bioinformatic evidence for the presence of classical PTSs in the protein factors potentially involved in β-oxidation in apicomplexan parasites. These proteins are subjected to stage specific expression supporting the existence of this process during the stage of sporulation or encystment within the parasites (Moog et al. 2017). *Tg*ACS1 was one of the proteins defined within the "high confidence" PTS1-targeted peroxisomal proteome for *T. gondii*. Vesicular localization and predicted PTS1 at the C-terminus of *Tg*ACS1 strongly suggests its role in putative β-oxidation of FA in *T. gondii.* Co-localization studies with peroxisomal markers like catalase and lipidomics can provide further confirmation.

Another functional aspect of ACSs is their involvement in FA transport across different organellar membrane compartments. Yeast ACSs Faa1p and Faa4p have been shown to function together with FA transport system (involving the transporter Fat1p) thereby linking import and activation of FA to further events in intracellular metabolism (Færgeman et al. 2001). In *E. coli*, the FA import is dependent on both outer membrane bound transporter FadL as well as acyl-CoA synthetase FadD (Black et al. 1992). In yet another study on human ACSs, it was found that the

N-terminal region of ACSL3 was responsible to FA uptake alongside its ER/LD localization (Poppelreuther et al. 2012). The transport of FA towards cellular fate can also be linked to metabolic trapping due to vectorial acylation of these FA by the ACSs, acting as the driving force of uptake of free FA from the extracellular environment. Human ACSL6 is required for cellular retention of omega-3-docohexaneoic acid in the brain which in turn protects against neurodegenerative disorders (Fernandez et al. 2018). The FA transporter function of ACSs in *Toxoplasma* can be elucidated through core lipidomics involving ^{13}C-Glc based fluxometrics.

In metabolically active hepatocyte cells Huh7, ACSL3 has been shown to specifically channel activated FA (esp. C18:1, oleic acid) into phosphatidylcholine. A siRNA mediated knockdown of ACSL3 decreases oleate incorporation to PC with concomitant rise in the levels of cellular-free oleic acid (Yao and Ye 2008). Similar to this study, the measured decrease of the total levels of FA content derived from phospholipids in the *Tg*ACS3-iKD alongside concomitant increase of free FA both corroborate with the functional role of the enzyme (Fig. 6).Lipidomic analysis of *Tg*ACS3-iKD +ATc illustrated a gross effect on the concentration of long chain fatty acids esp. C18:1. The short chain fatty acids, mostly apicoplast FASII derivatives like C12:0, C14:0, and C16:0 appeared to only slightly affected. This suggests that *Tg*ACS3 probably is a long chain fatty acyl-CoA ligase which thioesterifies long chain FA scavenged from the host (C18:1) rather than the apicoplast-FASII specific short chain fatty acids (C14:0 and C16:0). However, the source of FA substrate can be determined precisely from ^{13}C-Glc based flux analysis. Absence of human ACS, hsACSBG1, is linked to X-linked adrenoleukodystrophy (X-ALD) which is characterized by the presence of very long chain FAs in plasma and tissues causing neurodegeneration (Jia et al. 2004). The *A. thaliana* Δ*lacs4*Δ*lacs9* double mutant accumulates linoleic acid (C18:2) by up to 300% in leaf tissue due to abrogation of the corresponding acyl-CoA synthetase activity (Jessen et al. 2015).

The growth defect for the *Tg*ACS3-iKD was significantly more pronounced in 10% serum conditions. This observation can be explained by linking it to lipidomic data showing increase in the free FA content within *Tg*ACS3-iKD (+ATc). As per its expected function, due to loss of *Tg*ACS3 within the parasite there is a reduction in the metabolic utilization of fatty acids via thioesterification. In the presence of lipid enriched 10% serum DMEM, the parasites normally

uptake more FAs, however, are unable to balance its utilization due to absence of an important acyl-CoA synthetase *Tg*ACS3.

Despite having a negative phenotype score on *Toxoplasma* genome wide CRISPR-Cas9 screen (Sidik et al. 2016), the measured growth defect of *Tg*ACS3-iKD in normal nutrient conditions at 1% FBS was not as pronounced as predicted. However, in the presence of high host nutritional environment, the phenotype of *Tg*ACS3-iKD (+ATc) was more pronounced, correlating reported phenotype scores. These differences might be explained by a certain level of redundancy by the other *Tg*ACS when *Tg*ACS3 is depleted. However, the replication assay and egress defect demonstrated the importance of *Tg*ACS3 for the parasite intracellular development. The existence of several genes encoding the ACSs in different eukaryotes has been rooted as the cause of certain redundancy amongst their functionality and substrate specificity. In *A. thaliana*, the LACS9 and LACS4 functionally overlap with another ER-specific isoform LACS8 (Jessen et al. 2015). Another comprehensive study suggests that in plants cuticular wax biosynthesis majorly involves LACS1 alongside complementary assistance from LACS4 and LASC2. Male fertility is governed together by the function of LACS1 and LACS4 while as oil biosynthesis is controlled by combination of LACS1, LACS4 and LACS9 (Zhao et al. 2019).

MATERIALS AND METHODS

Protein sequence analysis and Phylogeny: Identification of TgACSs

Members of the Acyl CoA synthetase (ACS) gene family within *T. gondii* were identified using various online bioinformatic tools, Clustal omega (https://www.ebi.ac.uk/Tools/msa/clustalo/), (https://www.uniprot.org), EuPathDB (https://eupathdb.org/eupathdb). A phylogenetic tree of ACS proteins in several eukaryotes including apicomplexa, humans and plants was created using the online platform Phylogeny.fr. The organisms used for ACS protein sequences for generation of the phylogenetic tree include: *T. gondii_Tg*ACS1 (TGGT1_297220), *T. gondii_Tg*ACS2 (TGGT1_310150), *T. gondii_Tg*ACS3 (TGGT1_310080), *T. gondii_Tg*ACS4 (TGGT1_243800), *T. gondii_Tg*ACS5 (TGGT1_247760), *T. gondii_Tg*ACS6 (TGGT1_232580), *T. gondii_Tg*ACS7 (TGGT1_276155), *P. falciparum_Pf*ACS1a (PF3D7_1479000), *P. falciparum_Pf*ACS2 (PF3D7_0301000), *P. falciparum_Pf*ACS3 (PF3D7_1253400), *P. falciparum_Pf*ACS4 (PF3D7_1372400), *P. falciparum_Pf*ACS5 (PF3D7_0731600), *P. falciparum_Pf*ACS6 (PF3D7_0401900), *P. falciparum_Pf*ACS7 (PF3D7_1200700), *P. falciparum_Pf*ACS8 (PF3D7_0215300), *P. falciparum_Pf*ACS9 (PF3D7_0215000), *P. falciparum_Pf*ACS10 (PF3D7_0525100), *P. falciparum_Pf*ACS11 (PF3D7_1238800), *P. falciparum_Pf*ACS12 (PF3D7_0619500), *A. thaliana*_LACS1 (At2g47240), *A. thaliana*_LACS2 (At1g49430), *A. thaliana*_LACS3 (At1g57920), *A. thaliana*_LACS4 (At4g23850), *A. thaliana*_LACS5 (At4g11030), *A. thaliana*_LACS6 (At3g05970), *A. thaliana*_LACS7 (At5g27600), *A. thaliana*_LACS8 (At2g04350), *A. thaliana*_LACS9 (At1g77590); *Homo sapiens*_ACSS1 (NX_Q9NUB1), *H. sapiens*_ACSS2 (NX_Q9NR19), *H. sapiens*_ACSS3 (NX_Q9H6R3), *H. sapiens*_ACSVL1 (NX_O14975), *H. sapiens*_ACSVL2 (NX_Q9Y2P4), *H. sapiens*_ACSVL3 (NX_Q5K4L6), *H. sapiens*_ACSVL4 (NX_Q6P1M0), *H. sapiens*_ACSVL5 (NX_Q6PCB7), *H. sapiens*_ACSVL6 (NX_Q9Y2P5)*H. sapiens*_ACSL1 (NX_P33121), *H. sapiens*_ACSL3 (NX_O95573), *H. sapiens*_ACSL4 (NX_O60488), *H. sapiens*_ACSL5 (NX_Q9ULC5), *H. sapiens*_ACSL6 (NX_Q9UKU0), *H. sapiens*_ACSS3 (NX_Q9H6R3), *H. sapiens*_ACSM3 (NX_Q53FZ2), *H. sapiens*_ACSM2B (NX_Q68CK6), *H. sapiens*_ACSM1 (NX_Q08AH1), *H. sapiens*_ACSM4 (NX_P0C7M7), *H. sapiens*_ACSM5 (NX_Q6NUN0), *H. sapiens* ACSM6_(NX_Q6P461), *H. sapiens*_ACSBG1 (NX_Q96GR2), *H. sapiens*_ACSBG2 (NX_Q5FVE4); *Chromera velia* (Cvel_26948), *Chromera velia* (Cvel_29920), *C. velia* (Cve1_20092), *C. velia* (Cvel_8845)), *C. velia* (Cvel_24841), *C. velia* (Cvel_29002), *C. velia*

(Cvel_9659), *C. velia* (Cvel_3410), *C. velia* (Cvel_2306), *C. velia* (Cvel_26948) ; *Cryptosporidium parvum* (cgd5_3200), *C. parvum* (cdg3_2870), *C. parvum* (cdg3_2870) *C. parvum* (cdg3_640) ; *Hammondia hammondi* (HHA_310150), *H. hammondi* (HHA_310080), *H. hammondi* (HHA_276155), *H. hammondi* (HHA_232580), *H. hammondi* (HHA_297220), *H. hammondi* (HHA_243800), *H. hammondi* (HHA_247760); *Neospora caninum* (NCLIV_063970), *N. caninum* (NCLIV_006300), *N. caninum* (NCLIV_006990), *N. caninum* (NCLIV_054250), *N. caninum* (NCLIV_018500). First step involved the curation of these protein sequences. The protein sequences were aligned (Clustalomega) and then gaps were removed from the alignment. Finally, the phylogenetic tree was constructed using the maximum likelihood method in the PhyML program. The default substitution model (WAG) was selected. Graphical representation and edition of the phylogenetic tree were performed with cladogram.

T. gondii strains and cultures

The parasite host cells human foreskin fibroblasts (HFF) were cultured using Dulbecco's Modified Eagle's Medium (DMEM, Gibco) supplemented with 10% fetal bovine serum (FBS, Gibco), 2 mM glutamine (Gibco) and 25 µg/mL gentamicin (Gibco) at 37°C and 5% CO2.

T.gondii tachyzoite parental strains RH-ΔKu80 TATi, RH-ΔKu80 as well as mutant strains *Tg*LIPIN-iKD, *Tg*LIPIN-3*HA were propagated by serial passage within their host HFF using DMEM supplemented with 1% fetal bovine serum (FBS, Gibco), 2 mM glutamine (Gibco) and 25 µg/mL gentamicin (Gibco) at 37°C and 5% CO2.

Generation of HA-tagged lines for all TgACSs and inducible knockdown line for TgACS2 and TgACS3

All C-terminally tagged HA expressing parasite lines were generated from gene's endogenous locus using the classical pLIC strategy using homologous recombination in a RH-ΔKu80 strain. For the same, homology regions (HR) (respective lengths enlisted below: Table1) of all the *Tg*ACSs located towards to C-terminus excluding the stop codon, were amplified from the parasite genomic DNA using the primers enlisted in Table 1. The homology region was assembled into *PacI* digested pLIC-HA-DHFR plasmid using ligation independent cloning protocol. The assembled plasmid was linearized using single enzyme site specific to the parasite DNA sequence

within the plasmid just before transfection (enlisted in table 1). Parasites were selected with the drug pyrimethamine and cloned by limiting dilution

***Tg*ACS Gene ID**	**Primers** (gene specific sequence underlined)	**Length of HR** (in bp)
*Tg*ACS1 (TGGT1_297220)	Fw: TACTTCCAATCCAATTTAATGCAGCCTGGGGATGCCGATCAACT Rw: TCCTCCACTTCCAATTTTAGCCAGCTTTGCCTGCAGCGC	2501
*Tg*ACS2 (TGGT1_310150)	Fw: TACTTCCAATCCAATTTAATGCGCGCTCGGCGTTGAGTT Rw: TCCTCCACTTCCAATTTTAGCCGACCACCACGACCGCA	1956
*Tg*ACS3 (TGGT1_310080)	Fw: TACTTCCAATCCAATTTAATGCACTTGGCCATCTCCGCGTATCC Rw: TCCTCCACTTCCAATTTTAGCCACGCTGTGGCTGAGTTCGTC	2406
*Tg*ACS4 (TGGT1_243800)	Fw: TACTTCCAATCCAATTTAATGCCTTGCTTGGTGGCCATCATCG Rw: TCCTCCACTTCCAATTTTAGCAATCGCCTTCGCTCTCTCCG	1202
*Tg*ACS5 (TGGT1_247760)	Fw: TACTTCCAATCCAATTTAATGCCCTCGGATCATCGACCGAGC Rw: TCCTCCACTTCCAATTTTAGCATTGGCAGGATGGTGCCGT	1458

*Tg*ACS6 (TGGT1_232580)	Fw: TACTTCCAATCCAATTTAATGCGAAGATGAGATGACCGGGC Rw: TCCTCCACTTCCAATTTTAGCCTTATCTTCGACGTCCTTTACAG	986
*Tg*ACS7 (TGGT1_276155)	Fw: TACTTCCAATCCAATTTAATGCGAAGCAGGCGAACCTGGA Rw: TCCTCCACTTCCAATTTTAGCGTCGTCGTTCTTCAAAAGTTCG	770

For generation of an inducible knockdown parasite line for the gene *Tg*ACS2 and *Tg*ACS3 plasmid pPR2-DHFR (Katris et al. 2014) was used. For homologous recombination in RH-ΔKu80 TATi strain two separate homology flanks/regions were chosen. The 5' flank was amplified 1298 bp upstream of the *Tg*ACS3 start codon using the primers forward 5′-GGGCGCGCCGGATCCTTAATTAATCGCTGCGATGTCGATCGTTTTC-3' and reverse 5′-CGCCATGCATGGCCGGCCCATATGGCGACTACGAAAGACAAACGCC-3'. The pcr product was ligated to *PacI* and *NdeI* digested vector pPR2 using NEB assembly reaction. Next, the 3' flank was amplified as a 1263 bp fragment beginning at the start codon of *Tg*ACS3 with the primers forward 5′-TGTTCCAGATTATGCCTTACCCGGGATGGCACTCCAGTACGCCTACC-3' and reverse 5′-TGGAGCTCCACCGCGGTGGCGGCCGCCTGCTTCGAGGAGAATGGCTTTC-3'. The 3' homology flank was annealed to *XmaI* and *NotI* digested pPR-HA3-DHFR vector that already contained the *Tg*ACS3 5' flank. The final cloned vector positions the start codon of *Tg*ACS3 downstream of the ATc-regulatable t7s4 promoter and a 3xHA tag. Similar protocol was used for construction of *Tg*ACS2-pPR2-DHFR plasmid. For the same, a 1535 bp 5' homology flank was pcr amplified with primers forward 5'-TGTTCCAGATTATGCCTTACCCGGGATGCCTGTCTCGGGCGCT-3' and reverse 5'-TGGAGCTCCACCGCGGTGGCGCGGCCGCCGACCACCACGACCGCAG and a 1668 bp 3' homology flank was amplified using forward 5'-TGTTCCAGATTATGCCTTACCCGGGATGCCTGTCTCGGGCGCT and reverse 5'-

TGGAGCTCCACCGCGGTGGCGCGGCCGCCTGTTCGGCGATGCTTTTGAC. The resulting vector were linearized with NotI and transfected this into TATiΔku80 parasites. Parasites were selected with the drug pyrimethamine and cloned out by limiting dilution. Screening of parasite clones *Tg*ACS3-iKD where the t7s4 promoter had successfully replaced the native *Tg*ACS3 promoter, was done using the primers P1 5'- CGATGACCTGTGTCGACCTGT P2 5′- TCTTCTTTGAGGGAAGAGGAAACG, P3 5'- GGTACCGAGCTCGACTTTCAC, P4 5'- CAGCTGATCGGAGGTTGGTCT and P5 5'- CTCCACCGTTTCCGGTTCCGT in the combinations described in supplementary fig S2. All PCRs were performed with TaKara Primestar Max polymerase. The knockdown of *Tg*ACS3 was induced with 0.5 μg ml^{-1} of anhydrotetracycline (ATc).

Immunofluorescence assay

Primary antibodies anti-HA (Rat, Roche), anti-IMC1 (Mouse), anti-SAG1 (Mouse) were used at dilutions 1:500, 1:1000 and 1:1000 respectively. Secondary Alexa Fluor 488- and 546-conjugated anti-mouse, anti-rat and anti-rabbit antibodies (Life Technologies) were used at 1/2500. For the immunofluorescence assay (IFA) parasites were grown on confluent HFF on coverslips and fixed in PBS containing 2.5% paraformaldehyde (PFA) for 15 min at room temperature (RT). Samples were permeabilized with 0.25% Triton X-100 in PBS for 10 min at RT prior to blocking in PBS containing 3% BSA and subsequent incubation with primary antibodies then secondary antibodies diluted in the blocking solution. Labelled parasites were stained with Hoechst (1/10000, Life technologies) for 20 min and then washed three times in PBS before final mounting of the coverslips on a glass slide using fluorogel (reference). The fluorescence was visualized using fluorescence microscope (Axio Imager 2_apotome; ZEISS).

Confocal Microscopy and 3D reconstruction

Confocal microscopy was performed for *Tg*ACS2-HA co-localized with parasite specific mitochondrial marker (TOM40), to delineate the proximity between the two proteins. For image processing, 3D reconstruction was achieved with the UCSF ChimeraX software from the raw data (i.e., *Tg*ACS2-HA co-loc with mitochondrial TOM40) obtained after initial processing i.e. by cropping the region of interest and then applying the ''Iterative Deconvolve 3D'' plugin for each channel, separately.

Western blot analysis

Parasites were harvested for western blot after complete egress from their host. In order to remove any host cell debris, the parasites were passed through a 3 μm filter, then counted by hemocytometer and solubilized in SDS buffer at equivalent cell densities. Equal amount of protein was separated on a 4-12% gradient SDS-polyacrylamide (Life Technologies) and transferred to Nitrocellulose membrane (check this) using the XCellII Blot Module (Invitrogen). Primary antibodies anti-HA (Rat, Roche) and anti-TOM40 (Rabbit) (Van Dooren et al. 2008) were used at a dilution of 1:500 and 1:1000, respectively. Secondary goat anti-mouse and anti-rabbit horse radish peroxidase (HRP) conjugated antibodies (Thermo Scientific) were used at 1:2000. Protein signal was detected by chemiluminescence after membrane staining with Luminata Crescendo Western HRP detection kit (Millipore). The signal strength of protein was quantified using a BioRad Chemidoc imager (BioRad).

Phenotypic analysis

Plaque assay- The extracellular parasites were harvested after filtration and counted by hemocytometer. Then approx. 500 parasites were inoculated to confluent HFF flask (25 cm^2). The mutant parasites *Tg*AC2-iKD and *Tg*ACS3-ikD was grown for plaque assay in the presence or absence of ATc (0.5 μg ml^{-1}) for 7-10 days. Plaque sizes were visualized by crystal violet staining (30-60 min) after aspiration of culture media, and cells fixation with 100% ethanol (5 min) followed by phosphate-buffered saline (PBS) wash.

Replication assay- The parasites were grown for two days with or without ATc (0.5 μg ml^{-1}), harvested and filtered. Equal number of parasites were allowed to invade confluent HFF grown on coverslips. Following 2 h of invasion, the coverslips were washed thrice with ED1 (1% FBS containing DMEM), in order to remove any uninvaded parasites and promote synchronized replication. Anhydrotetracycline (ATc) (0.5 μg ml^{-1}) was added at the outset of the experiment, allowing the treatment for 24 h, alongside control parasites without ATc. These coverslips were then fixed and processed for IFA wherein the parasite number per parasitophorous vacuole was analyzed.

Egress assay- Like replication assay, the parasites were treated with ATc prior to the experiment. Equal number of parasites were allowed to invade confluent HFF grown on coverslips and allowed

to grow for 24-30 h for having big vacuoles with 16-32 parasites. For the egress assay, the culture media (ED1) was removed and replaced with either 5 µM of calcium ionophore A23187 or DMSO control. This was followed by a 4 min incubation at 37ºC. The parasites were immediately fixed with 2.5% paraformaldehyde+0.02% glutaraldehyde and proceeded for an IFA using anti-SAG1 antibody.

Lipidomic analysis

The parasites were grown for 24 h ad 48 h in conditions of +/- ATc on the confluent monolayer of HFF in flasks (175 cm^2). At each time point, parasites were harvested as the intracellular tachyzoites (1×10^7 cell equivalents per replicate) after syringe filtration with 3-µm pore size membrane. These parasites were metabolically quenched by rapid chilling in a dry ice-ethanol slurry bath and then centrifuged down at 4°C. The parasite pellet thus obtained was washed with ice-cold PBS thrice, before transferring the final pellet to a microcentrifuge tube. Then total lipids were extracted in chloroform/methanol/water (1:3:1, v/v/v) containing PC (C13:0/C13:0), 10 nmol and C21:0 (10 nmol) as internal standards for extraction) for 1 h at 4°C, with periodic sonication. Then polar and apolar metabolites were separated by phase partitioning by adding chloroform and water to give the ratio of Chloroform/Methanol/Water, 2:1:0.8 (v/v/v). For lipid analysis, the organic phase was dried under N_2 gas and dissolved in 1-butanol to obtain1µl butanol/10^7 parasites.

Total lipid analysis – Total lipid was then added with 1 nmol pentadecanoic acid (C15:0) as internal standard and derivatized to give fatty acid methyl ester (FAME) using trimethylsulfonium hydroxide (TMSH, Machenery Nagel) for total glycerolipid content. Resultant FAMEs were then analyzed by GC-MS as previously described (Dubois et al. 2018). All FAME were identified by comparison of retention time and mass spectra from GC-MS with authentic chemical standards. The concentration of FAMEs was quantified after initial normalization to different internal standards and finally to parasite number.

Phospholipid and neutral lipid analysis- For phospholipid analysis, total lipid extracted (as mentioned above) was separated with 1 nmol PA(C17:0/C17:0) (Avanti Polar lipids) by two-dimensional silica gel high-performance thin layer chromatography (HPTLC, Merck). The solvent system used for the 1st and 2nd dimension was chloroform/methanol/28% ammonium

hydroxide,12:7:1.6 (v/v) and chloroform/acetone/methanol/acetic acid/water, 10:4:2:2.6:1 (v/v/v/v/v), respectively. DAG, TAG, Free fatty acids (FFA) and cholesteryl ester (CE) analysis, total lipid fraction was separated by 1D-HPTLC using hexane/diethyl ether/formic acid, 80:20:2 (v/v/v) as solvent system. Thereafter, each lipid spot on the HPTLC plate was scrapped off and lipids were methanolized with 200 µl 0.5 M methanolic HCl in the presence of 1 nmol pentadecanoic acid (C15:0) as internal standard at 85ºC for 3 h. The resulting FAMEs were extracted with hexane and finally analyzed by GC-MS (Agilent).

Statistical analysis for all experiments

Entire graphical data for this study was generated using GraphPad prism software. Three biological replicates were used per experiment (n=3). The error bars are representative of standard error of mean (SEM) for each study. Statistical significance was determined for each experiment by t-test using GraphPad Prism. Range of statistical significance was signified as per the p value, wherein 0.01-0.05=*, 0.01-0.001=** and <0.001=***.

FIGURES

a

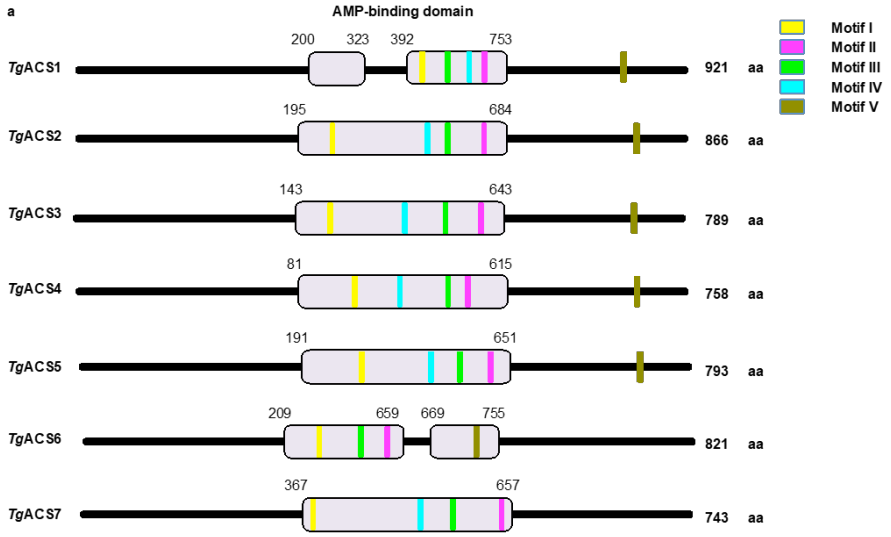

b

accession number	annotation	Motif I: {Y,F} TSG {T,S} TGXPK	Motif II: TGDX (7) GX hX (2) RX (4) Hx (3,4) GX (2) hX (4) hE	Motif III: YGXTE Or (WWQTE)	Motif IV: LPLXH	Motif V: PKTX{S,T} GKIX {R,K} (KXX {R,K})
TGGT1_297220:	*Tg*ACS1	455 YTSGTTGFPK 465	728 TGDLGYVDS----DGFVYLTGRKELIITAGGENVAPLLE 764	652 YGLSE 656	501 LPLSH 506	879 KLRR 882
TGGT1_310150:	*Tg*ACS2	379 YTSGTTGNPK 389	660 TGDVVEIQP----NGSMNIIDRKKSLIKLAQGEYLQTEKE 697	568 WGMTE 572	425 LPLSH 430	811 KSKR 814
TGGT1_310080:	*Tg*ACS3	295 YTSGTTGNPK 395	619 TGDIVEIQP----NGSIKIIDRKKSLIKLAQGEYLQTEKLE 654	521 WGMTE 525	333 LPLSH 338	764 KTKR 767
TGGT1_243800:	*Tg*ACS4	365 YTSGTTSRPK 375	590 SGDVAVIVP---GSNAVKIIDRKKNIFKLAQGEYVSPEKE 628	505 YGMTE 509	364 LPLAH 371	729 KIKR 732
TGGT1_247760:	*Tg*ACS5	380 FTSGTTGVPK 390	627 TGDVVELLP----SGAPRIIDRAKNIFKLAQGEYVAPERLE 664	544 WGMTE 549	406 LPQSH 411	764 KVVR 767
TGGT1_232580:	*Tg*ACS6	370 YTSGTTGDPK 380	635 TGDSGHFDD--DGYLHIEGRTDDVIN-VSAHRISGLSIEE 672	562 WWQSE 566	423 LGWVL 428	750 SGKTLR 758
TGGT1_276155:	*Tg*ACS7	369 FTSGTTGRPK 379	650 LGDVCFFLRPLAND G-QVDGDEEQEERREDEKEN RDEREEKETGEKEEKETGEKEKESRLD 709	541 FGSTE 545	414 LHHVN 419	Not found

Fig.1. Identification of seven acyl CoA synthetase encoding genes in T. gondii (TgACS).

a) Schematic representation of the characteristic AMP-binding domains within the 7 *Tg*ACSs (source: ToxoDB, https://toxodb.org/toxo/). The annotated amino acid sequences of *Tg*ACSs suggest similar protein sizes, with AMP-binding domains localizing mostly in the middle of the protein: *Tg*ACS1 (200-323 aa, 392-753 aa), *Tg*ACS2 (195-684 aa), *Tg*ACS3 (143-643 aa), *Tg*ACS4 (81-758 aa), *Tg*ACS5 (191-651 aa), *Tg*ACS6 (209-659 aa, 669-755 aa), *Tg*ACS7 (357-657 aa). b) Sequence alignment of *Tg*ACSs with other eukaryotic homologs, confirms the presence of 5 characteristic ACS motifs (Motif I-yellow, Motif II-purple, Motif III-green, Motif IV- cyan blue, Motif V- brown) described in table (b). In contrast to first 4 motifs which reside within the annotated AMP-binding domains of *Tg*ACSs, only a part of consensus sequence of Motif V exists, mostly outside of the annotated AMP-binding domains (except *Tg*ACS6). All sequence alignments were conducted using online toll Clustal omega (https://www.ebi.ac.uk/Tools/msa/clustalo).

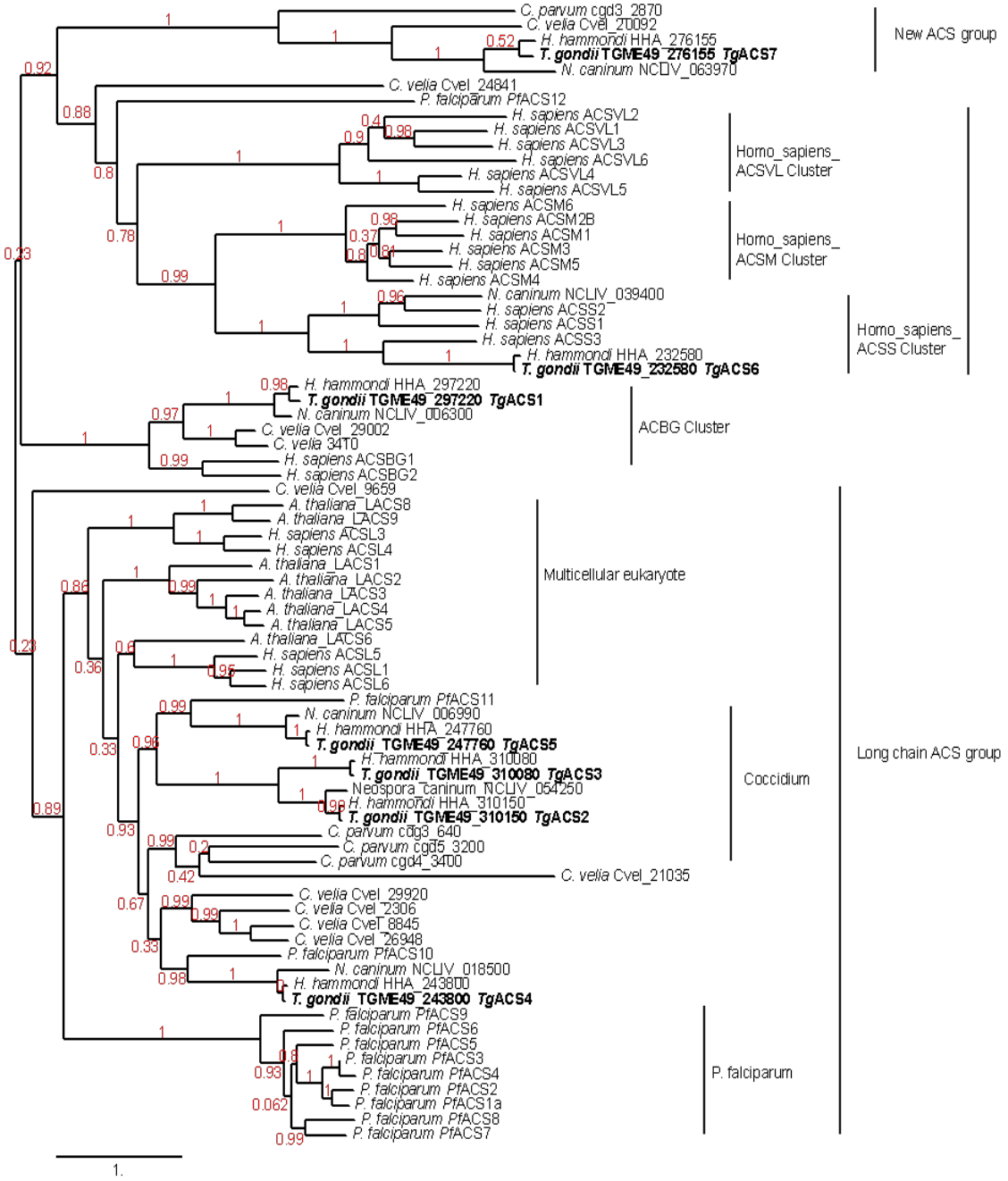

Fig.2. Phylogenetic analysis of the seven TgACSs with eukaryotic homologs

All 7 *Tg*ACSs appear in specified clusters based on their homology with their eukaryotic counterparts: *Tg*ACS1 in ACBG cluster; *Tg*ACS2, *Tg*ACS3, *Tg*ACS4, *Tg*ACS5 in the long chain ACS group; *Tg*ACS6 in the short chain ACS cluster; *Tg*ACS7 in a separate cluster specific to coccidia and chromerids. The phylogenetic tree was generated online using Phylogeny.fr.

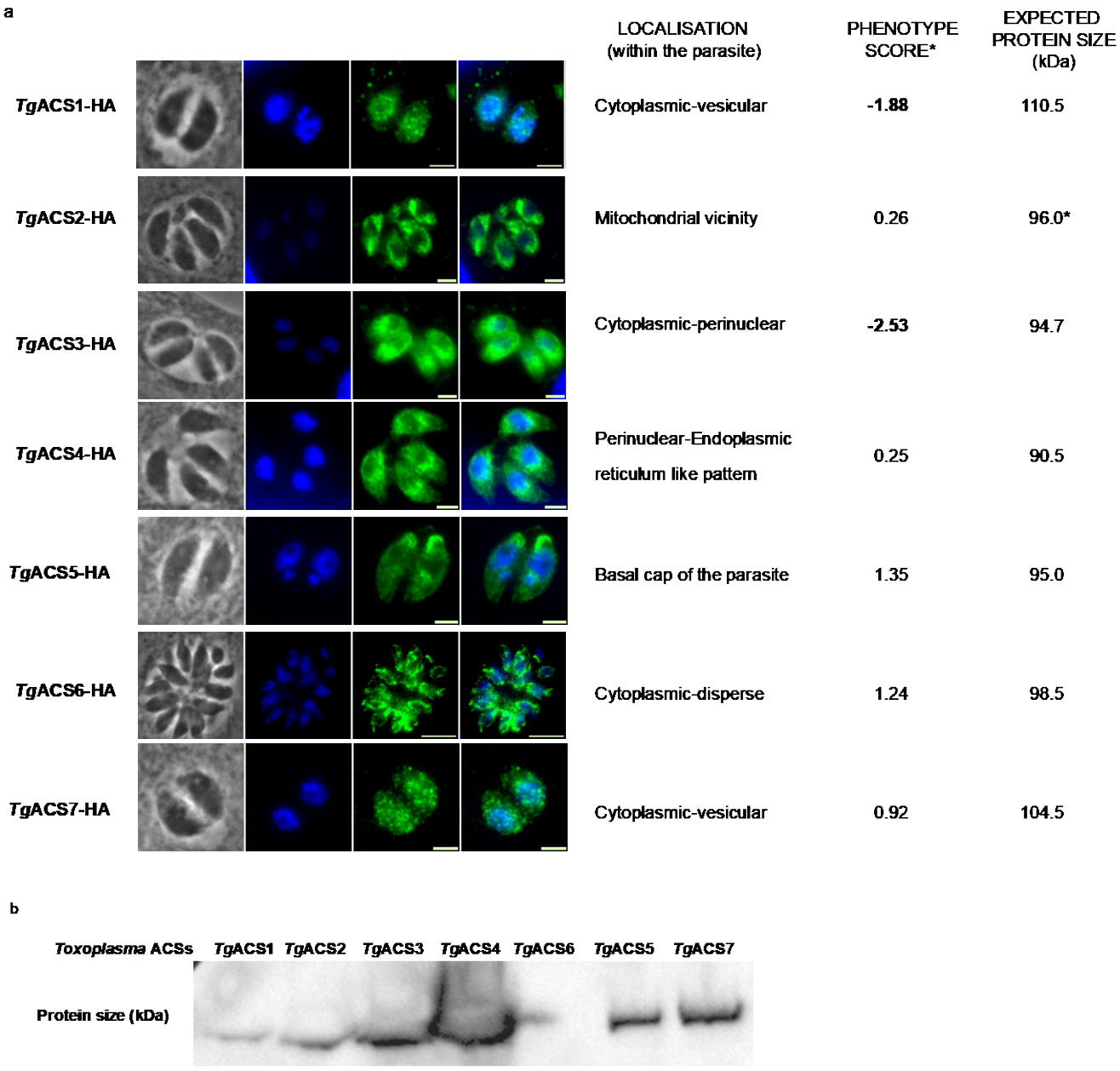

Fig.3. Endogenous localizations of the Toxoplasma ACSs

a) The 7 *Tg*ACSs were localized endogenously at their C-terminus with 3×HA. Immunofluorescence with anti-HA antibody shows that all seven proteins localize to non-overlapping compartments within the parasite: *Tg*ACS1 as cytoplasmic vesicular ; *Tg*ACS2 at the vicinity of mitochondria ; *Tg*ACS3 within the parasite cytoplasm, perinuclear ; *Tg*ACS4 as reminiscent of endoplasmic reticulum (ER) ; *Tg*ACS5 at the basal end of the parasite ; TgACS6 dispersed throughout parasite cytoplasm and *Tg*ACs7 showing vesicular localization within cytoplasm. Towards the right side of the IFA images is depicted the phenotype scores of all 7 *Tg*ACSs based on CRISPR-cas9 mediated whole genome screen in *T. gondii* (Sidik et al. 2016). b) Western blot analysis using anti-HA antibody shows all *Tg*ACSs migrating at their predicted protein sizes on ToxoDB (except *Tg*ACS2).

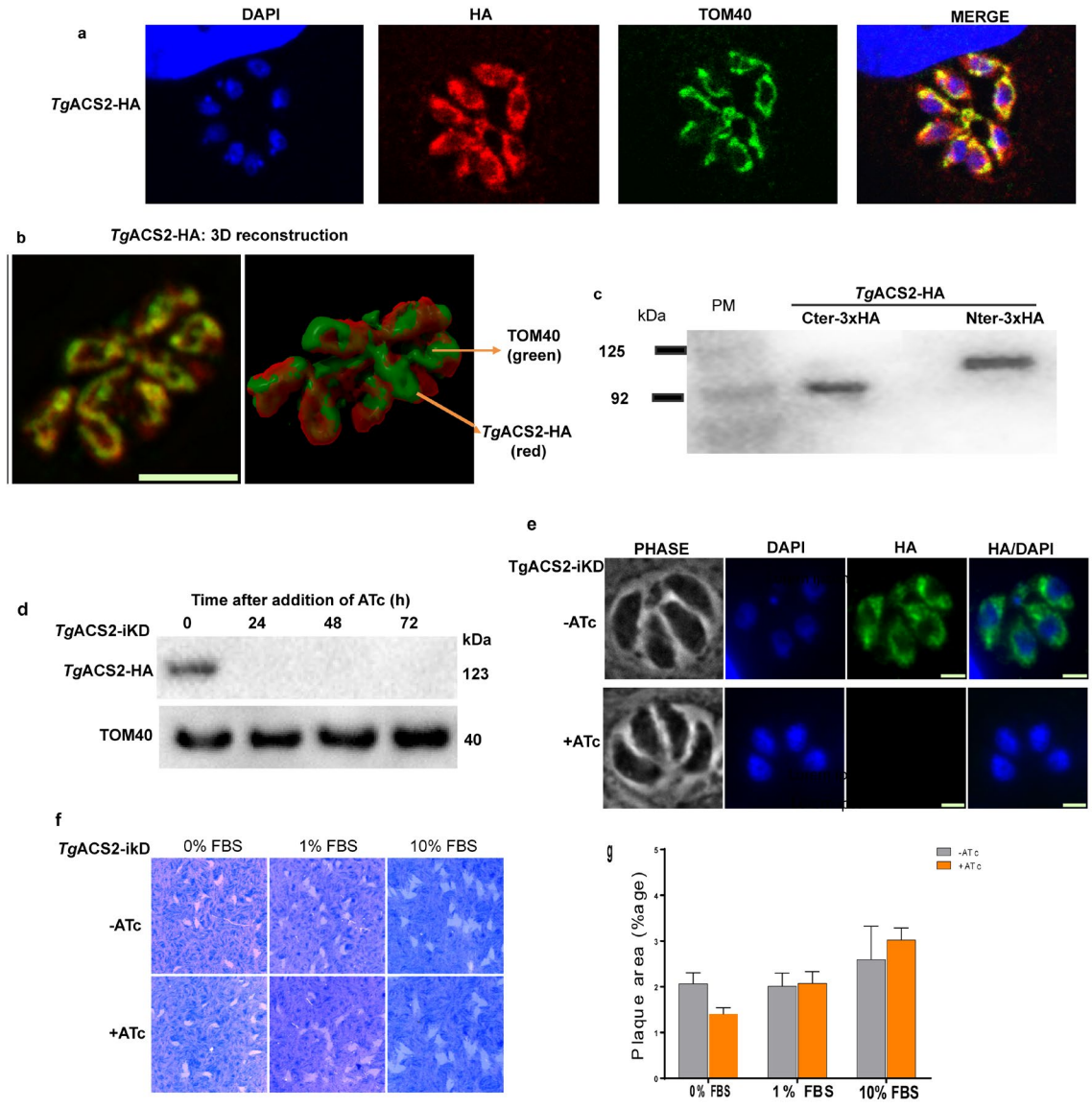

Fig.4. TgACS2 localizes to mitochondrial vicinity and is dispensable for growth of T. gondii.

a) Images generated using confocal microscopy depict that *Tg*ACS2 (HA-red) and mitochondrial marker (TOM40-green) co-localize with each other, thereby confirming mitochondrial vicinity of this ACS. b) 3D reconstruction of confocal images was obtained for *Tg*ACS2/mitochondrial co-location, using UCSF ChimeraX software. c) Western blot analysis using anti-HA antibody showing a size difference of approx. 10 kDa between *Tg*ACS2 tagged at C-terminus (endogenous promoter) and at the N-terminus (Tet-based promoter). d) Western blot and IFA (e) using anti-HA antibody shows downregulation of *Tg*ACS2 24 after induction with anhydrotetracycline (ATc). f) Plaque assays performed with *Tg*ACS2-iKD depict normal growth after depletion of *Tg*ACS2 using ATc, with no significant effect in the presence of 0, 1 and 10% FBS conditions. g) Graphical representation and statistical analysis of the plaque areas obtained confirms the dispensability of *Tg*ACS2 for parasite growth.

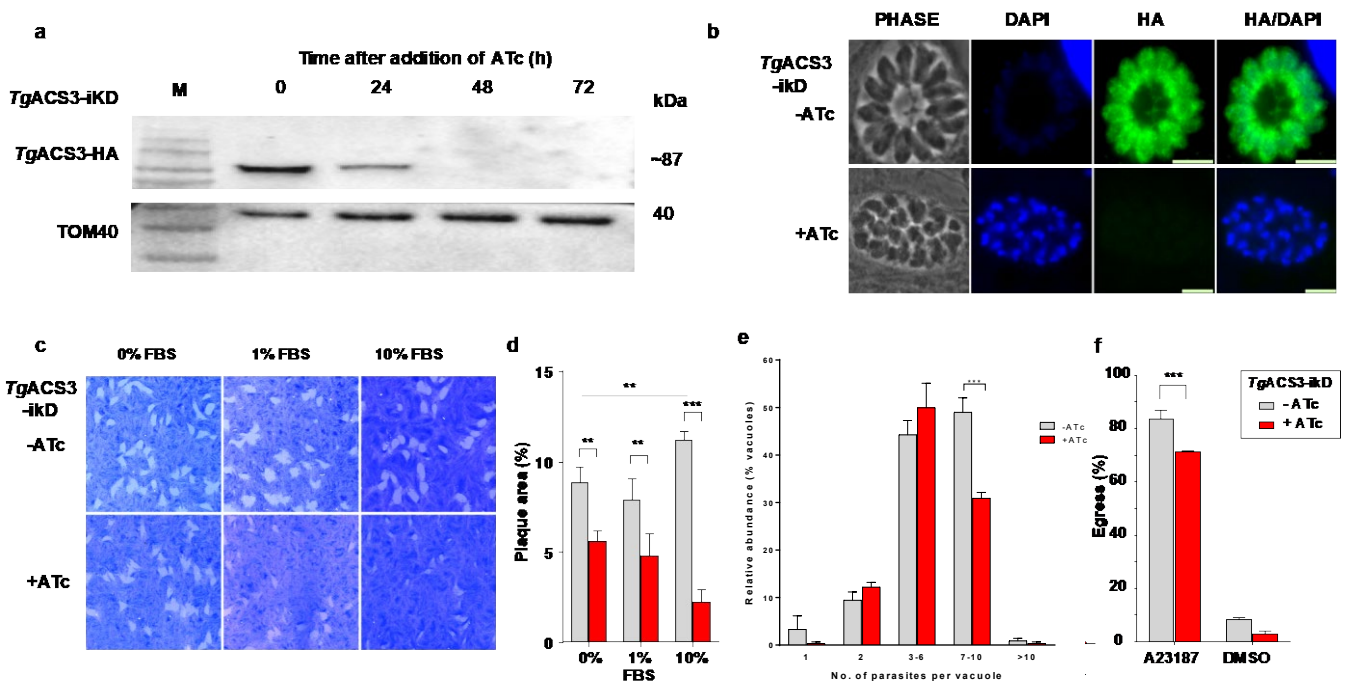

Fig.5. TgACS3 is required for parasite growth in vitro

Western blot (a) and IFA (b) analysis using anti-HA antibody show complete loss of *Tg*ACS3, 48 h after induction with ATc. c) Growth assays show reduction in plaque area upon *Tg*ACS3 depletion (+ATc), which is aggravated more in the presence of increased FBS content (10%), depicting effect of lipotoxicity in *Tg*ACS3-ikD (+ATc). d) The plaque area percentage of *Tg*ACS3-iKD (+ATc) declines by 4-5% in 0 and 1% FBS; by 8% in 10% FBS. e) The *Tg*ACS3-iKD showed a replication defect in the presence of ATc, with a significant decrease in the vacuoles with 7-10 parasites and consequent increase in vacuoles with 3-6 parasites. f) *Tg*ACS3-iKD + ATc parasites also exhibited a minor yet significant egress defect upon induction with calcium ionophore A23187. Three biological replicates were used per experiment (n=3). The error bars are representative of standard error of mean (SEM) for each study. Statistical significance was determined for each experiment by t-test using GraphPad Prism. Range of statistical significance was signified as per the p value, wherein 0.01-0.05=*, 0.01-0.001=** and <0.001=***.

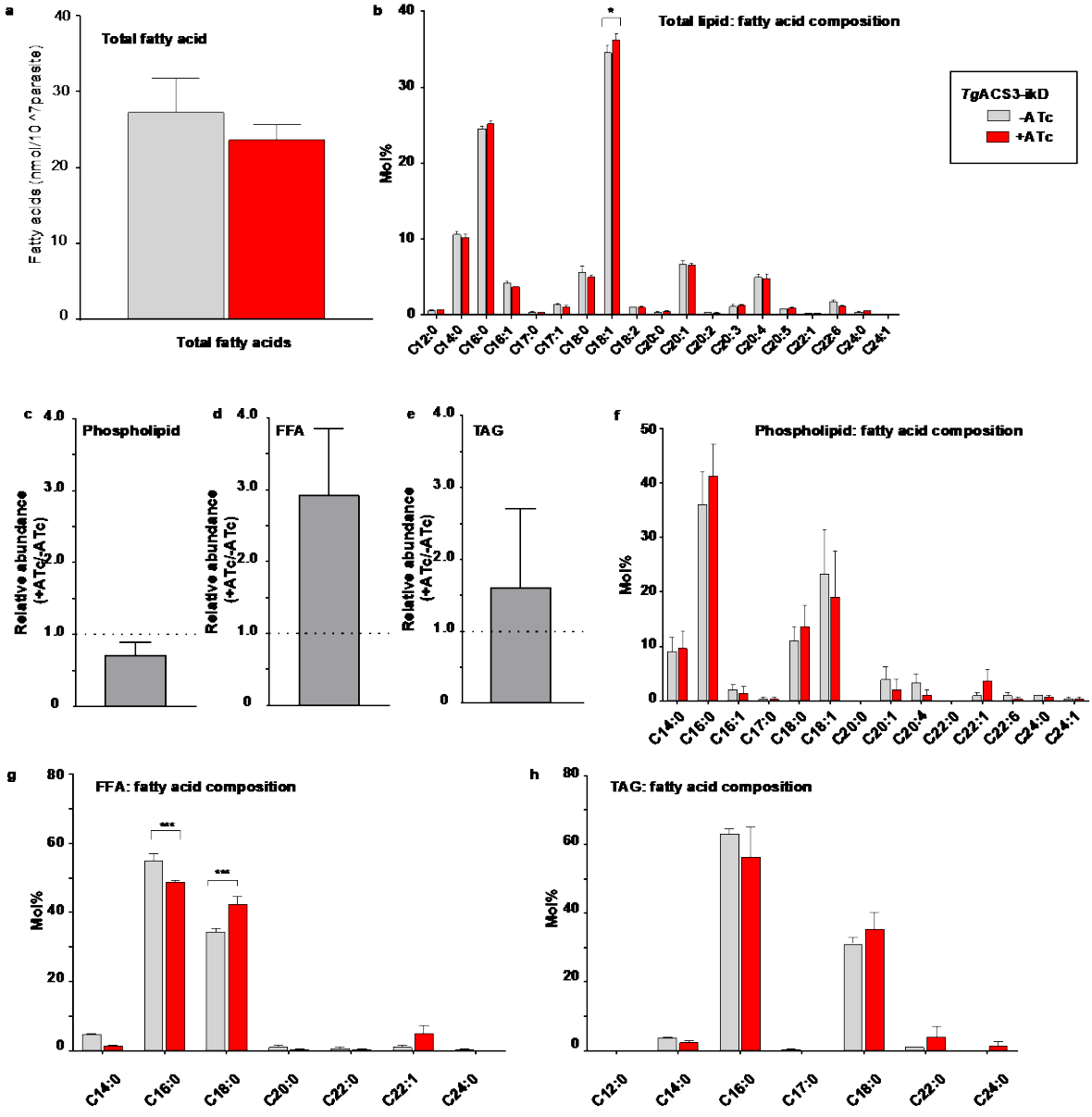

Fig.6. TgACS3 depletion results in specific decrease in the phospholipid fatty acid species within the parasite.

a) The total fatty acid (FA) content depicted by nmol FA/number of parasites, of *Tg*ACS3-iKD parasites showed no major difference in the presence of +ATc (red) or absence of –ATc (grey). b) The overall FA composition of *Tg*ACS3-iKD parasites depicted by mol%, show a minor yet significant increase in oleic acid (C18:1). *Tg*ACS3 depletion results in a significant decrease in the relative abundance (+ATc/-ATc) of total phospholipids (c) and possible consequent increase of free fatty acids (d). e) Graph showing slight increase in the relative abundance of triacylglycerols (TAGs). f) The FA composition of phospholipids in the *Tg*ACS3-ikD represented by mol%. Graphical representation of FA composition (mol%) of the FFA (g) and TAG (h) species within *Tg*ACS3-iKD. *Tg*ACS3-iKD+ATc in red and *Tg*ACS3-iKD-ATc in grey. g) *Tg*ACS3-iKD+ATc parasites were characterized with a significant decrease in C16:0 and increase in C18:0 derived from the FFA species. Three biological replicates were used per experiment (n=3). The

error bars are representative of standard error of mean (SEM) for each study. Statistical significance was determined for each experiment by t-test using GraphPad Prism. Range of statistical significance was signified as per the p value, wherein 0.01-0.05=*, 0.01-0.001=** and <0.001=***.

Supplementary figures

Fig. S1. Sequence alignment showing conservation of all 5 ACS motifs among various homologs of *Toxoplasma* ACSs

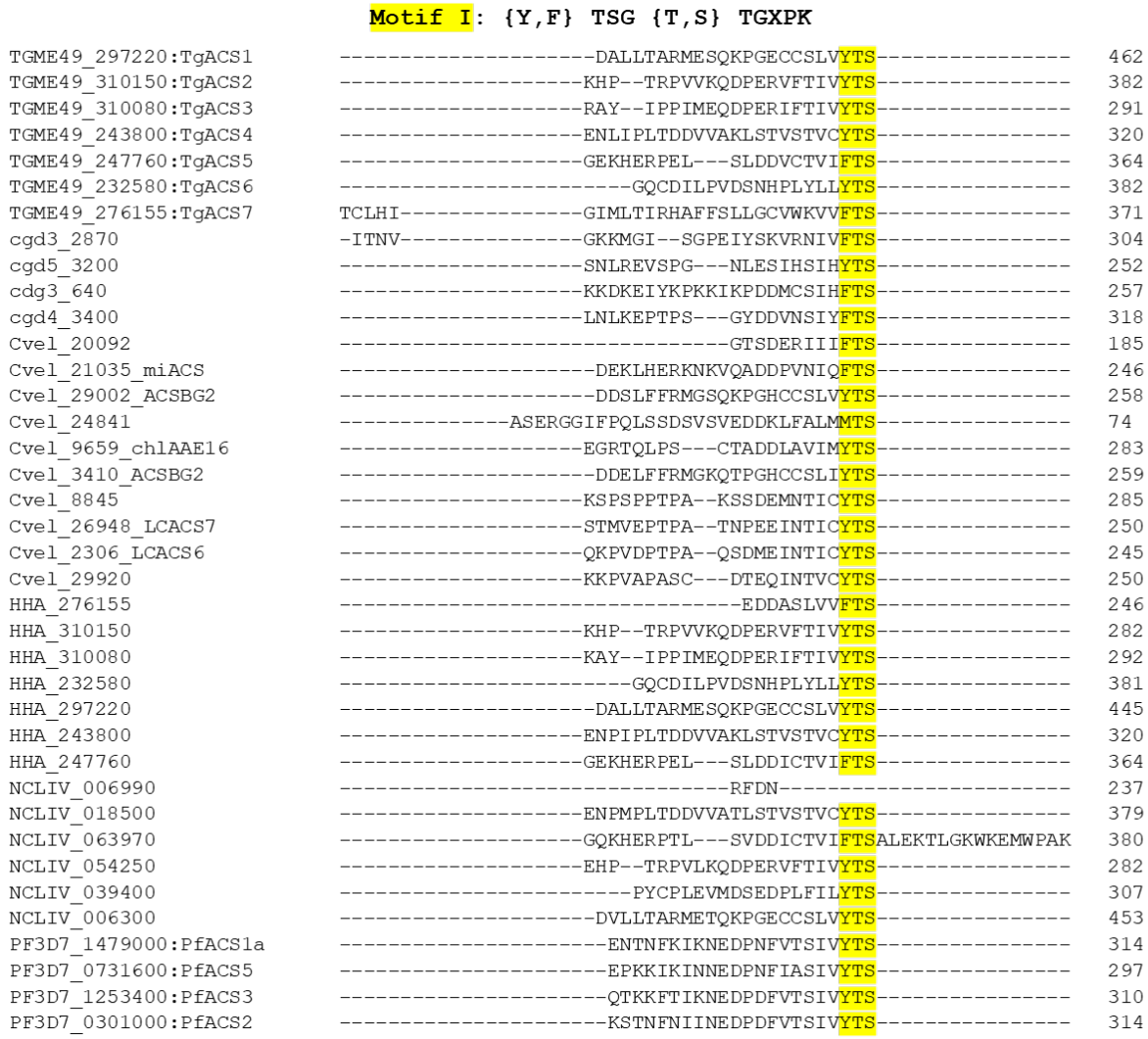

Motif I: {Y,F} TSG {T,S} TGXPK

```
PF3D7_0619500:PfACS12   ----------------------INKEEKNMLNSDICLHLHTS----------------   203
PF3D7_1372400:PfACS4    ---------------------QTKKFTIKNEDPDFVTSIVYTS----------------   310
PF3D7_0401900:PfACS6    ---------------------KKTNMKIQNEDPDFITSIVYTS----------------   363
PF3D7_0215000:PfACS9    --------------------NNMLTYNIQNDKENFISTIVYTS----------------   453
PF3D7_0215300:PfACS8    ---------------------PTKIYNIQNDEPDFITSIVYTS----------------   312
PF3D7_0525100:PfACS10   --------------------KKIVKVPQG---ALNNIFSICYTS----------------   245
PF3D7_1238800:PfACS11   NNNNIQKMNTNNRSIDERN-NYLMKQIKKNKGNLNDVCTIIFTS----------------   368
PF3D7_1200700:PfACS7    ----------------------KIANVTVQNEDPNFIASIVYTS----------------   306
HsACSL1                 --------------------ANRRKPKPP---APEDLAVICFTS----------------   277
ATLACS1                 --------------------EKPEDTNPP---KAFNICTIMYTS----------------   229
ATLACS2                 --------------------LDEANLPRK---RKTDICTIMYTS----------------   232
HsACSL3                 --------------------KASMENQPHSKPLPSDIAVIMYTS----------------   288
ATLACS3                 --------------------GKHYELPEK---RRSDVCTIMYTS----------------   232
HsACSL4                 --------------------NPENLGIPPSRPTPSDMAIVMYTS----------------   279
ATLACS4                 --------------------GKQYDLPIK---KKSDICTIMYTS----------------   232
HsACSL5                 --------------------EHFRKPVPP---SPEDLSVICFTS----------------   262
HsACSL6                 --------------------ENHQAPVPP---QPDDLSIVCFTS----------------   277
ATLACS5                 --------------------GKQYELPIK---KPSDICTIMYTS----------------   232
ATLACS6                 --------------------SNPQRFFPP---KPDDVATICYTS----------------   270
ATLACS8                 --------------------KN---AVQPILPSKNGVAVIMFTS----------------   283
ATLACS9                 --------------------EN---PVDPNFPLSADVAVIMYTS----------------   254
HsACSS3                 ------------------------QSHDCVPVLSEHPLYILYTS----------------   300
HsACSM3                 ------------------------DSHTCVKTKHNEIMAIFFTS----------------   236
HsACSM2B                ------------------------TTHHCVETGSQEASAIYFTS----------------   222
HsACSM1                 ------------------------PEHTCVKSKTLDPMVIFFTS----------------   227
HsACSM4                 ------------------------EEHSCVETGSQEPMTIYFTS----------------   230
HsACSM5                 ------------------------TEHNCMRTKSRDPLAIYFTS----------------   231
HsACSM6                 ------------------------PKQTYMRTKSQDPMAIFFTK----------------   227
HsACSBG1                --------------------EEALDAIIDTQQPNQCCVLVYTS----------------   283
HsACSBG2                --------------------DTQLEQVIESQKANQCAVLIYTS----------------   231
HsACSS1                 ------------------------PVCAPESMGSEDMLFMLYTS----------------   295
HsACSS2                 ------------------------DECEPEWCDAEDPLFILYTS----------------   222
HsACSVL1                --------------------TEPIPESWRSEVTFSTPALYIYTS----------------   226
HsACSVL2                --------------------DEPVPRSHHVVSLLKSTCLYIFTS----------------   225
HsACSVL3                --------------------DGPVPGYLSSPQSITDTCLYIFTS----------------   336
HsACSVL4                --------------------K-HLPSCP--DKGFTDKLFYIYTS----------------   247
HsACSVL5                --------------------TAPLAQIP--SKGMDDRLFYIYTS----------------   250
HsACSVL6                --------------------SHPVPADLRAGITWRSPALFIYTS----------------   296
```

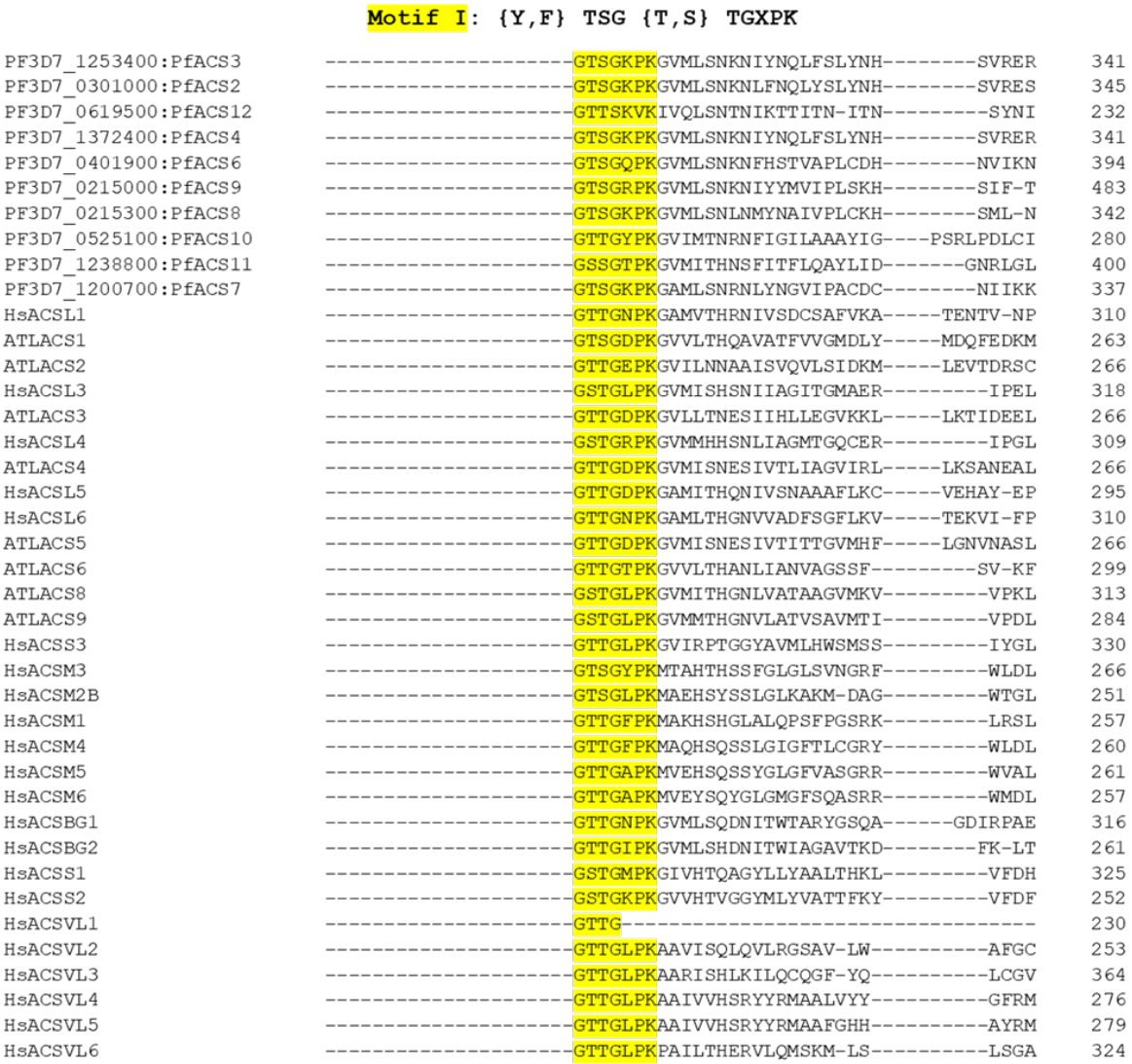
Motif I: {Y,F} TSG {T,S} TGXPK
PF3D7_1253400:PfACS3 ----------GTSGKPKGVMLSNKNIYNQLFSLYNH--------SVRER 341
PF3D7_0301000:PfACS2 ----------GTSGKPKGVMLSNKNLFNQLYSLYNH--------SVRES 345
PF3D7_0619500:PfACS12 ----------GTTSKVKIVQLSNTNIKTTITN-ITN---------SYNI 232
PF3D7_1372400:PfACS4 ----------GTSGKPKGVMLSNKNIYNQLFSLYNH--------SVRER 341
PF3D7_0401900:PfACS6 ----------GTSGQPKGVMLSNKNFHSTVAPLCDH--------NVIKN 394
PF3D7_0215000:PfACS9 ----------GTSGRPKGVMLSNKNIYYMVIPLSKH--------SIF-T 483
PF3D7_0215300:PfACS8 ----------GTSGKPKGVMLSNLNMYNAIVPLCKH--------SML-N 342
PF3D7_0525100:PFACS10 ----------GTTGYPKGVIMTNRNFIGILAAAYIG----PSRLPDLCI 280
PF3D7_1238800:PfACS11 ----------GSSGTPKGVMITHNSFITFLQAYLID-------GNRLGL 400
PF3D7_1200700:PfACS7 ----------GTSGKPKGAMLSNRNLYNGVIPACDC--------NIIKK 337
HsACSL1 ----------GTTGNPKGAMVTHRNIVSDCSAFVKA-----TENTV-NP 310
ATLACS1 ----------GTSGDPKGVVLTHQAVATFVVGMDLY-----MDQFEDKM 263
ATLACS2 ----------GTTGEPKGVILNNAAISVQVLSIDKM-----LEVTDRSC 266
HsACSL3 ----------GSTGLPKGVMISHSNIIAGITGMAER---------IPEL 318
ATLACS3 ----------GTTGDPKGVLLTNESIIHLLEGVKKL-----LKTIDEEL 266
HsACSL4 ----------GSTGRPKGVMMHHSNLIAGMTGQCER---------IPGL 309
ATLACS4 ----------GTTGDPKGVMISNESIVTLIAGVIRL-----LKSANEAL 266
HsACSL5 ----------GTTGDPKGAMITHQNIVSNAAAFLKC-----VEHAY-EP 295
HsACSL6 ----------GTTGNPKGAMLTHGNVVADFSGFLKV-----TEKVI-FP 310
ATLACS5 ----------GTTGDPKGVMISNESIVTITTGVMHF-----LGNVNASL 266
ATLACS6 ----------GTTGTPKGVVLTHANLIANVAGSSF---------SV-KF 299
ATLACS8 ----------GSTGLPKGVMITHGNLVATAAGVMKV---------VPKL 313
ATLACS9 ----------GSTGLPKGVMMTHGNVLATVSAVMTI---------VPDL 284
HsACSS3 ----------GTTGLPKGVIRPTGGYAVMLHWSMSS---------IYGL 330
HsACSM3 ----------GTSGYPKMTAHTHSSFGLGLSVNGRF---------WLDL 266
HsACSM2B ----------GTSGLPKMAEHSYSSLGLKAKM-DAG---------WTGL 251
HsACSM1 ----------GTTGFPKMAKHSHGLALQPSFPGSRK---------LRSL 257
HsACSM4 ----------GTTGFPKMAQHSQSSLGIGFTLCGRY---------WLDL 260
HsACSM5 ----------GTTGAPKMVEHSQSSYGLGFVASGRR---------WVAL 261
HsACSM6 ----------GTTGAPKMVEYSQYGLGMGFSQASRR---------WMDL 257
HsACSBG1 ----------GTTGNPKGVMLSQDNITWTARYGSQA------GDIRPAE 316
HsACSBG2 ----------GTTGIPKGVMLSHDNITWIAGAVTKD--------FK-LT 261
HsACSS1 ----------GSTGMPKGIVHTQAGYLLYAALTHKL---------VFDH 325
HsACSS2 ----------GSTGKPKGVVHTVGGYMLYVATTFKY---------VFDF 252
HsACSVL1 ----------GTTG---------- 230
HsACSVL2 ----------GTTGLPKAAVISQLQVLRGSAV-LW----------AFGC 253
HsACSVL3 ----------GTTGLPKAARISHLKILQCQGF-YQ----------LCGV 364
HsACSVL4 ----------GTTGLPKAAIVVHSRYYRMAALVYY----------GFRM 276
HsACSVL5 ----------GTTGLPKAAIVVHSRYYRMAAFGHH----------AYRM 279
HsACSVL6 ----------GTTGLPKPAILTHERVLQMSKM-LS----------LSGA 324

Motif I: {Y,F} TSG {T,S} TGXPK

```
TGME49_297220:TgACS1      --------------------GTTGFPKGVMLSHDNFTWTAACSSHM------MKI----    491
TGME49_310150:TgACS2      --------------------GTTGNPKGVMLTNRNWVAVIRALHIQ------NRTTLGI    415
TGME49_310080:TgACS3      --------------------GTTGNPKGVMMSNRNFVREIQGCLHI------NDYTLML    324
TGME49_243800:TgACS4      --------------------GTTSRPKGVLMSHGNFVATIAGAVRG----PLTVPSMAL    355
TGME49_247760:TgACS5      --------------------GTTGVPKGVVHTNGGFVATIAGYVGC-------NNRMNL    396
TGME49_232580:TgACS6      --------------------GTTGDPKGIVRDHAGQCVSSHYTASA---------IYGI    412
TGME49_276155:TgACS7      --------------------GTTGRPKGAILTNKNMETSCLALRQL--------LDLRD    402
cgd3_2870                 --------------------GSTGRPKGAKLTFGNYSGMISTLSVL--------CNNNN    335
cgd5_3200                 --------------------GTTGNPKGAVLTNRAWVSCTAAFVYG----QLGREGTKL    287
cdg3_640                  --------------------GTTGYPKGAILTHRCFLACVKSSYEH----LFSEKEIQL    292
cgd4_3400                 --------------------GTTGVPKGAIHTNGNWIAGASASLRS----FLNRSDCTL    353
Cvel_20092                --------------------GTTGLPKGVRLLYSNYDVNRKTFEKF--------LGVKE    216
Cvel_21035_miACS          --------------------GTTGRPKGATLSHHNIVNNGYFVG----------HRLGM    275
Cvel_29002_ACSBG2         --------------------GTTSFPKGVMLSHDNCTWTGSAGGPY------LDM----    287
Cvel_24841                --------------------GSTGSPKAAMFTDRMWTVDTGHAMY--------------     99
Cvel_9659_chlAAE16        --------------------GTTGQPKGVMLSHGNLLHQVYLNSFNDDAHKEGPGSVNP    322
Cvel_3410_ACSBG2          --------------------GTTSFPKGVMVSHDNCVWTGYSGGAF------LGL----    288
Cvel_8845                 --------------------GTTGNPKGAFVTHKQMLAAVSALKFI-----TEKNNLPF    319
Cvel_26948_LCACS7         --------------------GTTGNPKGAFVSHRQLLSAVNALFFI-----TQKNEVAF    284
Cvel_2306_LCACS6          --------------------GTTGNPKGVLVTHRALLTALSTSDEL-----FKKEGFKI    279
Cvel_29920                --------------------GTSGTPKGAMLPHRCFASNIAALDLA--GSDTEGGGLVI    287
HHA_276155                --------------------GTTGRPKGAILTNKNMETSCLALRQL--------LELRD    277
HHA_310150                --------------------GTTGNPKGVMLTNRNWVAVIRALHIQ------NRTTLGI    315
HHA_310080                --------------------GTTGNPKGVMMSNRNFVREIQGCLHI------NDYTLML    325
HHA_232580                --------------------GTTGDPKGIVRDHAGQCVSSHYTASA---------IYGI    411
HHA_297220                --------------------GTTGFPKGVMLSHDNFTWTAACSSHM------MKI----    474
HHA_243800                --------------------GTTSRPKGVLMSHGNFVATIAGAVRG----PLTVPSMAL    355
HHA_247760                --------------------GTTGVPKGVVHTNGGFVATIAGYVGC-------NNRMNL    396
NCLIV_006990              ------------------------------------------------------------    237
NCLIV_018500              --------------------GTTSSPKGVLMSHGNFVATVAGAVRG----PLTVPQMTL    414
NCLIV_063970              RRRGCVPEETPKRADLLRCAAGTTGVPKGVVHTNGGFVATIAGYAAC-------NNRMNL    433
NCLIV_054250              --------------------GTTGSPKGVMLTNKNWVAVIRSLYIQ------NPTTLGI    315
NCLIV_039400              --------------------GSTGKPKGLCHSTAGYLLYAALTHKF---------VFDY    337
NCLIV_006300              --------------------GTTGFPKGVMLSHDNFTWTAACSSHM------MKI----    482
PF3D7_1479000:PfACS1a     --------------------GSSGMPKGAMLSNKNLYNQLYSLYNH--------SVRKT    345
PF3D7_0731600:PfACS5      --------------------GTSGKPKGVMLSNENFHNTVVPLCDH--------NIIKE    328
```

Motif II: TGDX (7) GX hX (2) RX (4) Hx (3,4) GX (2) hX (4) hE

```
TGME49_297220:TgACS1        --FLHTGDLGYVDSD-------------------------------------------  737
TGME49_310150:TgACS2        KPWLLTGDVVEIQPN-------------------------------------------  669
TGME49_310080:TgACS3        SRWLATGDIVEIQPN-------------------------------------------  628
TGME49_243800:TgACS4        --WLHSGDVAVIVPG-------------------------------------------  599
TGME49_247760:TgACS5        --WMRTGDVVELLPS-------------------------------------------  636
TGME49_232580:TgACS6        --YYDTGDSGHFDDD-------------------------------------------  644
TGME49_276155:TgACS7        -WYLGLGDVCFFLRPLANDGQVDGDEEQEERREDEKENRDEREEKETGEKEEKETGEKEK  704
cgd3_2870                   -WYLGLGDQGYWTAEKINTNSEPSTVY---ILGEER------QVAHINKDPNIIIEEKLN  642
cgd5_3200                   --WIRTGDICQLLPN-------------------------------------------  524
cdg3_640                    --WLDTGDIAERQQD-------------------------------------------  532
cgd4_3400                   --WLHTGDIAELTDS-------------------------------------------  591
Cvel_20092                  -WYTNLGDICFWIEGEKC----------------------------------------  471
Cvel_21035_miACS            ARWMSTGDLAEMGED-------------------------------------------  485
Cvel_29002_ACSBG2           ------------------------------------------------------------  503
Cvel_24841                  --WYATGDLGRLDSE-------------------------------------------  315
Cvel_9659_chlAAE16          --WFVTGDLGQIMPS-------------------------------------------  594
Cvel_3410_ACSBG2            --FLHSGDLGYVDED-------------------------------------------  531
Cvel_8845                   --WFHTGDVVKVHPN-------------------------------------------  566
Cvel_26948_LCACS7           --WYHTGDVVKIHPN-------------------------------------------  531
Cvel_2306_LCACS6            --WLRTGDVCVINPN-------------------------------------------  526
Cvel_29920                  --WFRTGDIGLIRPN-------------------------------------------  533
HHA_276155                  -WYLGLGDVCFFLRPLENNGQVNGEEKQEERRDDEKESRDEREHKETG--------EKEE  571
HHA_310150                  KPWLLTGDVVEIQPN-------------------------------------------  569
HHA_310080                  SRWLATGDIVEIQPN-------------------------------------------  624
HHA_232580                  --YYDTGDSGFFDDD-------------------------------------------  643
HHA_297220                  --FLHTGDLGYVDSD-------------------------------------------  720
HHA_243800                  --WLHSGDVAVIVPG-------------------------------------------  599
HHA_247760                  --WMRTGDVVELLPS-------------------------------------------  636
NCLIV_006990                -WYLGLGDVCFFLRPLEKGDQARHGEEEREEHGEGRGGIRGREA-------------RLE  501
NCLIV_018500                --WLHSGDVAVIVPG-------------------------------------------  658
NCLIV_063970                --WMRTGDVVELLPS-------------------------------------------  673
NCLIV_054250                KPWLATGDVVEIQPD-------------------------------------------  565
NCLIV_039400                --YFFTGDGVFRDAD-------------------------------------------  551
NCLIV_006300                --FLHTGDLGYVDSD-------------------------------------------  728
PF3D7_1479000:PfACS1a       --YFKTGDVVQINKN-------------------------------------------  584
PF3D7_0731600:PfACS5        --YFKTGDVVQVNSD-------------------------------------------  567
PF3D7_1253400:PfACS3        --YFKTGDIVQINDN-------------------------------------------  580
PF3D7_0301000:PfACS2        --YFITGDVVQINRN-------------------------------------------  584
PF3D7_0619500:PfACS12       --FFKTGDIGYIDQD-------------------------------------------  492
```

Motif II: TGDX (7) GX hX (2) RX (4) Hx (3,4) GX (2) hX (4) hE

```
PF3D7_1372400:PfACS4        --YFKTGDIVQINDN-------------------------------------------  580
PF3D7_0401900:PfACS6        --YFKTGDVFQINED-------------------------------------------  633
PF3D7_0215000:PfACS9        --FFKTGDIVQINKN-------------------------------------------  722
PF3D7_0215300:PfACS8        --FFVTGDIVQINDN-------------------------------------------  581
PF3D7_0525100:PFACS10       --FIRTGDIALLSPN-------------------------------------------  522
PF3D7_1238800:PfACS11       --FFLTGDVVEVNEN-------------------------------------------  640
PF3D7_1200700:PfACS7        --YFKTGDIVQINDN-------------------------------------------  576
HsACSL1                     --WLHTGDIGKWLPN-------------------------------------------  547
ATLACS1                     --WFHTGDIGEILPN-------------------------------------------  506
ATLACS2                     --WFHTGDIGEWQED-------------------------------------------  510
HsACSL3                     --WLCTGDIGEFEPD-------------------------------------------  571
ATLACS3                     --WLHTGDVGEWQPD-------------------------------------------  509
HsACSL4                     --WFCTGDIGEFHPD-------------------------------------------  562
ATLACS4                     --WLHTGDVGEWQPD-------------------------------------------  509
HsACSL5                     --WLHTGDIGRWLPN-------------------------------------------  532
HsACSL6                     --WLHTGDIGKWLPA-------------------------------------------  547
ATLACS5                     --WLHTGDVGEWQPN-------------------------------------------  509
ATLACS6                     --WLHTGDIGLWLPG-------------------------------------------  540
ATLACS8                     --WFYTGDIGRFHPD-------------------------------------------  572
ATLACS9                     --WFYTGDIGRFHPD-------------------------------------------  543
HsACSS3                     --YYDTMDAGYMDEE-------------------------------------------  546
HsACSM3                     --FYITGDRGYMDKD-------------------------------------------  468
HsACSM2B                    --FWLLGDRGIKDED-------------------------------------------  453
HsACSM1                     --FYNTGDRGKMDEE-------------------------------------------  459
HsACSM4                     --FYVTGDRGVMDSD-------------------------------------------  462
HsACSM5                     --FYITGDRARMDKD-------------------------------------------  462
HsACSM6                     --LYLTGDRGIMDED-------------------------------------------  460
HsACSBG1                    --WLHTGDAGRLDAD-------------------------------------------  557
HsACSBG2                    --WLHSGDLGQLDGL-------------------------------------------  503
HsACSS1                     --YYFTGDGAYRTEG-------------------------------------------  538
HsACSS2                     --YYVTGDGCQRDQD-------------------------------------------  464
HsACSVL1                    --YFNSGDLLMVDHE-------------------------------------------  419
HsACSVL2                    --YLNTGDLIVQDQD-------------------------------------------  471
HsACSVL3                    --FFNTGDLLVCDDQ-------------------------------------------  582
HsACSVL4                    --AYLTGDVLVMDEL-------------------------------------------  496
HsACSVL5                    --AYLSGDVLVMDEL-------------------------------------------  499
HsACSVL6                    --YYNTGDVLAMDRE-------------------------------------------  542
```

Motif II: TGDX (7) GX hX (2) RX (4) Hx (3,4) GX (2) hX (4) hE

```
TGME49_297220:TgACS1      ----------G-FVYLTGRIKELIITAGGENVAPLLIESLLKQEMPQVLSNCMVVGDK    784
TGME49_310150:TgACS2      ----------G-SMNIIDRKKSLIKLAQGEYLQTEKLEGIYGA-SAF-VDNIFVHGYD    714
TGME49_310080:TgACS3      ----------G-SIKIIDRKKSLIKLAQGEYLQTEKLESIYGR-SAF-VDNIFVHGYD    673
TGME49_243800:TgACS4      ----------SNAVKIIDRKKNIFKLAQGEYVSPEKIENVYIQ-APL-VAQAFVTGYS    645
TGME49_247760:TgACS5      ----------G-APRIIDRAKNIFKLAQGEYVAPERLENIFSS-SPF-VEQIYLHGDS    681
TGME49_232580:TgACS6      ----------G-YLHIEGRTDDVINV-SAHRISGLSIEEVLTK-HPE-VASAAVVGVT    688
TGME49_276155:TgACS7      ESRL--DAGRARHLDYYWVTRSADVVIK-GGANYSCAQISDDIKNCLLR-L---YEGKLA    757
cgd3_2870                 SCACCKDNIFVDNIFLFWLSRSSSIIKI-GGVKYSSEEINDRIVSTLRN-L---NKKKFP    697
cgd5_3200                 ----------G-SIRIVDRRKNIFKLSQGEYVAPEKLENIFVICCEL-ISQALVIGRS    570
cdg3_640                  ----------G-SFKIIDRKKSLFKLSQGEYISPERIEGIYLSSSSL-IQHVYVYGQS    578
cgd4_3400                 ----------G-AIRIIDRRKHLFKLSQGEYISPETLENIYIAHSQI-VGQMFITAKT    637
Cvel_20092                -AST--EEGPSGSRDFFWLSRDSQMVIK-GGANYSCEQIGEELQSIAST-A---L--GCQ    521
Cvel_21035_miACS          ----------G-SIQIVGRLKDLI-IRGGENIYPREIEETMMK-HPA-VEDAHAVGVS    529
Cvel_29002_ACSBG2         ----------------------------------------------------------    503
Cvel_24841                ----------G-HLSCVGRVKHTFKLSSGEYYYPDELEKLYEG-AEG-VNAVCIHGEP    360
Cvel_9659_chlAAE16        ----------G-ELQLTGRQKDVIVLSNGENIEPEPLEITVAA-SAL-VDQIVCIGQD    639
Cvel_3410_ACSBG2          ----------G-FVFITGRIKELIITAGGENIPPVLIENVVKEELPF-VSNCQLIGDQ    577
Cvel_8845                 ----------G-AFQIIDRAKNIFKLAHGEYIAPEKIENVYVQ-AFS-VAQAFVYGTS    611
Cvel_26948_LCACS7         ----------G-AFQIIDRAKNIFKLAQGEYIAPEKIENVYIQ-APS-AAQAFVHGTS    576
Cvel_2306_LCACS6          ----------G-SFKIIDRAKNIFKLAQGEYVAPEKIENIYIQ-CES-VAQAFVTGYG    571
Cvel_29920                ----------G-AVKILDRAKNIFKLSHGEYVAPEKIENLSIQ-APL-VAQAFVYGYS    578
HHA_276155                ERRP--DAGRARHLDYYWVTRSADVVIK-GGANYSCAQISDDIKNCLLR-L---YEGKLA    624
HHA_310150                ----------G-SMNIIDRKKSLIKLAQGEYLQTEKLEGIYGA-SAF-VDNLLVHGYD    614
HHA_310080                ----------G-SIKIIDRKKSLIKLAQGEYLQTEKLESIYGR-SAF-VDNIFVHGYD    669
HHA_232580                ----------G-YLHIEGRTDDVINV-SAHRISGLSIEEVLTK-HPE-VASAAVVGVT    687
HHA_297220                ----------G-FVYLTGRIKELIITAGGENVAPLLIESLLKQEMPQILSNCMVVGDK    767
HHA_243800                ----------SNAVKIIDRKKNIFKLAQGEYVSPEKIENVYIQ-APL-VAQAFVTGYS    645
HHA_247760                ----------G-APRIIDRAKNIFKLAQGEYIAPERLENIFAS-SPF-VEQIYLHGDS    681
NCLIV_006990              GRQS--CQDSEACTDYYWVTRSADIVIK-GGANYSSAQISEDIKECLLR-L---YEGKLA    554
NCLIV_018500              ----------CNAVKIIDRKKNIFKLSQGEYVSPEKIENIYIQ-APL-VAQAFVTGSS    704
NCLIV_063970              ----------G-APRIIDRAKNIFKLAQGEYVAPERLENIFSS-SPF-VEQIYLHGDS    718
NCLIV_054250              ----------G-SMKIIDRKKSLIKLAQGEYLQTEKLEGIYGA-SAF-VENMLVHGYD    610
NCLIV_039400              ----------G-YYWITGRVDDTLNV-SGHRLTTAEIEHALVQ-HED-VAEAAVVGVP    595
NCLIV_006300              ----------G-FVYLTGRIKELIITAGGENVAPLLIESLLKQEMPQLLSNCMVVGDR    775
PF3D7_1479000:PfACS1a     ----------G-TLTFLDRSKGLVKLSQGEYIETDLLNNLYSQ-ISF-INNCVVYGDD    629
PF3D7_0731600:PfACS5      ----------G-SLTFLDRSKGLVKLSQGEYIETDLLNNLYSQ-ISF-INNCVVYGDD    612
PF3D7_1253400:PfACS3      ----------G-SVTFLDRSKGLVKLSQGEYIETDLLNNLYSQ-ISF-INNCVVYGDD    625
PF3D7_0301000:PfACS2      ----------G-SLKFLDRSKGLVKLSQGEYIETDMLNNLYSE-VLF-INFCVVYGDD    629
PF3D7_0619500:PfACS12     ----------N-FLFISGRIKDIINR-GGEKIIPNEIDDVLRN-HDL-VQDCLTFSCK    536
```

Motif II: TGDX (7) GX hX (2) RX (4) Hx (3,4) GX (2) hX (4) hE

```
PF3D7_1372400:PfACS4      ----------G-SVTFLDRSKGLVKLSQGEYIETDMLNNLYSQ-ITF-VNFCVVYGDD  625
PF3D7_0401900:PfACS6      ----------G-SLTFLDRSKGLVKLSQGEYIETDMLNNLYSV-ILF-VNFCVAYGDD  678
PF3D7_0215000:PfACS9      ----------G-SLTFLDRSKGLLKLAQGEYIQTDMLNSLYSE-IPF-INHCVVYADD  767
PF3D7_0215300:PfACS8      ----------G-SLTFLDRSKGLVKLSQGEYIETDLLNNIYSE-IPF-INNCVVYGDD  626
PF3D7_0525100:PFACS10     ----------G-SLTIIDRKKNIFKLAQGEYVAVEKVEASYKQ-SLF-ISQIFVFGYS  567
PF3D7_1238800:PfACS11     ----------NAYVKIIDRAKNIFKLAQGEYIEPEKLENLYSN-SIY-IENIFVHGYS  686
PF3D7_1200700:PfACS7      ----------G-SLTFLDRSKGLVKLSQGEYIETEMINNLYSQ-IPF-VNFCVAYGDD  621
HsACSL1                   ----------G-TLKIIDRKKHIFKLAQGEYIAPEKIENIYMR-SEP-VAQVFVHGES  592
ATLACS1                   ----------G-VLKIIDRKKNLIKLSQGEYVALEHLENIFGQ-NSV-VQDIWVYGDS  551
ATLACS2                   ----------G-SMKIIDRKKNIFKLSQGEYVAVENLENTYSR-CPL-IAQIWVYGNS  555
HsACSL3                   ----------G-CLKIIDRKKDLVKLQAGEYVSLGKVEAALKN-LPL-VDNICAYANS  616
ATLACS3                   ----------G-AMKIIDRKKNIFKLSQGEYVAVENLENIYSH-VAA-IESIWVYGNS  554
HsACSL4                   ----------G-CLQIIDRKKDLVKLQAGEYVSLGKVEAALKN-CPL-IDNICAFAKS  607
ATLACS4                   ----------G-SMKIIDRKKNIFKLSQGEYVAVENIENIYGE-VQA-VDSVWVYGNS  554
HsACSL5                   ----------G-TLKIIDRKKNIFKLAQGEYIAPEKIENIYNR-SQP-VLQIFVHGES  577
HsACSL6                   ----------G-TLKIIDRKKHIFKLAQGEYVAPEKIENIYIR-SQP-VAQIYVHGDS  592
ATLACS5                   ----------G-SMKIIDRKKNIFKLAQGEYVAVENLENVYSQ-VEV-IESIWVYGNS  554
ATLACS6                   ----------G-RLKIIDRKKNIFKLAQGEYIAPEKIENVYAK-CKF-VGQCFIYGDS  585
ATLACS8                   ----------G-CLEVIDRKKDIVKLQHGEYVSLGKVEAALGS-SNY-VDNIMVHADP  617
ATLACS9                   ----------G-CLEIIDRKKDIVKLQHGEYVSLGKVEAALSI-SPY-VENIMVHADS  588
HsACSS3                   ----------G-YLYVMSRVDDVINV-AGHRISAGAIEESILS-HGT-VADCAVVGKE  590
HsACSM3                   ----------G-YFWFVARADDVILS-SGYRIGPFEVENALNE-HPS-VAESAVVSSP  512
HsACSM2B                  ----------G-YFQFMGRADDIINS-SGYRIGPSEVENALMK-HPA-VVETAVISSP  497
HsACSM1                   ----------G-YICFLGRSDDIINA-SGYRIGPAEVESALVE-HPA-VAESAVVGSP  503
HsACSM4                   ----------G-YFWFVGRADDVIIS-SGYRIGPFEVESALIE-HPA-VVESAVVSSP  506
HsACSM5                   ----------G-YFWFMGRNDDVINS-SSYRIGPVEVESALAE-HPA-VLESAVVSSP  506
HsACSM6                   ----------G-YFWWSGRVDDVANA-LGQR--------------------------  479
HsACSBG1                  ----------G-FLYITGRLKELIITAGGENVPPVPIEEAVKMELPI-ISNAMLIGDQ  603
HsACSBG2                  ----------G-FLYVTGHIKEILITAGGENVPPIPVETLVKKKIPI-ISNAMLVGDK  549
HsACSS1                   ----------G-YYQITGRMDDVINI-SGHRLGTAEIEDAIAD-HPA-VPESAVIGYP  582
HsACSS2                   ----------G-YYWITGRIDDMLNV-SGHLLSTAEVESALVE-HEA-VAEAAVVGHP  508
HsACSVL1                  ----------N-FIYFHDRVGDTFRW-KGENVATTEVADTVGL-VDF-VQEVNVYGV-  462
HsACSVL2                  ----------N-FLYFWDRTGDTFRW-KGENVATTEVADVIGM-LDF-IQEANVYGV-  514
HsACSVL3                  ----------G-FLRFHDRTGDTFRW-KGENVATTEVAEVFEA-LDF-LQEVNVYGV-  625
HsACSVL4                  ----------G-YLYFRDRTGDTFRW-KGENVSTTEVEGTLSR-LLD-MADVAVYGV-  539
HsACSVL5                  ----------G-YMYFRDRSGDTFRW-RGENVSTTEVEGVLSR-LLG-QTDVAVYGV-  542
HsACSVL6                  ----------G-FLYFRDRLGDTFRW-KGENVSTHEVEGVLSQ-VDF-LQQVNVYGV-  585
```

Motif III: YGXTE (WWQTE)

```
TGME49_297220:TgACS1      --------MPINSIYGLSESTGPQTFILPAPG----------------------WYKVGS    675
TGME49_310150:TgACS2      --------LNIIQGWGMTETAGAGSWQAYRGD----------------------DAYD--S    591
TGME49_310080:TgACS3      --------TSFLQGWGMTETSGAGCWQARAGD----------------------GSLD--N    543
TGME49_243800:TgACS4      --------TPVVEGYGMTETMAASFISIAGEN----------------------TAG--H    526
TGME49_247760:TgACS5      --------APVCEGWGMTETGIC-FLQDLEDN----------------------EKG--T    566
TGME49_232580:TgACS6      TAYPSRTPPLVIDHWWQSETGWPMTCLMAGQ-PF--------------SEDDYTPLREGS    572
TGME49_276155:TgACS7      --------KLPAIRFGSTETCLQVMGTPFSLTDDEMMRALERGW---NHVFQGRPQKGFY    583
cgd3_2870                 --------KIPRIRFGSTETCLQLCGTDLLMDHSLLNAALKITSNINEINSKTKKKNGYF    508
cgd5_3200                 --------SYCFEGYGMTELLAACM-SEINDN----------------------SKN--I    453
cdg3_640                  --------CKLIEGFGMSECIGTL-GTRYSYA----------------------HLG--T    462
cgd4_3400                 --------THVVQGYGTTEALAA-FCPEFTDL----------------------SVN--N    521
Cvel_20092                --------KLPTVRFGSTETCLQVMGTPTDLSEEAALKAFQKGW---AHTFNGTPQKGYW    391
Cvel_21035_miACS          --------KEMTVCYGMTETSPVSFQTLRSDP----------------------PAKRCRT    413
Cvel_29002_ACSBG2         --------IPICDAYGMSECTGPECISEPRVG----------------------AYKLGS    468
Cvel_24841                --------CGVLESYGATECGAIATNGV--------------------------------    243
Cvel_9659_chlAAE16        --------VLLIEGYGLTETSPTLFNRRKEQN----------------------MRG--S    517
Cvel_3410_ACSBG2          --------MPICDAYGMSECTGPEVYAEPRHG----------------------AYKLGS    469
Cvel_8845                 --------CPLFEGYGMTETIACGGMTFSLDP----------------------NCG--I    490
Cvel_26948_LCACS7         --------CPLFEGYGSTETVCCGGMTYARDP----------------------KVG--T    455
Cvel_2306_LCACS6          --------CPMMEAFGMTETACCGTATAALDP----------------------TTG--H    450
Cvel_29920                --------CPILEGYGLTETCAATCVTSKFDP----------------------EVG--H    457
HHA_276155                --------KLPAIRFGSTETCLQVMGTPFSLTDEEMMKALERGW---NHVFQGRPQKGFY    458
HHA_310150                --------VNIIQGWGMTETAGAGSWQAYRGD----------------------DAYD--S    491
HHA_310080                --------TSFLQGWGMTETSGAGCWQARAGD----------------------GSLD--N    538
HHA_232580                TAYPSRTPPLVIDHWWQSETGWPMTCLMAGQ-SF--------------SEDDYTPCREGS    571
HHA_297220                --------MPINSIYGLSESTGPQTFILPAPG----------------------WYKVGS    658
HHA_243800                --------TPVVEGYGMTETMAASFISIAGEN----------------------TAG--H    526
HHA_247760                --------APVCEGWGMTETGIC-FLQDLEDN----------------------EKG--T    566
NCLIV_006990              --------KLPSIRFGSTETCLQVMGTPFSLTDEERMRALERGW---QHTYRGTPQPGYY    393
NCLIV_018500              --------VPLVEGYGMTETMAASFISLAGEN----------------------TAG--H    585
NCLIV_063970              --------SPVCEGWGMTETGIC-FLQDLSDN----------------------EKG--T    603
NCLIV_054250              --------LNIIQGWGMTETAGAGSWQAYRND----------------------DSYD--S    491
NCLIV_039400              -------RCSIVDTYWQTETGGHVLTPIPG----------------------ATVTKPGS    478
NCLIV_006300              --------MPINSIYGLSESTGPQTFILPAPG----------------------WYKVGS    666
PF3D7_1479000:PfACS1a     --------IKYCQGYGLTETGGAIFGKHVEDL----------------------NFE--C    515
PF3D7_0731600:PfACS5      --------INYYQGYGLTESTGPIFVQDTSDN----------------------NSE--S    498
PF3D7_1253400:PfACS3      --------IKYCQGYGLTETAGAILGNHADDE----------------------HFE--Y    511
PF3D7_0301000:PfACS2      --------INYCQGYGLTETGGGIFGNHAKDT----------------------NFL--C    515
PF3D7_0619500:PfACS12     KEIEEKFEVSVFQAYGMTEACHQVSSNKIIISSL--------------SSPNNLQICKKF    403
```

Motif III: YGXTE (WWQTE)

```
PF3D7_1372400:PfACS4      --------IKYCQGYGLTETAGAILGNHADDE----------------------HFE--Y    511
PF3D7_0401900:PfACS6      --------VDYIQGYGLTESTGALFVQDGLGC----------------------NTE--N    564
PF3D7_0215000:PfACS9      --------VSIQQGYGLTETTGPLFVQHRKDK----------------------DPE--S    653
PF3D7_0215300:PfACS8      --------VNFYQGYGLTETTGPIFVQQKRDY----------------------NTE--S    512
PF3D7_0525100:PFACS10     --------VPMFEGYGMTESLGASFITHSQDR----------------------NIG--H    451
PF3D7_1238800:PfACS11     --------SPISEGWGMTEVGVG-FLQHRFDS----------------------TKG--T    570
PF3D7_1200700:PfACS7      --------VKYYQGYGLTESTGPIFLQDVDDC----------------------NTE--S    507
HsACSL1                   --------CQFYEGYGQTECTAGCCLTMPGDW----------------------TAG--H    479
ATLACS1                   --------CFVVQGYGLTETLGGTALGFPDEM----------------------CMLG--T    437
ATLACS2                   --------SNLSQGYGLTESCGGSFTTLAGVF----------------------SMVG--T    440
HsACSL3                   --------CPVGQGYGLTESAGAGTISEVWDY----------------------NTG--R    496
ATLACS3                   --------AHVLQGYGLTESCGGTFVSIPNEL----------------------SMLG--T    440
HsACSL4                   --------CPIGQGYGLTESCGAGTVTEVTDY----------------------TTG--R    487
ATLACS4                   --------CHVLQGYGLTESCAGTFVSLPDEL----------------------GMLG--T    440
HsACSL5                   --------CQVYEAYGQTECTGGCTFTLPGDW----------------------TSG--H    464
HsACSL6                   --------CQVYEGYGQTECTAGCTFTTPGDW----------------------TSG--H    479
ATLACS5                   --------CNVLQGYGLTESCAGTFATFPDEL----------------------DMLG--T    440
ATLACS6                   --------GRVTEGYGMTETSCVISGMDEGDN----------------------LTG--H    469
ATLACS8                   --------SPIGQGYGLTETCAGATFSEWDDP----------------------AVG--R    497
ATLACS9                   --------APIGQGYGLTETCAGGTFSEFEDT----------------------SVG--R    468
HsACSS3                   --------VPVLDHWWQTETGSPITASCVGL-GN--------------S----KTPPPGQ    474
HsACSM3                   --------LDIYEGYGQTETVLICGNFK------------------------GMKIKPGS    397
HsACSM2B                  --------LDIREFYGQTETGLTCMVSK------------------------TMKIKPGY    382
HsACSM1                   --------LLLYENYGQSETGLICATYW------------------------GMKIKPGF    388
HsACSM4                   --------LELYEGYGQTEVGMICANQK------------------------GQEIKPGS    391
HsACSM5                   --------VELYEGYGQSETVVICANPK------------------------GMKIKSGS    391
HsACSM6                   --------LDIYEGYGQTETGLLCATSK------------------------TIKLKPSS    389
HsACSBG1                  --------IRLYAGYGLSETSGPHFMSS--PY----------------------NYRLYS    495
HsACSBG2                  --------IPIGELYGLSESSGPHTISN--QN----------------------NYRLLS    441
HsACSS1                   -------RCTLVDTWWQTGGICIAPRPSEE----------------------GAEILPAM    466
HsACSS2                   -------RCPIVDTFWQTETGGHMLTPLPG----------------------ATPMKPGS    393
HsACSVL1                  --------ICIYEFYAATEGNIGFMN-YARKV-------------------------GA    327
HsACSVL2                  --------IKVCELYAATESSISFMN-YTGRI-------------------------GA    379
HsACSVL3                  --------LQVLETYGLTEGNVATIN-YTGQR-------------------------GA    490
HsACSVL4                  --------PQVAEFYGATECNCSLGN-FDSQV-------------------------GA    402
HsACSVL5                  --------RQIGEFYGATECNCSIAN-MDGKV-------------------------GS    405
HsACSVL6                  --------IRIWEVYGSTEGNMGLVN-YVGRC-------------------------GA    450
```

Motif IV: LPLXH

```
PF3D7_1372400:PfACS4      YSFKNHLSYLPISHVFERTFAYSIL-MYGGTLNVWGKDIN--Y---------FSKDIYNT    389
PF3D7_0401900:PfACS6      MKPKTHFSYLPVSHVFERVLVYMAV-ILGIKINISSKDIS--C---------FSKDLYNS    442
PF3D7_0215000:PfACS9      YNVDTHLSYLPLSHIYERINIYLCF-VLTVEIHIWSKNLK--Y---------FSSDILVS    531
PF3D7_0215300:PfACS8      YHPKAHLSYLPVSHIYERVNVYVAF-LSGIKIDIWSKNIN--F---------FSRDIFNS    390
PF3D7_0525100:PFACS10     NENDIHISYLPLAHIYERLMIYLFM-AHGVKVGYYSGNVQ--T---------LLEDIQEL    328
PF3D7_1238800:PfACS11     KKYDVVFSYLPLAHVYERFIEYAVC-FFGHKIGYFSGNIK--E---------LVGDMNEL    448
PF3D7_1200700:PfACS7      YPLTTHLSYLPVSHIYERVVFFIAL-FLGVKINIWSRDIK--F---------LNTDICNS    385
HsACSL1                   CPDDTLISFLPLAHMFERVVECVML-CHGAKIGFFQGDIR--L---------LMDDLKVL    358
ATLACS1                   THDDVYLSFLPLAHILDRMNEEYFF-RKGASVGYYHGNLN--V---------LRDDIQEL    311
ATLACS2                   DTSDVFFSYLPLAHCYDQVMEIYFL-SRGSSVGYWRGDIR--Y---------LMDDVQAL    314
HsACSL3                   GEEDVYIGYLPLAHVLELSAELVCL-SHGCRIGYSSPQTL--ADQSSKIKKGSKGDTSML    375
ATLACS3                   TSKDVYLSYLPLAHIFDRVIEELCI-YEAASIGFWRGDVK--I---------LIEDIAAL    314
HsACSL4                   GPKDTYIGYLPLAHVLELTAEISCF-TYGCRIGYSSPLTL--SDQSSKIKKGSKGDCTVL    366
ATLACS4                   TVKDVYLSYLPLAHIFDRVIEECFI-QHGAAIGFWRGDVK--L---------LIEDLAEL    314
HsACSL5                   TPDDVAISYLPLAHMFERIVQAVVY-SCGARVGFFQGDIR--L---------LADDMKTL    343
HsACSL6                   RQDDVLISFLPLAHMFERVIQSVVY-CHGGRVGFFQGDIR--L---------LSDDMKAL    358
ATLACS5                   SEKDVYISYLPLAHVFDRAIEECII-QVGGSIGFWRGDVK--L---------LIEDLGEL    314
ATLACS6                   FSSDVYISYLPLAHIYERANQILTV-YFGVAVGFYQGDNM--K---------LLDDLAAL    347
ATLACS8                   DKNDTYIAYLPLAHVFELEAEIVVF-TSGSAIGYGSAMTL--TDTSNKVKKGTKGDVSAL    370
ATLACS9                   GKRDIYMAYLPLAHILELAAESVMA-TIGSAIGYGSPLTL--TDTSNKIKKGTKGDVTAL    341
HsACSS3                   QPGEVWWAASDLGWVVGHSYICYGPLLHGNTTVLYEGKPVGTPDA-----GAYFRVLAEH    385
HsACSM3                   TPSDVMWNTSDTGWAKSAWSSVFSPWIQGACVFTHHLPR---FEP-----TSILQTLSKY    318
HsACSM2B                  QASDIMWTISDTGWILNILGSLLESWTLGACTFVHLLPK---FDP-----LVILKTLSSY    303
HsACSM1                   KTSDVSWCLSDSGWIVATIWTLVEPWTAGCTVFIHHLPQ---FDT-----KVIIQTLLKY    309
HsACSM4                   KSSDIIWNMSDTGWVKAAIGSVFSSWLCGACVFVHRMAQ---FDT-----DTFLDTLTTY    312
HsACSM5                   TESDIFWNTTDTGWVKAAW-TLFSAWPNGSCIFVHELPR---VDA-----KVILNTLSKF    312
HsACSM6                   QPTDVLWSLGDAFGGSLSLSAVLGTWFQGACVFLCHMPT---FCP-----ETVLNVLSRF    309
HsACSBG1                  VQQEVVVSYLPLSHIAAQIYDLWTGIQWGAQVCFAEPDAL--K-------GSLVNTLREV    367
HsACSBG2                  DKHETVVSYLPLSHIAAQMMDIWVPIKIGALTYFAQADAL--K-------GTLVSTLKEV    312
HsACSS1                   QPGDIFGCVADIGWITGHSYVVYGPLCNGATSVLFESTPV-YPNA-----GRYWETVERL    379
HsACSS2                   HAEDVFWCTADIGWITGHSYVTYGPLANGATSVLFEGIPT-YPDV-----NRLWSIVDKY    306
HsACSVL1                  ----------------------------ATLALRTKFSA----------SQFWDDCRKY    251
HsACSVL2                  TAHDIVYITLPLYHSSAAILGISGCVELGATCVLKKKFSA----------SQFWSDCKKY    303
HsACSVL3                  HQEDVIYLALPLYHMSGSLLGIVGCMGIGATVVLKSKFSA----------GQFWEDCQQH    414
HsACSVL4                  RPNDIVYDCLPLYHSAGNIVGIGQCLLHGMTVVIRKKFSA----------SRFWDDCIKY    326
HsACSVL5                  QAADVLYDCLPLYHSAGNIIGVGQCLIYGLTVVLRKKFSA----------SRFWDDCIKY    329
HsACSVL6                  TADDVVYTVLPLYHVMGLVVGILGCLDLGATCVLAPKFST----------SCFWDDCRQH    374
```

Motif IV: LPLXH

```
PF3D7_1372400:PfACS4      YSFKNHLSYLPISHVFERTFAYSIL-MYGGTLNVWGKDIN--Y---------FSKDIYNT   389
PF3D7_0401900:PfACS6      MKPKTHFSYLPVSHVFERVLVYMAV-ILGIKINISSKDIS--C---------FSKDLYNS   442
PF3D7_0215000:PfACS9      YNVDTHLSYLPLSHIYERINIYLCF-VLTVEIHIWSKNLK--Y---------FSSDILVS   531
PF3D7_0215300:PfACS8      YHPKAHLSYLPVSHIYERVNVYVAF-LSGIKIDIWSKNIN--F---------FSRDIFNS   390
PF3D7_0525100:PFACS10     NENDIHISYLPLAHIYERLMIYLFM-AHGVKVGYYSGNVQ--T---------LLEDIQEL   328
PF3D7_1238800:PfACS11     KKYDVVFSYLPLAHVYERFIEYAVC-FFGHKIGYFSGNIK--E---------LVGDMNEL   448
PF3D7_1200700:PfACS7      YPLTTHLSYLPVSHIYERVVFFIAL-FLGVKINIWSRDIK--F---------LNTDICNS   385
HsACSL1                   CPDDTLISFLPLAHMFERVVECVML-CHGAKIGFFQGDIR--L---------LMDDLKVL   358
ATLACS1                   THDDVYLSFLPLAHILDRMNEEYFF-RKGASVGYYHGNLN--V---------LRDDIQEL   311
ATLACS2                   DTSDVFFSYLPLAHCYDQVMEIYFL-SRGSSVGYWRGDIR--Y---------LMDDVQAL   314
HsACSL3                   GEEDVYIGYLPLAHVLELSAELVCL-SHGCRIGYSSPQTL--ADQSSKIKKGSKGDTSML   375
ATLACS3                   TSKDVYLSYLPLAHIFDRVIEELCI-YEAASIGFWRGDVK--I---------LIEDIAAL   314
HsACSL4                   GPKDTYIGYLPLAHVLELTAEISCF-TYGCRIGYSSPLTL--SDQSSKIKKGSKGDCTVL   366
ATLACS4                   TVKDVYLSYLPLAHIFDRVIEECFI-QHGAAIGFWRGDVK--L---------LIEDLAEL   314
HsACSL5                   TPDDVAISYLPLAHMFERIVQAVVY-SCGARVGFFQGDIR--L---------LADDMKTL   343
HsACSL6                   RQDDVLISFLPLAHMFERVIQSVVY-CHGGRVGFFQGDIR--L---------LSDDMKAL   358
ATLACS5                   SEKDVYISYLPLAHVFDRAIEECII-QVGGSIGFWRGDVK--L---------LIEDLGEL   314
ATLACS6                   FSSDVYISYLPLAHIYERANQILTV-YFGVAVGFYQGDNM--K---------LLDDLAAL   347
ATLACS8                   DKNDTYIAYLPLAHVFELEAEIVVF-TSGSAIGYGSAMTL--TDTSNKVKKGTKGDVSAL   370
ATLACS9                   GKRDIYMAYLPLAHILELAAESVMA-TIGSAIGYGSPLTL--TDTSNKIKKGTKGDVTAL   341
HsACSS3                   QPGEVWWAASDLGWVVGHSYICYGPLLHGNTTVLYEGKPVGTPDA-----GAYFRVLAEH   385
HsACSM3                   TPSDVMWNTSDTGWAKSAWSSVFSPWIQGACVFTHHLPR---FEP-----TSILQTLSKY   318
HsACSM2B                  QASDIMWTISDTGWILNILGSLLESWTLGACTFVHLLPK---FDP-----LVILKTLSSY   303
HsACSM1                   KTSDVSWCLSDSGWIVATIWTLVEPWTAGCTVFIHHLPQ---FDT-----KVIIQTLLKY   309
HsACSM4                   KSSDIIWNMSDTGWVKAAIGSVFSSWLCGACVFVHRMAQ---FDT-----DTFLDTLTTY   312
HsACSM5                   TESDIFWNTTDTGWVKAAW-TLFSAWPNGSCIFVHELPR---VDA-----KVILNTLSKF   312
HsACSM6                   QPTDVLWSLGDAFGGSLSLSAVLGTWFQGACVFLCHMPT---FCP-----ETVLNVLSRF   309
HsACSBG1                  VQQEVVVSYLPLSHIAAQIYDLWTGIQWGAQVCFAEPDAL--K-------GSLVNTLREV   367
HsACSBG2                  DKHETVVSYLPLSHIAAQMMDIWVPIKIGALTYFAQADAL--K-------GTLVSTLKEV   312
HsACSS1                   QPGDIFGCVADIGWITGHSYVVYGPLCNGATSVLFESTPV-YPNA-----GRYWETVERL   379
HsACSS2                   HAEDVFWCTADIGWITGHSYVTYGPLANGATSVLFEGIPT-YPDV-----NRLWSIVDKY   306
HsACSVL1                  ----------------------------ATLALRTKFSA----------SQFWDDCRKY   251
HsACSVL2                  TAHDIVYITLPLYHSSAAILGISGCVELGATCVLKKKFSA----------SQFWSDCKKY   303
HsACSVL3                  HQEDVIYLALPLYHMSGSLLGIVGCMGIGATVVLKSKFSA----------GQFWEDCQQH   414
HsACSVL4                  RPNDIVYDCLPLYHSAGNIVGIGQCLLHGMTVVIRKKFSA----------SRFWDDCIKY   326
HsACSVL5                  QAADVLYDCLPLYHSAGNIIGVGQCLIYGLTVVLRKKFSA----------SRFWDDCIKY   329
HsACSVL6                  TADDVVYTVLPLYHVMGLVVGILGCLDLGATCVLAPKFST----------SCFWDDCRQH   374
```

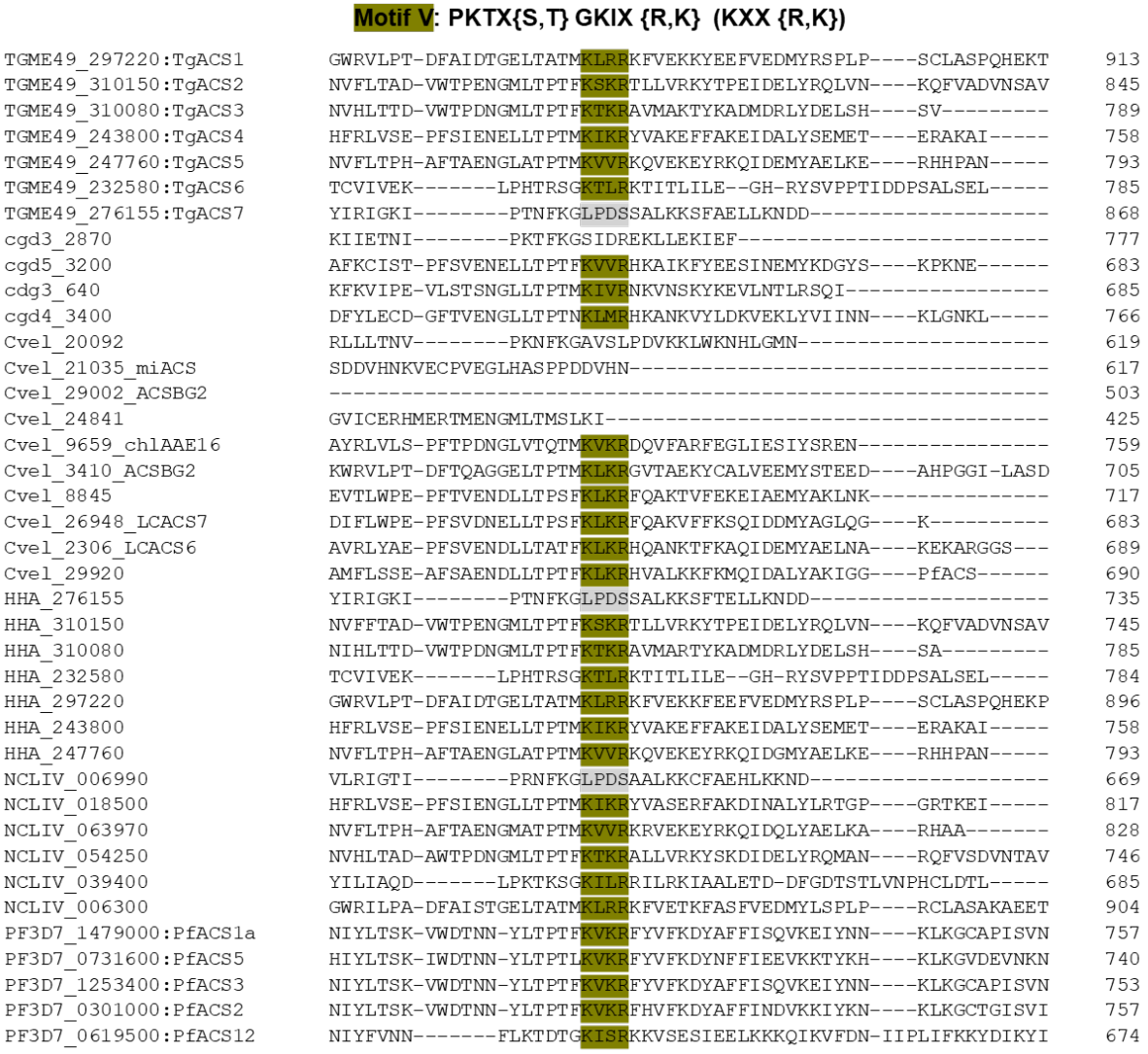
Motif V: PKTX{S,T} GKIX {R,K} (KXX {R,K})
TGME49_297220:TgACS1 GWRVLPT-DFAIDTGELTATMKLRRKFVEKKYEEFVEDMYRSPLP----SCLASPQHEKT 913
TGME49_310150:TgACS2 NVFLTAD-VWTPENGMLTPTFKSKRTLLVRKYTPEIDELYRQLVN----KQFVADVNSAV 845
TGME49_310080:TgACS3 NVHLTTD-VWTPDNGMLTPTFKTKRAVMAKTYKADMDRLYDELSH----SV--------- 789
TGME49_243800:TgACS4 HFRLVSE-PFSIENELLTPTMKIKRYVAKEFFAKEIDALYSEMET----ERAKAI----- 758
TGME49_247760:TgACS5 NVFLTPH-AFTAENGLATPTMKVVRKQVEKEYRKQIDEMYAELKE----RHHPAN----- 793
TGME49_232580:TgACS6 TCVIVEK-------LPHTRSGKTLRKTITLILE--GH-RYSVPPTIDDPSALSEL----- 785
TGME49_276155:TgACS7 YIRIGKI--------PTNFKGLPDSSALKKSFAELLKNDD-------------------- 868
cgd3_2870 KIIETNI--------PKTFKGSIDREKLLEKIEF------------------------- 777
cgd5_3200 AFKCIST-PFSVENELLTPTFKVVRHKAIKFYEESINEMYKDGYS----KPKNE------ 683
cdg3_640 KFKVIPE-VLSTSNGLLTPTMKIVRNKVNSKYKEVLNTLRSQI----------------- 685
cgd4_3400 DFYLECD-GFTVENGLLTPTNKLMRHKANKVYLDKVEKLYVIINN----KLGNKL----- 766
Cvel_20092 RLLLTNV--------PKNFKGAVSLPDVKKLWKNHLGMN-------------------- 619
Cvel_21035_miACS SDDVHNKVECPVEGLHASPPDDVHN---------------------------------- 617
Cvel_29002_ACSBG2 ---------- 503
Cvel_24841 GVICERHMERTMENGMLTMSLKI---------------------------------- 425
Cvel_9659_chlAAE16 AYRLVLS-PFTPDNGLVTQTMKVKRDQVFARFEGLIESIYSREN---------------- 759
Cvel_3410_ACSBG2 KWRVLPT-DFTQAGGELTPTMKLKRGVTAEKYCALVEEMYSTEED----AHPGGI-LASD 705
Cvel_8845 EVTLWPE-PFTVENDLLTPSFKLKRFQAKTVFEKEIAEMYAKLNK---------------- 717
Cvel_26948_LCACS7 DIFLWPE-PFSVDNELLTPSFKLKRFQAKVFFKSQIDDMYAGLQG----K---------- 683
Cvel_2306_LCACS6 AVRLYAE-PFSVENDLLTATFKLKRHQANKTFKAQIDEMYAELNA----KEKARGGS--- 689
Cvel_29920 AMFLSSE-AFSAENDLLTPTFKLKRHVALKKFKMQIDALYAKIGG----PfACS------ 690
HHA_276155 YIRIGKI--------PTNFKGLPDSSALKKSFTELLKNDD-------------------- 735
HHA_310150 NVFFTAD-VWTPENGMLTPTFKSKRTLLVRKYTPEIDELYRQLVN----KQFVADVNSAV 745
HHA_310080 NIHLTTD-VWTPDNGMLTPTFKTKRAVMARTYKADMDRLYDELSH----SA--------- 785
HHA_232580 TCVIVEK-------LPHTRSGKTLRKTITLILE--GH-RYSVPPTIDDPSALSEL----- 784
HHA_297220 GWRVLPT-DFAIDTGELTATMKLRRKFVEKKFEEFVEDMYRSPLP----SCLASPQHEKP 896
HHA_243800 HFRLVSE-PFSIENELLTPTMKIKRYVAKEFFAKEIDALYSEMET----ERAKAI----- 758
HHA_247760 NVFLTPH-AFTAENGLATPTMKVVRKQVEKEYRKQIDGMYAELKE----RHHPAN----- 793
NCLIV_006990 VLRIGTI--------PRNFKGLPDSAALKKCFAEHLKKND-------------------- 669
NCLIV_018500 HFRLVSE-PFSIENGLLTPTMKIKRYVASERFAKDINALYLRTGP----GRTKEI----- 817
NCLIV_063970 NVFLTPH-AFTAENGMATPTMKVVRKRVEKEYRKQIDQLYAELKA----RHAA------- 828
NCLIV_054250 NVHLTAD-AWTPDNGMLTPTFKTKRALLVRKYSKDIDELYRQMAN----RQFVSDVNTAV 746
NCLIV_039400 YILIAQD-------LPKTKSGKILRRILRKIAALETD-DFGDTSTLVNPHCLDTL----- 685
NCLIV_006300 GWRILPA-DFAISTGELTATMKLRRKFVETKFASFVEDMYLSPLP----RCLASAKAEET 904
PF3D7_1479000:PfACS1a NIYLTSK-VWDTNN-YLTPTFKVKRFYVFKDYAFFISQVKEIYNN----KLKGCAPISVN 757
PF3D7_0731600:PfACS5 HIYLTSK-IWDTNN-YLTPTLKVKRFYVFKDYNFFIEEVKKTYKH----KLKGVDEVNKN 740
PF3D7_1253400:PfACS3 NIYLTSK-VWDTNN-YLTPTFKVKRFYVFKDYAFFISQVKEIYNN----KLKGCAPISVN 753
PF3D7_0301000:PfACS2 NIYLTSK-VWDTNN-YLTPTFKVKRFHVFKDYAFFINDVKKIYKN----KLKGCTGISVI 757
PF3D7_0619500:PfACS12 NIYFVNN-------FLKTDTGKISRKKVSESIEELKKKQIKVFDN-IIPLIFKKYDIKYI 674

Motif V: PKTX{S,T} GKIX {R,K} (KXX {R,K})

```
PF3D7_1372400:PfACS4      DIYITSK-QWDTTN-YLTPTFKIKRFNVFKDFSFYIDAVKKKYEE----KLSGSSTGSMN  753
PF3D7_0401900:PfACS6      DIYLTSK-TWDMNN-YLTPTLKIRRFNVFKDFSFYIDQVKKKYED----KLKGSSTDSKS  806
PF3D7_0215000:PfACS9      HIYLTVK-VWDISN-YITPTFKIKRFHVFRDYAFFIDDIKKLYSS----K----------  885
PF3D7_0215300:PfACS8      HIYLTSK-TWDTTN-YLTPTMKVKRFSVIQDYAFFIDQVKNIFKK----KLKGQKERTKR  754
PF3D7_0525100:PFACS10     DIHFTLE-AFTIENDLMTPTGKIKRHEAKKRFKKEIDEMYEKLKQ---------------  673
PF3D7_1238800:PfACS11     LFHLTST-PFSVENKQLTPTHKIVRHVILADYKKVINDLYKSRNK---------------  792
PF3D7_1200700:PfACS7      DIYLTSK-PWDTTN-YLTPTLKIRRFNVFKDFSFFIDEVKKKYEE----KLSGNSTGSMN  749
HsACSL1                   GITLHPE-LFSIDNGLLTPTMKAKRPELRNYFRSQIDDLYSTIKV---------------  698
ATLACS1                   AVTVETK-PFDVERDLVTATLKNRRNNLLKYYQVQIDEMYRKLAS----KKI--------  660
ATLACS2                   AIHLEPN-PFDIERDLITPTFKLKRPQLLQHYKGIVDQLYSEAKR----SMA--------  665
HsACSL3                   KIRLSPE-PWTPETGLVTDAFKLKRKELKTHYQADIERMYGRK-----------------  720
ATLACS3                   GVHLDTV-PFDMERDLITPSYKMKRPQLLKYYQKEIDEMYKKNRE----VQLRV------  665
HsACSL4                   KVRLSPE-PWTPETGLVTDAFKLKRKELRNHYLKDIERMYGGK-----------------  711
ATLACS4                   AIHLDPV-PFDMERDLLTPTFKKKRPQLLKYYQSVIDEMYKTINA----KFASRG-----  666
HsACSL5                   AIFLHPE-PFSIENGLLTPTLKAKRGELSKYFRTQIDSLYEHIQD---------------  683
HsACSL6                   AIHIHSD-MFSVQNGLLTPTLKAKRPELREYFKKQIEELYSISM----------------  697
ATLACS5                   DVHLEPV-AFDMERDLLTPTYKKKRPQLLKYYQNVIHEMYKTTKE----SLASGQ-----  666
ATLACS6                   AVTLVLE-PFTLENGLLTPTFKIKRPQAKEYFAEAITNMYKELGA----SDPSANRGL--  701
ATLACS8                   KIKLLSE-PWTPESGLVTAALKIKREQIKSKFKDELSKLYA-------------------  720
ATLACS9                   KIKLLAS-PWTPESGLVTAALKLKRDVIRREFSEDLTKLYA-------------------  691
HsACSS3                   NAVFVKQ-------LPKTRSGKIPRSALSAIVN--GK-PYKITSTIEDPSIFGHV-----  679
HsACSM3                   KVEFIQE-------LPKTISGKTKRNELRKKEWKT-------I-----------------  586
HsACSM2B                  KIEFVLN-------LPKTVTGKIQRTKLRDKEWKM-------SGKARAQ----------  577
HsACSM1                   KVEFVSE-------LPKTITGKIERKELRKKETGQ-------M-----------------  577
HsACSM4                   KVEFVQE-------LPKTITGKIKRNVLRDQEWRG-------R-----------------  580
HsACSM5                   KVAFVSE-------LPKTVSGKIQRSKLRSQEWGK-------------------------  579
HsACSM6                   ------------------------------------------------------------  479
HsACSBG1                  KWAILER-DFSISGGELGPTMKLKRLTVLEKYKGIIDSFYQEQKM---------------  724
HsACSBG2                  KWVILEK-DFSIYGGELGPMMKLKRHFVAQKYKKQIDHMYH-------------------  666
HsACSS1                   EILVVKR-------LPKTRSGKVMRRLLRKIITSEAQ-ELGDTTTLEDPSIIAEI-----  672
HsACSS2                   YIQNAPG-------LPKTRSGKIMRRVLRKIAQN-DH-DLGDMSTVADPSVISHL-----  597
HsACSVL1                  KMTLVEE-GFNPAV-IKDALYF--LDDTAKMYVPMTEDIYNAISA----KTLKL------  567
HsACSVL2                  KHQLVED-GFNPLK-ISEPLYF--MDNLKKSYVLLTRELYDQIML----GEIKL------  619
HsACSVL3                  KVRMANE-GFDPST-LSDPLYV--LDQAVGAYLPLTTARYSALLA----GNLRI------  730
HsACSVL4                  KTELRKE-GFDPAI-VKDPLFY--LDAQKGRYVPLDQEAYSRIQA----GEEKL------  643
HsACSVL5                  KTRLQRE-GFDPRQ-TSDRLFF--LDLKQGHYLPLNEAVYTRICS----GAFAL------  646
HsACSVL6                  ------------------------------------------------------------  606
```

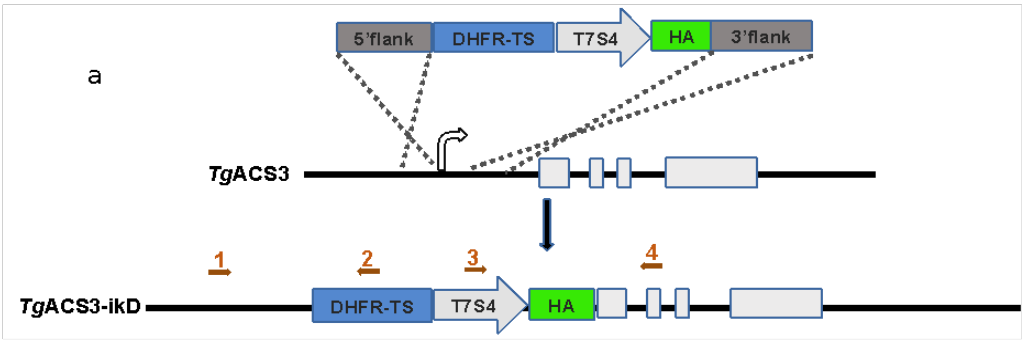

b

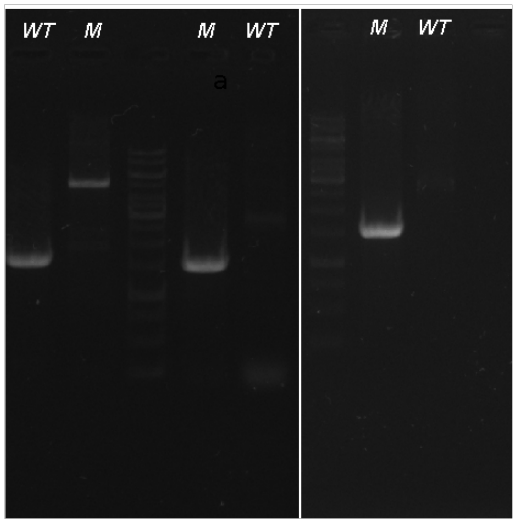

Fig. S2. Schematic of molecular strategy for generation of *Tg*ACS3-iKD tagged with 3*HA at its N-terminus. b) Confirmation of correct promoter replacement in the *Tg*ACS3-iKD line. Primers combinations during the screening PCR yielded products of expected amplicon size validating the mutant. The template genomic DNA was extracted from *Tg*ACS3-iKD line (M) and RHΔ Ku80 TATi strain (WT) (control). Primers 5+4 generated 1452 bp amplicon with RHΔ Ku80 TATi strain (WT) and approx. 4500 bp using *Tg*AC3-ikD gDNA (M), suggesting incorporation of tetracycline inducible elements along with DHFR cassette at the genome locus of *Tg*ACS3. Expectedly, primers combinations specific to Tet-regulatable elements (1+2, 3+4) generated an amplicon approx. 3000 bp in size only using *Tg*ACS3 (M) as the gDNA template.

REFERENCES (CHAPTER V)

Amiar, Souad, Nicholas J. Katris, Laurence Berry, Sheena Dass, Melanie J. Shears, Camille Brunet, Bastien Touquet, et al. 2019. "Division and Adaptation to Host Nutritional Environment of Apicomplexan Parasites Depend on Apicoplast Lipid Metabolic Plasticity and Host Organelles Remodelling." *BioRxiv*, 585737. https://doi.org/10.1101/585737.

Amiar, Souad, James I MacRae, Damien L Callahan, David Dubois, Giel G van Dooren, Melanie J Shears, Marie-France Cesbron-Delauw, et al. 2016. "Apicoplast-Localized Lysophosphatidic Acid Precursor Assembly Is Required for Bulk Phospholipid Synthesis in Toxoplasma Gondii and Relies on an Algal/Plant-Like Glycerol 3-Phosphate Acyltransferase." *PLoS Pathogens* 12 (8): e1005765. https://doi.org/10.1371/journal.ppat.1005765.

Babbitt, Patricia C., George L. Kenyon, Brian M. Martin, Hugues Charest, Michel Slyvestre, Jeffrey D. Scholten, Kai Hsuan Chang, Po Huang Liang, and Debra Dunaway-Mariano. 1992. "Ancestry of the 4-Chlorobenzoate Dehalogenase: Analysis of Amino Acid Sequence Identities among Families of AcyhAdenyl Ligases, Enoyl-CoA Hydratases/Isomerases, and Acyl-CoA Thioesterases." *Biochemistry* 31 (24): 5594–5604. https://doi.org/10.1021/bi00139a024.

Bethke, Lara L, Martine Zilversmit, Kaare Nielsen, Johanna Daily, Sarah K Volkman, Daouda Ndiaye, Elena R Lozovsky, Daniel L Hartl, and Dyann F Wirth. 2006. "Duplication, Gene Conversion, and Genetic Diversity in the Species-Specific Acyl-CoA Synthetase Gene Family of Plasmodium Falciparum." *Molecular and Biochemical Parasitology* 150 (1): 10–24. https://doi.org/10.1016/j.molbiopara.2006.06.004.

Bisio, Hugo, Matteo Lunghi, Mathieu Brochet, and Dominique Soldati-Favre. 2019. "Phosphatidic Acid Governs Natural Egress in Toxoplasma Gondii via a Guanylate Cyclase Receptor Platform." *Nature Microbiology* 4 (3): 420–28. https://doi.org/10.1038/s41564-018-0339-8.

Black, P N, C C DiRusso, A K Metzger, and T L Heimert. 1992. "Cloning, Sequencing, and Expression of the FadD Gene of Escherichia Coli Encoding Acyl Coenzyme A Synthetase." *The Journal of Biological Chemistry* 267 (35): 25513–20. http://www.ncbi.nlm.nih.gov/pubmed/1460045.

Bullen, Hayley E, Yonggen Jia, Yoshiki Yamaryo-Botté, Hugo Bisio, Ou Zhang, Natacha Klages Jemelin, Jean-Baptiste Marq, Vern Carruthers, Cyrille Y Botté, and Dominique Soldati-Favre. 2016. "Phosphatidic Acid-Mediated Signaling Regulates Microneme Secretion in Toxoplasma." *Cell Host & Microbe* 19 (3): 349–60. https://doi.org/10.1016/j.chom.2016.02.006.

Ding, M., C. Clayton, and D. Soldati. 2000. "Toxoplasma Gondii Catalase: Are There Peroxisomes in Toxoplasma." *Journal of Cell Science* 113 (13): 2409–19.

Dooren, Giel G. Van, Cveta Tomova, Swati Agrawal, Bruno M. Humbel, and Boris Striepen. 2008. "Toxoplasma

Gondii Tic20 Is Essential for Apicoplast Protein Import." *Proceedings of the National Academy of Sciences of the United States of America* 105 (36): 13574–79. https://doi.org/10.1073/pnas.0803862105.

Dooren, Giel G. Van, Lee M. Yeoh, Boris Striepen, and Geoffrey I. McFadden. 2016. "The Import of Proteins into the Mitochondrion of Toxoplasma Gondii." *Journal of Biological Chemistry*. https://doi.org/10.1074/jbc.M116.725069.

Dubois, David, Stella Fernandes, Souad Amiar, Sheena Dass, Nicholas J Katris, Cyrille Y Botté, and Yoshiki Yamaryo-Botté. 2018. "Toxoplasma Gondii Acetyl-CoA Synthetase Is Involved in Fatty Acid Elongation (of Long Fatty Acid Chains) during Tachyzoite Life Stages." *Journal of Lipid Research* 59 (6): 994–1004. https://doi.org/10.1194/jlr.M082891.

Ellis, Jessica M., Jennifer L. Frahm, Lei O. Li, and Rosalind A. Coleman. 2010. "Acyl-Coenzyme A Synthetases in Metabolic Control." *Current Opinion in Lipidology* 21 (3): 212–17. https://doi.org/10.1097/MOL.0b013e32833884bb.

Færgeman, Nils J., Paul N. Black, Xiao Dan Zhao, Jens Knudsen, and Concetta C. DiRusso. 2001. "The Acyl-CoA Synthetases Encoded within FAA1 and FAA4 in Saccharomyces Cerevisiae Function as Components of the Fatty Acid Transport System Linking Import, Activation, and Intracellular Utilization." *Journal of Biological Chemistry* 276 (40): 37051–59. https://doi.org/10.1074/jbc.M100884200.

Fernandez, Regina F., Sora Q. Kim, Yingwei Zhao, Rachel M. Foguth, Marcus M. Weera, Jessica L. Counihan, Daniel K. Nomura, Julia A. Chester, Jason R. Cannon, and Jessica M. Ellis. 2018. "Acyl-CoA Synthetase 6 Enriches the Neuroprotective Omega-3 Fatty Acid DHA in the Brain." *Proceedings of the National Academy of Sciences of the United States of America* 115 (49): 12525–30. https://doi.org/10.1073/pnas.1807958115.

Fu, Yong, Xia Cui, Sai Fan, Jing Liu, Xiao Zhang, Yihan Wu, and Qun Liu. 2018. "Comprehensive Characterization of Toxoplasma Acyl Coenzyme A-Binding Protein TgACBP2 and Its Critical Role in Parasite Cardiolipin Metabolism." *MBio* 9 (5): 1–20. https://doi.org/10.1128/mBio.01597-18.

Fu, Yong, Xia Cui, Jing Liu, Xiao Zhang, Heng Zhang, Congshan Yang, and Qun Liu. 2019. "Synergistic Roles of Acyl-CoA Binding Protein (ACBP1) and Sterol Carrier Protein 2 (SCP2) in Toxoplasma Lipid Metabolism." *Cellular Microbiology* 21 (3). https://doi.org/10.1111/cmi.12970.

Fulda, Martin, Judy Schnurr, Amine Abbadi, Ernst Heinz, and John Browse. 2004. "Peroxisomal Acyl-CoA Synthetase Activity Is Essential for Seedling Development in Arabidopsis Thaliana." *Plant Cell* 16 (2): 393–405. https://doi.org/10.1105/tpc.019646.

Fulda, Martin, Jay Shockey, Martin Werber, Frank P. Wolter, and Ernst Heinz. 2002. "Two Long-Chain Acyl-CoA Synthetases from Arabidopsis Thaliana Involved in Peroxisomal Fatty Acid β-Oxidation." *Plant Journal* 32 (1): 93–103. https://doi.org/10.1046/j.1365-313X.2002.01405.x.

Grevengoed, Trisha J., Eric L. Klett, and Rosalind A. Coleman. 2014. “Acyl-CoA Metabolism and Partitioning.” *Annual Review of Nutrition* 34 (1): 1–30. https://doi.org/10.1146/annurev-nutr-071813-105541.

Gulick, Andrew M. 2009. “Conformational Dynamics in the Acyl-CoA Synthetases, Adenylation Domains of Non-Ribosomal Peptide Synthetases, and Firefly Luciferase.” *ACS Chemical Biology* 4 (10): 811–27. https://doi.org/10.1021/cb900156h.

Guo, Fengguang, Haili Zhang, Jason M. Fritzler, S. Dean Rider, Lixin Xiang, Nina N. Mcnair, Jan R. Mead, and Guan Zhu. 2014. “Amelioration of Cryptosporidium Parvum Infection in Vitro and in Vivo by Targeting Parasite Fatty Acyl-Coenzyme a Synthetases.” *Journal of Infectious Diseases* 209 (8): 1279–87. https://doi.org/10.1093/infdis/jit645.

Guo, Fengguang, Haili Zhang, Harold Ross Payne, and Guan Zhu. 2016. “Differential Gene Expression and Protein Localization of Cryptosporidium Parvum Fatty Acyl-CoA Synthetase Isoforms.” *Journal of Eukaryotic Microbiology*. https://doi.org/10.1111/jeu.12272.

Hu, Ke. 2008. “Organizational Changes of the Daughter Basal Complex during the Parasite Replication of Toxoplasma Gondii.” *PLoS Pathogens*. https://doi.org/10.1371/journal.ppat.0040010.

Huynh, My Hang, and Vern B. Carruthers. 2009. “Tagging of Endogenous Genes in a Toxoplasma Gondii Strain Lacking Ku80.” *Eukaryotic Cell* 8 (4): 530–39. https://doi.org/10.1128/EC.00358-08.

Jessen, Dirk, Charlotte Roth, Marcel Wiermer, and Martin Fulda. 2015. “Two Activities of Long-Chain Acyl-Coenzyme A Synthetase Are Involved in Lipid Trafficking between the Endoplasmic Reticulum and the Plastid in Arabidopsis.” *Plant Physiology* 167 (2): 351–66. https://doi.org/10.1104/pp.114.250365.

Jia, Zhenzhen, Zhengtong Pei, Yuanyuan Li, Liumei Wei, Kirby D. Smith, and Paul A. Watkins. 2004. “X-Linked Adrenoleukodystrophy: Role of Very Long-Chain Acyl-CoA Synthetases.” *Molecular Genetics and Metabolism* 83 (1–2): 117–27. https://doi.org/10.1016/j.ymgme.2004.06.015.

Kaasch, Achim J., and Keith A. Joiner. 2000. “Targeting and Subcellular Localization of Toxoplasma Gondii Catalase. Identification of Peroxisomes in an Apicomplexan Parasite.” *Journal of Biological Chemistry* 275 (2): 1112–18. https://doi.org/10.1074/jbc.275.2.1112.

Katris, Nicholas J, Giel G van Dooren, Paul J McMillan, Eric Hanssen, Leann Tilley, and Ross F Waller. 2014. “The Apical Complex Provides a Regulated Gateway for Secretion of Invasion Factors in Toxoplasma.” *PLoS Pathogens* 10 (4): e1004074. https://doi.org/10.1371/journal.ppat.1004074.

Lee, Kwangwon, Janos Kerner, and Charles L. Hoppel. 2011. “Mitochondrial Carnitine Palmitoyltransferase 1a (CPT1a) Is Part of an Outer Membrane Fatty Acid Transfer Complex.” *Journal of Biological Chemistry* 286 (29): 25655–62. https://doi.org/10.1074/jbc.M111.228692.

Li, Lei O., Jessica M. Ellis, Heather A. Paich, Shuli Wang, Nan Gong, George Altshuller, Randy J. Thresher, et al. 2009. “Liver-Specific Loss of Long Chain Acyl-CoA Synthetase-1 Decreases Triacylglycerol Synthesis and β-Oxidation and Alters Phospholipid Fatty Acid Composition.” *Journal of Biological Chemistry* 284 (41): 27816–26. https://doi.org/10.1074/jbc.M109.022467.

Lopes-Marques, Mónica, André M. Machado, Raquel Ruivo, Elza Fonseca, Estela Carvalho, and L. Filipe C. Castro. 2018. “Expansion, Retention and Loss in the Acyl-CoA Synthetase ‘Bubblegum’ (Acsbg) Gene Family in Vertebrate History.” *Gene* 664 (November 2017): 111–18. https://doi.org/10.1016/j.gene.2018.04.058.

Mazumdar, Jolly, and Boris Striepen. 2007. “Make It or Take It: Fatty Acid Metabolism of Apicomplexan Parasites.” *Eukaryotic Cell* 6 (10): 1727–35. https://doi.org/10.1128/EC.00255-07.

Mazumdar, Jolly, Emma H. Wilson, Kate Masek, Christopher A. Hunter, and Boris Striepen. 2006. “Apicoplast Fatty Acid Synthesis Is Essential for Organelle Biogenesis and Parasite Survival in Toxoplasma Gondii.” *Proceedings of the National Academy of Sciences of the United States of America* 103 (35): 13192–97. https://doi.org/10.1073/pnas.0603391103.

Meissner, Markus, Dirk Schlüter, and Dominique Soldati. 2002. “Role of Toxoplasma Gondii Myosin a in Powering Parasite Gliding and Host Cell Invasion.” *Science* 298 (5594): 837–40. https://doi.org/10.1126/science.1074553.

Moog, Daniel, Jude M. Przyborski, and Uwe G. Maier. 2017. “Genomic and Proteomic Evidence for the Presence of a Peroxisome in the Apicomplexan Parasite Toxoplasma Gondii and Other Coccidia.” *Genome Biology and Evolution* 9 (11): 3108–21. https://doi.org/10.1093/gbe/evx231.

Nolan, Sabrina J., Julia D. Romano, John T. Kline, and Isabelle Coppens. 2018. “Novel Approaches to Kill Toxoplasma Gondii by Exploiting the Uncontrolled Uptake of Unsaturated Fatty Acids and Vulnerability to Lipid Storage Inhibition of the Parasite.” *Antimicrobial Agents and Chemotherapy* 62 (10): 1–34. https://doi.org/10.1128/AAC.00347-18.

Pei, Zhengtong, Nadia A. Oey, Maartje M. Zuidervaart, Zhenzhen Jia, Yuanyuan Li, Steven J. Steinberg, Kirby D. Smith, and Paul A. Watkins. 2003. “The Acyl-CoA Synthetase ‘Bubblegum’ (Lipidosin).” *Journal of Biological Chemistry* 278 (47): 47070–78. https://doi.org/10.1074/jbc.M310075200.

Pernas, Lena, Camilla Bean, John C. Boothroyd, and Luca Scorrano. 2018. “Mitochondria Restrict Growth of the Intracellular Parasite Toxoplasma Gondii by Limiting Its Uptake of Fatty Acids.” *Cell Metabolism* 27 (4): 886-897.e4. https://doi.org/10.1016/j.cmet.2018.02.018.

Poppelreuther, Margarete, Berenice Rudolph, Chen Du, Regina Großmann, Melanie Becker, Christoph Thiele, Robert Ehehalt, and Joachim Füllekrug. 2012. “The N-Terminal Region of Acyl-CoA Synthetase 3 Is Essential for Both the Localization on Lipid Droplets and the Function in Fatty Acid Uptake.” *Journal of Lipid*

Research 53 (5): 888–900. https://doi.org/10.1194/jlr.M024562.

Ramakrishnan, Srinivasan, Melissa D. Docampo, James I. MacRae, François M. Pujol, Carrie F. Brooks, Giel G. Van Dooren, J. Kalervo Hiltunen, Alexander J. Kastaniotis, Malcolm J. McConville, and Boris Striepen. 2012. "Apicoplast and Endoplasmic Reticulum Cooperate in Fatty Acid Biosynthesis in Apicomplexan Parasite Toxoplasma Gondii." *Journal of Biological Chemistry* 287 (7): 4957–71. https://doi.org/10.1074/jbc.M111.310144.

Schnurr, Judy A., Jay M. Shockey, Gert Jan De Boer, and John A. Browse. 2002. "Fatty Acid Export from the Chloroplast. Molecular Characterization of a Major Plastidial Acyl-Coenzyme A Synthetase from Arabidopsis." *Plant Physiology* 129 (4): 1700–1709. https://doi.org/10.1104/pp.003251.

Sheiner, Lilach, Jessica L Demerly, Nicole Poulsen, Wandy L Beatty, Olivier Lucas, Michael S Behnke, Michael W White, and Boris Striepen. 2011. "A Systematic Screen to Discover and Analyze Apicoplast Proteins Identifies a Conserved and Essential Protein Import Factor." *PLoS Pathogens* 7 (12): e1002392. https://doi.org/10.1371/journal.ppat.1002392.

Shockey, J M, M S Fulda, and J A Browse. 2002. "Arabidopsis Contains Nine Long-Chain Acyl-Coenzyme A Synthetase Genes That Participate in Fatty Acid and Glycerolipid Metabolism." *Plant Physiology* 129 (4): 1710–22. https://doi.org/10.1104/pp.003269.

Sidik, Saima M., Diego Huet, Suresh M. Ganesan, My Hang Huynh, Tim Wang, Armiyaw S. Nasamu, Prathapan Thiru, et al. 2016. "A Genome-Wide CRISPR Screen in Toxoplasma Identifies Essential Apicomplexan Genes." *Cell* 166 (6): 1423-1435.e12. https://doi.org/10.1016/j.cell.2016.08.019.

Watkins, Paul A., Dony Maiguel, Zhenzhen Jia, and Jonathan Pevsner. 2007. "Evidence for 26 Distinct Acyl-Coenzyme A Synthetase Genes in the Human Genome." *Journal of Lipid Research* 48 (12): 2736–50. https://doi.org/10.1194/jlr.M700378-JLR200.

Yao, Hongbing, and Jin Ye. 2008. "Long Chain Acyl-CoA Synthetase 3-Mediated Phosphatidylcholine Synthesis Is Required for Assembly of Very Low Density Lipoproteins in Human Hepatoma Huh7 Cells." *Journal of Biological Chemistry* 283 (2): 849–54. https://doi.org/10.1074/jbc.M706160200.

Zhao, Lifang, Tegan M. Haslam, Annika Sonntag, Isabel Molina, and Ljerka Kunst. 2019. "Functional Overlap of Long-Chain Acyl-CoA Synthetases in Arabidopsis." *Plant and Cell Physiology* 60 (5): 1041–54. https://doi.org/10.1093/pcp/pcz019.

CHAPTER VI: GENERAL DISCUSSION AND FUTURE PERSPECTIVES

The survival of apicomplexan parasites within their hosts is predominantly dependent on lipids, which play an essential role by regulating metabolic flux, acting as signaling molecules, storage fuels and structural building blocks of membranes. To sustain rapid replication during the intracellular stages, these parasites rely on active lipid synthesis fed by fatty acids derived from both *de novo* FASII and the host. The essential mechanism allowing these parasites to maintain a proper flux between the two sources of FA remains largely unknown. In pursuit of the same, my PhD focused on ascertaining pivotal roles of 2 key proteins in parasite FA metabolism: a) acyl coA synthetases (ACS) converting free FA to activated acyl coA-FA and b) Lipin: a phosphatidic acid phosphatase utilizing the activated FA to generate and control the bulk synthesis of central lipid precursors, phosphatidic acid (PA) and diacylglycerol (DAG).

Tg*LIPIN: key enzyme regulating FA fluxes via PA metabolism in *Toxoplasma

Functional characterization of *Tg*LIPIN established its pivotal function as an active phosphatidate phosphatase, regulating the critical levels of PA through the generation of its enzymatic product DAG. Fatty acid scavenging from the host can only support the proper intracellular growth of *Toxoplasma* tachyzoites in specific amount below a certain lipotoxic threshold (Nolan *et al.*, 2018). This suggests that the parasite is reliant on a delicate tuning allowing these FA to be properly repurposed for metabolic use rather than accumulating in excess resulting in parasite growth arrest. The parasite and the host work in a concerted manner to regulate and maintain the FA flux/homeostasis. We propose that *Tg*LIPIN is an essential control switch that channels the host-derived FA flux to either membrane phospholipids or storage lipids (TAG). The role of PA in parasite pathogenicity has previously been attributed to (i) its function as a signaling lipid mediating key parasite processes like invasion, motility and egress (Bullen *et al.*, 2016; Bisio *et al.*, 2019), (b) as central precursor for generation of membrane phospholipids and regulator of LPA/PA levels which governs parasite cell division and cytokinesis (Amiar *et al.*, 2016, 2019; Shears *et al.*, 2017). We, through this study, determined the unprecedented and key role of PA as the limiting component between glycerolipid synthesis and storage pathways in apicomplexa, particularly in *T. gondii*.

Identifying the protein regulators of the metabolic tap, *Tg*LIPIN

In other eukaryotic systems, lipin functionality has been proposed to be under control of multi-regulatory mechanisms involving various protein kinases and phosphatases (Zhang and Reue,

2017; Carman and Han, 2019). Data from our collaborative studies involving phospho-proteomic screen of a cyclin-dependent protein kinase-*Tg*CDPK7 knockout strain (personal communication C. Botté, collaboration Botté-Sharma) showed that *Tg*LIPIN was hypophosphorylated at serine residue in the *Tg*CDPK7-KO strain (amino acid position-serine 1019). Interestingly, the phosphorylation of the yeast lipin Pah1 that controls its localization, catalytic activity and stability, is regulated by several protein kinases including cyclin dependent protein kinases, protein kinase A, protein kinase C (Carman and Han, 2019). Together, these data orientated my PhD project further towards the identification of potential regulators of *Tg*LIPIN. In contrast to multi-site phosphorylation events governing the regulation of eukaryotic homologs of *Tg*LIPIN, lipin-1 (in mammals) and Pah1 (in yeast), are activated by a single-site dephosphorylation event (Kim *et al.*, 2007; Pascual and Carman, 2013; Reue and Wang, 2019). This activating dephosphorylation is controlled by a specific protein phosphatase family: The Dullard protein phosphatase for the human lipin-1 and the related Nem1p (part of the Nem1p-Spo7p complex) for the yeast Pah1. Using bioinformatic tools I identified a homolog of the Dullard/Nem1p phosphatase in *T. gondii*, which was named as *Tg*DULL. We think that could be a putative regulator of *Tg*LIPIN metabolic function. This Nem1p/Dullard homolog is predicted to be a protein phosphatase sharing the characteristic HAD motif with its potential/probable substrate *Tg*LIPIN. I endogenously tagged *Tg*DULL at its C-terminus with 3×HA tag. The corresponding *Tg*DULL-HA was found co-localizing with the ER of the parasite placing it into the perspective of ER vicinity localization of *Tg*LIPIN. I generated an inducible knockdown line for this protein, within which *Tg*LIPIN will be endogenously tagged. The future aim and continuation of my PhD project is to determine the effect of *Tg*DULL downregulation on localization and phosphorylation status of *Tg*LIPIN. Subsequently, parasite development and survival will be sought to establish *Tg*DULL role as the potential 'activator' of *Tg*LIPIN.

Does the presence of a predicted Nuclear Localizing Signal, NLS, in *Plasmodium falciparum* Lipin (*Pf*LIPIN) mean that *Pf*LIPIN has retained a link to phospholipid gene regulation like its human homolog lipin-1?

Another important future perspective of my lipin project is to complete the functional characterization of *Pf*LIPIN. In contrast to *Tg*LIPIN, *Pf*LIPIN, was found to have a predicted nuclear localization signal (NLS) like its other eukaryotic counterparts (Csaki and Reue, 2010; Ren *et al.*, 2010; Han and Carman, 2017; Carman and Han, 2018). Although *Pf*LIPIN is predicted

to be mutable via the *P. falciparum* whole genome KO screen (Zhang *et al.*, 2018), an intriguing localization of this protein in the vicinity/near overlap with the parasite nucleus, instils a potentially unexplored and important role. In humans, lipin-1 translocates to the nucleus to function as an inducible amplifier of PGC1 alpha/PPAR alpha pathway in hepatocytes to control the hepatic lipid metabolism (Finck *et al.*, 2006). Another astounding study by Romanauska and Köhler (Romanauska and Köhler, 2018), showed that the inner nuclear membrane (INM) of a eukaryotic cell is a metabolically active site that can, generate nuclear lipid droplets (nLDs). They examined the INM lipid composition and found that the INM was enriched with DAG and that the nLDs lipid monolayer comprised appropriate levels of PA/DAG controlling the cell's storage vs growth functions. This fine balance between PA and DAG is notably regulated via the nuclear activity of the lipin homolog in yeast, Pah1. Thus, the predicted NLS and interesting localization, could place *Pf*LIPIN in the perspective of a possible link between nuclear metabolic activity and gene regulation in *P. falciparum*.

_Tg_ACSs: Role of the fatty acid 'activating' enzymes in _Toxoplasma_ lipid metabolism

Acyl CoA syntheses (ACS) are enzymes that catalyze the initial and mandatory reaction of all FA metabolic pathways. Within apicomplexa, 13 ACSs have been identified in *P. falciparum* and 3 in *C. parvum* (Bethke *et al.*, 2006; Guo *et al.*, 2016). The extension of the *Pf*ACS9 into a family into 10 paralogs (*Pf*Acs1a-*Pf*Acs8) within the sub-telomeric region of the chromosomes, which is otherwise well known for harboring parasite virulence specific 'var/rifin' genes, strongly confer that lipid metabolism in important for the pathogenicity of the parasite(Bethke *et al.*, 2006).

With the help of bioinformatic and genetic tools, we were able to identify 7 putative acyl CoA synthetases in *T. gondii*. Phylogeny helped segregate the 7 ACSs with their closest eukaryotic counterparts with an interesting separation of *Tg*ACS7 to sub-group specific to coccidia and chromerids. This protein could be an evolutionary link between apicomplexan sub-group coccidia and plant-like ancestors, chromerids, which was lost in *P. falciparum.*

Characterization and lipidomics on mutant parasites lacking the predicted most important member of the *Toxoplasma ACS* gene family, *Tg*ACS3, provided insights into the functional aspect and importance of the protein family for the parasite. First, the increase in FFA species with simultaneous decrease in the FA levels of the phospholipid classes within this mutant parasite (*Tg*ACS3-iKD), strongly supported its functional aspect of being an ACS. Importantly, it

determines its likely role for activating FA for their downstream metabolic flux for phospholipid synthesis, membrane biogenesis and parasite division.

Functional and metabolic confirmation of all *Tg*ACSs may require further biochemical assays involving activity assay using purified recombinant *Tg*ACS and/ or heterologous complementation of appropriate yeast strains lacking ACS activity. Such assays have been reported previously (Shockey, Fulda and Browse, 2002). We have initiated this work, but I was unfortunately not able to fully conduct and report it in this manuscript. To further determine the functional role of the remaining *Tg*ACS, we are currently generating CRISPR-cas9 mediated knockout strains for each ACS identified in *T. gondii* genome. One of the future prospects of my PhD project is thus to assert the effect of the disruption of all *Tg*ACSs on parasite growth/fitness of the parasite, which will be followed by core lipidomics to ascertain their FA specificities and role for parasite lipid synthesis.

It is interesting to note that of all the ACSs that we identified in *Toxoplasma*, none was localizing to one of the major metabolic hubs, apicoplast. Despite being highly active in PA biosynthesis, the absence of ACS suggests that the substrates utilized in this process are 'acyl-ACPs' directly obtained from FASII rather than fatty acyl-CoA thioesters.

ACSs also participate in the vectorial acylation of FAs, a process coupling the import and activation of FA. An evidence of physical interaction between an ACS, FACS and an acyl-CoA transporter, Fat1p, in yeast, also indicates vectorial esterification and metabolic trapping of the FAs (Zou *et al.*, 2003). A PVM specific ACS in *C. parvum, Cp*ACS1, has been proposed to activate FA acquired from the host, in order to facilitate their entry into the parasite cytoplasm. Thus, it is plausible that some of these *Tg*ACSs could participate in vectorial acylation of FAs. The mitochondrial localization of *Tg*ACS2 and *Tg*ACBP2 suggest their potential participation in vectorial acylation of fatty acids across the mitochondrial membrane. It is probably the case with other ACSs, ACBPs, and potentially other (lyso)phospholipases at other key metabolic active sites for parasite lipid synthesis. The results of my project will potentially help answering such questions on the metabolic organization of the key parasite enzymes that maintain lipid synthesis and homeostasis.

Lastly, FA flux analysis using stable isotope labelling with ^{13}C-Glucose, including our novel lipidomic approach to monitor host scavenging, will help determine the role of ACS at the cross-

roads of utilization of FA from the two key parasite sources: *de novo* machinery and scavenging from host. Determining these will be key to unravel the complex mechanisms sustaining lipid synthesis and parasite propagation and survival.

Understanding the bigger perspective: Metabolic co-evolution of the host with its parasite

By nature of its intracellular development parasite metabolism cannot be studied exclusive of the host. As a part of their survival regime, these parasites hijack their host cell machinery to acquire nutrients and evade immune response. These parasites infect multiple host cell types and are able to establish successful infection owing to consistent remodeling within the metabolic capacities. Recent study showed that malaria infection in humans is potentially impacted by the host dietary calorie alterations (Mancio-Silva *et al.*, 2017). Use of restricted diet regime in mouse models prior to infection with *P. berghei* resulted in attenuated parasitemia and virulence. The basis of this nutrient sensing was identified as a homolog of SNF1/AMPKα, a putative serine/threonine kinase called KIN which modulated the transcription of genes in response to host nutritional status. The calorie restriction mediated effects on parasite replication within the host were in fact rescued by addition of glucose. This shows the impact of host nutritional environment on parasite metabolic characteristics which in turn impacts their infection rate within the host. An interesting epidemiological study of African ethnic tribes revealed natural resistance of Fulani tribe to malaria. The basis on this divergence has been long rooted into genetic polymorphisms and immune responses. However, it is interesting to note that these resistant tribes also diverge in their dietary habits which involves intake of food rich in saturated fatty acids. Although, there is no evidence of direct link between resistance to malaria infection and food intake, it plausible to co-relate the dietary intake to host nutritional environment affecting parasite infection (Zuzarte-Luís and Mota, 2018). The sexual stages of *P. falciparum* respond to levels of host derived lysophosphatidylcholine (LPC). High levels of LPC suppresses the development of gametocytes in vitro (Brancucci *et al.*, 2017; Wein *et al.*, 2018). Consistently, the deprivation of lipids from growth culture media resulted in decline in the growth of otherwise unessential FASII-FabI knockout asexual blood stage *P. falciparum* parasites (Amiar *et al.*, 2019). When subjected to weak host nutritional environment, the *Toxoplasma* tachyzoites are able to suffice their lipidic needs by upregulation of fatty acid synthesis *de novo* via FASII (Amiar *et al.*, 2019). It can thus be said that the parasites endure adept metabolic capacity to ensure survival in less-favorable metabolic landscape.

The sexual development of *Toxoplasma* is restricted to feline intestine due to the excessive presence of linoleic acid (18:2) owing to the absence of the enzyme Δdesaturase responsible for metabolism of 18:2 (Di Genova *et al.*, 2019). This study represents a classic example of co-evolution of the host and parasite based on metabolic reprogramming, which in this case occurs within the host. As a part of its innate defence mechanism, the host, embarks a competitive streak by limiting the parasites from fatty acid uptake by enwrapping their PV in host mitochondria (Pernas *et al.*, 2018). Host cells infected with *T. gondii* exhibit enhanced lipid droplet biogenesis due to increased levels of neutral lipid TAGs (Hu, Binns and Reese, 2017). Later, it was shown by Nolan et al that indeed the parasites acquire the host lipids through host Rab7 labelled vesicles/LDs originating from host Golgi to the parasite PV lumen (Nolan, Romano and Coppens, 2017).

Lessons from other apicomplexan parasites: *De novo* synthesis vs scavenging

So far, this thesis has extensively discussed the fatty acid biosynthesis and host/environmental scavenging in two sub-groups of apicomplexa, Coccidia (with ref to *T. gondii)* and Haemosporidia with ref to (*P. falciparum*). Further ahead, I briefly discuss the fatty acid metabolism in other apicomplexan parasites:

a) Piroplasmida

   These livestock affecting parasites reside within a vertebrate host (as sporozoite and merozoite forms) and in their tick host (as zygote and ookinete form). Once inside the mammalian host, these protists sequentially parasitize nucleated lymphocytes followed by enucleated erythrocytes. This part of the life cycle bears resemblance to an extent with Haemosporidia (*Plasmodium falciparum)*. An interesting aspect of the survival of these parasites within their lymphocyte host is that post 15 min of invasion and establishment of infection, the parasite escapes from the enclosing host cell membrane to lie freely in the host cytoplasm, surrounded by host microtubules (Shaw 2003). Thus, during its intracellular development, this parasite is not surrounded by any parasitophorous vacuolar membrane. There are studies suggesting that these intracellular free parasite forms phagocytose or pinocytose the host cytoplasm (Jalovecka et al. 2018).

   As a part of their eubacterial ancestry, the piroplasms have retained organelle apicoplast, however its importance as the central metabolic hub still holds many questions. For

instance, despite the presence of apicoplast, *Theileria annulata* lacks the enzymes involved in heme and fatty acid synthesis. No enoyl ACP reductase or acetyl-CoA carboxylase is apparent in the *Theileria* genomes(Goodman and McFadden 2006). Similarly, despite the presence of an ACP in *Babesia bovis* apicoplast, the FASII pathway has been shown to be dispensable by triclosan treatment, during intraerythrocytic stages(Caballero et al. 2012).

The indispensability and/or absence of key enzymes involved in FASII pathway in the piroplasms residing within mammalian hosts suggests the complete dependency of these parasites on their host for fatty acids and other essential nutrients. This explains the 'no-barrier' nature of its intracellular development i.e. the complete absence of PVM to facilitate maximum uptake from the host. Nevertheless, it would be interesting to identify the nutrient transporters that actively participate in this the process of a 'regulated' uptake from the host cell in these parasites.

A study distinguishing the lipid composition of *B. bovis* infected erythrocytes from uninfected RBCs showed trend similar to *P. falciparum* with an increase in lipid species- PC, PA, DAG , CE. This study also showed by uptake studies that *Babesia* was able to scavenge resources including choline, myo-inositol and ^{14}C labelled stearic acid from the extracellular environment (Jalovecka et al. 2000).

b) Cryptosporidida

This parasite completes both its asexual and sexual part of the lifecycle within epithelial cells lining the intestines of its human host. The parasites belonging to this sub-group have developed a unique epicellular lifestyle wherein they develop intracellularly within a parasitophorous vacuole bulging out of the apical end of cytoplasm of the host cell (Elliott and Clark 2000).

Biochemical and genetic data suggests that *Cryptosporidium* has lost a plastid as well as the genomes of both plastid and mitochondria. Subsequently, *Cryptosporidium* is unable to *de novo* synthesize amino acids, nucleotides and fatty acids (Cacciò and Widmer 2014). Due to the absence of several *de novo* synthesis pathways, a considerable amount of the metabolites is up taken from host and or extracellular environment. *Cryptosporidium* has been known to have several transporters specific to each metabolite like amino acids

(~11transporters), sugars (~9), and nucleotides (at least one). These parasites are also known to have approx. 24 ABC transporters (Cacciò and Widmer 2014).

Despite extensive reliance on host FA scavenging due to absence of apicoplast FASII, *Cryptosporidium* possesses a type I intron less fatty acid mega synthase which is similar to bacterial polyketide synthase. The specificity of the *Cp*FASI for very long chain fatty acids (>C20) suggests that rather than *de novo* synthesis, this enzyme is potentially rewired to function as a fatty acid elongase. Apart from the *Cp*FASI, these parasites also possess a membrane protein called LCE i.e long chain elongase and a bacterial like polyketide synthase (*Cp*PKS1). The LCE enzyme accepts acyl CoA thioesters as its substrate rather than acyl-ACPs. *Cp*LCE1 is able to elongate its substrate fatty acyl CoA ester by a single C2 subunit and was shown to have a preference towards myristyl CoA and palmityl CoA. This enzyme is present on the plasma membrane of sporozoites as well as in the PVM, to utilise the incoming scavenged fatty acids which prior to, are activated to corresponding thioesters by acyl-CoA synthetases (also localised towards the parasite's PM and PVM). It seems that all the plasma membrane bound important enzymes like ACS, ACBP and LCE are purposed towards these locations in order to achieve proper uptake of fatty acids via transport, activation and further elongation.

Based on simplified metabolic features and a compact genome, the Cryptosporidida can be placed phylogenetically closer to Gregarines rather than other coccidians and haemosporidians.

c) Gregarinida

Parasites belonging to Gregarinida and Cryptosporidida likely share a monophyletic relationship, meaning they may a common immediate ancestor. However, Gregarines are able to parasitize only invertebrates. Like *Cryptosporidium*, the *Gregarina* also lacks a plastid but in contrast possesses a respiring mitochondrion. Genome analysis of *Ascogregarina sp* hints at *de novo* fatty acid biosynthesis due to the retention of wide set of fatty acid (FA) biosynthetic enzymes including a type I fatty acid synthase, FA desaturases and fatty acid CoA ligases (Templeton et al. 2010).

REFERENCES (Chapter VI)

Aly, Ahmed S.I., Ashley M. Vaughan, and Stefan H.I. Kappe. 2009. "Malaria Parasite Development in the Mosquito and Infection of the Mammalian Host." *Annual Review of Microbiology*. https://doi.org/10.1146/annurev.micro.091208.073403.

Amiar, S. *et al.* (2016) 'Apicoplast-Localized Lysophosphatidic Acid Precursor Assembly Is Required for Bulk Phospholipid Synthesis in Toxoplasma gondii and Relies on an Algal/Plant-Like Glycerol 3-Phosphate Acyltransferase.', *PLoS pathogens*, 12(8), p. e1005765. doi: 10.1371/journal.ppat.1005765.

Amiar, S. *et al.* (2019) 'Division and adaptation to host nutritional environment of apicomplexan parasites depend on apicoplast lipid metabolic plasticity and host organelles remodelling', *bioRxiv*, p. 585737. doi: 10.1101/585737.

Bethke, L. L. *et al.* (2006) 'Duplication, gene conversion, and genetic diversity in the species-specific acyl-CoA synthetase gene family of Plasmodium falciparum.', *Molecular and biochemical parasitology*, 150(1), pp. 10–24. doi: 10.1016/j.molbiopara.2006.06.004.

Bisio, H. *et al.* (2019) 'Phosphatidic acid governs natural egress in Toxoplasma gondii via a guanylate cyclase receptor platform', *Nature Microbiology*. doi: 10.1038/s41564-018-0339-8.

Brancucci, N. M. B. *et al.* (2017) 'Lysophosphatidylcholine Regulates Sexual Stage Differentiation in the Human Malaria Parasite Plasmodium falciparum', *Cell*. doi: 10.1016/j.cell.2017.10.020.

Bullen, H. E. *et al.* (2016) 'Phosphatidic Acid-Mediated Signaling Regulates Microneme Secretion in Toxoplasma.', *Cell host & microbe*, 19(3), pp. 349–60. doi: 10.1016/j.chom.2016.02.006.

Caballero, Marina C., Monica J. Pedroni, Guy H. Palmer, Carlos E. Suarez, Christine Davitt, and Audrey O.T. Lau. 2012. "Characterization of Acyl Carrier Protein and LytB in Babesia Bovis Apicoplast." *Molecular and Biochemical Parasitology* 181 (2): 125–33. https://doi.org/10.1016/j.molbiopara.2011.10.009.

Cacciò, Simone M., and Giovanni Widmer. 2014. "Cryptosporidium: Parasite and Disease." *Cryptosporidium: Parasite and Disease*, 1–564. https://doi.org/10.1007/978-3-7091-1562-6.

Carman, G. M. and Han, G. S. (2018) 'Phosphatidate phosphatase regulates membrane phospholipid synthesis via phosphatidylserine synthase', *Advances in Biological Regulation*. doi: 10.1016/j.jbior.2017.08.001.

Carman, G. M. and Han, G. S. (2019) 'Fat-regulating phosphatidic acid phosphatase: A review of its roles and regulation in lipid homeostasis', *Journal of Lipid Research*, 60(1), pp. 2–6. doi: 10.1194/jlr.S087452.

Csaki, L. S. and Reue, K. (2010) 'Lipins: Multifunctional Lipid Metabolism Proteins', *Annual Review of Nutrition*. doi: 10.1146/annurev.nutr.012809.104729.

Finck, B. N. *et al.* (2006) 'Lipin 1 is an inducible amplifier of the hepatic PGC-1α/PPARα regulatory pathway', *Cell*

Metabolism. doi: 10.1016/j.cmet.2006.08.005.

Di Genova, B. M. *et al.* (2019) 'Intestinal delta-6-desaturase activity determines host range for Toxoplasma sexual reproduction', *PLoS Biology*, 17(8), pp. 1–19. doi: 10.1371/journal.pbio.3000364.

Elliott, David A., and Douglas P. Clark. 2000. "Cryptosporidium Parvum Induces Host Cell Actin Accumulation at the Host- Parasite Interface." *Infection and Immunity*. https://doi.org/10.1128/IAI.68.4.2315-2322.2000.

Goodman, C., and G. McFadden. 2006. "Fatty Acid Biosynthesis as a Drug Target in Apicomplexan Parasites." *Current Drug Targets* 8 (1): 15–30. https://doi.org/10.2174/138945007779315579.

Guo, F. *et al.* (2016) 'Differential Gene Expression and Protein Localization of Cryptosporidium parvum Fatty Acyl-CoA Synthetase Isoforms', *Journal of Eukaryotic Microbiology*. doi: 10.1111/jeu.12272.

Han, G. S. and Carman, G. M. (2017) 'Yeast PAH1-encoded phosphatidate phosphatase controls the expression of CHO1-encoded phosphatidylserine synthase for membrane phospholipid synthesis', *Journal of Biological Chemistry*. doi: 10.1074/jbc.M117.801720.

Hu, X., Binns, D. and Reese, M. L. (2017) 'The coccidian parasites Toxoplasma and Neospora dysregulate mammalian lipid droplet biogenesis', *Journal of Biological Chemistry*, 292(26), pp. 11009–11020. doi: 10.1074/jbc.M116.768176.

Jalovecka, Marie, Ondrej Hajdusek, Daniel Sojka, Petr Kopacek, Laurence Malandrin, Michael K. Shaw, Alexis Valentin, et al. 2000. "Phosphatidylcholine Formation Is the Predominant Lipid Biosynthetic Event in the Hemoparasite Babesia Bovis." *Biology of the Cell* 73 (1): 1–22. https://doi.org/10.1016/0248-4900(91)90010-K.

Kim, Y. *et al.* (2007) 'A conserved phosphatase cascade that regulates nuclear membrane biogenesis', *Proceedings of the National Academy of Sciences of the United States of America*. doi: 10.1073/pnas.0702099104.

Mancio-Silva, L. *et al.* (2017) 'Nutrient sensing modulates malaria parasite virulence', *Nature*. doi: 10.1038/nature23009.

Nolan, S. J. *et al.* (2018) 'Novel approaches to kill toxoplasma gondii by exploiting the uncontrolled uptake of unsaturated fatty acids and vulnerability to lipid storage inhibition of the parasite', *Antimicrobial Agents and Chemotherapy*, 62(10), pp. 1–34. doi: 10.1128/AAC.00347-18.

Nolan, S. J., Romano, J. D. and Coppens, I. (2017) *Host lipid droplets: An important source of lipids salvaged by the intracellular parasite Toxoplasma gondii*, *PLoS Pathogens*. doi: 10.1371/journal.ppat.1006362.

Pascual, F. and Carman, G. M. (2013) 'Phosphatidate phosphatase, a key regulator of lipid homeostasis.', *Biochimica et biophysica acta*, 1831(3), pp. 514–22. doi: 10.1016/j.bbalip.2012.08.006.

Pernas, L. *et al.* (2018) 'Mitochondria Restrict Growth of the Intracellular Parasite Toxoplasma gondii by Limiting Its Uptake of Fatty Acids', *Cell Metabolism*. Elsevier Inc., 27(4), pp. 886-897.e4. doi: 10.1016/j.cmet.2018.02.018.

Ren, H. *et al.* (2010) 'A phosphatidic acid binding/nuclear localization motif determines lipin1 function in lipid metabolism and adipogenesis', *Molecular Biology of the Cell*. doi: 10.1091/mbc.E10-01-0073.

Reue, K. and Wang, H. (2019) 'Mammalian lipin phosphatidic acid phosphatases in lipid synthesis and beyond: Metabolic and inflammatory disorders', *Journal of Lipid Research*. doi: 10.1194/jlr.S091769.

Romanauska, A. and Köhler, A. (2018) 'The Inner Nuclear Membrane Is a Metabolically Active Territory that Generates Nuclear Lipid Droplets', *Cell*. doi: 10.1016/j.cell.2018.05.047.

Shaw, Michael K. 2003. "Cell Invasion by Theileria Sporozoites." *Trends in Parasitology*. https://doi.org/10.1016/S1471-4922(02)00015-6.

Shears, M. J. *et al.* (2017) 'Characterization of the Plasmodium falciparum and P. berghei glycerol 3-phosphate acyltransferase involved in FASII fatty acid utilization in the malaria parasite apicoplast', *Cellular Microbiology*, 19(1). doi: 10.1111/cmi.12633.

Shockey, J. M., Fulda, M. S. and Browse, J. A. (2002) 'Arabidopsis contains nine long-chain acyl-coenzyme A synthetase genes that participate in fatty acid and glycerolipid metabolism', *Plant Physiology*, 129(4), pp. 1710–1722. doi: 10.1104/pp.003269.

Templeton, Thomas J., Shinichiro Enomoto, Wei June Chen, Chin Gi Huang, Cheryl A. Lancto, Mitchell S. Abrahamsen, and Guan Zhu. 2010. "A Genome-Sequence Survey for Ascogregarina Taiwanensis Supports Evolutionary Affiliation but Metabolic Diversity between a Gregarine and Cryptosporidium." *Molecular Biology and Evolution* 27 (2): 235–48. https://doi.org/10.1093/molbev/msp226.

Wein, S. *et al.* (2018) 'Contribution of the precursors and interplay of the pathways in the phospholipid metabolism of the malaria parasite', *Journal of Lipid Research*. doi: 10.1194/jlr.M085589.

Zhang, M. *et al.* (2018) 'Uncovering the essential genes of the human malaria parasite Plasmodium falciparum by saturation mutagenesis', *Science*. doi: 10.1126/science.aap7847.

Zhang, P. and Reue, K. (2017) 'Lipin proteins and glycerolipid metabolism: Roles at the ER membrane and beyond', *Biochimica et Biophysica Acta - Biomembranes*. doi: 10.1016/j.bbamem.2017.04.007.

Zou, Z. *et al.* (2003) 'Vectorial acylation in Saccharomyces cerevisiae: Fat1p and fatty acyl-CoA synthetase are interacting components of a fatty acid import complex', *Journal of Biological Chemistry*. doi: 10.1074/jbc.M210557200.

Zuzarte-Luís, V. and Mota, M. M. (2018) 'Parasite Sensing of Host Nutrients and Environmental Cues.', *Cell host & microbe*, 23(6), pp. 749–758. doi: 10.1016/j.chom.2018.05.018.

ANNEX

The annex contains collaborative papers obtained during my PhD

- Amiar, Souad, Nicholas J. Katris, Laurence Berry, **Sheena Dass**, Melanie J. Shears, Camille Brunet, Bastien Touquet, et al. 2019. "**Division and Adaptation to Host Nutritional Environment of Apicomplexan Parasites Depend on Apicoplast Lipid Metabolic Plasticity and Host Organelles Remodelling.**" *BioRxiv*, 585737. https://doi.org/10.1101/585737.
  In this study, I assessed the role of nutrient starvation on host cells and intracellular parasites, separately by analysing the lipid droplets and a host-specific mitochondrial lipid anti-lyso-bi-phosphatidic acid (LBPA). The import of lipid droplets was increased within the parasite was upregulated in conditions of FBS starvation. Host LBPA was found surrounding the PVM in the infected host cell, within the PV and the parasite, but its localization and intensity remained unchanged in response to reduced FBS content.

- Dubois, David, Stella Fernandes, Souad Amiar, **Sheena Dass**, Nicholas J Katris, Cyrille Y Botté, and Yoshiki Yamaryo-Botté. 2018. "**Toxoplasma Gondii Acetyl-CoA Synthetase Is Involved in Fatty Acid Elongation (of Long Fatty Acid Chains) during Tachyzoite Life Stages.**" *Journal of Lipid Research* 59 (6): 994–1004. https://doi.org/10.1194/jlr.M082891.
  I performed and analysed all immunofluorescence assays of mutant lacking acetyl CoA synthetase

- Soleilhac, Emmanuelle, Loraine Brillet-Guéguen, Véronique Roussel, Renaud Prudent, Bastien Touquet, **Sheena Dass**, Samia Aci-Sèche, et al. 2018. "**Specific Targeting of Plant and Apicomplexa Parasite Tubulin through Differential Screening Using in Silico and Assay-Based Approaches.**" *International Journal of Molecular Sciences*. https://doi.org/10.3390/ijms19103085
  In this study**,**I performed and analyzed SYBR green based drug test for assessing the effect of dinitroanilines compounds on*Plasmodium falciparum.* Dinitroanilines are chemical compounds with high selectivity for plant cell α-tubulin in which they promote microtubule depolymerization

Article

Cell Reports

Division and Adaptation to Host Environment of Apicomplexan Parasites Depend on Apicoplast Lipid Metabolic Plasticity and Host Organelle Remodeling

Graphical Abstract

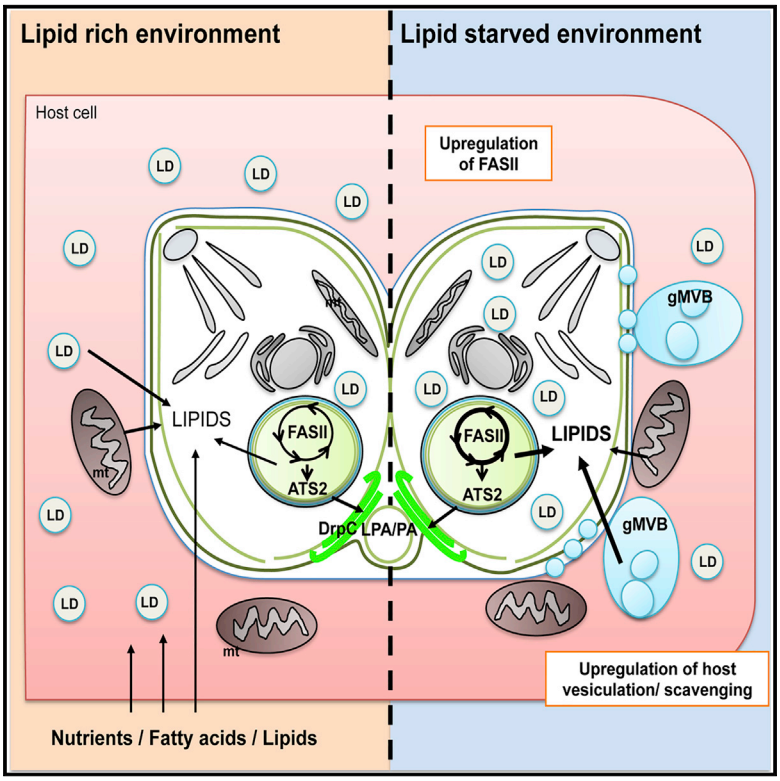

Highlights

- Knockout of apicoplast *Tg*ATS2 disrupts LPA/PA for DrpC recruitment during cytokinesis
- *T. gondii* can sense host environment and adapt to low host nutritional content
- Under lipid starvation, parasite FASII and other lipid metabolic genes become essential
- Upon nutrient deprivation, *T. gondii* induces host organelle remodeling and vesiculation

Authors

Souad Amiar, Nicholas J. Katris, Laurence Berry, ..., Geoffrey I. McFadden, Yoshiki Yamaryo-Botté, Cyrille Y. Botté

Correspondence

yoshiki.yamaryo@gmail.com (Y.Y.-B.), cyrille.botte@univ-grenoble-alpes.fr (C.Y.B.)

In Brief

Apicoplast *de novo* lipid synthesis and lipid host scavenging are both critical for apicomplexan intracellular development. Amiar et al. show that the parasite adapts to the fluctuations of host nutritional content to regulate the metabolic activity of both apicoplast and scavenging pathways and maintain parasite development and division.

Amiar et al., 2020, Cell Reports *30*, 3778–3792
March 17, 2020
https://doi.org/10.1016/j.celrep.2020.02.072

CellPress

OPEN ACCESS
CellPress

Cell Reports
Article

Division and Adaptation to Host Environment of Apicomplexan Parasites Depend on Apicoplast Lipid Metabolic Plasticity and Host Organelle Remodeling

Souad Amiar,[1,5] Nicholas J. Katris,[1,5] Laurence Berry,[2] Sheena Dass,[1] Samuel Duley,[1] Christophe-Sebastien Arnold,[1] Melanie J. Shears,[3] Camille Brunet,[1] Bastien Touquet,[4] Geoffrey I. McFadden,[3] Yoshiki Yamaryo-Botté,[1,6,*] and Cyrille Y. Botté[1,6,7,*]

[1]ApicoLipid Team, Institute for Advanced Biosciences, CNRS UMR5309, Université Grenoble Alpes, INSERM U1209, Grenoble, France
[2]Dynamique des interactions Membranaires normales et pathologiques, UMR5235, Université Montpellier II, Montpellier, France
[3]McFadden Laboratory, School of Biosciences, University of Melbourne, Melbourne, VIC 3010, Australia
[4]Team Cell and Membrane Dynamics of Parasite-Host Interaction, Institute for Advanced Biosciences, INSERM 1209, CNRS UMR5309, Université Grenoble Alpes, Grenoble, France
[5]These authors contributed equally
[6]Senior author
[7]Lead Contact
*Correspondence: yoshiki.yamaryo@gmail.com (Y.Y.-B.), cyrille.botte@univ-grenoble-alpes.fr (C.Y.B.)
https://doi.org/10.1016/j.celrep.2020.02.072

SUMMARY

Apicomplexan parasites are unicellular eukaryotic pathogens that must obtain and combine lipids from both host cell scavenging and *de novo* synthesis to maintain parasite propagation and survival within their human host. Major questions on the role and regulation of each lipid source upon fluctuating host nutritional conditions remain unanswered. Characterization of an apicoplast acyltransferase, *Tg*ATS2, shows that the apicoplast provides (lyso) phosphatidic acid, required for the recruitment of a critical dynamin (*Tg*DrpC) during parasite cytokinesis. Disruption of *Tg*ATS2 also leads parasites to shift metabolic lipid acquisition from *de novo* synthesis toward host scavenging. We show that both lipid scavenging and *de novo* synthesis pathways in wild-type parasites exhibit major metabolic and cellular plasticity upon sensing host lipid-deprived environments through concomitant (1) upregulation of *de novo* fatty acid synthesis capacities in the apicoplast and (2) parasite-driven host remodeling to generate multi-membrane-bound structures from host organelles that are imported toward the parasite.

INTRODUCTION

Apicomplexa are intracellular protozoan parasites that cause serious infectious diseases in humans, including malaria and toxoplasmosis. Most Apicomplexa harbor a relict non-photosynthetic plastid, the apicoplast, acquired by the secondary endosymbiosis of a red alga (Janouskovec et al., 2010). The apicoplast lost photosynthetic capability during the conversion to a parasitic lifestyle (Botté et al., 2013). However, it still contains plant-like pathways, including a prokaryotic type II fatty acid synthesis pathway (FASII) (Waller et al., 1998). The apicoplast is essential for parasite survival in both *T. gondii* and *P. falciparum* (MacRae et al., 2012).

However, the FASII pathway is thought to be essential only during specific life stages. Indeed, in *Plasmodium*, disruption of FASII was demonstrated to be dispensable in asexual blood stages but essential for late liver stage in rodent malaria parasites and for sporozoite schizogony during mosquito stages (Vaughan et al., 2009). Nevertheless, changes in *P. falciparum* blood stage growth conditions, such as lipid starvation during *in vitro* growth and physiological stress in human patients, induced re-activation of apicoplast FASII (Daily et al., 2007; Botté et al., 2013), suggesting plasticity of FASII in response to nutritional environment. In *T. gondii*, FASII is essential during tachyzoite development (Mazumdar et al., 2006).

Apicomplexan parasite membranes are constituted of up to 80% phospholipid (PL), primarily phosphatidylcholine (PC), phosphatidylethanolamine (PE), phosphatidylserine (PS), and phosphatidylinositol (PI; Welti et al., 2007; Gulati et al., 2015). *T. gondii* can readily scavenge PL and triacylglycerols (TAGs) from the host but is also capable of, and dependent on, *de novo* synthesis of several PL classes (Hu et al., 2017; Amiar et al., 2016; Nolan et al., 2017). Like other eukaryotes, apicomplexan *de novo* PL synthesis is initiated by the assembly of fatty acid (FA) (i.e., esterification onto a glycerol-phosphate backbone) into specific PL precursors. In *T. gondii*, FAs to be used for PLs synthesis derive from three sources: (1) apicoplast FASII generating short FA chains (C12:0, C14:0, and C16:0) (Ramakrishnan et al., 2012), (2) FA elongases located on the parasite endoplasmic reticulum (ER) generating C16:1, C18:1, C20:1, C22:1, and C26:1 (Dubois et al., 2018), and (3) FAs directly scavenged from the host cell (Bisanz et al., 2006). Lipidomics reveals that most *T. gondii* PLs are hybrid/patchwork molecules, comprising one FA moiety from the apicoplast *de novo* synthesis pathway and a second one scavenged from the host (Amiar et al., 2016). Thus, both scavenging and *de novo* synthesis of FA are critical for intracellular development.

Typically, phosphatidic acid (PA) is the central precursor for the *de novo* synthesis of all PL classes by the two-step esterification of FAs onto a glycerol-3-phosphate backbone; first by glycerol-3-phosphate acyltransferases (GPATs) to form lysophosphatidic acid (LPA) and then by acyl-glycerol-3-phosphate acyltransferases (AGPATs) to convert LPA to PA. In eukaryotic cells, GPATs and AGPATs of diverse origins work as a set at several locations within the cell. Apicomplexans have two sets of acyltransferases: one plastid-like set putatively in the apicoplast (prokaryotic pathway) (Amiar et al., 2016) and another pair predicted to be in the ER (the so-called eukaryotic pathway). In *T. gondii*, the apicoplast GPAT, *Tg*ATS1 is essential for tachyzoite development, where it generates LPA from apicoplast-FA for the bulk synthesis of PL (Amiar et al., 2016). The role of parasite AGPATs for lipid synthesis is yet to be determined. Beyond their roles as lipid precursors, PA (and LPA) also have important biophysical properties by controlling the formation of positive or negative membrane curvatures, and thereby influence the recruitment of proteins involved in membrane fusion/fission events such as endocytosis in other eukaryotic models (Schmidt et al., 1999; Kooijman et al., 2005; Brown et al., 2008).

Here we characterize *T. gondii* AGPATs, focusing on one localized to the apicoplast, *Tg*ATS2. We confirm that *Tg*ATS2 is an acyltransferase by heterologous complemention of a bacterial mutant. We then generate a knockout (KO) mutant, which was defective parasite cytokinesis and normal lipid profile. Particularly, the impact of LPA/PA changes on the localization of a dynamin-related protein (Drp), *Tg*DrpC, in the *Tg*ATS2 mutant is described and provides a rationale for cytokinesis defects associated with drug inhibition of apicoplast FASII (Martins-Duarte et al., 2015). Finally, changes in parasite lipid composition and lipid fluxes led us to subject parasites to lipid starvation to explore how host nutritional environment affects parasite growth. Analysis of lipid fluxes and growth screening under adverse lipid conditions show that parasites can sense the environment and respond by (1) upregulation of *de novo* lipid synthesis in the apicoplast and (2) manipulation of the human host through vesiculation from host organelles and import of such material to the parasitophorous vacuole (PVM) mediated by export of parasite effectors to improve their lipid scavenging. Our analysis provides unprecedented mechanistic insights into parasite metabolic adaption under host nutritional challenge, which was poorly understood until now.

RESULTS

Deletion of *Toxoplasma gondii* Apicoplast Acyltransferase *Tg*ATS2 Results in Aberrant Cytokinesis and Residual Body Formation during Replication

To explore *de novo* PA synthesis in *T. gondii*, we searched the genome for AGPATs capable of catalyzing the esterification of an activated FA (i.e., acyl-CoA or acyl-ACP) onto LPA to make PA. We found two AGPAT candidates with conserved motifs: ToxoDB: TGME49_297640 and ToxoDB: TGME49_240860. Phylogenetic analyses reveal that TGME49_297640 clusters with the prokaryotic clade of the pathway with plant and algal sequences and that TGME49_240860 clusters with the eukaryotic clade of the pathway (Figure S1). We termed these enzymes *Tg*ATS2 and *Tg*AGPAT on the basis of the plant and eukaryotic terminology, respectively. We generated parasite lines expressing *Tg*ATS2 and *Tg*AGPAT endogenously tagged at the C terminus with a triple HA tag, under control of their respective promoters (Figures S2A–S2C). Immunofluorescence assays (IFAs) confirmed *Tg*ATS2 targets to the apicoplast (Figure 1A), and transient expression of *Tg*AGPAT-HA showed a perinuclear structure corresponding to the parasite ER (Figure 1B).

To test if *Tg*ATS2 and *Tg*AGPAT are functional AGPAT, we complemented an *E. coli* temperature-sensitive mutant SM2-1 Δ*plsC* lacking AGPAT activity (Coleman, 1990) with recombinant *TgATS2* and *TgAGPAT*. All transformants grew at the permissive temperature of 30°C (Figure 1C). Only those complemented with bacterial *Ec*PlsC and *Tg*ATS2 grew at the non-permissive 42°C (Figure 1C). Constructs with *TgAGPAT* including or not its long N-Ter extension did not grow at 42°C, likely because of *TgAGPAT* eukaryotic origin (Figure S1). Indeed, eukaryotic AGPATs favor acyl-CoA substrates over acyl-ACP substrates used in bacterial and plastid systems. Thus, it is unclear if *Tg*AGPAT has acyltransferase activity, but *Tg*ATS2 complements defective *E. coli* SM2-1 AGPAT enzymatic activity *in vivo*, confirming LPA-to-PA synthetic capability.

To investigate the importance of apicoplast *Tg*ATS2 during tachyzoite life stages, the *TgATS2* locus was disrupted to generate knock-in (KI) and KO mutants of *Tg*ATS2 using CRISPR-Cas9 strategies (Figures S2D–S2F). Loss of the protein product was confirmed by western blot (Figures 1D and 1E), IFA (Figure 1F), and PCR (Figures S2E and S2F). Both Δ*Tg*ATS2 mutants were viable, but plaque and replication assays revealed that Δ*Tg*ATS2 had a mild yet significant growth defect with significantly more small (two to four parasites) vacuoles and significantly fewer large vacuoles (Figures 1G–1I).

Parasite egress was significantly affected in the Δ*Tg*ATS2 mutant (Figure S2G), but invasion ability showed no difference with the parental line, nor was there a defect in microneme secretion (Figures S2H and S2I). Morphology of different intracellular tachyzoite organelles showed no obvious defects except the apicoplast displaying a mild biogenesis defect (Figures S2J and S2K).

Upon closer inspection of parasite morphology, Δ*Tg*ATS2 parasites appeared fused to each other at their basal poles (Figure 2A), suggesting a cytokinesis defect, which provided a rationale for the egress defect (Figure S2G). Cytokinesis was monitored by localizing MORN1, which curiously displayed no obvious basal mis-localization (Figure 2B). However, Δ*Tg*ATS2 parasites showed important enlargement of the residual body (Figure 2C). Residual body size was quantified by IFA using GAP45 antibody as a marker for the inner membrane complex (IMC). Δ*Tg*ATS2 parasites displayed a significantly larger residual body at the center of big vacuoles (more than four parasites), (Figures 2B and 2C). Accordingly, egressed extracellular parasites often remained tethered at their basal pole via a plasma membrane (PM) structure (Figure 2D). Electron microscopy (EM) of Δ*Tg*ATS2 parasites supported the segregation defects seen by IFA (Figure 2E). In dividing parasites, it is commonly seen that the PM is kept connected between two recently divided cells so that the cells are stuck together and distributed

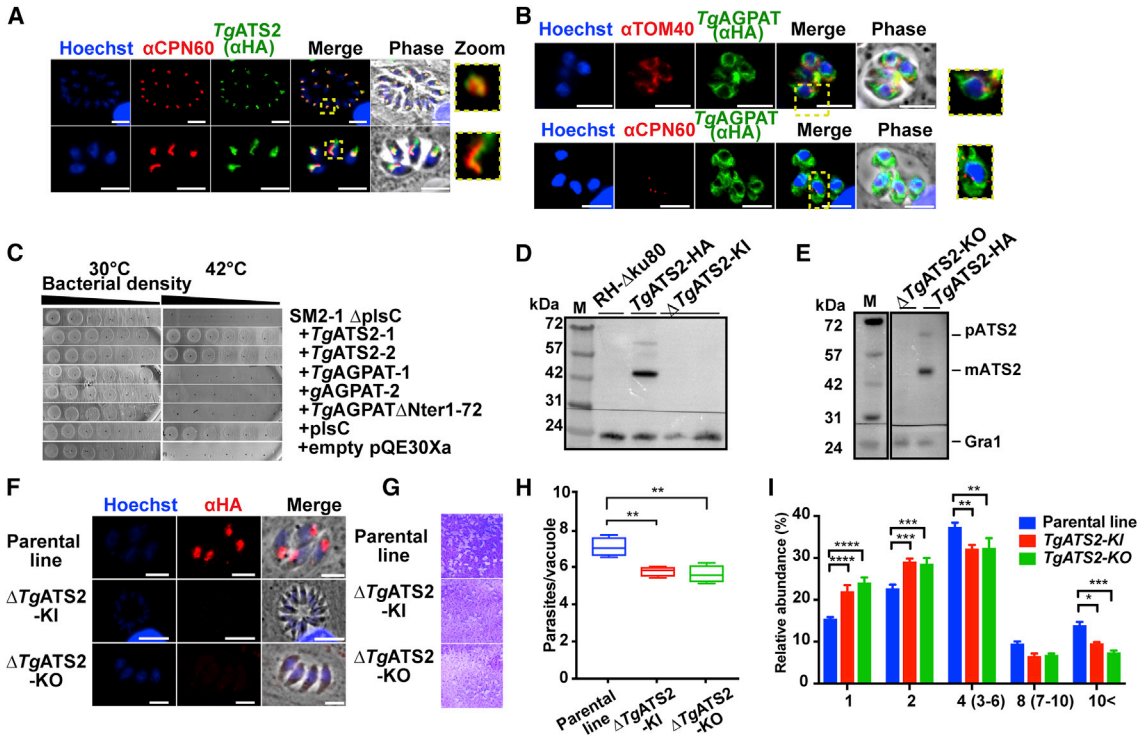

Figure 1. *Tg*ATS2 Is an Apicoplast Lysophosphatidic Acid Acyltransferase Important for Parasite Proliferation

(A and B) IFA of stable *Tg*ATS2-HA expressing parasites (A) and transient *Tg*AGPAT-HA expression (B). CPN60, apicoplast marker; TOM40, mitochondrial marker. Scale bars, 2 μm.

(C) Expression of *Tg*ATS2 and *Tg*AGPAT in LPAAT-deficient *E. coli* strain SM2-1. SM2-1Δ*plsC E. coli* mutant transformed with *Tg*ATS2 (1, 2), *Tg*AGPAT (1, 2), $TgAGPAT_{\Delta Nter1\text{-}72}$, *Ec*plsC, or empty pQE30Xa expression vector were grown at 30°C (permissive) or 42°C (non-permissive) for 20 h (n = 3).

(D and E) Confirmation of *Tg*ATS2-HA loss by western blot analysis in *Tg*ATS2-KI (D) and *Tg*ATS2-KO (E) using anti-HA (anti-Gra1, loading control).

(F) Confirmation of *Tg*ATS2-HA signal loss in Δ*Tg*ATS2 by IFA using anti-HA. Scale bars, 2 μm.

(G) Plaque assay showing a mild growth defect in Δ*Tg*ATS2 mutants.

(H) Cell-based growth fitness assay confirmed the growth defect in the Δ*Tg*ATS2 mutants 30 h post-infection (n = 3).

(I) Proliferation assay confirmed a replication defect in Δ*Tg*ATS2 mutants (n = 3).

*p ≤ 0.05, **p ≤ 0.01, ***p ≤ 0.001, and ****p ≤ 0.0001.

to daughter cells during cytokinesis. Very little is known on the molecular mechanisms of PM segregation during cytokinesis. In the parental parasites, initial steps of endodyogeny showed the formation of the daughter cell apical pole along with organelle division before the formation of the daughter cells within the mother cell (Figure 2E). Emergence of the daughter cells initiates the apical-to-basal biogenesis of their PM, partly recycled from the mother (Figures 2E1–2E5), and ends by a constriction of both IMC and PM at the basal poles, leaving a small basal residual body (Figure 2E6). In contrast, there were many division and cytokinesis defects in Δ*Tg*ATS2, which were unable to separate, although a new round of daughter formation could be initiated (Figure 2E1). Furthermore, parasite organelles were frequently found in the residual body as if ejected from improper segregation, likely contributing to the enlarged residual body phenotype (Figure 2E). Affected vacuoles thus displayed enlarged residual bodies that often contained various organelles—including the nucleus, mitochondrion, acidocalcisome vesicles, and other cytosolic material—that appeared to be ejected from the dividing cells because of improper segregation (Figures 2E3 and 2E4). Pieces of mitochondria were a particular feature within enlarged residual bodies (Figures 2E5 and 2E6).

We attempted to disrupt *TgAGPAT* using CRISPR-Cas9 as per Δ*Tg*ATS2 in wild-type (WT) (Δ*Tg*AGPAT) and Δ*TgATS2* (Δ*Tg*AGPAT-Δ*Tg*ATS2) genetic backgrounds, but parasites were not viable (Figures S2L–S2O), suggesting that *Tg*AGPAT is indispensable, consistent with its phenotype score (Sidik et al., 2016).

*Tg*ATS2 Disruption Reduces C14:0 FA Incorporation into *T. gondii* Lipids, Skews the LPA/PA Ratio, and Alters PL Abundance and Composition

To investigate the role of *Tg*ATS2 in lipid metabolism, we performed lipidomic analysis on the Δ*Tg*ATS2 mutant. Disruption of *Tg*ATS2 resulted in a large significant reduction of the relative amount of C14:0, the main product of the apicoplast FASII (Figures 3A and 3B). Significant decreases in C18:1 and C20:1 were also observed (Figures 3A and 3B). In contrast, there were significant increases in the abundance of C18:0, C22:1, C24:1, C20:4, C20:5, and C22:6 (Figures 3A–3C), most of which can be

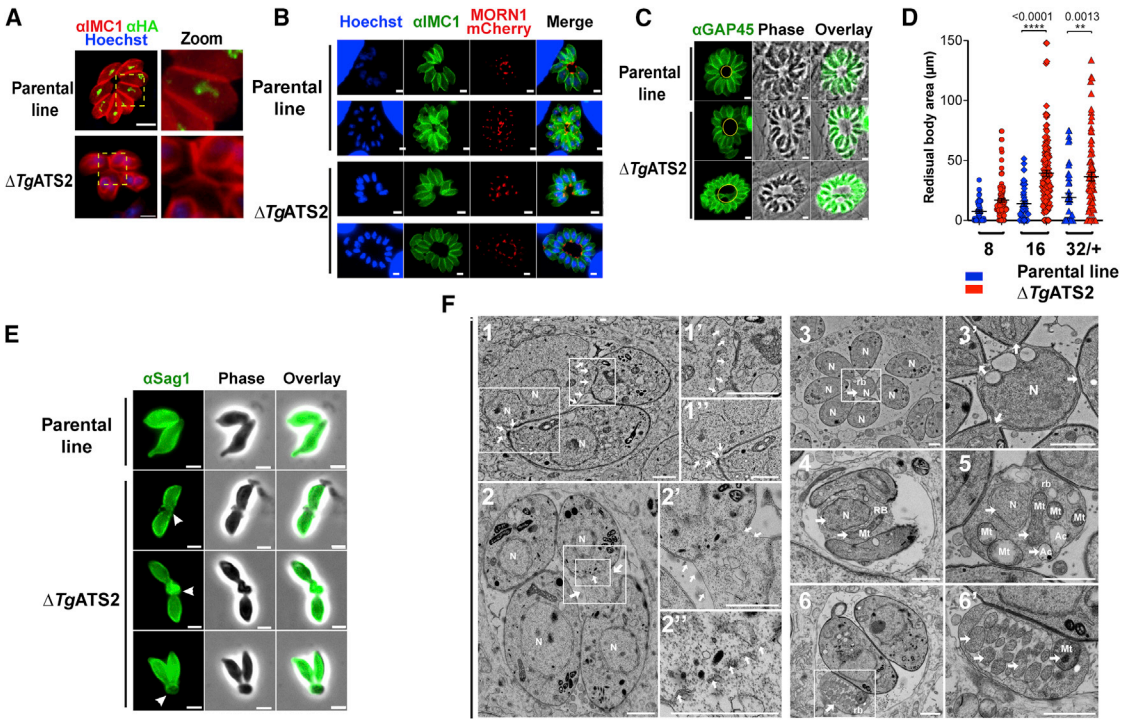

Figure 2. Disruption of *Tg*ATS2 Induces Parasite Cytokinetic Defect, Residual Body Enlargement, and Organelle Segregation Deficiency

(A) IFA of Δ*Tg*ATS2-HA and parental line using anti-HA and anti-IMC1 shows that Δ*Tg*ATS2-HA has a cytokinetic defect phenotype (scale bars, 2 μm).

(B) IFA of Δ*Tg*ATS2 and parental line transiently expressing MORN1-mCherry (IMC basal tip) and anti-IMC1 (scale bars, 2 μm).

(C and D) Confirmation of enlarged residual bodies in Δ*Tg*ATS2 by IFA using anti-GAP45 (IMC marker) (C) and by statistical analysis of residual body size (D). Scale bars, 2 μm.

(E) IFA observation of extracellular parasites using anti-SAG1 reveals egressed parasites tethered at their basal ends (white arrowhead, PM tether). Scale bars, 2 μm.

(F) Electron microscopic image of Δ*Tg*ATS2 mutants reveals important cytokinesis defects: major enlargement of the PM, defects in mother cell membrane constriction and cell daughter attachment at the basal pole (F1 and F2; enlarged in F1′, F1′′, and F2′, white arrows), and IMC fragmentation at the separation sites between dividing parasites (F2′′). Residual bodies containing unevenly separated nuclei (F1, F3, F3′, F4, and F5), mitochondria (F4, F5, F6, and F6′), and acidocalcisomes (F5). N, nucleus; Mt, mitochondria; rb, residual body; Ac, acidocalcisome. Scale bars, 1 μm.

scavenged from the host, such as C20:4 and C20:5 (Welti et al., 2007; Ramakrishnan et al., 2012; Amiar et al., 2016; Figures S3A and S3B). Comparison of the relative FA abundance between Δ*Tg*ATS2 and its parental line showed significant decreases of C14:0, C20:0, C20:1, and C22:2 (Figure 3C). These results indicate that in addition to the aforementioned cytokinesis defect, Δ*Tg*ATS2 has a highly modified lipid content that relies more on long-chain FAs scavenged from the host (Figures 3A–3C).

To further investigate Δ*Tg*ATS2 lipid defects, we analyzed and quantified each PL class and its individual FA content. The Δ*Tg*ATS2 mutant accumulates significantly more LPA compared with the control parental line and significantly less PA (Figures 3D and 3E), consistent given that LPA and PA are the likely substrate and product, respectively, of ATS2 (Figure 1C). The slight reduction in PA suggests that *Tg*ATS2 is not responsible for the bulk PA synthesis but rather for a specialist function. Importantly, the LPA/PA ratio was significantly affected in Δ*Tg*ATS2 (Figure 3E). We investigated diacylglycerol (DAG) and other related PLs, namely PC, PE, PI, PS, phosphatidylglycerol (PG) and cardiolipin (CL; Figure 3D). The relative abundance of both DAG and PG significantly decreased in Δ*Tg*ATS2 (Figure 3D). This is relevant because DAG can be a direct product of PA, and PG is the sole PL made from PA in plant chloroplasts (Ohlrogge and Browse, 1995). In contrast, the relative abundance of PS, PI, and PE increased in the mutant (Figure 3D).

We then examined the FA profiles of each of these lipid classes. LPA had significant increases in the amounts of C16:0 and C18:0 in Δ*Tg*ATS2 parasites, whereas significant decreases in the apicoplast-specific FAs C12:0 and C14:0 were measured in the mutant (Figure 3F). No major difference was observed in PA composition in Δ*Tg*ATS2 parasites (Figure 3G). Strikingly, though, DAG, PC, PI, and PE all had significantly reduced C14:0 content (Figures 3D and S3C–S3H), which is the main product of FASII and is used by *Tg*ATS1 for bulk *de novo* synthesis of PC, PI, and PE (Amiar et al., 2016). This indicates that *Tg*ATS2 likely uses apicoplast-generated C14:0 as its major substrate to make these lipids. In contrast, the levels of two long polyunsaturated FAs (PUFAs), C20:4 and C20:5, in all three major PLs (PC, PI, and PE) were significantly increased in Δ*Tg*ATS2 (Figures S3C–S3H), which is again consistent with mutant parasites compensating for the lack of *de novo*-made FAs by increasing scavenging long-chain FAs from the host. The FA composition of fetal bovine serum (FBS) and HFF host cells (Figures S3C–S3H) confirmed that C20:4 and C20:5 PUFAs were

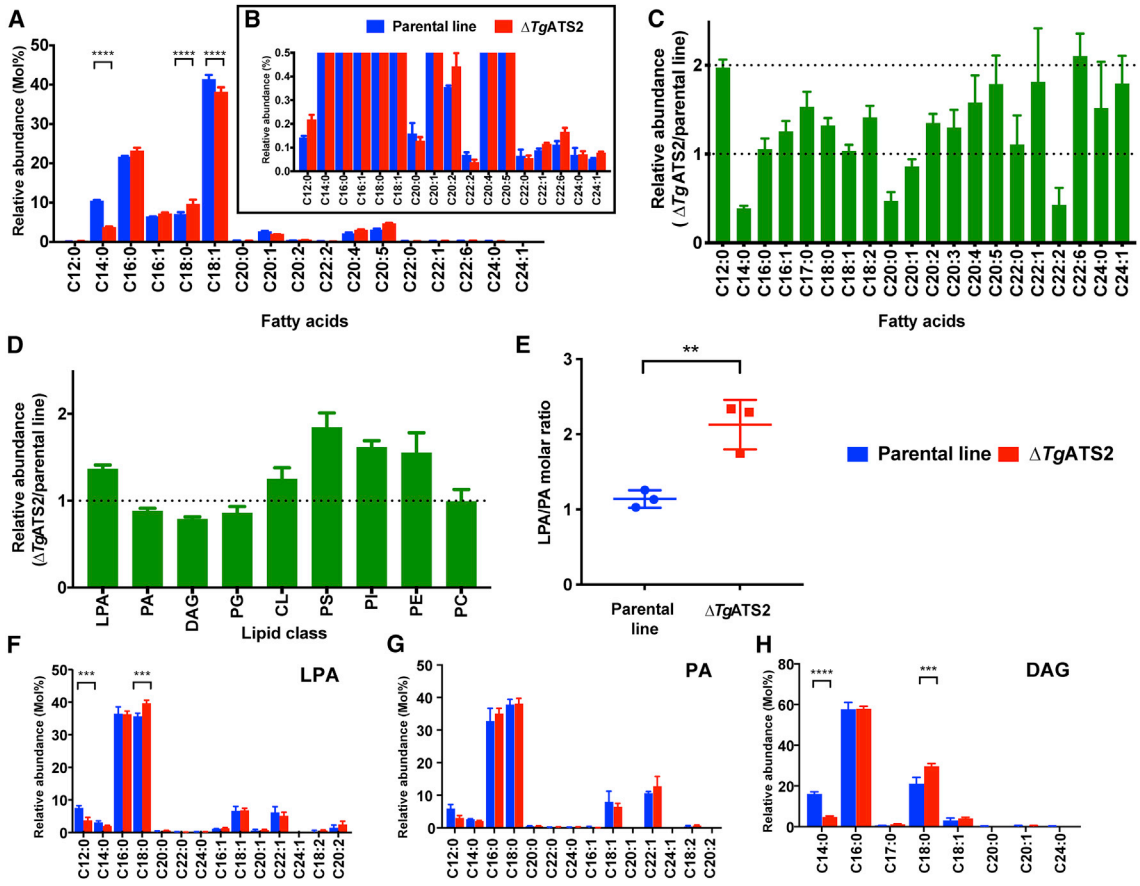

Figure 3. Lipidomic Analysis of Δ*Tg*ATS2 Mutant

(A) Fatty acid composition of total lipid extracted 72 h post-infection.

(B) is enlargement of A.

(C) Relative fatty acid abundance of Δ*Tg*ATS2 to the parental line.

(D) Relative major phospholipid abundance of Δ*Tg*ATS2 to parental line.

(E) LPA/PA ratio.

(F–H) Individual molecular species of LPA (F), PA (G), and DAG (H). Fatty acids are shown as Cx:y, where x is the number of carbons and y is the number of unsaturations.

n = 4; *p ≤ 0.05, **p ≤ 0.01, ***p ≤ 0.001, and ****p ≤ 0.0001.

present from the host environment. This is consistent with the Δ*Tg*ATS2 mutants' increasing scavenging of these PUFAs to make PC, PI, and PE. We complemented Δ*Tg*ATS2 and WT parasites (Figure S3I) using exogenous PA(14:0;14:0), the putative product of *Tg*ATS2, and PA(16:0;18:1) as host-derived PAs. Proliferation assays showed that both exogenous PA sources could significantly boost parasite growth (Figures S3I and S3J) but could not rescue Δ*Tg*ATS2 growth phenotype. This indicates that the PA source needs to be made *de novo* via *Tg*ATS2 for proper division. Because parasites are capable of scavenging lipids from the host and medium, we determined whether the Δ*Tg*ATS2 imported more PA, using PC as a control. Δ*Tg*ATS2 imported significantly more PA and PC than the parental control line (Figure S3K). Together these data on extracellular Δ*Tg*ATS2 corroborate our lipidomic analyses (Figure 3), indicating that the mutant scavenges more lipids to compensate for reduced *de novo* synthesis.

Disruption of *Tg*ATS2 Induces a Mis-localization of the Parasite DrpC Perturbing Parasite Cytokinesis, IMC Formation, and PM Stability

Lipidomic analyses revealed a drastic LPA/PA imbalance in the Δ*Tg*ATS2 mutant (Figure 3E). LPA and PA have important structural influences on membrane architecture and endocytosis by inducing local membrane curvatures, which can affect the recruitment and functions of specific dynamins at precise membrane domains for organelle/vesicle fission (Adachi et al., 2016; Schmidt et al., 1999; Gras et al., 2019). For example, synaptic vesicle transport between neurons requires a protein complex composed of a dynamin and an endophilin that exert acyltransferase activity to create the proper membrane groove where the dynamin can pinch and release the synaptic vesicle, or in human mitochondrial fission by the protein Dynamin-like 1, *Hs*Drp1, which requires insertion, recruitment, and regulation through PA. In *T. gondii*, there are three known dynamin-related

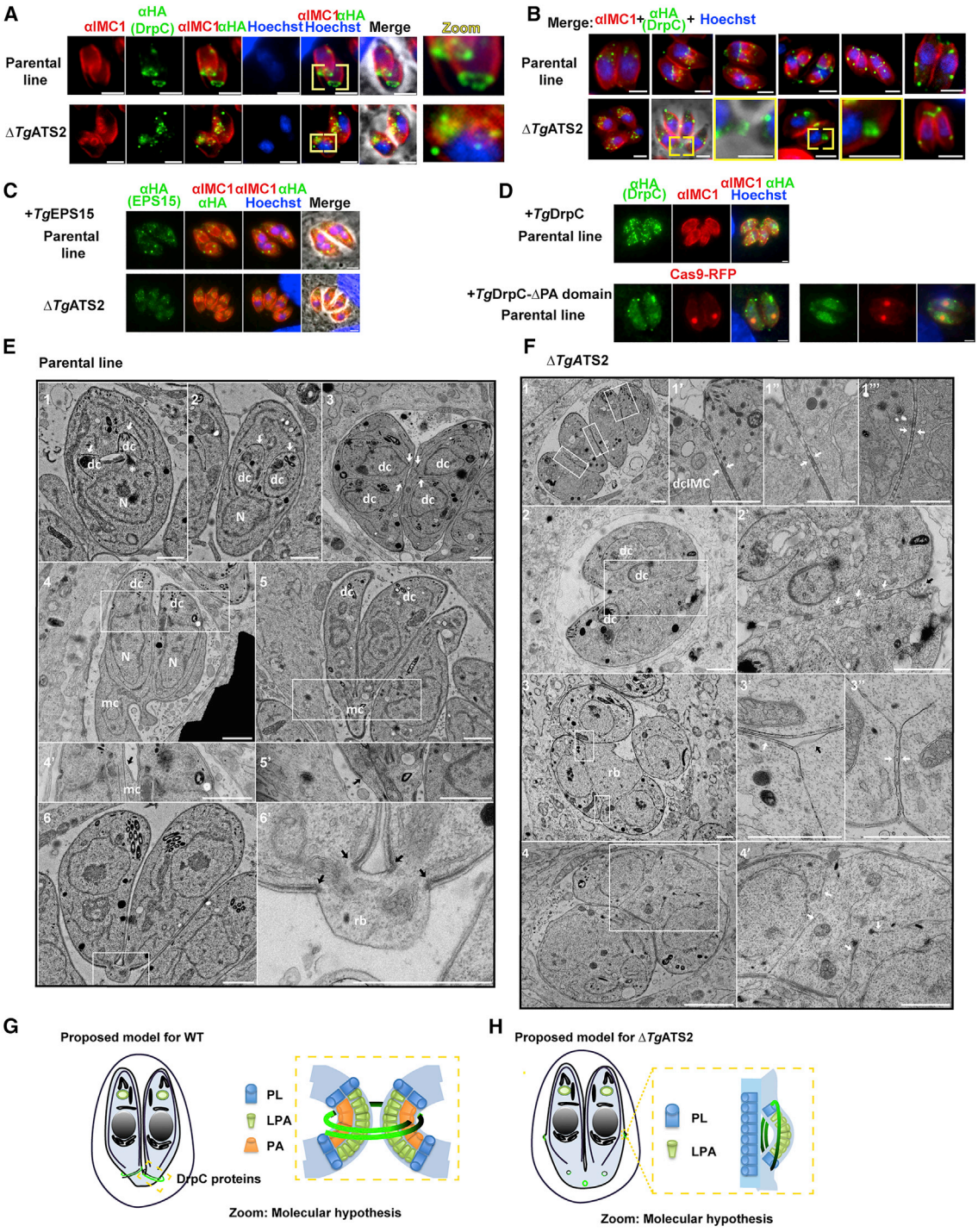

Figure 4. Δ*Tg*ATS2 Induces the Specific Mis-localization of *Tg*DrpC, a Dynamin-Related Protein Involved in Endodyogeny, Leading to Cytokinetic Defects during Tachyzoite Division

(A) IFA localization of *Tg*DrpC-HA expressed in parental line shows ring structures at the growing ends of daughter cells during division (top panel) but fails to do so when expressed in Δ*Tg*ATS2 (bottom panel). Scale bars, 2 μm.

(B) *Tg*DrpC-HA localization during tachyzoite division cycle in the parental line (top panel) and its mis-localization in Δ*Tg*ATS2 mutant. Scale bars, 2 μm.

(C) IFA localization of TgESP15, a known interactor of TgDrpC, in Δ*Tg*ATS2 and parental line using anti-HA and anti-IMC1. Scale bars, 2 μm.

(D) IFA localization of *Tg*DrpC and *Tg*DrpC-ΔPA domain-Cas9-RFP using anti-HA and anti-IMC1 (scale bars, 2 μm) reveals the mis-localization of TgDrpCΔPA domain during endodyogeny.

(legend continued on next page)

proteins (Drps): *Tg*DrpA, *Tg*DrpB, and *Tg*DrpC. *Tg*DrpA and *Tg*DrpB have roles in apicoplast fission and secretory organelle biogenesis, respectively (van Dooren et al., 2009; Breinich et al., 2009). *Tg*DrpC was recently localized to the basal poles of dividing daughter cells (Heredero-Bermejo et al., 2019). We generated a parasite line expressing *Tg*DrpC fused to a 3xHA tag under the control of its endogenous promoter using CRISPR-Cas9 (Figures S4A and S4B) and localized *Tg*DrpC-HA during the tachyzoite intracellular division cycle in Δ*Tg*ATS2 and its parental line (Figure 4A). In parental-line parasites, *Tg*DrpC-HA clustered in small punctate-like compartments in the apical post-Golgi area during interphase (Figure 4A). During daughter budding, *Tg*DrpC re-localized to form two distinct ring-like structures coinciding with the growing ends of the IMC from the budding daughter cells, which constricted at the base of the mother cell during cytokinesis and eventually formed basal caps on the each newly divided parasite (Figures 4A and 4B).

In Δ*Tg*ATS2, localization of *Tg*DrpC-HA was only mildly affected during interphase but was drastically affected during division (Figures 4A and 4B). Indeed, *Tg*DrpC-HA frequently failed to form the typical ring structures at daughter cells (Figures 4A and 4B). Instead, DrpC-HA was scattered in the cytosol, or formed rings pushing on the side of mother IMC, or improperly constricted at the daughter basal pole (Figures 4A and 4B). This contrasted with the normal localization of MORN1, which appears to be a more cytoskeletal component, as its localization remains unaffected during endodyogeny (Figure 2B). We further examined other known interactors of DrpC and thus localized the dynamin-like protein EPS15 (Heredero-Bermejo et al., 2019) by C-terminally tagging by CRISPR-Cas9 (Figures 4C and 4D). In parental strains, EPS15-HA localized to clear punctate dots during interphase similarly to DrpC. During endodyogeny, EPS15 remained as punctate dots and did not re-localize to the daughter rings like DrpC (Figure 4C). In Δ*Tg*ATS2 background, EPS15 was unaffected during interphase though more scattered than in the parental line. However, during endodyogeny, EPS15-HA mis-localized in the cytosol of the parasite when expressed in the Δ*Tg*ATS2 background (Figure 4C), consistent with its role as a DrpC interactor (Heredero-Bermejo et al., 2019).

In silico sequence alignment showed that (1) *Tg*DrpC is the closest *Tg*Drp homolog to the *Hs*Drp1, which allows mitochondrial fission through its interaction with PA via its Stalk domain including a loop with specific hydrophobic residues (Adachi et al., 2016, 2018), and (2) the Stalk domain and the PA binding loop seem conserved in *Tg*DrC (3) but are absent in *Tg*DrpA and *Tg*DrpB (Figures S4C–S4E). To confirm this, we tagged and monitored the localization of other *Tg*Drps in the Δ*Tg*ATS2 background. No obvious change in localization of *Tg*Drp*A* was observed in Δ*Tg*ATS2 parasites, even during the fission of the apicoplast (Figure S4B).

On the basis of homology with *Hs*Drp1, we disrupted the putative PA-binding region of *Tg*DrpC. We expressed this *Tg*DrpC-ΔPA version of the protein in the parasite to test the importance of the putative PA-binding domain for the localization of *Tg*DrpC. To do so, we transfected a WT *Tg*DrpC-HA cell line with a Cas9-RFP and a PCR product targeting the DrpC PA domain. IFAs on parasites with no Cas9-RFP had typical DrpC-HA localization (Figure 4D). However, parasites with positive Cas9-RFP expression showed that DrpC was mis-localized and scattered throughout the cytosol in a similar manner as in *TgΔATS2* parasites. These results are also consistent with the cytosolic mis-localization of truncated *Tg*DrpC, excluding the putative PA-binding domain recently reported (Melatti et al., 2019).

Further detailed evidence of improper cytokinesis could be observed under EM. In the parental line, initial steps of endodyogeny showed the formation of the daughter cell apical pole along with organelle division before the formation of the daughter cells within the mother cell (Figure 4E). Emergence of the daughter cells initiates the apical-to-basal biogenesis of their PM, partly recycled from the mother (Figures 4E1–4E5), and ends by a constriction of both IMC and PM at the basal poles, leaving a small basal residual body (Figure 3F6). IMC biogenesis and aberrant endocytosis can be seen in *TgΔATS2* cells upon closer inspection under EM. In contrast Δ*Tg*ATS2 were unable to separate, although a new round of daughter formation could be initiated (Figure 4F1). Daughter cells were found tightly apposed at normal emergence sites, and their PMs were often missing between daughter IMCs. Instead, interconnection of PM, vesicles, or cisternae could be observed at these apposition sites and at the basal end of dividing cells (Figures 4F1 and 4F2). Mother cells were frequently observed to be fused to each other, with vesicle fusion frequently occurring between the two at the site of the PM (Figure 4F2). These defects suggested issues at the PM composition and/or problems in membrane fusion/fission sites. Furthermore, there was no constriction of both IMC and PM from daughter cells, resulting in enlarged residual bodies containing organelles and cytosol portions (Figures 4F3 and 4F4). In particular, these membrane invaginations were frequently seen at the junction between two parasites in a process resembling endocytosis.

(E and F) Electron microscopic observation of endodyogenic division in parental line (E) and ΔTgATS2 (F). (E1–E3) Endodyogeny starts with the formation of daughter cells (dc) by growth of IMC (white arrows) and organelle segregation. IMC scaffolding then grows toward the basal pole (white arrows) encompassing divided organelles (e.g., nucleus N). (E4–E5′) Recycling and biogenesis of PM (black arrow) ends daughter cell emergence from mother cell (mc). (E6 and E6′) Division ends by cytokinesis through constriction of both IMC and PM at basal pole (black arrows) to form a small residual body (rb). (F) Δ*Tg*ATS2 shows an incomplete separation of daughter cells during cytokinesis with absence of PM biogenesis between closely apposed IMC (F1 and F3 and insets, white arrows), presence of vesicle/cisternae inside membrane structures at the inter-IMC space (F2′, white arrows), absence of mother IMC (F3′, black arrow), absence of basal constriction forming large residual bodies leaving floating daughter IMC (F3, F4, and 4′, white arrows). Scale bar, 1 μm.

(G and H) Proposed molecular model for *Tg*DrpC function during endodyogeny and cytokinesis in WT parasite (G) and Δ*Tg*ATS2 (H). LPA and PA molecules induce positive and negative curvature, creating grooves in membranes for *Tg*DrpC to insert at specific sites during division for a pinching function during endodyogeny (G).

Nutrient Starvation Enhances the Synthesis of FA by Apicoplast FASII in *T. gondii* and Blocks Intracellular Proliferation of *P. falciparum* Blood Stages Lacking a Functional FASII

Because *Tg*ATS2 has a role in maintaining parasite lipid homeostasis, we set out to determine the balance of *de novo* synthesized versus scavenged lipids in Δ*Tg*ATS2 using a stable isotope precursor of apicoplast synthesized FAs, U-^{13}C-glucose. (Ramakrishnan et al., 2012; Amiar et al., 2016; Dubois et al., 2018). Incorporation of ^{13}C within FA is detected by increase of mass and determined in relation to non-labeled FA. Distribution of ^{13}C incorporation to each FA isotopologue is shown as its own mass (M) plus number of ^{13}C carbon incorporation (i.e., M + x). In both parental and Δ*Tg*ATS2 mutant lines, we observed significant differences of ^{13}C incorporation in C14:0, C16:1, C18:0, and C18:1 (Figure 5A). Isotopologue distribution of apicoplast-signature C14:0 showed that Δ*Tg*ATS2 had ^{13}C incorporation up to M + 14, but major incorporation occurred at lower masses (M + 8, M + 10) than the parental (M + 12, M + 14; Figure 5B). This indicates that FASII is active in Δ*Tg*ATS2 but slowed down in the process of making C14:0, thus explaining the C14:0 reduction previously detected (Figure 3A). Similar significant results were observed for C16:0 isotopologue distribution, although overall incorporation was similar between parental and Δ*Tg*ATS2 (Figure 5C). C18:0 in Δ*Tg*ATS2 had higher ^{13}C incorporation than the parental, and its isotopologue distribution showed more short FA from the apicoplast (Figure 5D).

Lipidomic analyses thus indicate that both scavenged and *de novo* lipid fluxes are modified in Δ*Tg*ATS2. To tease out the impact of host nutritional environment on both pathways, we sought to measure parasite lipid fluxes under adverse host nutritional/lipid conditions, through limitations in FBS concentrations in parasite culture media. Interestingly, gas chromatography-mass spectrometry (GC-MS) analysis revealed that ^{13}C incorporation into all FASII-generated and further ER-elongated FA products (i.e., C14:0, C16:0, C16:1, C18:0, C18:1, and C20:1) was significantly higher by 5%–15% under FBS starvation in the parental line (Figures 5E, 5F, and S5A). In addition, ^{13}C incorporation into most FAs is increased in the WT parental line (Figure 5F). These results suggest that apicoplast *de novo* FA/lipid synthesis can be upregulated during FBS starvation to compensate for the lack of nutrients in the external environment. However, in Δ*Tg*ATS2, the ^{13}C incorporation into each FA was decreased by FBS starvation (Figure 5F). No morphological changes could be observed by IFA in the FBS-starved WT or Δ*Tg*ATS2 mutant (Figure S5B). Both parental line and Δ*Tg*ATS2 mutant showed a significant reduction in the synthesis of C18:0 in FBS-starved conditions, suggesting that C18:0 is obtained predominantly by scavenging from the host cell (Figure 5F). Because the availability of lipids from the environment is limited, the FA abundance in the parental line was decreased (Figure 5G). Interestingly however, the FA abundance in Δ*Tg*ATS2 was increased in most of its FA species during FBS starvation (Figure 5G).

Although we observed a defect in the activation of FASII in Δ*Tg*ATS2, FASII was nevertheless viable during FBS starvation. This suggests that if FASII is active, regardless of the level of FASII activity, the parasites are viable under FBS starvation, consistent with its essential role in tachyzoites. However, in *P. falciparum*, FASII is not essential during nutrient-replete blood stage but is activated under lipid starvation, apparently to compensate for reduced availability of scavenge-able lipids (Yu et al., 2008; Botté et al., 2013). Our results in *T. gondii* led us to re-think the current hypothesis regarding the dispensability of the apicoplast FASII in *P. falciparum* blood stages and to test the essentiality of malaria parasite apicoplast FASII under nutrient/lipid-starved conditions. We grew *P. falciparum* FASII KO, Δ*Pf*FabI (Yu et al., 2008), and its parental line (NF54) in either regular (i.e., lipid-rich) culture medium or in "lipid-starved" minimal medium (Mi-Ichi et al., 2007; Botté et al., 2013). Both NF54 and Δ*Pf*FabI grew normally in the regular culture medium (Figure 5H). In the lipid-starved medium, NF54 was viable but grew significantly slower than in lipid-replete conditions, as previously reported (Shears et al., 2017). However, Δ*Pf*FabI grew only for the first 2 days in lipid-starved media, but after 4 days, a sharp decrease in growth occurred, and this led to a complete loss of detectable parasites after 8 days and showed no sign of further recovery in the next monitored cycles (Figure 5H). This shows that FASII is required for the malaria parasite blood stages to adapt its lipid metabolism in response to an adverse host lipid environment, a similar situation to that revealed here for *T. gondii*.

Because environmental FBS starvation induces an increase of *de novo* lipid synthesis, we investigated the effect the lipid-nutrient-depleted conditions (i.e., 0%, 1%, and 10% of FBS) on various mutants involved in lipid metabolism in *T. gondii*. We assessed parasite growth by plaque assay and quantified plaque area. The WT and parental parasite lines could grow equally well in DMEM supplemented with 0%, 1%, or 10% FBS (Figures 5I–5R and S5C), without affecting the integrity of HFF host cells. FBS starvation reduced growth of Δ*Tg*ATS2 under 0% FBS (Figure 5I). *Tg*ATS1-depleted cells grew sharply less in the regular culture conditions (i.e., 1% FBS), but starvation under 0% FBS led to the quasi-absence of plaques, whereas an increase to 10% FBS partially rescued the growth defect seen in 1% FBS (Figure 5J). This suggested that in the absence of the major *de novo* PL precursor synthesis pathway, the parasite could partially compensate the growth defect by accessing more host lipid resources. The acetyl-CoA synthetase *Tg*ACS (Dubois et al., 2018) was adequately responsive to FBS starvation (Figure 5K). Interestingly, proteins not involved in bulk membrane/lipid synthesis, such as *Tg*PKA-iKO, could not be rescued by excess nutrients (Figure 5L; Uboldi et al., 2018).

Because host FA binding proteins (FABPs) are upregulated upon tachyzoite invasion (Hu et al., 2017), we searched the genome of *T. gondii* for homologs of FABPs that could be responsible for the transport of FAs in the parasite during starvation but found none. Instead, we found two proteins belonging to the closely related family of acyl-CoA binding protein (ACBP): *Tg*ACBP1 and *Tg*ACBP2. We found that *Tg*ACBP1 and *Tg*ACBP2 localized at the parasite cytosol and mitochondrion, respectively (Figures S5D–S5G). We generated inducible knockdown parasite lines for both (Figures S5D and S5E). However, plaque assays showed that both proteins were dispensable during tachyzoite life stages, and neither was responding to FBS starvation (Figures 5M and 5N), suggesting that neither of the

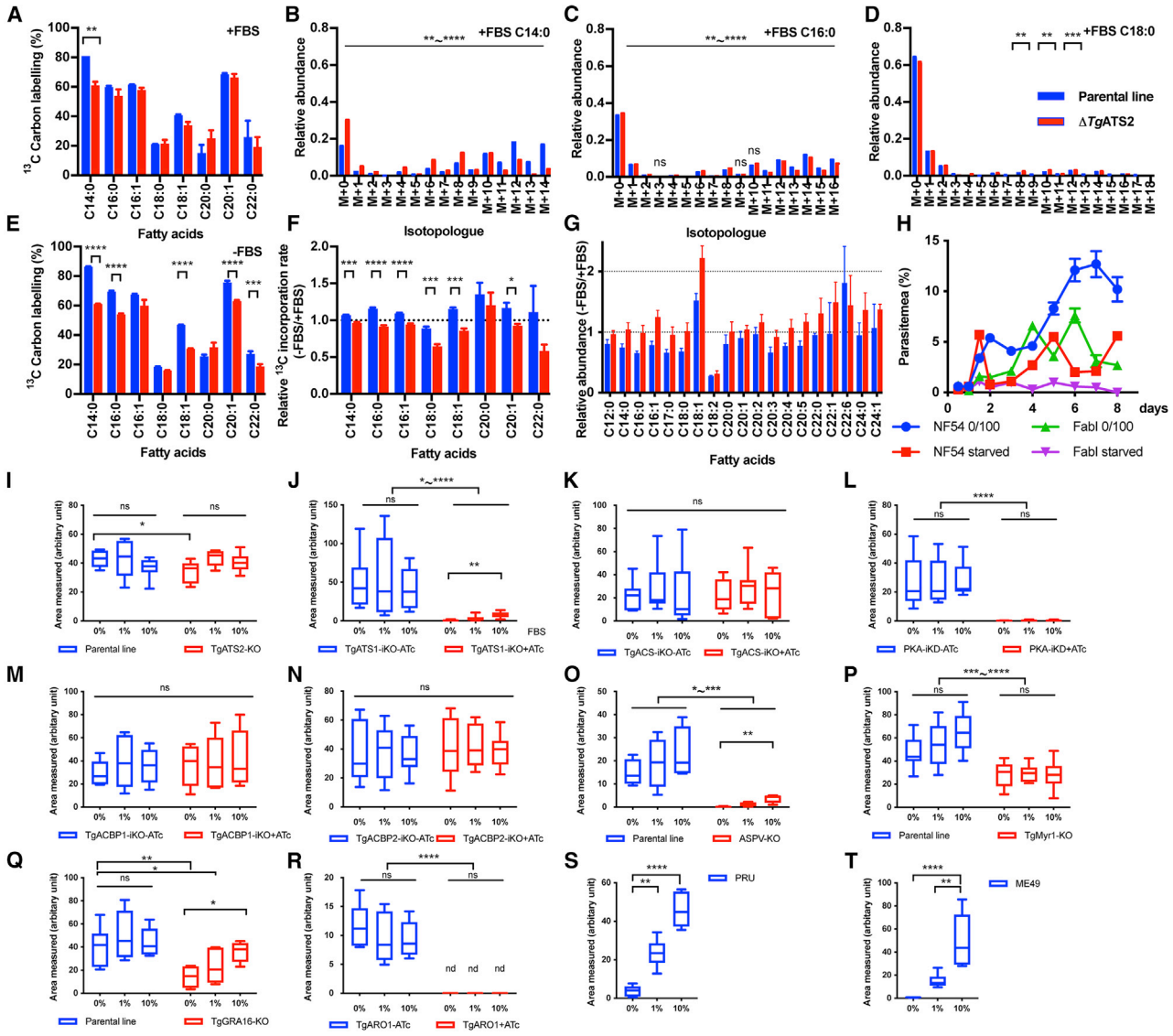

Figure 5. Changes in Host Nutritional Environment Induces an Upregulation of the Apicoplast FASII Metabolic Capacities in *T. gondii* Tachyzoites and *P. falciparum* Blood Stages and Are Pivotal for Enzymes Involved in Metabolic Adaptation

(A–G) U-^{13}C-glucose labeling for 72 h to monitor apicoplast FA synthesis by ^{13}C incorporation to fatty acids (blue, parental line; red, Δ*Tg*ATS2). (A) ^{13}C incorporation to each fatty acid in 1% FBS. (B–D) Mass isotopologue distribution in 1% FBS for C14:0 (B), C16:0 (C), and C18:0 (D). The x axis shown as "M + X" represents mass with "X" ^{13}C atoms incorporated during the FA synthesis. (E) ^{13}C incorporation to each fatty acid in 0.2% FBS. FASII metabolic activity increased upon FBS starvation in the parental line but not in Δ*Tg*ATS2. (F) Change in ^{13}C incorporation between 0.2% FBS and 1% FBS (−FBS/+FBS). (G) The relative abundance of each FA (−FBS/+FBS).

(H) Asexual blood stage growth assay of *P. falciparum* FabI-KO and its parental line (NF54) in regular (lipid-rich) culture medium and lipid-starved medium reveals that FASII is essential in blood stage in low-lipid environment.

(I–T) Growth assays conducted in 0%, 1%, or 10% FBS in different *T. gondii* mutants and strains: *Tg*ATS2 (I), *Tg*ATS1 (J), *Tg*ACS (K), *Tg*PKA (L), *Tg*ACBP1 (M), *Tg*ACBP2 (N), *Tg*ASP5 (O), *Tg*Myr1 (P), *Tg*GRA16 (Q), *Tg*ARO1 (R), type II PRU (S), and type II ME49 (T).

n ≥ 3. ns, not significant; *p ≤ 0.05, **p ≤ 0.01, ***p ≤ 0.001, and ****p ≤ 0.0001.

*Tg*ACBPs is involved as an effector for the adaptation to nutritional environment. We generated a *Tg*ACBP1 and *Tg*ABCP2 double KO and a double ACBP1iKD/sterol carrier protein (SCP2) KO cell line, which we also found to be viable and not responsive to starvation (Figures S5H and S5I).

We then hypothesized that parasite effectors putatively exported into the PVM or toward the host cell could be used by the parasite to collect putative host membrane material generated during FBS starvation. To test this, we investigated *Tg*ASP5, a Golgi-resident aspartyl protease that controls the non-canonical trafficking pathway of parasite effectors toward the PVM and the host cell, during FBS starvation (Bougdour et al., 2014). Strikingly, FBS starvation significantly exacerbated the growth defect in Δ*Tg*ASP5 (Figures 5O and S5). By contrast,

the mutant cell line Δ*Tg*MYR1 (the canonical system to export effectors toward the host; Franco et al., 2016) showed overall less growth than the parental cell line, although Δ*Tg*MYR1 grew equally well among the 0%, 1%, and 10% FBS conditions (Figure 5P). To examine the effects of some specific GRA effectors, we examined a GRA16-KO cell line, which we observed to have a minor but significant growth defect under FBS starvation, suggesting that at least some GRA proteins are important, likely in combination (Figure 5O). We also examined a mutant for rhoptry secretion *Tg*ARO-iKO (Mueller et al., 2013) but found that under ATc treatment, the mutant died regardless of FBS concentration (Figure 5R), suggesting a primary role in host invasion prior to host re-wiring.

Last, we explored strain-specific differences between in *Toxoplasma* between the hypervirulent type I RH strain and type II strains (Prugniaud, ME49) capable of forming chronic stages (bradyzoites). Both type II strains showed significantly reduced growth in lipid-depleted medium (Figures 5S and 5T), unlike type I strain.

Together, these data provide evidence that in response to nutrient starvation, parasite effectors can be trafficked to the host cell, primarily via the *Tg*ASP5 export pathway, likely to enhance the ability to scavenge resources.

Nutrient Starvation Induces the Formation of Multi-membrane-Bound Vesicles in Host Cells that Are Taken up by the Parasite

To investigate potential changes to the host cell and hence host-parasite interactions during lipid starvation, we performed EM on starved (0%, 1%, or 10% FBS) HFF host cells infected with either the parental parasite line or Δ*Tg*ATS2. Growth in 10% FBS led to no obvious phenotype changes in the hosts cells or the parental parasite line or the Δ*Tg*ATS2 mutant (Figures 6A and 6B), but reduction to 1% and 0% FBS induced striking changes in the host cells, which became extensively vesiculated irrespective of whether they were infected with the parental line or Δ*Tg*ATS2 (Figures 6A and 6B). Such vesiculation was not observed in uninfected HFF host cells put under nutrient starvation. Giant multi-vesicular bodies (gMVBs; i.e., large membrane-bound compartments containing various smaller vesicles) were frequent in 1% FBS-grown cells (Figures 6A and 6B) and very numerous at 0% FBS (Figures 6A and 6B). The gMVBs are distinct from host autophagosome, as they lack the typical double/multiple surrounding membranes and the cytosolic material defining autophagosomes (Ylä-Anttila et al., 2009). This was confirmed by IFA using the typical autophagosome marker anti-LC3, which showed no accumulation of autophagosome under 10%, 1%, or 0% FBS (Figure S6). The gMVBs could arise from the host ER, as the ER could be seen swelling and forming networks containing large lipid bodies (Figure 6B3). gMVBs were also often seen in close apposition or contact with the mitochondria and/or ER network, indicating that material could also be transferred from both (Figures 6B3 and 6B5). However, gMVBs were more often observed arising directly from the host nuclear envelope, potentially a major contributor to their formation (Figures 6B6–6B8). The gMVB accumulated in close vicinity with the PVM, which houses the parasite during its intracellular development and serves as the exchange interphase between the host and the parasite. The gMVBs were not only close to the PVM but appeared to be interacting with the PVM with host material and vesicles from the gMVB, apparently "percolating" through the PVM (Figure 6B4) or directly from their originating organelles (Figure 6B5) to eventually be found in the PVM (Figures 6A and 6B1). These vesicles appeared in both WT and Δ*Tg*ATS2, suggesting that the host cell is responding to the nutrient deficiency in the same way. The Δ*Tg*ATS2 parasite cytokinesis phenotype (e.g., Figure 2A) was still observed and apparently exacerbated in 0% and 1% FBS growth medium (Figure 6B). This vesicle/gMVB formation and trafficking to and within the PVM was not apparent in high (10%) FBS medium, suggesting that host gMVBs somehow allow the parasite to increase its lipid scavenging in the absence of nutrient rich serum. Together this indicates that gMVBs contain multiple vesicles that (1) are dependent and induced by nutrient availability and (2) originate directly from diverse host organelles. The gMVBs are distinct from lipid droplets of host cell origin used as a lipid source by *T. gondii* (Nolan et al., 2017; Romano et al., 2017).

However, it is possible that FBS starvation leads to increased host cell lipid droplet import. Nile red staining confirmed that FBS starvation induced a significant increase of the amount of lipid droplets into the parasites and its PVM (Figure 6C). In contrast, low FBS content resulted in a reduced amount of lipid droplets in uninfected host cells, while high FBS content increased their presence in the host cells alone (Figure 6D). This further indicates that increase of import of lipid droplets to the parasite is upregulated by the parasite during FBS starvation.

Because gMVBs also seem to arise from host mitochondria, we used an anti-lyso-bi-PA (LBPA; i.e., a degradation product of mitochondrial CL) antibody (Kobayashi et al., 1998), a lipid that can also be scavenged by intracellular parasites (Romano et al., 2017; Figure 6E). LBPA was found surrounding the PVM in the host cell, within the PV and the parasite, but its localization and intensity remained unchanged in response to reduced FBS content (Figure 6E). Direct salvage of mitochondrial CL per se might not be the primary upregulated scavenging pathway during lipid starvation.

To determine whether host mitochondrial sequestration could affect parasite adaptation to low host nutrient, we measured the levels of mitochondrial sequestration in type I parasites (prone to host mitochondrial sequestration) and type II parasites (not sequestering host mitochondria) (Pernas et al., 2014). Host mitochondria was monitored with MitoTracker. Both RH type I and type II ME49 parasites showed no major difference in host mitochondrial sequestration after FBS starvation (Figure S6).

DISCUSSION

We have shown that *Tg*ATS2 is an apicoplast acyltransferase able to esterify FAs on LPA to generate PA, a precursor for a wide range of parasite lipids. KO of *Tg*ATS2 resulted in perturbed lipid fluxes, which affects LPA/PA lipid balance, causing mislocalization of *Tg*DrpC and vesiculation during cytokinesis. Furthermore, changes in lipid profiles of Δ*Tg*ATS2 showed the capacity of WT parasites to exhibit considerable metabolic plasticity at both *de novo* FA synthesis in the apicoplast and host modification for organelle membrane scavenging, together

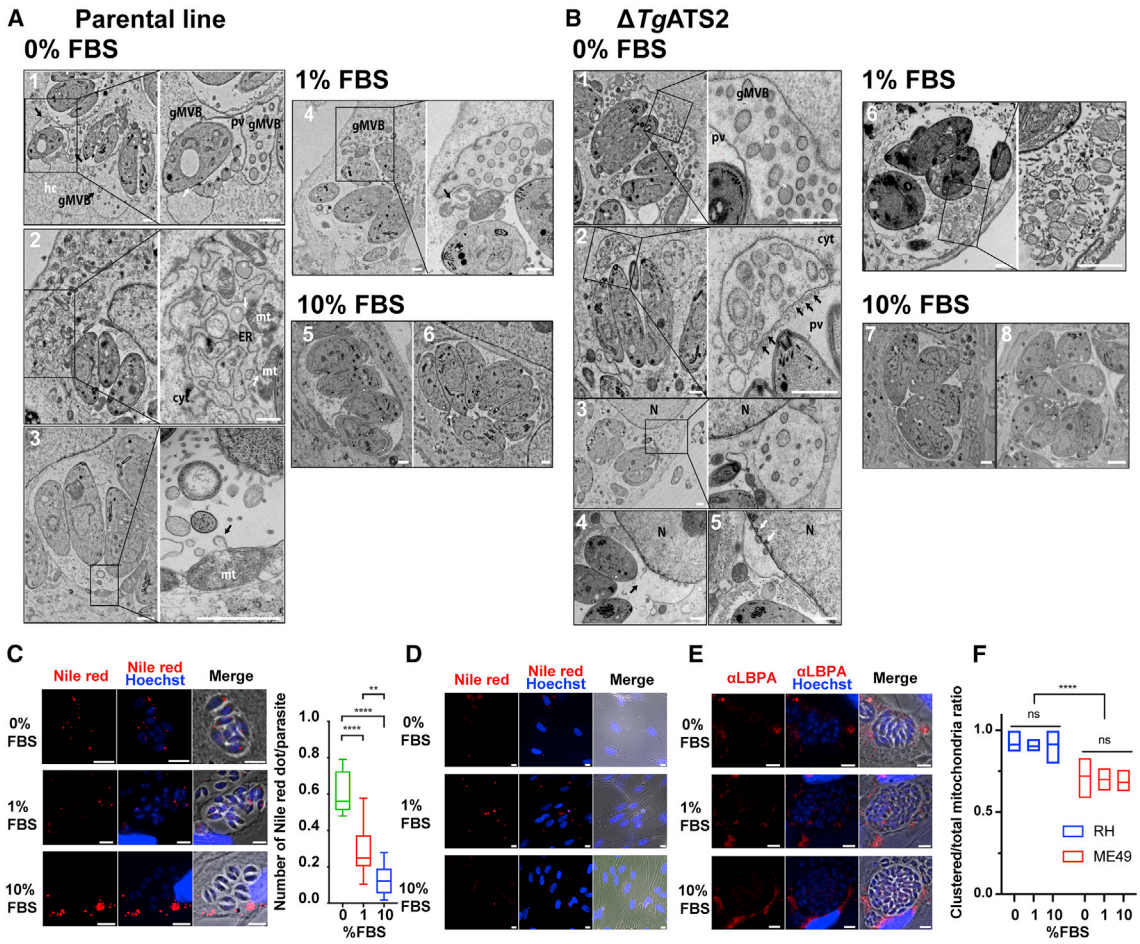

Figure 6. Nutrient Starvation Unveils the Formation of Multi-vesicular Bodies from Host Cell Organelles, Whose Content Is Imported toward Parasites

(A and B) Transmission electron micrographs of intracellular WT tachyzoites (A) and Δ*Tg*ATS2 mutant parasites (B) grown in 0%, 1%, and 10% FBS. Nutrient starvation (i.e., 0% and 1% FBS) induces formation of giant multi-vesicular bodies (gMVBs) in the host cell (hc), containing various vesicles, including lipid body-like (white stars). In starvation, gMVBs localized in the cytosol (cyt) in contact with the parasitophorous vacuole (pv) (A1, A2, A4, B1, and B2), and their content was imported through and into the PV (A1, black stars; B2 and B6, black arrows); gMVBs were arising from host endoplasmic reticulum (ER; A2), mitochondria (mt; A2 and A3), and mainly swollen nuclear envelope (N; B3–B5). Ten percent FBS did not induce gMVB formation in both parental and Δ*Tg*ATS2. Scale bar, 1 μm.

(C) Nutrient starvation induces a significant increase of lipid droplets within the parasite and its PV as measured by IFA using Nile red (Nile red dots were counted for 100 or more parasites; n = 3; ns, not significant; *p ≤ 0.05, **p ≤ 0.01, ***p ≤ 0.001, and ****p ≤ 0.0001). Scale bar, 2 μm.

(D) Nutrient starvation induces a decrease of lipid bodies in uninfected HFF host cells as measured by IFA using Nile red. Scale bar, 2 μm.

(E) IFA shows that import into parasites of LBPA (anti-LBPA) is not affected by nutrient starvation. Scale bar, 2 μm.

(F) Nutrient starvation induces a significant growth defect in *T. gondii* tachyzoites ME49 type II strain compared with RH type I strain. p values are as mentioned as above.

critical for adaptation to nutrient-limiting conditions in the host (Figure 7; Table S1).

Roles of PA and LPA in Membrane Curvature and Cell Division

Membrane PLs have different physical shapes according to the relative sizes between the polar head and the FA tails. Most PLs are cylindrical, while PA is cone shaped and LPA adopts an inverted cone shape; thus their insertion into membrane bilayers facilitates curvature and in- or evagination (Kooijman et al., 2005).

Furthermore, in human cells, dynamin pinching requires endophilin-1, an ATS2 homolog, as a partner to create LPA/PA curvatures (Burger et al., 2000; Shin and Loewen, 2011), improving penetration of a larger part of dynamin into the lipid monolayer (Burger et al., 2000; Shin and Loewen, 2011), similar to the relationship between *Tg*ATS2 and *Tg*DrpC. Our results reveal the previously unrecognized importance of the apicoplast in maintaining internal lipid homeostasis. Furthermore, the functional role of *Tg*ATS2 for PA synthesis during division provides a mechanism for the long-standing question of why drugs targeting the apicoplast display a secondary cytokinetic defect (Martins-Duarte et al., 2015).

Our results nicely complement those of a recent study that identified the basal complex as a major site of endocytosis in

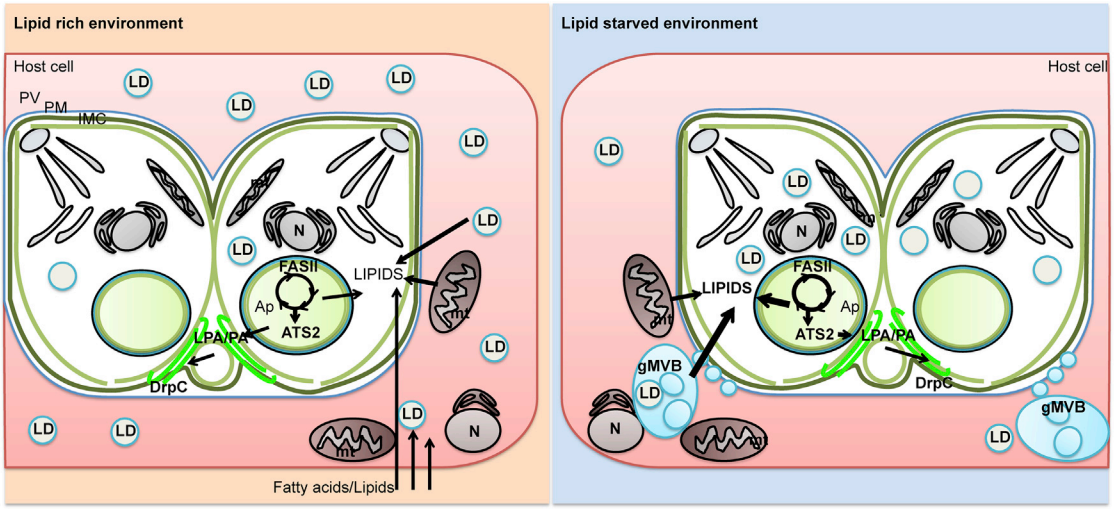

Figure 7. Proposed Model for Cytokinesis, Lipid Acquisition, and Metabolic Adaptation under Adverse Host Lipid Environment in *T. gondii*

Left: under lipid-rich environment, *T. gondii* can readily acquire FAs and lipids by *de novo* synthesis (apicoplast) and host cell scavenging. The apicoplast ATS2 generates PA and regulates the balance of LPA/PA, necessary for DrpC. Right: in a host lipid-starved environment, the parasite adapts its metabolism by increasing FASII to produce more fatty acids to compensate their absence from the host cell. Concomitantly, the parasite induces morphological changes in the host to increase scavenged resources, including the nucleus, ER, and gMVBs.

motile tachyzoites, consistent with the basal complex localization of DrpC (Figure 4; (Heredero-Bermejo et al., 2019). Our results show that endocytosis occurs during intracellular stages and that aberrant LPA/PA ratios caused by the loss of ATS2 disrupt this process.

Furthermore, many DrpC-interacting proteins have been identified as part of a larger endocytic protein complex, including EPS15, AP2 adaptins, and, intriguingly, Kelch13 (Heredero-Bermejo et al., 2019). Kelch13 is the infamous protein found mutated in artemisinin-resistant malaria spreading throughout Asia (Menard and Dondorp, 2017). Kelch13 therefore likely has a role in endocytosis consistent with DrpC and other interacting partners (Heredero-Bermejo et al., 2019). Intriguingly, it has been shown that FASII activity is often increased in artemisinin-resistant parasites (Chen et al., 2014). Our evidence here demonstrates that the upregulation of FASII produces LPA that modulates cytokinesis and endocytosis processes. Again, this highlights the previously unrecognized importance of the apicoplast in maintaining internal lipid homeostasis in parasites.

Environmental and Nutritional Conditions Drive the Adaptation of the Apicoplast Metabolic Capacities as Well as the Scavenging Capacities

Importantly, *Toxoplasma* could increase production of FA in the FASII pathway in nutrient/lipid-deprived medium similarly to *P. falciparum* (Botté et al., 2013). Hence, apicomplexan parasites show high metabolic flexibility to obtain FA for the major membrane building blocks required for growth, as pointed out by recent studies exploring *Plasmodium* survival in nutrient-depleted conditions (Mancio-Silva et al., 2017; Zuzarte-Luís et al., 2017). Importantly, our results demonstrate that *P. falciparum* lacking a FASII and grown in lipid-deprived conditions was unable to properly proliferate, ultimately dying. This suggests that apicoplast FASII is facultative rather than totally dispensable in malaria parasite blood stage and can be activated during lipid starvation to meet PL needs. This FASII flexibility is consistent with a growing pool of evidence including the upregulation of FASII and the apicoplast acyltransferase PfG3apiGPAt (a homolog of *Tg*ATS1) transcripts in starved patients (Daily et al., 2007) and the essentiality of most FASII enzymes, including the central acyl-carrier protein ACP in both *T. gondii* and *P. falciparum* (Sidik et al., 2016; Zhang et al., 2018), summarized in Table S1. Therefore, environmental factors could have important consequences in treating patients. Indeed, if patients are under stress, nutrient deprivation, or malnourished conditions, the FASII pathway could become a secondary target of choice to help eradicate the parasites. Altogether these data question whether isopentenyl pyrophosphate (IPP) synthesis is the sole essential function of the apicoplast during *Plasmodium* blood stage (Yeh and DeRisi, 2011). Rather, our data put the parasite back into its physiological context, where nutrient availability and environmental conditions drive the requirement and regulation of a given metabolic pathway. Furthermore, the scavenging of *Toxoplasma* can also be seen to be upregulated through exported effectors by evidence that ASP5 KO is partially rescued by excess host lipids and the induction of host remodeling to make gMVBs, although the identity of these gMVBs warrants further investigation. This redefines what we call an essential gene, where phenotypes might only be seen under starvation conditions.

A major question raised here is the nature the signaling factor(s) responsible for environmental sensing and metabolic adaption of both apicoplast *de novo* synthesis and scavenging pathways. Both *T. gondii* and *P. falciparum* lack the canonical mTOR-based nutrient-sensing pathways present in other eukaryotes, but a recent study showed that *P. berghei* is capable

of sensing nutrient deprivation by a SNF1-related kinase, KIN1 (Mancio-Silva et al., 2017).

Together, our results reveal the central role of the apicoplast to provide specific precursors for membrane biogenesis during cytokinesis and, most important, to be a central metabolic hub to adapt the parasite metabolic capacities upon nutrient availability and environmental changes. The data also point to major modifications in vesiculation and the use and scavenging of these membrane structures by the parasite upon such environmental changes. The data also corroborate recent results showing that the mosquito lipid environment regulates the metabolic activity of transmissible sporozoites (Costa et al., 2018). The fundamental role of these physiological changes induced by the parasite in response to host environment provides novel insights into parasite biology and offers new avenues to explore in the fight against toxoplasmosis and malaria.

STAR★METHODS

Detailed methods are provided in the online version of this paper and include the following:

- KEY RESOURCES TABLE
- MATERIALS AND METHODS
- LEAD CONTACT AND MATERIALS AVAILABILITY
- EXPERIMENTAL MODEL AND SUBJECT DETAILS
  - T. gondii culture
  - P. falciparum culture
- METHOD DETAILS
  - Gene identification and sequence analysis
  - T. gondii plasmid constructs
  - T. gondii transfection
  - T. gondii growth assays
  - T. gondii Red/Green parasite invasion assay
  - Plasmodium falciparum growth assays
  - Immunofluorescence assay and Microscopy
  - Nile red staining of lipid droplets
  - Activity analysis in LPAAT-deficient *E. coli* strains
  - Transmission electron microscopy
  - Lipidomic analysis by GCMS extraction from T. gondii tachyzoites
  - Stable isotope labeling of T. gondii
  - Phospholipid import assay
- QUANTIFICATION AND STATISTICAL ANALYSIS
- DATA AND CODE AVAILABILITY

SUPPLEMENTAL INFORMATION

Supplemental Information can be found online at https://doi.org/10.1016/j.celrep.2020.02.072.

ACKNOWLEDGMENTS

We would like to thank Prof. Alan Cowman and Dr. Ali Hakimi for sharing parasite strains, reagents, and fruitful advice. This work and C.Y.B., Y.Y.-B., S.A., N.J.K., and C.B. are supported by Agence Nationale de la Recherche, France (grant ANR-12-PDOC-0028, Project Apicolipid), the Atip-Avenir and Finovi programs (CNRS-INSERM-FinoviAtip-AvenirApicolipid projects), and Laboratoire d'Excellence Parafrap, France (grant ANR-11-LABX-0024). C.Y.B. and G.I.M. are supported by the LIA-IRP CNRS Program (Apicolipid project).

AUTHOR CONTRIBUTIONS

S.A. and N.J.K. designed and performed experiments, analyzed and interpreted data, and wrote the manuscript. L.B. performed, analyzed, and interpreted data for EM. S.D. performed Nile red/LBPA and related IFAs. S.D. generated and analyzed the *Tg*DrpC-ΔPA mutant. C.S.A. generated and analyzed the double ACBP1-ACBP2- and ACBP1iKD/SCP2-KO mutants. M.J.S. helped perform and analyze the *P. falciparum* lipid starvation growth assay. C.B. helped perform *E. coli* complementation assays. B.T. performed and analyzed *T. gondii* proliferation assays and the related statistical analyses. G.I.M. supervised the *P. falciparum* lipid starvation growth assay. Y.Y.-B. performed, analyzed, interpreted, and supervised lipidomic analyses and wrote the manuscript. C.Y.B. led the project, designed and interpreted data, and wrote the manuscript.

DECLARATION OF INTERESTS

The authors declare no competing interests.

Received: March 22, 2019
Revised: November 12, 2019
Accepted: February 19, 2020
Published: March 17, 2020

REFERENCES

Adachi, Y., Itoh, K., Yamada, T., Cerveny, K.L., Suzuki, T.L., Macdonald, P., Frohman, M.A., Ramachandran, R., Iijima, M., and Sesaki, H. (2016). Coincident phosphatidic acid interaction restrains Drp1 in mitochondrial division. Mol. Cell *63*, 1034–1043.

Adachi, Y., Iijima, M., and Sesaki, H. (2018). An unstructured loop that is critical for interactions of the stalk domain of Drp1 with saturated phosphatidic acid. Small GTPases *9*, 472–479.

Amiar, S., MacRae, J.I., Callahan, D.L., Dubois, D., van Dooren, G.G., Shears, M.J., Cesbron-Delauw, M.-F., Maréchal, E., McConville, M.J., McFadden, G.I., et al. (2016). Apicoplast-localized lysophosphatidic acid precursor assembly is required for bulk phospholipid synthesis in toxoplasma gondii and relies on an algal/plant-like glycerol 3-phosphate acyltransferase. PLoS Pathog. *12*, e1005765.

Bisanz, C., Bastien, O., Grando, D., Jouhet, J., Maréchal, E., and Cesbron-Delauw, M.F. (2006). Toxoplasma gondii acyl-lipid metabolism: de novo synthesis from apicoplast-generated fatty acids versus scavenging of host cell precursors. Biochem. J. *394*, 197–205.

Botté, C.Y., Yamaryo-Botté, Y., Rupasinghe, T.W., Mullin, K.A., MacRae, J.I., Spurck, T.P., Kalanon, M., Shears, M.J., Coppel, R.L., Crellin, P.K., et al. (2013). Atypical lipid composition in the purified relict plastid (apicoplast) of malaria parasites. Proc. Natl. Acad. Sci. U S A *110*, 7506–7511.

Bougdour, A., Durandau, E., Brenier-Pinchart, M.-P., Ortet, P., Barakat, M., Kieffer, S., Curt-Varesano, A., Curt-Bertini, R.-L., Bastien, O., Coute, Y., Pelloux, H., and Hakimi, M.-A. (2013). Host cell subversion by Toxoplasma GRA16, an exported dense granule protein that targets the host cell nucleus and alters gene expression. Cell Host Microbe. *13*, 489–500.

Bougdour, A., Tardieux, I., and Hakimi, M.A. (2014). Toxoplasma exports dense granule proteins beyond the vacuole to the host cell nucleus and rewires the host genome expression. Cell. Microbiol. *16*, 334–343.

Braun, L., Brenier-Pinchart, M.-P., Hammoudi, P.-M., Cannella, D., Kieffer-Jaquinod, S., Vollaire, J., Josserand, V., Touquet, B., Couté, Y., Tardieux, I., Bougdour, A., and Hakimi, M.-A. (2019). The Toxoplasma effector TEEGR promotes parasite persistence by modulating NF-κB signalling via EZH2. Nat. Microbiol. *4*, 1208–1220.

Breinich, M.S., Ferguson, D.J., Foth, B.J., van Dooren, G.G., Lebrun, M., Quon, D.V., Striepen, B., Bradley, P.J., Frischknecht, F., Carruthers, V.B., and Meissner, M. (2009). A dynamin is required for the biogenesis of secretory organelles in Toxoplasma gondii. Curr. Biol. *19*, 277–286.

Brown, W.J., Plutner, H., Drecktrah, D., Judson, B.L., and Balch, W.E. (2008). The lysophospholipid acyltransferase antagonist CI-976 inhibits a late step in COPII vesicle budding. Traffic *9*, 786–797.

Burger, K.N.J., Demel, R.A., Schmid, S.L., and de Kruijff, B. (2000). Dynamin is membrane-active: lipid insertion is induced by phosphoinositides and phosphatidic acid. Biochemistry *39*, 12485–12493.

Chen, N., LaCrue, A.N., Teuscher, F., Waters, N.C., Gatton, M.L., Kyle, D.E., and Cheng, Q. (2014). Fatty acid synthesis and pyruvate metabolism pathways remain active in dihydroartemisinin-induced dormant ring stages of Plasmodium falciparum. Antimicrob Agents Chemother *58*, 4773–4781.

Coleman, J. (1990). Characterization of Escherichia coli cells deficient in 1-acyl-sn-glycerol-3- phosphate acyltransferase activity. J. Biol. Chem. *265*, 17215–17221.

Costa, G., Gildenhard, M., Eldering, M., Lindquist, R.L., Hauser, A.E., Sauerwein, R., Goosmann, C., Brinkmann, V., Carrillo-Bustamante, P., and Levashina, E.A. (2018). Non-competitive resource exploitation within mosquito shapes within-host malaria infectivity and virulence. Nat. Commun. *9*, 3474.

Curt-Varesano, A., Braun, L., Ranquet, C., Hakimi, M.-A., and Bougdour, A. (2016). The aspartyl protease TgASP5 mediates the export of the Toxoplasma GRA16 and GRA24 effectors into host cells. Cell. Microbiol. *18*, 151–167.

Daily, J.P., Scanfeld, D., Pochet, N., Le Roch, K., Plouffe, D., Kamal, M., Sarr, O., Mboup, S., Ndir, O., Wypij, D., et al. (2007). Distinct physiological states of Plasmodium falciparum in malaria-infected patients. Nature *450*, 1091–1095.

Dereeper, A., Guignon, V., Blanc, G., Audic, S., Buffet, S., Chevenet, F., Dufayard, J.-F., Guindon, S., Lefort, V., Lescot, M., et al. (2008). Phylogeny.fr: robust phylogenetic analysis for the non-specialist. Nucleic Acids Res. *36*, W465–W469.

Dubois, D., Fernandes, S., Amiar, S., Dass, S., Katris, N.J., Botté, C.Y., and Yamaryo-Botté, Y. (2018). *Toxoplasma gondii* acetyl-CoA synthetase is involved in fatty acid elongation (of long fatty acid chains) during tachyzoite life stages. J. Lipid Res. *59*, 994–1004.

Franco, M., Panas, M.W., Marino, N.D., Lee, M.C., Buchholz, K.R., Kelly, F.D., Bednarski, J.J., Sleckman, B.P., Pourmand, N., and Boothroyd, J.C. (2016). A novel secreted protein, MYR1, is central to Toxoplasma's manipulation of host cells. MBio *7*, e02231-15.

Gras, S., Jimenez-Ruiz, E., Klinger, C.M., Schneider, K., Klingl, A., Lemgruber, L., and Meissner, M. (2019). An endocytic-secretory cycle participates in Toxoplasma gondii in motility. PLoS Biol. *17*, e3000060.

Guindon, S., Dufayard, J.F., Lefort, V., Anisimova, M., Hordijk, W., and Gascuel, O. (2010). New algorithms and methods to estimate maximum-likelihood phylogenies: assessing the performance of PhyML 3.0. Syst. Biol. *59*, 307–321.

Gulati, S., Ekland, E.H., Ruggles, K.V., Chan, R.B., Jayabalasingham, B., Zhou, B., Mantel, P.Y., Lee, M.C., Spottiswoode, N., Coburn-Flynn, O., et al. (2015). Profiling the Essential nature of lipid metabolism in asexual blood and gametocyte stages of Plasmodium falciparum. Cell Host Microbe *18*, 371–381.

Heredero-Bermejo, I., Varberg, J.M., Charvat, R., Jacobs, K., Garbuz, T., Sullivan, W.J., Jr., and Arrizabalaga, G. (2019). TgDrpC, an atypical dynamin-related protein in Toxoplasma gondii, is associated with vesicular transport factors and parasite division. Mol. Microbiol. *111*, 46–64.

Hu, X., Binns, D., and Reese, M.L. (2017). The coccidian parasites *Toxoplasma* and *Neospora* dysregulate mammalian lipid droplet biogenesis. J. Biol. Chem. *292*, 11009–11020.

Huynh, M.H., and Carruthers, V.B. (2009). Tagging of endogenous genes in a Toxoplasma gondii strain lacking Ku80. Eukaryot. Cell *8*, 530–539.

Janouskovec, J., Horák, A., Oborník, M., Lukeš, J., and Keeling, P.J. (2010). A common red algal origin of the apicomplexan, dinoflagellate, and heterokont plastids. Proc. Natl. Acad. Sci. U S A *107*, 10949–10954.

Katris, N.J., van Dooren, G.G., McMillan, P.J., Hanssen, E., Tilley, L., and Waller, R.F. (2014). The apical complex provides a regulated gateway for secretion of invasion factors in Toxoplasma. PLoS Pathog. *10*, e1004074.

Kim, K., Soldati, D., and Boothroyd, J.C. (1993). Gene replacement in Toxoplasma gondii with chloramphenicol acetyltransferase as selectable marker. Science *262*, 911–914.

Kobayashi, T., Stang, E., Fang, K.S., de Moerloose, P., Parton, R.G., and Gruenberg, J. (1998). A lipid associated with the antiphospholipid syndrome regulates endosome structure and function. Nature *392*, 193–197.

Kooijman, E.E., Chupin, V., Fuller, N.L., Kozlov, M.M., de Kruijff, B., Burger, K.N.J., and Rand, P.R. (2005). Spontaneous curvature of phosphatidic acid and lysophosphatidic acid. Biochemistry *44*, 2097–2102.

Larkin, M.A., Blackshields, G., Brown, N.P., Chenna, R., McGettigan, P.A., McWilliam, H., Valentin, F., Wallace, I.M., Wilm, A., Lopez, R., et al. (2007). Clustal W and Clustal X version 2.0. Bioinformatics *23*, 2947–2948.

Li, W., Cowley, A., Uludag, M., Gur, T., McWilliam, H., Squizzato, S., Park, Y.M., Buso, N., and Lopez, R. (2015). The EMBL-EBI bioinformatics web and programmatic tools framework. Nucleic Acids Res. *43* (*W1*), W580–W584.

MacRae, J.I., Maréchal, E., Biot, C., and Botté, C.Y. (2012). The apicoplast: a key target to cure malaria. Curr. Pharm. Des. *18*, 3490–3504.

Mancio-Silva, L., Slavic, K., Grilo Ruivo, M.T., Grosso, A.R., Modrzynska, K.K., Vera, I.M., Sales-Dias, J., Gomes, A.R., MacPherson, C.R., Crozet, P., et al. (2017). Nutrient sensing modulates malaria parasite virulence. Nature *547*, 213–216.

Martins-Duarte, E.S., Dubar, F., Lawton, P., da Silva, C.F., Soeiro, Mde.N., de Souza, W., Biot, C., and Vommaro, R.C. (2015). Ciprofloxacin derivatives affect parasite cell division and increase the survival of mice infected with Toxoplasma gondii. PLoS ONE *10*, e0125705.

Mazumdar, J., H Wilson, E., Masek, K., A Hunter, C., and Striepen, B. (2006). Apicoplast fatty acid synthesis is essential for organelle biogenesis and parasite survival in Toxoplasma gondii. Proc. Natl. Acad. Sci. U S A *103*, 13192–13197.

Melatti, C., Pieperhoff, M., Lemgruber, L., Pohl, E., Sheiner, L., and Meissner, M. (2019). A unique dynamin-related protein is essential for mitochondrial fission in Toxoplasma gondii. PLoS Pathog. *15*, e1007512.

Menard, D., and Dondorp, A. (2017). Antimalarial drug resistance: a threat to malaria elimination. Cold Spring Harb. Perspect. Med. *7*, a025619.

Mi-Ichi, F., Kita, K., and Mitamura, T. (2006). Intraerythrocytic Plasmodium falciparum utilize a broad range of serum-derived fatty acids with limited modification for their growth. Parasitology *133*, 399–410.

Mi-Ichi, F., Kano, S., and Mitamura, T. (2007). Oleic acid is indispensable for intraerythrocytic proliferation of *Plasmodium falciparum*. Parasitology *134*, 1671–1677.

Mitamura, T., Hanada, K., Ko-Mitamura, E.P., Nishijima, M., and Horii, T. (2000). Serum factors governing intraerythrocytic development and cell cycle progression of Plasmodium falciparum. Parasitol. Int. *49*, 219–229.

Mueller, C., Klages, N., Jacot, D., Santos, J.M., Cabrera, A., Gilberger, T.W., Dubremetz, J.-F., and Soldati-Favre, D. (2013). The Toxoplasma protein ARO mediates the apical positioning of rhoptry organelles, a prerequisite for host cell invasion. Cell Host Microbe *13*, 289–301.

Nolan, S.J., Romano, J.D., and Coppens, I. (2017). Host lipid droplets: an important source of lipids salvaged by the intracellular parasite Toxoplasma gondii. PLoS Pathog. *13*, e1006362.

Ohlrogge, J., and Browse, J. (1995). Lipid biosynthesis. Plant Cell *7*, 957–970.

Pernas, L., Adomako-Ankomah, Y., Shastri, A.J., Ewald, S.E., Treeck, M., Boyle, J.P., and Boothroyd, J.C. (2014). Toxoplasma effector MAF1 mediates recruitment of host mitochondria and impacts the host response. PLoS Biol. *12*, e1001845.

Ramakrishnan, S., Docampo, M.D., Macrae, J.I., Pujol, F.M., Brooks, C.F., van Dooren, G.G., Hiltunen, J.K., Kastaniotis, A.J., McConville, M.J., and Striepen, B. (2012). Apicoplast and endoplasmic reticulum cooperate in fatty acid biosynthesis in apicomplexan parasite *Toxoplasma gondii*. J. Biol. Chem. *287*, 4957–4971.

Romano, J.D., Nolan, S.J., Porter, C., Ehrenman, K., Hartman, E.J., Hsia, R.C., and Coppens, I. (2017). The parasite *Toxoplasma* sequesters diverse Rab host vesicles within an intravacuolar network. J. Cell Biol. *216*, 4235–4254.

Schmidt, A., Wolde, M., Thiele, C., Fest, W., Kratzin, H., Podtelejnikov, A.V., Witke, W., Huttner, W.B., and Söling, H.D. (1999). Endophilin I mediates synaptic vesicle formation by transfer of arachidonate to lysophosphatidic acid. Nature *401*, 133–141.

Shears, M.J., MacRae, J.I., Mollard, V., Goodman, C.D., Sturm, A., Orchard, L.M., Llinás, M., McConville, M.J., Botté, C.Y., and McFadden, G.I. (2017). Characterization of the Plasmodium falciparum and P. berghei glycerol 3-phosphate acyltransferase involved in FASII fatty acid utilization in the malaria parasite apicoplast. Cell. Microbiol. *19*.

Sheiner, L., Demerly, J.L., Poulsen, N., Beatty, W.L., Lucas, O., Behnke, M.S., White, M.W., and Striepen, B. (2011). A systematic screen to discover and analyze apicoplast proteins identifies a conserved and essential protein import factor. PLoS Pathog. *7*, e1002392.

Shin, J.J.H., and Loewen, C.J.R. (2011). Putting the pH into phosphatidic acid signaling. BMC Biol. *9*, 85.

Sidik, S.M., Hackett, C.G., Tran, F., Westwood, N.J., and Lourido, S. (2014). Efficient genome engineering of Toxoplasma gondii using CRISPR/Cas9. PLoS ONE *9*, e100450.

Sidik, S.M., Huet, D., Ganesan, S.M., Huynh, M.H., Wang, T., Nasamu, A.S., Thiru, P., Saeij, J.P.J., Carruthers, V.B., Niles, J.C., and Lourido, S. (2016). A genome-wide CRISPR screen in Toxoplasma identifies essential apicomplexan genes. Cell *166*, 1423–1435.e12.

Trager, W., and Jensen, J.B. (1976). Human malaria parasites in continuous culture. Science *196*, 673–675.

Uboldi, A.D., Wilde, M.-L., McRae, E.A., Stewart, R.J., Dagley, L.F., Yang, L., Katris, N.J., Hapuarachchi, S.V., Coffey, M.J., Lehane, A.M., Botte, C.Y., Waller, R.F., Webb, A.I., McConville, M.J., and Tonkin, C.J. (2018). Protein kinase A negatively regulates Ca^{2+} signalling in *Toxoplasma gondii*. PLOS Biology *16*, e2005642.

van Dooren, G.G., Reiff, S.B., Tomova, C., Meissner, M., Humbel, B.M., and Striepen, B. (2009). A novel dynamin-related protein has been recruited for apicoplast fission in Toxoplasma gondii. Curr. Biol. *19*, 267–276.

Vaughan, A.M., O'Neill, M.T., Tarun, A.S., Camargo, N., Phuong, T.M., Aly, A.S., Cowman, A.F., and Kappe, S.H. (2009). Type II fatty acid synthesis is essential only for malaria parasite late liver stage development. Cell. Microbiol. *11*, 506–520.

Waller, R.F., Keeling, P.J., Donald, R.G., Striepen, B., Handman, E., Lang-Unnasch, N., Cowman, A.F., Besra, G.S., Roos, D.S., and McFadden, G.I. (1998). Nuclear-encoded proteins target to the plastid in *Toxoplasma gondii* and *Plasmodium falciparum*. Proc. Natl. Acad. Sci. U S A *95*, 12352–12357.

Welti, R., Mui, E., Sparks, A., Wernimont, S., Isaac, G., Kirisits, M., Roth, M., Roberts, C.W., Botté, C., Maréchal, E., and McLeod, R. (2007). Lipidomic analysis of Toxoplasma gondii reveals unusual polar lipids. Biochemistry *46*, 13882–13890.

Yeh, E., and DeRisi, J.L. (2011). Chemical rescue of malaria parasites lacking an apicoplast defines organelle function in blood-stage Plasmodium falciparum. PLoS Biol. *9*, e1001138.

Ylä-Anttila, P., Vihinen, H., Jokitalo, E., and Eskelinen, E.L. (2009). Monitoring autophagy by electron microscopy in mammalian cells. Methods Enzymol. *452*, 143–164.

Yu, M., Kumar, T.R., Nkrumah, L.J., Coppi, A., Retzlaff, S., Li, C.D., Kelly, B.J., Moura, P.A., Lakshmanan, V., Freundlich, J.S., et al. (2008). The fatty acid biosynthesis enzyme FabI plays a key role in the development of liver-stage malarial parasites. Cell Host Microbe *4*, 567–578.

Zhang, M., Wang, C., Otto, T.D., Oberstaller, J., Liao, X., Adapa, S.R., Udenze, K., Bronner, I.F., Casandra, D., Mayho, M., et al. (2018). Uncovering the essential genes of the human malaria parasite *Plasmodium falciparum* by saturation mutagenesis. Science *360*, eaap7847.

Zuzarte-Luís, V., Mello-Vieira, J., Marreiros, I.M., Liehl, P., Chora, A.F., Carret, C.K., Carvalho, T., and Mota, M.M. (2017). Dietary alterations modulate susceptibility to Plasmodium infection. Nat. Microbiol. *2*, 1600–1607.

STAR★METHODS

KEY RESOURCES TABLE

REAGENT or RESOURCE	SOURCE	IDENTIFIER
Antibodies		
Mouse anti-HA	Roche	Cat#: 11867423001; RRID:AB_390918
anti-CPN60	Boris Striepen	N/A
anti-LBPA	Echelon Biosciences	Cat#: 117Z-PLBPA-50ug
Mouse anti-Sag1	Abcam	N/A
Anti-LC3B antibody produced in rabbit	Sigma	Cat#: L7543; RRID:AB_796155
Rabbit anti-TOM40	Giel van Dooren	N/A
rabbit anti-GAP45	Dominique Soldati Lab	N/A
rabbit polyclonal anti-IMC1	Gary Ward Lab	N/A
Anti-MIC2	David Sibley	N/A
Anti-GRA1	Cesbron-Delauw Lab	N/A
Rabbit anti-ACP	McFadden lab	N/A
Rabbit polyclonal anti-MIC4	Dominique Soldati Lab	N/A
rabbit anti-Sumo21	Hakimi lab	N/A
Goat a Mouse Alexa 488	ThermoFisher Scientific	Cat#: A11001; RRID:AB_2534069
Goat a Rb Alexa 546	ThermoFisher Scientific	Cat#: A11003; RRID:AB_141370
Goat a Mouse Alexa 546	ThermoFisher Scientific	Cat#: A11010; RRID:AB_2534077
Goat a Rb Alexa 488	ThermoFisher Scientific	Cat#: A11008; RRID:AB_143165
Bacterial and Virus Strains		
E. coli SM2-1 ΔplsC	Coleman, 1990	Coli Genetic Stock Center #7587, Yale University
Biological Samples		
Red Blood Cells	Etablissement francais du sang (EFS)	N/A
Chemicals, Peptides, and Recombinant Proteins		
DMEM, High Glucose	GIBCO, ThermoFisher Scientific	Cat#: 41965-062
DMEM, no Glucose	GIBCO, ThermoFisher Scientific	Cat#: 11966-025
RPMI 1640 Medium, HEPES	GIBCO, ThermoFisher Scientific	Cat#: 52400-025
Fetal Calf Serum, Sourced from South America (EU Approved).	ThermoFisher Scientific	Cat#: 10270-106
AlbuMAX® II	ThermoFisher Scientific	Cat#: 11021-045
GLUCOSE-D U-13C6 99%13C 10 g	Cambridge Isotope Laboratories (Eurisotop)	Cat#: CLM-1396-10
Sorbitol	Sigma	Cat#: S1876
Giemsa's azur eosin methylene blue solution	Merck	Cat#: MEF1092040500
fatty acid free bovine serum albumin	Sigma	Cat#: A8806
palmitic acid (C16:0)	Sigma	Cat#: P0500-10G
oleic acid (C18:1)	Sigma	Cat#: 75090-5ML
tridecanoic acid (C13:0)	Sigma	Cat#: 91988-5G
pentadecanoic acid C15:0	Sigma	Cat#: P6125-1G
MethPrep II (Alltech)	Alltech	Grace 5122149
HCl	Sigma	Cat#: 258148
1-butanol	Sigma	N/A
Chloroform	Sigma	Cat#: 34854
Hexane	Sigma	Cat#: 34484
Methanol	Sigma	Cat#: 34860

(*Continued on next page*)

Continued

REAGENT or RESOURCE	SOURCE	IDENTIFIER
Acetone	Sigma	Cat#: 34850
Ammonium hydroxie	Sigma	Cat#: 221228
Acetic acid	Sigma	Cat#: 27221
Fluorescent NBD PA18:1, 12:0	Avanti Polar Lipids	Cat#: 810176P-1mg
Fluorescent NBD PC 18:1, 12:0	Avanti Polar Lipids	Cat#: 810133P-1mg
PA 18:1, 16:0	Avanti Polar Lipids	Cat#: 840857
PA 14:0, 14:0	Avanti Polar Lipids	Cat#: 830845
PA(C17:0/C17:0)	Avanti Polar lipids	Cat#: 830856
HPTLC60	Merck	Cat#: MEF1056330001
Nile red	Sigma	Cat#: 72485
Chloramphenicol	Sigma	Cat#: C0378-5G
Pyrimethamine	Sigma	Cat#: 46706
Mycophenolic acid	Sigma	Cat#: M3536
Xanthine	Sigma	Cat#: X3627
Fluoro-Gel, (with Tris Buffer)	Electron Micrsoscopy Sciences	Cat#: 17985-10
0.1 M cacodylate buffer	Electron Micrsoscopy Sciences	Cat#: 11650
25% glutaraldehyde	Electron Microscopy Sciences	Cat#: 16220
4% osmium tetroxide	Electron Micrsoscopy Sciences	Cat#: 19150?
uranyl acetate	Electron Micrsoscopy Sciences	Cat#: 22400
Epon812	Electron Micrsoscopy Sciences	Cat#: 13940
Crystal Violet	Sigma	Cat#: C0775
Hoechst 33342	ThermoFisher Scientific	Cat#: 1015-0888
A23187	Sigma	Cat#: C7522
DIMETHYL SULFOXIDE,	Sigma	Cat#: D2438
16% Paraformaldehyde	Electron Microscopy Sciences	Cat#: 15710
Triton X-100	Sigma	Cat#: T9284-100ML
K_2SO_4	Sigma	Cat#: 60528
$MgSO_4$	Sigma	Cat#: M2643
sucrose	Sigma	Cat#: 84100
glucose	Sigma	Cat#: G5400
Tris	Dutscher	Cat#: 091572
BSA	Sigma	Cat#: A9418
HEPES	Sigma	Cat#: H4034
DAPI	Sigma	Cat #: D9542
Critical Commercial Assays		
NucleoSpin Gel and PCR Clean-up	Macherey-Nagel	Cat #: 740609
NucleoSpin Plasmid	Macherey-Nagel	Cat #: 740588
NucleoBond Xtra Midi	Macherey-Nagel	Cat #: 740410
Nucleo spin RNA II	Macherey-Nagel	Cat #: 740955
DNA sequencing	Eurofins Genomics	N/A
Oligo nucleotide synthesis	Sigma	N/A
Q5® Site-Directed Mutagenesis Kit	NEB	Cat#: E0554S
Experimental Models: Cell Lines		
Human Foreskin fibroblasts	ATCC® CCL-171	N/A
Experimental Models: Organisms/Strains		
T. gondii RH TATi1-*ΔKu80*	Sheiner et al., 2011	N/A
T. gondii RHΔKu80	Huynh and Carruthers, 2009	N/A
T. gondii PRU Type II	Marie-France Cesbron Delauw	N/A

(*Continued on next page*)

Continued

REAGENT or RESOURCE	SOURCE	IDENTIFIER
T. gondii ME49 Type II	Jeroen Saeij	N/A
T. gondii ASPV KO	Curt-Varesano et al., 2016	N/A
T. gondii MYR1 KO	Braun et al., 2019	N/A
T. gondii ACASiKD	Dubois et al., 2018	N/A
T. gondii ARO-iKD	Mueller et al., 2013	N/A
T. gondii PKA-iKD	Uboldi et al., 2018	N/A
T. gondii GRA16	Bougdour et al., 2013	N/A
T. gondii ATS1	Amiar et al., 2016	N/A
P. falciparum PfFabI KO	Vaughan et al., 2009	N/A
P. falciparum NF54	Walter and Eliza Hall Institute	N/A
T. gondii ACBP1 iKD	This study	N/A
T. gondii ACBP2 iKD	This study	N/A
T. gondii ACBP1/ACBP3 double KO	This study	N/A
T. gondii ACBP1/SCP2 double KO	This study	N/A
T. gondii ATS2-HA	This study	N/A
T. gondii ATS2-KI	This study	N/A
T. gondii ATS2-KO	This study	N/A
Oligonucleotides		
All primers outlined in materials and methods section.		N/A
Recombinant DNA		
U6-Unversal Plasmid	Sidik et al., 2014 (Addgene)	N/A
Cas9-RFP plasmid	Dominique Soldati	N/A
pTOXO_Cas9-CRISPR	Hakimi Lab, Grenoble, France	N/A
pTOXO_Cas9-CRISPR::g*Tg*ATS2-KI	This study	N/A
pTOXO_Cas9-CRISPR::g*Tg*ATS2-KO	This study	N/A
pTOXO_Cas9-CRISPR::g*Tg*AGPAT-KO	This study	N/A
graCAT-sagMcherry	This study	N/A
pLIC HA3 DHFR	Huynh and Carruthers, 2009	N/A
pLIC HA3 CAT	Sheiner et al., 2011	N/A
ATS2 KO plasmid MAH	This Study	N/A
pPR2 HA3 DHFR	Katris et al., 2014	N/A
graCAT sagmCherry KO plasmid	This study	N/A
Morn1-myc	Marc-Jan Gubbels	N/A
pLIC-*Tg*ATS2-3HA-DHFR	This study	N/A
pLIC-*Tg*AGPAT-3HA-DHFR	This study	N/A
pMORN1-CherryRFP-MORN1/SagCAT	This study	N/A
pQE30Xa vector	Quiagen	33203
Software and Algorithms		
Prism software	GraphPad	N/A
ImageJ	NIH	N/A
Mass Hunter Quantification software	Agilent	N/A
Other		
Gas chromatography-mass spectrometry	Agilent	5977A-7890B

MATERIALS AND METHODS

See STAR Methods **KEY RESOURCES** Table

LEAD CONTACT AND MATERIALS AVAILABILITY

Materials generated in this study are available upon request. Information and requests for resources and reagents should be directed to the Lead Contact, Cyrille Botte (cyrille.botte@univ-grenoble-alpes.fr). Plasmids and parasite lines generated in this study will be made freely available by the Lead Contact upon request which may require the completion of a Material Transfer Agreement.

EXPERIMENTAL MODEL AND SUBJECT DETAILS

T. gondii culture

Toxoplasma gondii parental lines RH TATi1-ΔKu80 (Sheiner et al., 2011) and RH-ΔKu80 (Huynh and Carruthers, 2009) and derived transgenic cell lines were grown in confluent human foreskin fibroblasts (HFFs) in high glucose DMEM supplemented with 1% Foetal Bovine Serum, as described (Amiar et al., 2016). ME49 parental cell cultures were additionally supplemented with 10 mM HEPES.

P. falciparum culture

P. falciparum NF54 wild-type parasites were maintained as previously described (Trager and Jensen, 1976). Briefly, *Plasmodium* blood stage parasites were maintained at 2% hematocrit in 1640 RPMI-HEPES supplemented with 10% AlbuMAX II (GIBCO) and 0.25% gentamycin. Parasites were grown sealed Perspex chambers gassed with beta mix gas (1%O_2 5%CO_2, 94% N_2) at 37°C and maintained on 48-hour cycles.

METHOD DETAILS

Gene identification and sequence analysis
T.gondii plasmid constructs
T.gondii transfection
T.gondii growth assays
T.gondii Red/Green parasite invasion assay:
Plasmodium falciparum growth assays:
Immunofluorescence assay and Microscopy
Nile red staining of lipid droplets
Activity analysis in LPAAT-deficient *E. coli* strains
Transmission electron microscopy:
Lipidomic analysis by GCMS extraction from *T. gondii* tachyzoites
Stable isotope labeling of *T. gondii*
Phospholipid import assay:
Quantification and statistical analysis

Gene identification and sequence analysis

Arabidopsis thaliana sequence of ATS2 (GenBankTM and TAIRTM IDs: NP_194787 and AT4G30580 respectively) was used as a query sequences for BLAST searches against the Toxoplasma gondii genome on ToxoDB database (https://www.toxodb.org/). Phylogenetic analysis of AGPAT related proteins was performed on the Phylogeny.fr platform (Dereeper et al., 2008). Protein sequences were then aligned by ClustalW software (Larkin et al., 2007) and the maximum likelihood phylogeny was generated using the PhyML (Guindon et al., 2010). We generated multiple sequence alignment using Clustal Omega (Li et al., 2015).

T. gondii plasmid constructs

Plasmid LIC-3HA-DHFR was used to generate a 3′ endogenous tagging with 3xHA coding sequence of ToxoDB: TGME49_297640 (*Tg*ATS2) and ToxoDB: TGME49_240860 (*Tg*AGPAT). A 2229 bp fragment corresponding to the 3′ of TgATS2 was amplified from genomic DNA using primer sets 5′-TCCTCCACTTCCAATTTTAGCGTTCGTCTCGGTGGCGGC-3′ and 5′-TACTTCCAATC CAATGCTTCAGACACTCGGTGCAAA-3. A 5466 bp fragment corresponding to promoter and gene sequence of TgAGPAT was amplified using primer sets 5′-TACTTCCAATCCAATGCAGCCAGCAAAGGACGAAAGG-3′ and 5′-TCCTCCACTTCCAATTTTAGC GAGACCGTGGCCTCGGTGGG-3′. These fragments were cloned into pLIC-3HA-DHFR vector as described previously (Huynh and Carruthers, 2009). Vectors LIC-TgATS2-3HA-DHFR and LIC-TgAGPAT-3HA-DHFR were confirmed by PCR screen using primer sets 5′-GCATAATCGGGCACATCATA-3′ and 5′-ATACGCATAATCGGGCACATCATA-3′and by sequencing (Eurofin genomicsTM).

Plasmid pTOXO_Cas9-CRISPR (gift from Hakimi Lab, Grenoble, France) was used to integrate a gRNA within BsaI restriction site as previously described (Sidik et al., 2014). Briefly, Crisp-Fwd and Crisp-Rv primer sets were phosphorylated and annealed: *Tg*ATS2-KI: 5′-AAGTTACGGGTGTGCGCCGCCTTGCG-3′ and 5′-AAAACGCAAGGCGGCGCACACCCGTA-3′, *Tg*ATS2-KO: 5′-AAGTTG GAGCGCCGACGGGCGACTGG-3′ and 5′-AAAACCAGTCGCCCGTCGGCGCTCCA-3′, *Tg*AGPAT-KO: 5′-AAGTTCTCTGCCGAGT TCCAATCGCG-3′ and 5′-AAAACGCGATTGGAACTCGGCAGAGA-3′. The gRNAs were then ligated into pTOXO_Cas9-CRISPR plasmid linearized with BsaI, yielding pTOXO_Cas9-CRISPR::gTgATS2-KI, pTOXO_Cas9-CRISPR::gTgATS2-KO and pTOXO_Cas9-CRISPR::gTgAGPAT-KO, respectively.

For *Tg*ATS2 knockout by CRISPR-CAs9, an appropriate HXGPRT cassette amplified by PCR from pMini (kind gift from the Hakimi laboratory) using those primer sets, TgATS2-KI: 5′-GAGGCCCTGCGTCTCCTCAAGCG- AAAGGCGCCGCCACAGTCGACGGGTGT GCGCC-GCCTCAGCACGAAACCT-TGCATTCAAACC-3′ and 5′-GCTACTCCTTCTTCCCCTCTCG- CGTTGTGTGTCTCCCCGTCG CGTTCTGCGTCGCCAGCAGTGTCACTGTAGCCTGCCAGAACA-3′; *Tg*ATS2-KO: 5′-GACACACAACGCGAGAGGGGAAGAAGGA GTAGCTCTCG-TCGCCTTTCCAGAAGGTACTCCAGCACGAAACCTTGCATTCAAACC −3′ and 5′-CTTCG- CTGCTCGTTCGTCTTC ATGTGGGGAAGGAGCAGCACGAAACCTTG- CATTCAAACC-3′.

DrpA and DrpC were localized by CRISPR Cas9 strategy. Guides were inserted into Cas9 U6 universal plasmid (Sidik et al., 2014) by either standard ligation of annealed primers or Q5 mutagenesis. Cells were transfected together with PCR product encoding either HA3-CAT and DrpC homology flanks, for DrpC or GFP sequence without selection and DrpA homology flanks for DrpA.

For DrpC HA3 CAT CRISPR Cas9 tagging, DrpC was tagged at the 3′ terminus by CRISPR Cas9 (Sidik et al., 2014). For DrpC, the protospacer gaatggggcttgaaactgtg was chosen and primers 5′ AAGTTgaatggggcttgaaactgtgG 3′ and 5′ AAAACcacagtttcaagccc cattcA 3′ were annealed together and ligated into U6 universal plasmid (Sidik et al., 2014). The HA3-CAT cassette was PCR amplified by primers with 50 bp homology flanks (FOR aggaagttccggtcggcttccgtcaccgtt- gaatggggctAAAATTGGAAGTGGAGGACGGG and REV gttcttcccagtgctctggcga- agtgggccagcacaagccaGTTGTAAAACGACGGCCAGTG) and overhang corresponding to the 3′ end of DrpC and in frame with HAx3. 50 μg of both plasmid and PCR product were transfected and placed under chloramphenicol selection (Kim et al., 1993). DrpC was also localized by pLIC-HA3-CAT using primers TACTTCCAATCCAATTTAGCgcacggtctgttgttc tacg and TCCTCCACTTCCAATTTTAGCagccccattcaacggtg (Sheiner et al., 2011). For DrpA, the protospacer gatggaggagttgattcctg was inserted into the Universal Cas9 Plasmid using the NEB Q5 site directed mutagenesis Kit with the oligos 5′ gatggaggagtt gattcctgGTTTTAGAGCTAGAAATAGC 3′ and 5′ AACTTGACATCCCCATTTAC 3′. PCR product was amplified using 5′- gttgccctggctt cctcctctttctctcctctctctcaagATGGCGGTGAGCAAGGGC3′ 5′- cgtcctgcaggcgattgacAacaggaatcaactcctccatCCCGGGCTTGTA CAGC 3′ using GFP cDNA as a template and co-transfected with U6 guide RNA plasmid described above. Transfected parasites were seeded onto coverslips and then transiently observed after 24 hours growth.

For the DrpC PA domain mutation, a guide was identified within a DrpC exon and the 20 bp protospacer (5′ ggcgagctgatcctcgag gt 3′) was inserted into a CRISPR Cas9 plasmid using Q5 with primers 5′ ggcgagctgatcctcgaggt-GTTTTAGAGCTAGAAATAGCA AG 3′ and 5′ AACTTGACATCCCCATTTAC 3′ (Sidik et al., 2014). The PCR product was amplified with the following primers 5′ cgtcgccttgtacggaaacgctt-ggagacgcaaaaacggattGCGGTGAGCAAGGGCG 3′ and 5′ agccccattcaacggtgacggaagccgaccggaacttcc tgcCCCGGGCTTGTACAGC 3′. The guide and the PCR product were transfected together and parasites were seeded onto HFFs on coverslips and grown for 24 h. Cells were labeled with anti-IMC and anti-HA antibodies and viewed under the microscope. Cas9 expression was visualized by the Cas9-RFP tag to observe parasites with DrpC-HA normally (Cas9-RFP absent) or with the PA binding domain disrupted (Cas9-RFP present).

For TgACBP1i-HA KD, the 5′ UTR flank was PCR amplified using primers ACACGGGCCCACGATCAGTTGAGTTCCGAGG and GACACATATGAAGG -TCGAAAGAAGGCTCC and inserted into ApaI/NdeI sites of pPR2-HA3 (Katris et al., 2014). The 3′ flank was amplified using primers CTTGCCCGGGATGGCCTCGCgtaaggaagg and CAGAGCGGCCGCCTGT -GTCGTGAGCGAGTGAC and then inserted in frame with a Tet7O/SAG4 promoter using XmaI/NotI sites. Plasmid was linearized with NotI prior to transfection and selected using pyrimethamine. For ACBP2, flanks were PCR amplified using respective primers below into the plasmid pPR2-GFP or pPR2-mCherry (adapted from pPR2-HA3, (Katris et al., 2014). The 5′ UTR flank was amplified using CTGAGGGCCCGC GACGCTCCAGAAGACTCC and GTACCATA -TGTTATTATATGGTTGAAAGAAGC inserted first using ApaI/NdeI sites. Next, the 3′ UTR flank was amplified using GACTGATATCGATT -ACGGCTTCAACTCCGTC and ATTAGCGGCCGCCTTCATAGGAC -CAGAGCC and inserted using MscI/NotI sites. ACBP2 cDNA sequence was amplified using GATCAGATCTAAAATGGCGAGGCCTGTA CATCTTGGG and GTACCCTAGGAGTAGCTTTTGAGGCGGTG inserted last into BglII/AvrII sites then selected using pyrimethamine. ACBP1 pLIC was PCR amplified using pLIC primers TACTTCCAATCCAATTTAGCTACAACGGAGCAGACAGAGG and TCCTCCACTTCCAATTTTAGCCGCGCTTTTCTCGCGCC into pLIC-HA3-CAT (Sheiner et al., 2011), and linearized prior to transfection and selection on chloramphenicol.

For ACBP1 KO/ACBP2iKD the following protospacer was selected, 5′ GGGGCGTTCCACTGAGAGAA 3′, inserted into a U6-Cas9 expression construct (Sidik et al., 2014). A PCR product w homology flanks for ACBP1 was made with the following primers 5′ ATTTTTTCCAAAGTCCATGCTGGGTTTCTCCCCTG-TGTCTAGGGAGCCTTAAAACCCTCGAAGGCTGCTAGTAC 3′ and

5′ AGATGATTTGACGACACGCGCCTCGGAAGTCGCTCTGTTTACG- CGCTTTTTGCCAGAACACTTGTCAACCG3′ using a graCAT-sag-mcherry resistance cassette as a template and transfected with U6 construct and selected for with Chloramphenicol. For SCP2 KO/ACBP1iKD, the following protospacer5′ GTACGCTTGCTGTGGAAAAA 3′ was inserted into a U6-Cas9 construct and co-transfected with the following primers 5′

gaacaggtgctgacacttgctcgagaatcctgtcgctgcaagttctgagttAAAACCCTCGAAGGCTGCTAGTAC 3′ and 5′ agggcgagtttcacgaaatc ttcgt -ccaacaaagtgatggtgcagtcgcaTGCCAGAACACTTGTCAACCG 3′ using a graCAT-sag-mcherry resistance cassette and selected for with chloramphenicol.

T. gondii transfection

RH-ΔKu80 parasite line was transfected with 100 μg of pLIC-TgATS2-3HA-DHFR linearized with BlpI for stable integration of HA-tag at C terminus of TgATS2. 150 μg pTOXO_Cas9-CRISPR::gTgATS2-KO and pTOXO_Cas9-CRISPR::gTgAGPAT-KO were transfected in TgATS2-HA line with 10 μg of appropriate HXGPRT cassette for *Tg*ATS2-KI and *Tg*ATS2-KO, PCR product as described above. Electroporations were performed in a 2-mm cuvette in a BTX ECM 630 (Harvard Apparatus, at 1,100 V, 25 Ω, and 25 μF. Stable lines expressing the tagged constructs were selected selected in media with 1 μM pyrimethamine or 25 μg/ml mycophenolic acid and 50 μg/ml xanthine and cloned by limiting dilution.

RH-ΔKu80 parasites were also transiently transfected with pLIC-TgAGPAT-3HA-DHFR. pTOXO_Cas9-CRISPR::gTgAGPAT-KO was transfected in RH-ΔKu80 parasites for a simple mutant ΔTgAGPAT and in ΔTgATS2 parasites to obtain a double mutant ΔTgATS2/ΔTgAGPAT. The plasmid pMORN1-CherryRFP-MORN1/SagCAT were transfected in both RH-ΔKu80 and ΔTgATS2 parasite lines.

All other transfections were performed with 50 μg of DNA and electroporation conditions were as described above. Transfected parasites were incubated at different concentration with HFF cell 48 h prior to immunofluorescence assay.

T. gondii growth assays

- Plaque Assay

HFF monolayers were infected with 500 parasites and allowed to develop for 10 days before staining with Crystal Violet (Sigma) and cell growth assessment by light microscopy for the presence of intact HFF. To obtain statistical assessment, each strain was grown in each condition in triplicate and the plaque area in the same square unit (n = 6) are measured. Boxplot with whiskers from minimum to maximum with median.

- Cell-based assay

T. gondii growth was determined with an automatic microscope-based screening (Olympus ScanR, Japan). HFFs were seeded at a density of 10,000 cells per well into 96-well plates and were allowed to grow and equilibrate for 48 h at 37°C. Cells were then infected with 4 × 104 parasites/well. Invasion was synchronized by briefly centrifugation of plate at 250 g and placed at 37°C for 2 h. The assay was run for 30 h. Hoechst 33342 (Life technologies) stain was then loaded on live cells/parasites at 5 μg/ml for 20 min. Infected cells were fixed with PFA (3.7%) for 10 min at 37°C. A mouse anti-GRA1/Alexa488 labeling (dilution 1:500) was used to identify parasitophorous vacuoles. A total of 20 fields per well were taken using the 20X objective. Images were collected for the distinct fluorescence channels (Hoechst 33342: e.g., 360-370 nm, em. 420-460 nm and Alexa488: ex. 460-495, em. 510-550 nm). Images were then analyzed using the ScanR analysis software (Olympus, Tokyo, Japan). For Alexa488 channels images (vacuoles) an intensity algorithm module was used where a fixe threshold was defined with a minimum of 100 pixels size in order to segment the smallest vacuoles (one or two parasite). For Hoechst channel images (parasites nuclei), image process consists to apply a strong background correction and detected parasites with an edge algorithm. A minimum object size of 5 pixels and a maximum object 20 pixels larger one was chosen to discriminate each parasite. ScanR analysis module interface as in flow cytometry allow us to extract and display data as scatterplots and histograms. Using a "gating" procedure we were able to hierarchically filter selected data points with precise boundaries (e.g., number of vacuoles versus number of parasite/vacuoles). The proliferative index was evaluated by parasite/vacuole number ratio. To assess statistically, the samples were prepared in quadruplicate (n = 4).

T. gondii egress assay

WT or Δ*T*gATS2 parasites were incubated on HFF cells for approximately 26 h before aspirating medium and replacing with DMEM containing 2 μM A23187 or DMSO in quadruplicate (n = 4). Parasites were incubated for 3 min before addition of an equivalent volume of 2x fixative containing 5% Paraformaldehyde, 0.05% glutaraldehyde in PBS (final concentration 2.5% Paraformaldehyde, 0.025% glutaraldehyde). Cells were fixed for 15 min before permeabilizing with 0.025% Triton X-100 in PBS for 10 min and then Blocking overnight in blocking solution (2% FBS in PBS). Samples were then probed by immunofluorescence assay and counted manually for egress.

T. gondii Red/Green parasite invasion assay

Experiment was performed as per (Katris et al., 2014). Parasites were grown for 2 days in quadruplicate (n = 4). and harvested intracellular after replacing medium with ENDO buffer (44.7 mM K2SO4, 10 mM MgSO4, 106 mM sucrose, 5 mM glucose, 20 mM Tris-H2SO4, 3.5 mg/ml BSA, pH 8.2). Cells were scraped, needle passed, filtered and centrifuged at 1800 rpm for 10 min. Cells were resuspended to a concentration of 2.5 × 107 cells ml-1 in ENDO buffer and settled for 20 min onto host cells. Once settled, medium was aspirated and replaced with Invasion buffer (DMEM, 3% FBS and 10 mM HEPES). Parasites were allowed to invade for 15 min before fixation with 2.5% Paraformaldehyde and 0.02% glutaraldehyde. Samples were then blocked in 2% FBS in PBS overnight at 4oC. Samples were probed with mouse anti-SAG1, before washing with PBS, then permeabilized with 0.25% Triton

X-100 in PBS. Cells were then probed with rabbit anti-GAP45 and washed in PBS. Samples were then probed with Alexafluor anti-mouse 546 and anti-rabbit 488 before mounting onto slides. Cells were imaged by microscopy and invasion rate determined using ImageJ.

Plasmodium falciparum growth assays

P. falciparum NF54 wild-type parasites and FabI-KO (Vaughan et al., 2009) were maintained as previously described (Trager and Jensen, 1976) at 2% hematocrit in RPMI-HEPES supplemented with AlbuMAX II (GIBCO). Intra-erythrocytic growth assays in standard media were performed by monitoring the replication of tightly synchronous parasites (5% sorbitol) over four asexual cycles as previously described (Mi-Ichi et al., 2006; Mitamura et al., 2000). Media was replaced daily, sub-culturing were performed every 48 h when required, and parasitemia monitored by Giemsa stained blood smears. Growth assays in lipid-depleted media were performed by synchronizing parasites, before transferring trophozoites to lipid-depleted media as previously reported (Botté et al., 2013; Shears et al., 2017). Briefly, lipid-rich AlbuMAX II was replaced by complementing culture media with an equivalent amount of fatty acid free bovine serum albumin (Sigma), 30 μM palmitic acid (C16:0; Sigma) and 45 μM oleic acid (C18:1; Sigma). All assays were performed in triplicates on different days.

Immunofluorescence assay and Microscopy

Parasites were infected to HFF cells grown on coverslips as previously mentioned (Amiar et al., 2016). Primary antibodies used: Mouse anti-HA antibody (Roche, 1:1000), anti CPN60 (1:1000), anti GAP45 (1:1000), rabbit anti-ACP (1:2000), rabbit anti-TOM40 (1:3000), polyclonal rabbit anti-IMC1, anti-MIC4 antibodies (1:1000), rabbit anti-Sumo21 at (1:500) and mouse anti-Sag1 (1:500), anti-LBPA (1:500) or anti-LC3 (1:500). Secondary antibodies: anti-mouse Alexa 488 or 546, anti-rabbit Alexa 546- (ThermoFisher Scientific, 1:10000). Mitotracker (1mM) was diluted in DMEM 1:5000 (100-300 nM working concentration).

For the immunofluorescence assay (IFA) parasites were grown on confluent HFF on coverslips and fixed in PBS containing 2.5% paraformaldehyde (PFA) for 15 min at room temperature (RT). Samples were permeabilized with 0.25% Triton X-100 in PBS for 10 min at RT prior to blocking in PBS containing 3% BSA and subsequent incubation with primary antibodies then secondary antibodies diluted in the blocking solution. Labeled parasites were stained with Hoechst (1:10000, ThermoFisher Scientific) for 20 min and then washed three times in PBS before final mounting of the coverslips on a glass slide using Fluoro-Gel (Electron Microscopy Sciences). The fluorescence was visualized using fluorescence microscope (Axio Imager 2_apotome; ZEISS) with 63x objective.

Nile red staining of lipid droplets

The parasites were allowed to infect and growth in confluent monolayer HFF grown on coverslips, in the ± ATc conditions for x days and then fixed in PBS containing 2.5% paraformaldehyde (PFA) for 15 min at room temperature (RT). Samples were permeabilized with 0.25% Triton X-100 in PBS for 10 min at RT and stained with primary rat anti-HA antibody followed by detection with secondary AlexaFluor 488- conjugated goat anti-rat antibody. Thereafter, the sample coverslips were incubated for 1 h with Nile red in 1X. Lastly, three washing steps with 1X PBS were performed before proceeding to DNA staining with Hoechst. The coverslips were mounted onto a glass slide in fluorogel vefore proceeding to imaging using fluorescence microscope (Axio Imager 2_apotome; ZEISS). For visualizing nile red stained droplets yellow-gold fluorescence (excitation, 450-500 nm; emission, greater than 528 nm) was used on the axio imager. Quantification in ± ATc condition was done by counting the no. of lipid droplets per parasite.

Activity analysis in LPAAT-deficient *E. coli* strains

Escherichia coli strain deficient in LPAAT/AGPAT activity [SM2-1 ΔplsC, Coli Genetic Stock Center #7587, Yale University] (Coleman, 1990) was used to confirm LPAAT activity in both TgATS2 and TgAGPAT.

Coding sequence of *Tg*ATS2 was synthesized (Genscript). TgAGPAT coding sequence was amplified by RT-PCR using primer sets 5′-ATGGCGTCCACGCCGCTGC-3′/5′-TTAGAGACCGTGGCCTCGGTG-3′ and TgAGPATΔN-ter1-72 coding was amplified by RT-PCR using primer sets 5′-CTCAACCGCCCGCCCAGGAATTA-3′/5′-TTAGAGACCGTGGCCTCGGTG-3′. These sequences were digested and ligated into HindIII restriction site on pQE30Xa vector (Quiagen) to generate expression vectors. Additionally, gene coding for *E. coli* LPAAT activity plsC, was amplified from *E. coli* DH5alpha genomic DNA using primer sets 5′-CTATATATCTTTCGTCTTAT TATTAC-3′/ 5′-AACTTTTCCGGCGGCTTC-3′ and ligated into pQE30Xa vector. Then these acyltransferase vectors and empty pQE30Xa vector as negative control were transfected to electrocompetent cells of SM2-1 ΔplsC deficient E.coli. pREP4 repressor vector to regulate Lac promotor activity. Transformed bacterial populations were grown at 37°C in order to promote growth of all isolates. Two independent clones of each bacterial strain that harbors each plasmid-of-interest were isolated for this study. Rescue of LPAAT activity in SM2-1ΔplsC mutant was measured by the ability to grow at elevated temperature, 42°C, non-permissive temperature in LB medium as previously described (Coleman, 1990). Bacteria were first grown in LB media at 37°C to stationary phase, then the cultures were diluted to OD600 = 0.04 and finally inoculated with several dilutions (at 10-1 to 10-6) on LB plates and incubated for 24 h at permissive (30°C) and non-permissive (42°C) temperatures. All experiments were conducted in triplicate with both independent clones.

Transmission electron microscopy

Parasites were grown for 24 h in Labteks (Nunc, Thermofisher) before fixation in 0.1 M cacodylate buffer with 2.5% glutaraldehyde for 2 h. Samples were then kept in fixative. at 4oC until further processing. Sample were then post-fixed 1h with 1% osmium tetroxide in cacodylate buffer followed by overnight in 2% uranyl acetate in distilled water. After dehydration in graded series of acetonitrile, samples were progressively impregnated in Epon812, the wells were then filled with fresh resin and allowed to polymerize 48 h at 60°C. Ultrathin 70 nm section were obtained with a Leica UCT Ultramicrotome and collected on copper grids. Grids were post-stained with uranyl acetate and lead citrate before their observation on a Jeol1200EXII Transmission Electron Microscope. All chemicals were from Electron Micrsoscopy Sciences.

Lipidomic analysis by GCMS extraction from T. gondii tachyzoites

Lipid extraction and analysis of tachyzoites was performed as previously described (Ramakrishnan et al., 2012; Amiar et al., 2016; Dubois et al., 2018). Freshly egressed tachyzoites (1 × 10^8 cell equivalents) grown in standard culture (n = 4) or in starvation culture (n = 3), were metabolically quenched by rapid chilling of the cell suspension in a dry ice/ethanol bath and lipids were extracted in chloroform/methanol/water (2:1:0.8, v/v/v containing 25 nmol tridecanoic acid C13:0 as extraction internal standard) for total lipid analysis.

- For lipid quantification

Total lipid extraction was performed as described previously (Amiar et al., 2016). Parasites were prepared as described above except for the addition of 0.1 M HCl to promote PA and LPA extraction. Pooled organic phase was subjected to biphasic separation by adding 0.1 M HCl. In both protocols, the organic phase was dried with speed vaccum and dissolved in 1-butanol.

- Total lipids analysis

An aliquot of the lipid extract was dried in vacuum concentrator with 1 nmol pentadecanoic acid C15:0 as internal standard. Then the dried lipid was dissolved in the chloroform/methanol, (2:1, v/v) and derivatised with MethPrep II (Alltech). The resulting fatty acid methyl esters was analyzed by GC-MS as described previously (Amiar et al., 2016). Fatty acid methyl esters were identified by their mass spectrum and retention time compared to authentic standards. Lipid data was analyzed using Agilent® Masshunter software.

- Lipid quantification

Total lipid fraction was separated by 2D-HPTLC (Merck) with 5 μg PA(C17:0/C17:0) and 5 μg LPA(C17:0) (Avanti Polar lipids) using chloroform/methanol/28% NH4OH, 60:35:8 (v/v) as the 1st dimension solvent system and chloroform/acetone/methanol/acetic acid/water, 50:20:10:13:5 (v/v/v/v/v) as the 2nd dimension solvent system (Amiar et al., 2016). For DAG analysis, total lipid fraction was separated by 1D-HPTLC using hexane/diethlether/formic acid, 80:20:2 (v/v/v) as solvent system. The spot on the HPTLC corresponding to each lipid was scrapped off and lipids were directly derivatised with 0.5 M methanoic HCl in the presence of 1 nmol pentadecanoic acid (C15:0) as internal standard. The resulting fatty acid methyl esters were extracted with hexane and analyzed by GC-MS (Amiar et al., 2016). Resulted FAME and cholesterol-TMS was analyzed by GC-MS (5977A-7890B, Agilent). FAME was then quantified using Mass Hunter Quantification software (Agilent). All statistical analyses were conducted using GraphPad Prism software. P values of $\leq$ 0.05 from statistical analyses (Ttests) were considered statistically significant.

Stable isotope labeling of T. gondii

Stable isotope labeling using U-^{13}C-glucose (Cambridge Isotope Laboratories, USA), lipid extraction, and GC-MS analysis was performed as previously described in Ramakrishnan et al. (2012) and Amiar et al. (2016). Freshly infected HFF were incubated in glucose-free medium supplemented with 8 mM U-^{13}C-glucose. For FBS starvation study, 5% FBS was add to U-^{13}C-glucose medium in standard culture conditions and 1% FBS was add to U-^{13}C-glucose medium in starvation culture condition. Parasites were harvested 72 h post-infection and metabolites extracted as above.

Phospholipid import assay

Freshly lysed cultures of WT or ΔTgATS2 parasites (n = 3) were harvested, filtered and resuspended in DMEM to a concentration of approximately 2 × 108 cells ml-1. Cells were then mixed with a 2x solution containing 10 μg ml-1 NBD-PA or NBD-PC (5 μg/mL final) and incubated at 37oC. Parasites were then spun down, resuspended in PBS. PFA was then added to a final concentration of 2.5%, and cells were fixed for 15 min before being spun down again and resuspended in 1xPBS. Parasites were smeared onto polyethyleneimine coated coverslips, and then probed with anti-SAG1 primary (1:1000) and anti-mouse Alexa 546 secondary antibodies (1:10000) by immunofluorescence microscopy, stained with DAPI (1:10000) and mounted onto slides. Samples were imaged by microscopy. SAG1 labeling was used to identify parasites using ImageJ and then estimate the amount of NBD-lipid uptaken by the parasites.

QUANTIFICATION AND STATISTICAL ANALYSIS

Statistical analyses for all experiments were performed with Prism software v7 (GraphPad). In experiments comparing only two groups, t test with Holm-Sidak correction were used to compare the experimental group with the control group. For other experiments including 3 groups, non-parametric ANOVA tests (Sidak correction for multiple tests) were used. Individual p values are indicated in each figure. Each experiment was done in n = 3 otherwise mentioned in material metthods. For lipidomic analysis,

Agilent® Masshunter software, was used for fatty acid analysis and subjected to statistical analysis as described above. All error bars present standard error of mean, otherwise mentioned individually.

DATA AND CODE AVAILABILITY

No unique code or software was generated in this study. All datasets generated and analyzed during this study are available upon request to the lead contact Cyrille Botte (cyrille.botte@univ-grenoble-alpes.fr).

Title: *Toxoplasma gondii* acetyl-CoA synthetase is involved in fatty acid elongation (of long fatty acid chains) during tachyzoite life stages

Authors: David Dubois, Stella Fernandes, Souad Amiar, Sheena Dass, Nicholas J. Katris, Cyrille Y. Botté[*¶] and Yoshiki Yamaryo-Botté[*¶]

Affiliation: ApicoLipid Team, Institute of Advanced Biosciences, CNRS UMR5309, Université Grenoble Alpes, INSERM U1209, Grenoble, France.

Summary:

[¶] These authors contributed equally

*Corresponding authors: cyrille.botte@univ-grenoble-alpes.fr; cyrille.botte@gmail.com / yoshiki.yamaryo@gmail.com

Running title: *Tg*ACS is involved in the elongation of fatty acids

Key words: *Toxoplasma gondii*, fatty acid synthesis and elongation, apicoplast, membrane biogenesis, lipidomics, stable isotope labelling

Abstract

Apicomplexan parasites are pathogens responsible for major human diseases such as toxoplasmosis caused by *Toxoplasma gondii* and malaria caused by *Plasmodium* spp.. Throughout their intracellular division cycle, the parasites require vast and specific amounts of lipids to divide and survive. This demand for lipids relies on a fine balance between *de novo* synthesized lipids and scavenged lipids from the host. Acetyl-CoA is a major and central precursor for many metabolic pathways especially for lipid biosynthesis. *Toxoplasma gondii* possesses a single cytosolic acetyl-CoA synthetase (*Tg*ACS). Its role in the parasite lipid synthesis is unclear. Here we generated an inducible *Tg*ACS knockout parasite line and confirmed the cytosolic localization of the protein. We conducted ^{13}C-stable isotope labelling combined to mass spectrometry-based lipidomic analyses to unravel its putative role in the parasite lipid synthesis pathway. We show that its disruption has a minor effect on the global fatty acid composition due the metabolic changes induced to compensate for its loss. However, we could demonstrate that *Tg*ACS is involved in providing acetyl-CoA for the essential fatty elongation pathway to generate fatty acids used for membrane biogenesis. This work provides novel metabolic insight to decipher the complex lipid synthesis in *T. gondii*.

Introduction:

Apicomplexa are unicellular eukaryotes, which most organisms are obligate intracellular parasites. The Apicomplexa phylum comprises important human pathogens such as *Toxoplasma gondii* causing toxoplasmosis and *Plasmodium* spp., the causative agent of malaria. These pathogens represent a global human and social threat against which there is no efficient vaccine and which are becoming increasingly resistant to all marketed drugs, especially in the case of *Plasmodium falciparum,* the major agent of lethal human malaria (1). There is a pressing need for the identification of new drug targets and for the development of novel inhibitors.

Understanding the complex metabolic pathways by which these parasites can obtain the nutrients essential for their survival is an important avenue for drug development. Specifically, lipid synthesis is a pivotal and essential pathway for the parasite during its intracellular development for membrane biogenesis, proper lipid homeostasis and lipid signalling. Due to its complex and unique evolution, the lipid synthesis pathway is highly compartmentalized and forms a puzzle pathway with enzymes of different origins. Indeed, most Apicomplexa (to the exception of Cryptosporidium) harbour a relict non-photosynthetic

plastid named the apicoplast (Apicomplexa plastid) (2, 3), which has been acquired by the secondary endosymbiosis of a red algal ancestor (4). Similarly as in plant and algal plastids, the apicoplast contains a prokaryotic type II fatty acid synthesis pathway, or FASII pathway, that is essential in both *T. gondii* and *P. falciparum (5-10)*. The apicoplast also has the capacity to use FASII fatty acids and form lysophosphatidic acid (LPA) and phosphatidic acid (PA), which are crucial precursors used for the bulk membrane biogenesis and for the survival of the parasite (8, 10-16). Apicoplast-generated fatty acids and LPA are then exported towards the endoplasmic reticulum where they can be elongated and desaturated by elongases and dehydratase to expand the FA range used to maintain the parasite lipid homeostasis in each of its intracellular compartment (7, 15, 17).

In addition to these *de novo* lipid synthesis pathways, parasites are also capable of scavenging lipids and other resources from the host and the external environment. The parasite lipid synthesis, composition and homeostasis depend on a fine-tuning between the *de novo* synthetic pathways, the scavenged lipid moieties and the trafficking of these lipids. Furthermore, parasites can sense the availability of lipids and other nutrients from the environment to modulate the balance between *de novo* and scavenging metabolic pathways and thus maintain membrane biogenesis, proper growth, division, and thus survival and pathogenesis (18-20).

Acetyl co-enzyme A (acetyl-CoA) is a crucial metabolite in the central carbon metabolism of Apicomplexan parasites, including lipid synthesis, and the mitochondrial TCA cycle(7, 21-25). Indeed, the main precursor of the apicoplast FASII is acetyl-CoA, which is generated via the apicoplast pyruvate dehydrogenase (PDH) (6). The apicoplast PDH is fuelled via the import of phosphoenolpyruvate, which is generated via the cytosolic glycolysis pathway and then transported via the apicoplast phosphate transporter (APT, also named the apicoplast triose phosphate transporter in *P. falciparum (7, 23)*, in a similar manner as in plant plastids (26-29). The ER fatty acid elongation pathway also requires acetyl-CoA as a carbon source to elongate the apicoplast generated fatty acids. Unlike plants and most eukaryotes, Apicomplexan mitochondria lack a canonical PDH to synthesise Acetyl-CoA, essential for the TCA cycle (21). Instead, the parasite uses a Branched-chain Keto acid dehydrogenase (BCKDH) that possesses a dual function to also make acetyl-CoA for the TCA cycle (21, 30). In *T. gondii,* acetyl-CoA can also be made via a cytosolic ATP-citrate lyase (*Tg*ACL) using a by-product of the TCA cycle, oxaloacetate, unlike *P.*

falciparum that seems to lack a homolog of *Tg*ACL. However, both *T. gondii* and *P. falciparum* possess a single acetyl-CoA synthetase (ACS) that can use acetate imported from the host and/or the external environment to for acetyl-CoA by active transfer of acetate to the Co-enzyme A (CoA) (22). Recent analysis of the *T. gondii* ACS and ACL showed that each enzyme is dispensable alone but that the dual knockout parasite strain for *Tg*ACS and *Tg*ACL is not viable (30). Taken together these data point at the importance of acetyl-CoA and its synthesis in the metabolism of these parasites. To date, no metabolomic analysis has been performed to unravel the metabolic role of *Tg*ACL and especially *Tg*ACS, which is the sole enzyme capable of using a scavenged substrate, *i.e.* acetate, for acetyl-CoA synthesis.

Here we generated an inducible knock-down of the *T. gondii* ACS, *Tg*ACS-iKO. We conducted state of the art stable isotope labelling, using ^{13}C-Uglucose and ^{13}C-U-acetate, combined to mass spectrometry-based lipidomic analysis of the *Tg*ACS-iKO to determine its putative role in fatty acid synthesis and fatty acid elongation, respectively. We report that the enzyme contributes to the parasite lipid synthesis pathways, specifically for the elongation of fatty acid by the ER elongases whereas it does not participate in the *de novo* synthesis pathways for fatty acid synthesis. This is the first report that *Tg*ACS has a role beyond being a source of acetyl-CoA for protein acylation and histone acylation and shows the versatility of the parasite to confront its metabolic demand and nutrient availabilities.

Results

*Tg*ACS is a cytosolic protein that is not essential during tachyzoite stage.

In order to identify the role of acetyl-CoA synthetase (ACS), we first searched for a candidate ACS in *T. gondii* genome using the ToxoDB website (http://toxodb.org/toxo/). We found a predicted gene annotated as ACS (accession number: TGGT1-266640) based on sequence homology with other characterised ACSs (31-33). The candidate protein was bearing typical domains for ACS such as AMP binding (PF13193) and CoA binding (TIGR02188). Comparison of *Tg*ACS protein sequence against the one of *Salmonella enterica*, *Se*ACS, which protein was crystallized (34), showed a high level of conservation between the two proteins. Indeed, alignment showed a 52% identity over 91% of the protein covered when comparing *Se*ACS to *Tg*ACS. Most residues involved in CoA binding, (*i.e.* F222, A223, G224, R250, K253, I255, A417, S585, G586, H587, R588, K642, R646) and AMP binding (*i.e.* I370, V446, T472, Y473, W474, 8475, T476, E477, I574) (**Fig1. A**) are identical or highly conserved as well. Furthermore, we searched for homologs of ACS in

Plasmodium falciparum and the chromerids, *Chromera velia* and *Vitrella brassicaformis*, and found putative candidates, *Pf*ACS (PF3D7_0627800, the enzyme likely responsible for the acetyl-CoA synthesis from acetate described in (22) *Cv*ACS (Cve1_1982) and *Vb*ACS (VBra_8944), respectively. We compared those to protein sequence of *Se*ACS, *Tg*ACS, and human ACS, which showed that there is a high homology amongst these divergent organisms (**Fig. S1**). This, added to the fact that recombinant *Hs*ACS was shown to generate acetyl-CoA from acetate (35), strongly supports that the *Tg*ACS gene locus is encoding for an active ACS. We furthermore performed *in silico* protein threading (or homology modelling) against the crystal structure of *S. enterica*. Predicted *Tg*ACS structure can merge together with that of *S. enterica* and conserves the structural amino acids localization of predicted substrates binding Co-A and AMP with high scores and confidence from the prediction software. This high structural conservation is indicative of an important and fundamental requirement of ACS in the cellular function and homology to characterized ACS (**Fig. 1B-F**).

In order to localize *Tg*ACS, we generated a construct that expressed *Tg*ACS fused to a C-terminal triple haemaglutinin (3×HA) epitope-tag under control of an anhydrotetracycline (ATc)-regulated promoter (*Tg*ACS-HA-iKO, **Fig. 2A, B, C**). This *Tg*ACS-HA-iKO strain enables us to analyze the effect of disruption of *Tg*ACS. Two independent mutants were generated within a *T. gondii* TATi_Δ*Ku80* background(36), the successful replacement of the endogenous locus was confirmed via PCR (Fig.2C). Immunofluorescence assays (IFA) using anti-HA antibody showed that *Tg*ACS-HA was localised within the cytosol of the parasite similarly to previous reports (30, 37) (**Fig. 3A, upper panels**). The effect of repression of *TgACS* was observed by IFA after the addition of ATc (0.5 μg/mL) to the parasite culture (**Fig. 3A, lower panels**). The addition of ATc led to significant loss of HA signal within two days post after the treatment with ATc (**Fig. 3A**), suggesting that *TgACS* most likely is not essential for *in vitro* growth for parasites.

We then analysed the effect of ATc on the *Tg*ACS-HA protein level via western blot analysis. *Tg*ACS-HA protein was detected as a single distinct band with an apparent molecular mass of 80 kDa corresponding to its predicted molecular weight of 79.8 kDa. The addition of 0.5 μg/mL ATc to the culture medium down-regulated *TgACS*-HA expression and the protein was undetectable after three days of ATc treatment (**Fig. 3B**). This kinetics complements the rapid loss of *Tg*ACS-HA signal observed during IFA.

While the loss of *Tg*ACS-HA did not affect parasite morphology, we investigated possible growth defects through plaque assays. The knockdown of *TgACS* lead to no

discernable alteration in plaque size so as ATc treatment of the parental lines produced no detectable growth retardation (**Fig. 3CD**). This suggested that *TgACS* is not essential in accordance with a recent genome wide analysis of essential genes in *Toxoplasma* by CRISPR-Cas9 knockout, which pointed at the likely non-essential role of *TgACS* (38).

***TgACS* disruption slightly alters the total fatty acid content of the parasite.**

Since the *ACS* gene encodes for an enzyme to produce acetyl-CoA, a major precursor for fatty acid synthesis and fatty acid elongation, it is possible that loss of *TgACS* may alter the lipid profile of the parasite. We first qualified and quantified the fatty acid content in the *Tg*ACS-HA-iKO parasite in the absence and presence of ATc for 4 days. Fatty acid moieties of glycerolipids were derivatised to fatty acid methyl ester (FAME), then FAMEs were quantified by gas chromatography-mass spectrometry (GC-MS, 5977A-7890B, Agilent Technology). There was no major difference in total fatty acid content between the reference and induced *Tg*ACS knockout strains (**Fig. 4A**). However, slight differences in the fatty acid composition could be detected (**Fig. 4BC**). Although *Tg*ACS can generate acetyl-CoA that is hypothesized to be used for the elongation of fatty acids, there was slight yet non-significant decrease in the longer chain fatty acids amount known to be produced via the elongation pathway(7) such as C20:1, C22:1, C24:1. Interestingly, however, in the ATc treated parasite, the apicoplast FASII-generated C12:0 and C14:0 were decreased significantly, while C22:6, a fatty acid source believed to be scavenged from the host, was significantly increased.

***TgACS* disruption does not impair apicoplast fatty acid synthesis.**

To determine the potential role of *Tg*ACS for fatty acid synthesis, including *de novo* fatty acid synthesis in the apicoplast and FA elongation in the ER, we performed metabolic labelling on ATc-treated and untreated *Tg*ACS-iKO-HA parasites with stable isotope precursors, *i.e.* ^{13}C-universally labelled carbon substrate, U-^{13}C-glucose or U-^{13}C-acetate, respectively. These substrates can be incorporated to the parasites and are used for the fatty acid synthesis in different pathways (7, 15, 39). Incorporation of ^{13}C-glucose to fatty acids determines the *de novo* synthesized fatty acids via FASII in apicoplast (7, 15, 39), whereas the incorporation of ^{13}C-acetate to fatty acids determines the elongation of fatty acids in cytosol (7, 17). The resulting labelled fatty acids can be distinguished by the shift of mass by GC-MS. The degree of the incorporation of ^{13}C into fatty acids (%carbon incorporation) is determined by the mass isotopomer distribution (MID) of each FAMEs. These together can delineate the exact effect on lipid metabolism of *Tg*ACS knockdown. MID can be obtained

from the shift in isotopic mass dependent on the amount of ^{12}C carbons compared to the integration of ^{13}C carbon atoms. For example, myristic acid (C14:0) consists of a carbon backbone of 14 carbons in length, the most common isotope would contain only ^{12}C with a detectable mass-to-charge ratio of m/z=228, as no ^{13}C has been incorporated we call this isotope mass 0 (M0). Integration patterns vary from one carbon to fully labelled, incorporation of four ^{13}C leads to an increase in mass by four, M+4, m/z=232. These isotopic distributions allow us to determine the metabolic flux and processes involved in lipid biosynthesis.

To investigate the role *TgACS* in the *de novo* lipid synthesis, we first labelled *Tg*ACS-HA-iKO parasites with U-^{13}C-glucose for 4 days continuously with ATc to disrupt *Tg*ACS similarly to the condition analysed for the total fatty acid composition (**Fig. 4**). Labelling for 4 days of ATc treatment and labelling with U-^{13}C-glucose showed no significant alteration for ^{13}C incorporation for all the fatty acid species analysed (**Fig. 5A**). MID analysis of C14:0 showed the typical two by two mass increase up to the M+14 mass due to ^{13}C from 6 carbon glucose was metabolised to 2 carbon acetyl-CoA in the apicoplast (**Fig. 5B**). This two by two went up to M+14 to show the full synthesis of C14:0 by the apicoplast FASII as we previously reported (15). Similarly, the MID analysis of C20:0, showed the full synthesis up to M+14 and M+16, mainly, correlating the origin of C20:0 from the apicoplast FASII major products C14:0 and C16:0 (**Fig. 5C**) (7, 15).

Since 4 days of labelling still includes 2 days of expression of active *Tg*ACS protein (**Fig. 3B**), most of the ^{13}C-Carbon integration may have occurred before the loss of *Tg*ACS potentially masking obvious difference between the knock-down mutant and its parental line. To measure the direct effect of loss of *Tg*ACS, we grew parasites with or without ATc for 48 h prior to the addition of U-^{13}C-glucose (pre-treatment 2 days). Then parasites were incubated with U-^{13}C-glucose for the next 72 h. In this condition, overall incorporation of ^{13}C-Carbon integration was reduced to approximately half of 4-day labelling (**Fig. 5D**). Here again, there was no significant difference between ATc treated and non-treated parasites in the integration of ^{13}C-carbon in fatty acids from glucose. In addition, the integration pattern of ^{13}C to apicoplast generated fatty acids, C14:0, showed clear two by two increase of mass up to M+14 in both condition (**Fig. 5E**), suggesting there was no activation or alteration of FASII upon the loss of *Tg*ACS. MID analysis of C14:0, however, showed a significant reduction of ^{13}C incoporation in the M+12 and M+14 isotopologues in the *Tg*ACS knock-down mutant.

This slight reduction of relative abundance for the M+14 (and M+12) could be a sign of slight reduction of the FASII activity.

TgACS disruption significantly alters endoplasmic reticulum fatty acid elongation pathway

To investigate if acetyl-CoA generated by *Tg*ACS is involved in the elongation of fatty acid, we first labelled parasites with U-^{13}C-acetate continuously for 4 days with or without ATc (**Fig. 6**). In this condition, there was incorporation of ^{13}C label to all fatty acids analysed in both with or without ATc. Interestingly, the ^{13}C incorporation from acetate to shorter fatty acids, C14:0, C16:0 in the *Tg*ACAS- HA-iKO with ATc was significantly higher than that without ATc (**Fig. 6A**). In the meantime ^{13}C incorporation to longer fatty acids known to be products of the elongation pathway, especially C18:1, C20:0 and C20:1, was significantly reduced (**Fig. 6A**). MID analysis of ^{13}C integration into C14:0 and C16:0 showed that the measured labelling increase displayed an unusual pattern of M+1 incoporation from M+2 to M+8 (**Fig. 6BC**). However, there was no sign of two by two increase of the mass, which was seen in the U-^{13}C-glucose as signature of apicoplast FASII suggesting acetate was not directly incorporated into the apicoplast as a substrate for FASII but rather that acetate was catabolised to a single carbon molecule and then metabolised to be used in FASII pathway. MID analysis of C20:0 did not show clear increase of M+2, M+4, a usual signature for the elongation pathway (**Fig. 6D**). Although ^{13}C incorporation from acetate was altered, there was no total abrogation of such incorporation. Taken together, this also suggest 4 days of incubation with U-^{13}C-acetate with or without ATc was likely too long and may not be the best suited approach to determine effect of the loss of *Tg*ACS.

We thus treated parasites with ATc for two days prior to addition of U-^{13}C-acetate and grown for a further two-days (pre-treatment 2 days) to suppress most of *Tg*ACS presence in the parasite. In this condition, ^{13}C integration from ^{13}C-acetate was almost abrogated in most long fatty acid chains C18:0, C20:0, C22:0 and C24:0 generated via the elongation pathway (**Fig. 6E**). Here, no incorporation of ^{13}C to C14:0, C16:0 in both strains was observed (**Fig. 6FG**) suggesting that what observed in **Fig. 6BC** was probably due to the catabolism of acetate due to long incubation in the course of *Tg*ACS deactivation. The MID analysis of C20:0, showed a clear increase of M+2, and M+4, in the absence of ATc (*i.e.* wild type condition), which is the signature of elongation of the FASII products C18:0 and C16:0 (15). However, in the presence of ATc, *i.e.* lack of *Tg*ACS, labelled C20:0 did not contain any

increase of M+2 and M+4 (**Fig. 6H**). This clearly suggests that the loss of *Tg*ACS could not provide the substrate, acetyl-CoA for the elongation of fatty acids. Similar results were measured for the other altered FA chains, suggesting that C18:0 is elongated from C16:0, C22:0 from C18:0 and C16:0, C20:1 predominantly from C18:1mainly and slightly from C16:1/0 and C24:0, C16:0 and C14:0 (**Fig. S2**). Collectively these metabolic results indicate that the loss of *Tg*ACS leads to a reduction in the elongation of FA by the lack of acetyl-CoA it produces for the pathway.

Discussion:

In this study we determined the role of the sole enzyme capable of generating acetyl-CoA from a scavenged substrate (*i.e*. acetate) for lipid synthesis in *T. gondii*. Indeed, acetyl-CoA is a central metabolite that is involved in the TCA cycle, fatty acid synthesis, fatty acid elongation and post-translational protein acylation, including histone acylation for genetic regulation. The apicoplast FASII pathway generates its own pool of acetyl-CoA via the apicoplast PDH and the mitochondrial BCKDH generates the acetyl-CoA required to initiate the TCA cycle(30). The source and role of acetyl-CoA for cytosolic fatty acid synthesis via the FASI pathway and the endoplasmic reticulum elongation pathway remain to be fully understood. Previous studies showed that *T. gondii* possesses two enzymes capable of generating acetyl-CoA: the acetyl-CoA synthetase (*Tg*ACS) and the ATP-citrate lyase (ACL) (30). Where *Tg*ACS is theoretically capable of using acetate and binds it to CoA, *Tg*ACL uses existing citrate from the TCA to generate acetyl-CoA. Interestingly the localization of *Tg*ACS shows a uniform cytosolic and nuclear localization, as previously described (30, 37). The nuclear localization supports the potential role of *Tg*ACS for providing acetyl-CoA in the nucleus for histone acetylation. Further analysis to determine its putative role in histone modification and chromatin remodelling by determining *T. gondii* acetylome on the *Tg*ACS-iKO mutant would be important to conduct. Here, we disrupted *Tg*ACS and were able to determine its role in generating acetyl-Coa for fatty acid biosynthesis.

The loss of *TgACS* disrupts the typical mechanism of FA elongation, which relies on three elongases together essential for parasite survival (7). Here our results clearly demonstrate that the acetyl-CoA generated by *Tg*ACS is used by the elongases to contribute to the production of many elongated FA initially produced by the apicoplast FASII (C18:0, C18:1, C20:0, C20:1, C22:0, C24:0) (**Fig. 7,** 15). The lack of major changes in the FA composition and the non-lethal phenotype of *Tg*ACS-iKO mutant clearly support the

presence of another source of acetyl-CoA for the essential FA elongation pathway. This is likely a redundant role of *Tg*ACL as previously shown when both *Tg*ACS and *Tg*ACL were knocked out, which eventually killed the parasite. (30)This hypothesis is also strengthened by the increase of ACL abundance when *Tg*ACS is disrupted (30). Interestingly, *P. falciparum* seems to lack a homolog to the citrate lyase and possesses the sole ACS to generate acetyl-CoA from acetate (22), which seems essential for the parasite (40). Further analyses are a prerequisite to understand the differences between *T. gondii* and *P. falciparum* lipid synthesis and use of acetyl-CoA.

Genetic ablation of *Tg*ACS does not kill the parasite; however, metabolic plasticity enables continued parasite survival via providing alternate substrate options maintaining elongation at a suitable level as measured by the absence of major changes in the total FA composition. As an evidence of such compensation, upon the loss of *Tg*ACS, C12:0 and C14:0, major products of FASII (15), decrease, whilst C22:6, a FA chain believed to be scavenged (7, 41), increases. When we incubated parasites with ^{13}C-U-acetate for 4 days, the incorporation of labelling was observed in both *Tg*ACS-iKO with or without ATc although ^{13}C-U-acetate was not supposed to be used as substrate for the *de novo* fatty acid synthesis, i.e. incorporation to short chain fatty acids, C14:0 fatty acids. In addition, the labelling in C14:0 was more abundant upon the loss of *Tg*ACS suggesting that parasite enhanced some metabolic pathway and used acetate for *de novo* fatty acid synthesis upon the loss of *Tg*ACS. First of all, it should be noted that both *Tg*ACS-iKO with or without ATc had incorporation of ^{13}C-U-acetate to C14:0 only up to M+7 and to C16:0 only up to M+8 in each masses. This means only one carbon of acetyl-CoA was labelled with ^{13}C, therefore parasites have only half of number of fatty acid chain is labelled in continuous manner without two by two steps. This was only observed when parasites were incubated for four days with ^{13}C-U-acetate with or without ATc but not in two days even in the –ATc condition. This suggests that acetate was not directly used for the TCA cycle similarly shown in *Plasmodium*, that^{13}C labeled acetate is rapidly incorporated to acetyl-CoA and then to acetylated alanine and acetylated glutamate but not to keto-glutarate, TCA intermediate (22). It is possible that acetate was recycled from those acetylated amino acid to be metabolized to pyruvate probably via TCA cycle to serve a precursor for the *de novo* fatty acid synthesis. Another potential explanation for these is the un-used acetate was catabolised to give single carbon molecule, bicarbonate and CO_2 to be used in another metabolic pathway. Finally, *T. gondii* is able to generate propionyl-CoA from the degradation of leucine, isoleucine, and valine (42). This propionyl-

CoA is toxic for the cell and needs to be detoxified. One alternative way to degrade it would be through its utilization as a substrate in place of acetyl-CoA, which would potentially explain the +1 increase that we measured (**Fig. 6**).

Interestingly, accumulation of acetate in rats has been shown to down-regulate the expression of lipogenic genes such as (a) pyruvate kinase (PyK), which catalyses the synthesis of pyruvate for the generation of acetyl-CoA for fatty acid synthesis by the FAS, (b) acetyl-CoA carboxylase (ACCase), which catalyses the synthesis of malonyl-CoA the other essential substrate for the FAS pathways (both type I and II), and (c) FAS (43). All of these enzymes are present in *T. gondii* and could putatively be regulated by an accumulation of acetate following *Tg*ACS disruption; pyruvate kinase is present in two essential isoforms in *T. gondii, Tg*PyKI, likely in the cytosol and *Tg*PyKII dually localized in the mitochondrion and the apicoplast (44, 45), ACCase is also present in two copies one in the apicoplast to fuel the FASII and one likely in the cytosol potentially for FASI and/or elongases (46). Furthermore, it has also been shown that ACCase can be down regulated when there is the accumulation of the FASII products (47). So it is possible that the accumulation of C14:0 that is not elongated anymore due to the lack of acetyl-CoA provided by *Tg*ACS could indeed inhibit the FASII pathway as we observed in this work. Similarly, the abrogation of ^{13}C incorporation from acetate in C18:1 in the 2 days pre-treatment (**Fig. 6E**) might be explained by a massive scavenging of C18:1 from the external environment to compensate for the loss of its synthesis via the elongation pathway. Altogether our observations conclude that *Tg*ACS loss perturbed the fatty acid metabolism the causing modification of lipid balance in the induced knockout due to its role in providing acetyl-CoA for FA elongation.

One of the important questions that remain unanswered is the origin of the acetate used by *Tg*ACS. In human blood, it is said to contain 50-200 μM of acetate. Here in vitro, supplemented FBS also contains certain amount acetate (48), but this is possibly irrelevant because thus far, no transporter for acetate has been identified in Apicomplexa. Furthermore ^{13}C-Glucose labelling in *P. falciparum* shows that a small part of the intracellular acetate pool originates from glucose but that most of it is of unknown origin (22). Although acetate can be found in the extracellular environment, its origin in Apicomplexa might not be from importing it but maybe as a downstream product of host or parasite metabolism.

In summary, we demonstrated that (a) *Tg*ACS is a non essential enzyme present as a uniform protein of the cytosol and likely the nucleus, (b) it does not participate in providing substrate for the de novo synthesis of FA by the apicoplast FASII, (c) that its disruption does not have

much influence over the parasite FA composition but (d) that it provides acetyl-CoA for the elongation of FA, and actively participates to this pathway, essential for parasite survival (7). These data show for the first time that one of the enzymes capable of the synthesis of Acetyl-CoA is also involved in the parasite lipid synthesis and the plasticity of *T. gondii* to compensate for the loss of proteins participating in these crucial pathways for membrane biogenesis.

Materials and Methods

Sequence analysis and structure generation

*Tg*ACS gene (TGGT1-266640) was identified by using toxoDB (http://toxodb.org/toxo/) and alignment with *Salmonella enterica,* was performed on Multalin (http://multalin.toulouse.inra.fr/multalin/multalin.html (49). The 3D structure was determined via protein threading against the previously crystallized *S. enterica* ACS, (34) using SwissProt bioinformatics (https://swissmodel.expasy.org/).

T. gondii strains and cultures

T. gondii tachyzoites (RH-ΔKu80 TATi (36) and *TgACS*-iKO-HA) were maintained in human foreskin fibroblasts (HFF) using Dulbecco's Modified Eagle's Medium (DMEM, Gibco) supplemented with 1% foetal bovine serum (FBS, Gibco), 2 mM glutamine (Gibco) and 25 μg/mL gentamicin (Gibco) at 37°C and 5% CO_2.

Construct design

TgACS (TGGT1-266640) gene sequences was obtained from ToxoDB. The *TgACS* open reading frame was PCR amplified using primers 5'- GAAGATCT ATGGAGAAAGATAGGAACACTATGGAGGG and 5'-. TGGCCTAGGAGCTTTCGCA-AGAGAGCCCC, *TgACS* un-translated flanking regions were generated using the following primers, 5' UTR 5'-GGAATTCCATATGTACTTTCCACATACGTCTGCTTGTGC and 5'-GGAATTCCATATGGGTGTTCCTGGTTCTGAAATGTTGC and the 3'UTR with 5'- AT-ACCCGGGACGATTTATACACATGGTTAGACCAGGC and 5'- ATAAGAATGCG-GCCGCACGTCCTTCATTAGCCATCTGTTGC. PCR was performed using PrimeSTAR Max DNA Polymerase (TaKaRa, Japan) denaturing at 98ºC for 10 s and annealing at 60ºC for 10 s and extension at 72ºC (1 min/kbp). These PCR products were then inserted into the vector pDt7s4H (Fig. 1B) (50, 51)). The resulting construct was transfected into *T. gondii* RH Ku80_TATi strain parasites as described (15). Transfected parasites were then selected on

pyrimethamine and cloned. Mutant clones with successful replacement of the native *Tg*ACS gene locus with the resistant cassette and inducible promoter together with CDS was confirmed by PCR using their genomic DNA as template and following primers as indicated in the figure2: Primer1,5'_AACGCACACACAAATGCTCC_3'; Primer2, 5'_GCGTCGTTTTTGTCAC-ACGA_3'; Primer3, 5'_ACGAACCATGTCGA-GGCTTT_3'; Primer4, 5'_CGTAG-TCCGGGACATCGTAC_3'; Primer5, 5'_GTACGATG-TCCCGGACTACG_3' and Primer6, 5'_ACCTTCATAGAGGCAGCCGA _3'.

Antibodies and immunofluorescence assays

Primary anti-CPN60 (rabbit) antibodies were used at a dilution of 1/6000, anti-HA at 1/1000 (Mouse, Invivogen). Secondary AlexaFluor 488- and 546-conjugated anti-mouse and anti-rabbit antibodies (Life Technologies) were used at 1/10000. Parasites were grown on confluent HFF on coverslips and fixed in PBS containing 4% paraformaldehyde for 30 min, at room temperature (RT). Samples were permeabilized with 0.1% Triton X-100 in PBS for 10 min at RT before blocking in PBS containing 3% BSA and incubation with primary antibodies then secondary antibodies diluted in the blocking solution. Labelled parasites were stained with Hoechst (1/10000, Life technologies) for 20 min and then washed three times in PBS then H_2O. Coverslips were mounted onto slides prior to observation using an epifluorescent microscope (Zeiss, Germany).

Western blotting

Protein expression was analysed by western-blot on freshly egressed parasites. Equal amount (50 μg) of protein were boiled in SDS-PAGE buffer separated on a 4–12% gradient SDS-polyacrylamide (Life Technologies) and transferred to PVDF membrane (Millipore) using the XCellII Blot Module (Invitrogen). The membrane was blocked with skim milk and then probed with monoclonal mouse anti-HA antibodies (InvivoGen) at 1:2000 and mouse anti-Gra1 antibodies at 1:3000. Secondary Goat anti-mouse HRP conjugated antibodies (Thermo Scientific) were used at 1:20000. Signal was detected after membrane staining with Luminata Crescendo Western HRP detection kit (Millipore).

Phenotypic analysis

Plaque assays were performed with 500 parasites infected to HFF confluent monolayers in culture flasks (25 cm^2). *Tg*ACS-HA-iKO parasites were grown in the presence or absence of ATc 0.5 μg/mL for 10 days. Then cells were fixed with ethanol and followed by staining with Crystal Violet (Sigma).

Lipid extraction from *T. gondii* tachyzoites and gas-chromatography mass spectrometry analysis

Intracellular tachyzoites (1×10^8 cell equivalents per replicate) were harvested after metabolic quenching in dry ice-ethanol (100%) to rapidly stop the metabolism as previously described (7, 52). Then total lipids were extracted in chloroform/methanol/water (1:3:1, v/v/v containing 25 nmol tridecanoic acid (C13:0) as internal standard for extraction) for 1 h at 4°C, with periodic sonication. Then polar and apolar metabolites were separated by phase partitioning. For lipid analysis, the organic phase was dried under N_2 gas and dissolved in chloroform/methanol, 2:1 (v/v). Then the lipid was mixed with 1 nmol pentadecanoic acid (C15:0) as internal standard and derivatised using MethPrep II (Alltech). The resulting fatty acid methyl esters were analysed by GC-MS as previously described (7, 52). All fatty acid methyl esters were identified by comparison of retention time and mass spectra from GC-MS with authentic chemical standards. Then fatty acid methyl esters were normalized to cell number and extraction efficiency and quantified. The experiments were repeated as indicated using each independent mutant line as a biological replicate.

Stable isotope metabolic labelling of *T. gondii* fatty acids.

Stable isotope metabolic labelling experiment using U-^{13}C-glucose or U-^{13}C-acetate (Cambridge Isotope Laboratories, USA) followed by lipid extraction and GC-MS analysis was performed as previously described (7, 15, 52). Parasites were infected to confluent HFF and incubated in the presence or absence of ATc (2 μM, Sigma-Aldrich). For the change of ^{13}C labelling in the course of *Tg*ACS-HA suppression by ATc, glucose-free medium supplemented with a U-^{13}C-glucose or U-^{13}C-acetate at a final concentration of 8 mM was used concomitant with the inoculation of parasites, and parasites were harvested after four days. For the change of ^{13}C labelling after the loss of *Tg*ACS protein by ATc, parasites were grown for 72 h in the normal media. Then medium was replaced with glucose-free medium supplemented with ^{13}C-U-carbon source (concentration as above) while presence or absence of ATc is maintained. 24 h the incubation with ^{13}C source medium, parasites were harvested for the lipid analysis as above. Other supplements (glutamine, sodium bicarbonate, and foetal bovine serum) were added according to normal culture conditions, minimal concentration of ^{12}C-glucose (800 μM final concentration) was added to the cultures for ^{13}C-U-acetate labelling experiment. All lipids were then analysed by GC-MS after derivatisation using Methprep II (Alltech). Mass shift in each mass spectra of each fatty acids were analysed to assess the incorporation of ^{13}C to fatty acids.

Acknowledgments

This work was supported by Agence Nationale de la Recherche, France (Grant ANR-12-PDOC-0028- Project Apicolipid), the Atip-Avenir and Finovi programs (CNRS-INSERM-Finovi Atip-Avenir Apicolipid projects), and the Laboratoire d'Excellence Parafrap, France (grant number ANR-11-LABX-0024). CYB is a CNRS Atip-Avenir Fellow.

Reference:

1. W.H.O. 2017. World malaria report 2017. *In*. World Health Organization, Geneva.
2. McFadden, G. I., M. E. Reith, J. Munholland, and N. Lang-Unnasch. 1996. Plastid in human parasites. *Nature* **381**: 482-482.
3. Kohler, S. 1997. A Plastid of Probable Green Algal Origin in Apicomplexan Parasites. *Science (New York, NY)* **275**: 1485-1489.
4. Janouskovec, J., A. Horák, M. Oborník, J. Lukeš, and P. J. Keeling. 2010. A common red algal origin of the apicomplexan, dinoflagellate, and heterokont plastids. *Proc. Natl. Acad. Sci. U. S. A.* **107**: 10949-10954.
5. Waller, R. F., P. J. Keeling, R. G. Donald, B. Striepen, E. Handman, N. Lang-Unnasch, A. F. Cowman, G. S. Besra, D. S. Roos, and G. I. McFadden. 1998. Nuclear-encoded proteins target to the plastid in Toxoplasma gondii and Plasmodium falciparum. *Proc. Natl. Acad. Sci. U. S. A.* **95**: 12352-12357.
6. Mazumdar, J., E. H Wilson, K. Masek, C. A Hunter, and B. Striepen. 2006. Apicoplast fatty acid synthesis is essential for organelle biogenesis and parasite survival in Toxoplasma gondii. *Proc. Natl. Acad. Sci. U. S. A.* **103**: 13192-13197.
7. Ramakrishnan, S., M. D. Docampo, J. I. Macrae, F. M. Pujol, C. F. Brooks, G. G. van Dooren, J. K. Hiltunen, A. J. Kastaniotis, M. J. McConville, and B. Striepen. 2012. Apicoplast and Endoplasmic Reticulum Cooperate in Fatty Acid Biosynthesis in Apicomplexan Parasite Toxoplasma gondii. *J. Biol. Chem.* **287**: 4957-4971.
8. Yu, M., T. R. S. Kumar, L. J. Nkrumah, A. Coppi, S. Retzlaff, C. D. Li, B. J. Kelly, P. A. Moura, V. Lakshmanan, J. S. Freundlich, J.-C. Valderramos, C. Vilcheze, M. Siedner, J. H. C. Tsai, B. Falkard, A. b. S. Sidhu, L. A. Purcell, P. Gratraud, L. Kremer, A. P. Waters, G. Schiehser, D. P. Jacobus, C. J. Janse, A. Ager, W. R. J. Jr, J. C. Sacchettini, V. Heussler, P. Sinnis, and D. A. Fidock. 2008. The fatty acid biosynthesis enzyme FabI plays a key role in the development of liver-stage malarial parasites. *Cell Host Microbe* **4**: 567-578.
9. van Schaijk, B. C. L., T. R. S. Kumar, M. W. Vos, A. Richman, G. J. van Gemert, T. Li, A. G. Eappen, K. C. Williamson, B. J. Morahan, M. Fishbaugher, M. Kennedy, N. Camargo, S. M. Khan, C. J. Janse, K. L. Sim, S. L. Hoffman, S. H. I. Kappe, R. W. Sauerwein, D. A. Fidock, and A. M. Vaughan. 2014. Type II Fatty Acid Biosynthesis Is Essential for Plasmodium falciparum Sporozoite Development in the Midgut of Anopheles Mosquitoes. *Eukaryot. Cell* **13**: 550-559.
10. Vaughan, A. M., M. T. O'Neill, A. S. Tarun, N. Camargo, T. M. Phuong, A. S. I. Aly, A. F. Cowman, and S. H. I. Kappe. 2009. Type II fatty acid synthesis is essential only for malaria parasite late liver stage development. *Cell. Microbiol.* **11**: 506-520.
11. Waller, R. F., P. J. Keeling, R. G. Donald, B. Striepen, E. Handman, N. Lang-Unnasch, A. F. Cowman, G. S. Besra, D. S. Roos, and G. I. McFadden. 1998. Nuclear-encoded proteins target to the plastid in *Toxoplasma gondii* and *Plasmodium falciparum*. *Proc Natl Acad Sci U S A* **95**: 12352-12357.
12. Fichera, M. E., and D. S. Roos. 1997. A plastid organelle as a drug target in apicomplexan parasites. *Nature* **390**: 407-409.
13. He, C. Y., M. K. Shaw, C. H. Pletcher, B. Striepen, L. G. Tilney, and D. S. Roos. 2001. A plastid segregation defect in the protozoan parasite *Toxoplasma gondii*. *EMBO J* **20**: 330-339.
14. Lindner, S. E., M. J. Sartain, K. Hayes, A. Harupa, R. L. Moritz, S. H. Kappe, and A. M. Vaughan. 2014. Enzymes involved in plastid-targeted phosphatidic acid synthesis are essential for *Plasmodium yoelii* liver-stage development. *Mol. Microbiol.* **91**: 679-693.
15. Amiar, S., J. I. Macrae, D. L. Callahan, D. Dubois, G. G. van Dooren, M. J. Shears, M.-F. Cesbron-Delauw, E. Maréchal, M. J. McConville, G. I. McFadden, Y. Yamaryo-Botte, and C. Y. Botté. 2016. Apicoplast-Localized Lysophosphatidic Acid Precursor Assembly Is Required for Bulk Phospholipid Synthesis in Toxoplasma gondii and Relies on an Algal/Plant-Like Glycerol 3-Phosphate Acyltransferase. *PLoS Pathog.* **12**: e1005765.
16. Shears, M. J., J. I. Macrae, V. Mollard, C. D. Goodman, A. Sturm, L. M. Orchard, M. Llinás, M. J. McConville, C. Y. Botté, and G. I. McFadden. 2017. Characterization of the Plasmodium falciparum

and P. berghei glycerol 3-phosphate acyltransferase involved in FASII fatty acid utilization in the malaria parasite apicoplast. *Cell. Microbiol.* **19**: e12633.
17. Ramakrishnan, S., M. D. Docampo, J. I. Macrae, J. E. Ralton, T. Rupasinghe, M. J. McConville, and B. Striepen. 2015. The intracellular parasite Toxoplasma gondiidepends on the synthesis of long-chain and very long-chain unsaturated fatty acids not supplied by the host cell. *Mol. Microbiol.* **97**: 64-76.
18. Botté, C. Y., Y. Yamaryo-Botte, T. W. T. Rupasinghe, K. A. Mullin, J. I. Macrae, T. P. Spurck, M. Kalanon, M. J. Shears, R. L. Coppel, P. K. Crellin, E. Maréchal, M. J. McConville, and G. I. McFadden. 2013. Atypical lipid composition in the purified relict plastid (apicoplast) of malaria parasites. *Proc Natl Acad Sci USA* **110**: 7506-7511.
19. Brancucci, N. M. B., J. P. Gerdt, C. Wang, M. De Niz, N. Philip, S. R. Adapa, M. Zhang, E. Hitz, I. Niederwieser, S. D. Boltryk, M. C. Laffitte, M. A. Clark, C. Gruring, D. Ravel, A. Blancke Soares, A. Demas, S. Bopp, B. Rubio-Ruiz, A. Conejo-Garcia, D. F. Wirth, E. Gendaszewska-Darmach, M. T. Duraisingh, J. H. Adams, T. S. Voss, A. P. Waters, R. H. Y. Jiang, J. Clardy, and M. Marti. 2017. Lysophosphatidylcholine Regulates Sexual Stage Differentiation in the Human Malaria Parasite Plasmodium falciparum. *Cell* **171**: 1532-1544.
20. Mancio-Silva, L., K. Slavic, M. T. Grilo Ruivo, A. R. Grosso, K. K. Modrzynska, I. M. Vera, J. Sales-Dias, A. R. Gomes, C. R. MacPherson, P. Crozet, M. Adamo, E. Baena-Gonzalez, R. Tewari, M. Llinas, O. Billker, and M. M. Mota. 2017. Nutrient sensing modulates malaria parasite virulence. *Nature* **547**: 213-216.
21. Oppenheim, R. D., D. J. Creek, J. I. Macrae, K. K. Modrzynska, P. Pino, J. Limenitakis, V. Polonais, F. Seeber, M. P. Barrett, O. Billker, M. J. McConville, and D. Soldati-Favre. 2014. BCKDH: the missing link in apicomplexan mitochondrial metabolism is required for full virulence of Toxoplasma gondii and Plasmodium berghei. *PLoS Pathog.* **10**: e1004263.
22. Cobbold, S. A., A. M. Vaughan, I. A. Lewis, H. J. Painter, N. Camargo, D. H. Perlman, M. Fishbaugher, J. Healer, A. F. Cowman, S. H. I. Kappe, and M. Llinas. 2013. Kinetic Flux Profiling Elucidates Two Independent Acetyl-CoA Biosynthetic Pathways in Plasmodium falciparum. *J. Biol. Chem.* **288**: 36338-36350.
23. Botte, C. Y., Y. Yamaryo-Botte, T. W. T. Rupasinghe, K. A. Mullin, J. I. MacRae, T. P. Spurck, M. Kalanon, M. J. Shears, R. L. Coppel, P. K. Crellin, E. Maréchal, M. J. McConville, and G. I. McFadden. 2013. Atypical lipid composition in the purified relict plastid (apicoplast) of malaria parasites. *Proc. Natl. Acad. Sci. U. S. A.* **110**: 7506-7511.
24. Foth, B. J., L. M. Stimmler, E. Handman, B. S. Crabb, A. N. Hodder, and G. I. McFadden. 2005. The malaria parasite Plasmodium falciparum has only one pyruvate dehydrogenase complex, which is located in the apicoplast. *Mol. Microbiol.* **55**: 39-53.
25. Pei, Y., A. S. Tarun, A. M. Vaughan, R. W. Herman, J. M. Soliman, A. Erickson-Wayman, and S. H. Kappe. 2010. Plasmodium pyruvate dehydrogenase activity is only essential for the parasite's progression from liver infection to blood infection. *Mol. Microbiol.* **75**: 957-971.
26. Mullin, K. A., L. Lim, S. A. Ralph, T. P. Spurck, E. Handman, and G. I. McFadden. 2006. Membrane transporters in the relict plastid of malaria parasites. *Proc. Natl. Acad. Sci. U. S. A.* **103**: 9572-9577.
27. Karnataki, A., A. Derocher, I. Coppens, C. Nash, J. E. Feagin, and M. Parsons. 2007. Cell cycle-regulated vesicular trafficking of Toxoplasma APT1, a protein localized to multiple apicoplast membranes. *Mol. Microbiol.* **63**: 1653-1668.
28. Lim, L., M. Linka, K. A. Mullin, A. P. M. Weber, and G. I. McFadden. 2009. The carbon and energy sources of the non-photosynthetic plastid in the malaria parasite. *FEBS Lett.* **584**: 1-6.
29. Brooks, C. F., H. Johnsen, G. G. van Dooren, M. Muthalagi, S. S. Lin, W. Bohne, K. Fischer, and B. Striepen. 2010. The Toxoplasma Apicoplast Phosphate Translocator Links Cytosolic and Apicoplast Metabolism and Is Essential for Parasite Survival. *Cell Host Microbe* **7**: 62-73.

30. Tymoshenko, S., R. D. Oppenheim, R. Agren, J. Nielsen, D. Soldati-Favre, and V. Hatzimanikatis. 2015. Metabolic Needs and Capabilities of Toxoplasma gondii through Combined Computational and Experimental Analysis. *PLoS Comput. Biol.* **11**: e1004261.
31. Starai, V. J., J. Garrity, and J. C. Escalante-Semerena. 2005. Acetate excretion during growth of Salmonella enterica on ethanolamine requires phosphotransacetylase (EutD) activity, and acetate recapture requires acetyl-CoA synthetase (Acs) and phosphotransacetylase (Pta) activities. *Microbiology* **151**: 3793-3801.
32. Reger, A. S., J. M. Carney, and A. M. Gulick. 2007. Biochemical and crystallographic analysis of substrate binding and conformational changes in acetyl-CoA synthetase. *Biochemistry* **46**: 6536-6546.
33. Hur, H., Y. B. Kim, I. H. Ham, and D. Lee. 2015. Loss of ACSS2 expression predicts poor prognosis in patients with gastric cancer. *J. Surg. Oncol.* **112**: 585-591.
34. Gulick, A. M., V. J. Starai, A. R. Horswill, K. M. Homick, and J. C. Escalante-Semerena. 2003. The 1.75 A crystal structure of acetyl-CoA synthetase bound to adenosine-5'-propylphosphate and coenzyme A. *Biochemistry* **42**: 2866-2873.
35. Luong, A., V. C. Hannah, M. S. Brown, and J. L. Goldstein. 2000. Molecular characterization of human acetyl-CoA synthetase, an enzyme regulated by sterol regulatory element-binding proteins. *J. Biol. Chem.* **275**: 26458-26466.
36. Sheiner, L., J. L. Demerly, N. Poulsen, W. L. Beatty, O. Lucas, M. S. Behnke, M. W. White, and B. Striepen. 2011. A Systematic Screen to Discover and Analyze Apicoplast Proteins Identifies a Conserved and Essential Protein Import Factor. *PLoS Pathog.* **7**: e1002392.
37. Nitzsche, R., V. Zagoriy, R. Lucius, and N. Gupta. 2016. Metabolic Cooperation of Glucose and Glutamine Is Essential for the Lytic Cycle of Obligate Intracellular Parasite Toxoplasma gondii. *J. Biol. Chem.* **291**: 126-141.
38. Sidik, S. M., D. Huet, S. M. Ganesan, M. H. Huynh, T. Wang, A. S. Nasamu, P. Thiru, J. P. J. Saeij, V. B. Carruthers, J. C. Niles, and S. Lourido. 2016. A Genome-wide CRISPR Screen in Toxoplasma Identifies Essential Apicomplexan Genes. *Cell* **166**: 1423-1435.e1412.
39. Leveque, M. F., L. Berry, Y. Yamaryo-Botte, H. M. Nguyen, M. Galera, C. Y. Botte, and S. Besteiro. 2017. TgPL2, a patatin-like phospholipase domain-containing protein, is involved in the maintenance of apicoplast lipids homeostasis in Toxoplasma. *Mol. Microbiol.* **105**: 158-174.
40. Gomes, A. R., E. Bushell, F. Schwach, G. Girling, B. Anar, M. A. Quail, C. Herd, C. Pfander, K. Modrzynska, J. C. Rayner, and O. Billker. 2015. A genome-scale vector resource enables high-throughput reverse genetic screening in a malaria parasite. *Cell Host Microbe* **17**: 404-413.
41. Welti, R., E. Mui, A. Sparks, S. Wernimont, G. Isaac, M. Kirisits, M. Roth, C. W. Roberts, C. Botté, E. Maréchal, and R. McLeod. 2007. Lipidomic analysis of Toxoplasma gondii reveals unusual polar lipids. *Biochemistry* **46**: 13882-13890.
42. Limenitakis, J., R. D. Oppenheim, D. J. Creek, B. J. Foth, M. P. Barrett, and D. Soldati-Favre. 2013. The 2-methylcitrate cycle is implicated in the detoxification of propionate in Toxoplasma gondii. *Mol. Microbiol.* **87**: 894-908.
43. Yamashita, H., K. Fujisawa, E. Ito, S. Idei, N. Kawaguchi, M. Kimoto, M. Hiemori, and H. Tsuji. 2007. Improvement of obesity and glucose tolerance by acetate in Type 2 diabetic Otsuka Long-Evans Tokushima Fatty (OLETF) rats. *Biosci. Biotechnol. Biochem.* **71**: 1236-1243.
44. Saito, T., M. Nishi, M. I. Lim, B. Wu, T. Maeda, H. Hashimoto, T. Takeuchi, D. S. Roos, and T. Asai. 2008. A novel GDP-dependent pyruvate kinase isozyme from Toxoplasma gondii localizes to both the apicoplast and the mitochondrion. *J. Biol. Chem.* **283**: 14041-14052.
45. Bakszt, R., A. Wernimont, A. Allali-Hassani, M. W. Mok, T. Hills, R. Hui, and J. C. Pizarro. 2010. The crystal structure of Toxoplasma gondii pyruvate kinase 1. *PLoS One* **5**: e12736.
46. Jelenska, J., M. J. Crawford, O. S. Harb, E. Zuther, R. Haselkorn, D. S. Roos, and P. Gornicki. 2001. Subcellular localization of acetyl-CoA carboxylase in the apicomplexan parasite Toxoplasma gondii. *Proc. Natl. Acad. Sci. U. S. A.* **98**: 2723-2728.
47. Faergeman, N. J., and J. Knudsen. 1997. Role of long-chain fatty acyl-CoA esters in the regulation of metabolism and in cell signalling. *The Biochemical journal* **323 (Pt 1)**: 1-12.

48. Hosios, A. M., and M. G. Vander Heiden. 2014. Acetate metabolism in cancer cells. *Cancer & Metabolism* **2**: 27.
49. Corpet, F. 1988. Multiple sequence alignment with hierarchical clustering. *Nucleic Acids Res.* **16**: 10881-10890.
50. Agrawal, S., G. G. van Dooren, W. L. Beatty, and B. Striepen. 2009. Genetic evidence that an endosymbiont-derived endoplasmic reticulum-associated protein degradation (ERAD) system functions in import of apicoplast proteins. *J Biol Chem* **284**: 33683-33691.
51. Agrawal, G. K., S. Tamogami, O. Han, H. Iwahashi, and R. Rakwal. 2004. Rice octadecanoid pathway. *Biochem. Biophys. Res. Commun.* **317**: 1-15.
52. Macrae, J. I., L. Sheiner, A. Nahid, C. Tonkin, B. Striepen, and M. J. McConville. 2012. Mitochondrial Metabolism of Glucose and Glutamine Is Required for Intracellular Growth of Toxoplasma gondii. *Cell Host Microbe* **12**: 682-692.

FIGURE 1

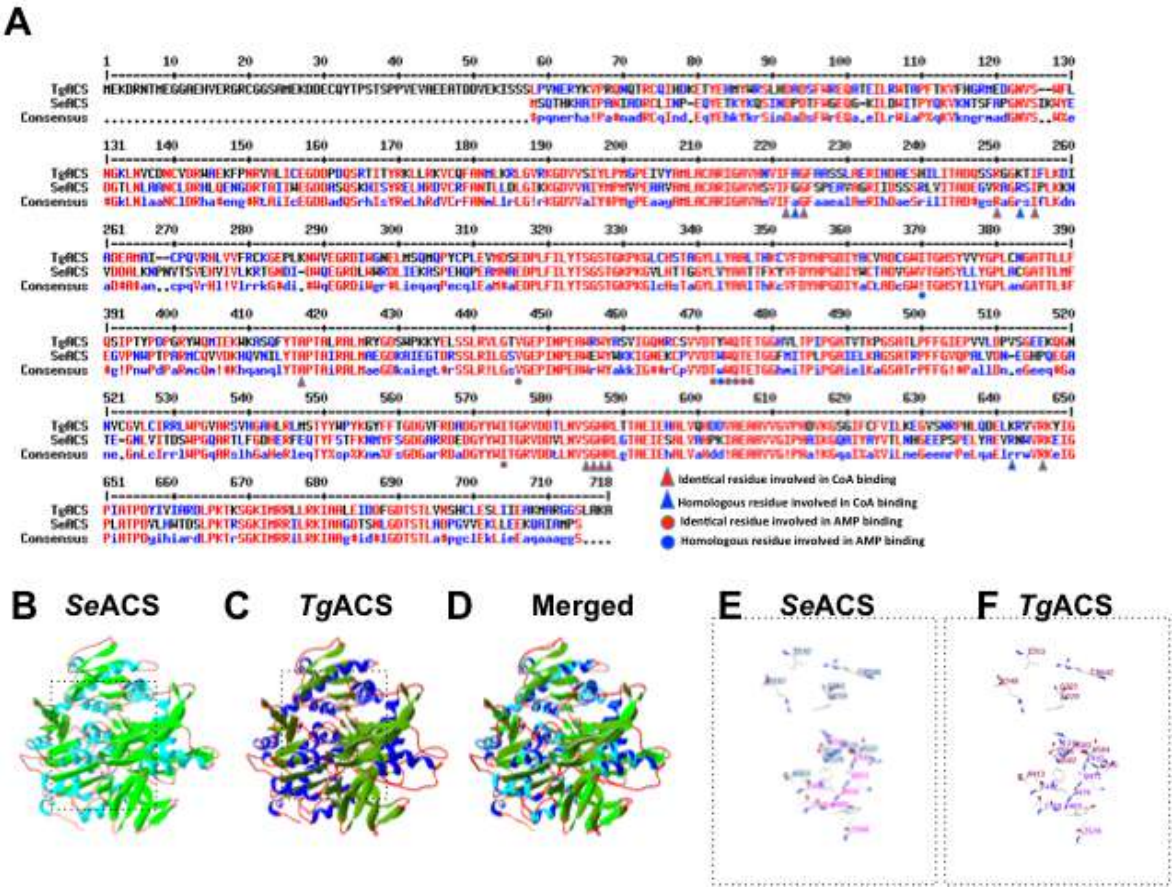

Fig. 1 Structural analysis of the predicted *Tg*ACS. A : Alignment of protein sequences from *Tg*ACS and *Sc*ACS. High consensus or identity in the residues are shown in red and lower consensus is shown in blue, whilst black depicts neutrality. Amino acid residues for the CoA binding are depicted by red triangles, homologous residues for the CoA binding with blue triangles, identical residues involved in AMP binding are shown by red circles and homologous residues for AMP binding with blue circles are shown. **B :** Crystal structure of Salmonella enterica (*Se*ACS). **C** : Predicted model of *Tg*ACS based on *Se*ACS crystal structure. **D** : Overlay of the *Se*ACS crystal structure and the homology model of *Tg*ACS. The overall structure of *Tg*ACS is conserved and highly similar as observed in the ribbon representation. **E** : Three dimensional representation of the amino acid residues involved in AMP and CoA in *Se*ACS. **F** : Three dimensional representation of the predicted residues involved in AMP and CoA binding in TgACS.

FIGURE 2

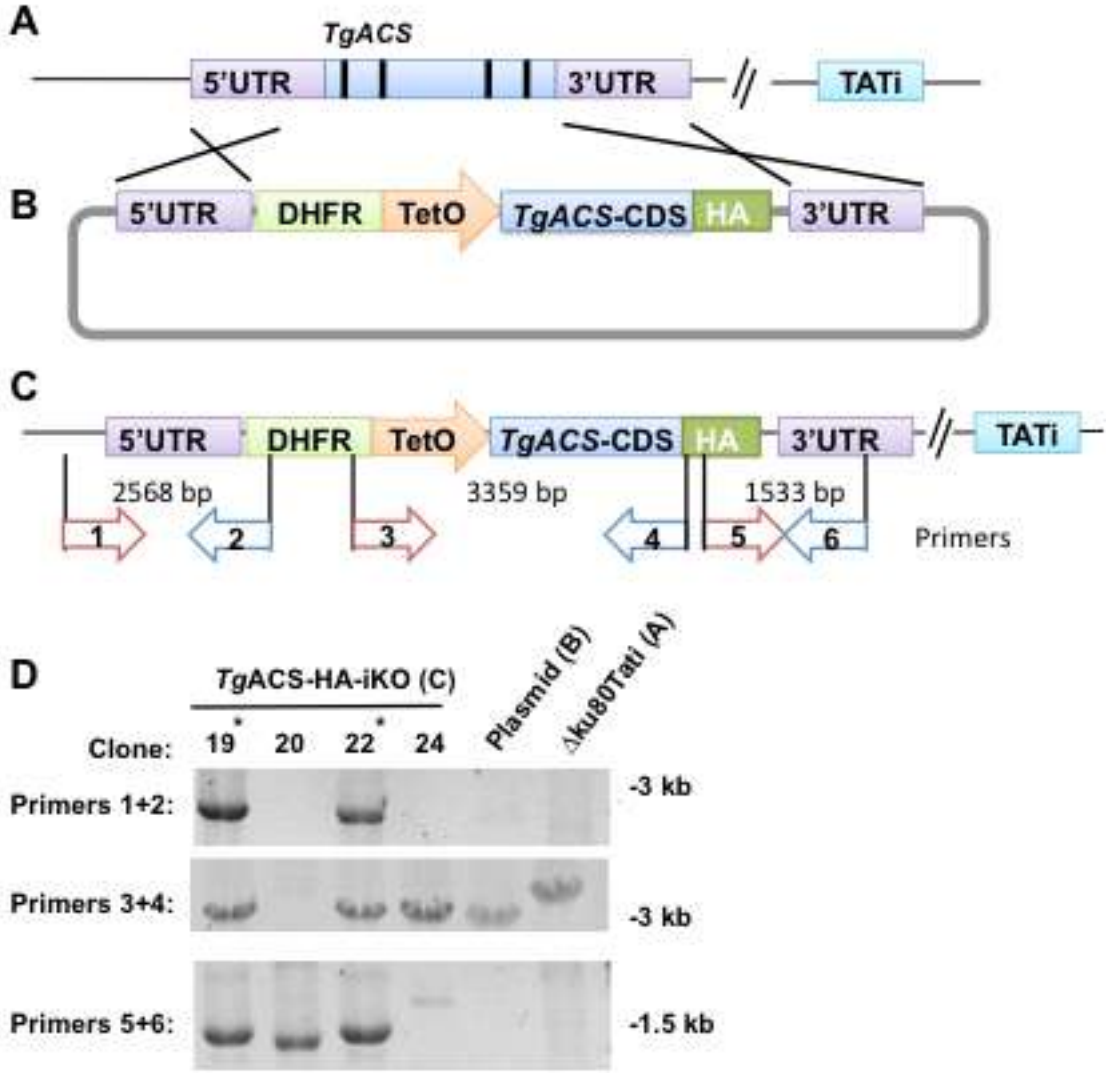

Fig. 2 Generating *Tg*ACS-HA-iKO. A: A tetracycline-regulated transactivator (TATi) expressing strain. **B**: Modified pDT7s4H plasmid for promoter replacement and tagging. **C**: Modified gene locus and primers used for (D). **D**: Confirmation of replacement of gene locus by PCR.

FIGURE 3

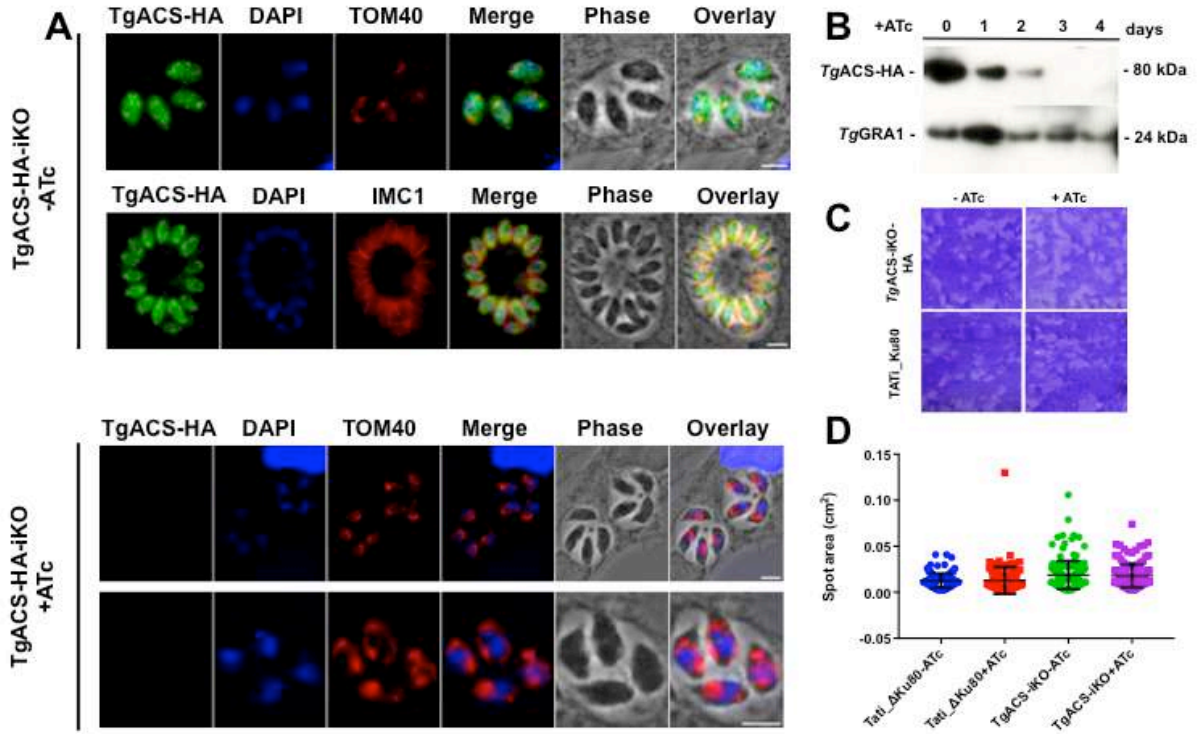

Fig. 3 *Tg*ACS-HA-iKO is a dispensable cytosolic protein that can be downregulated to determine its cellular function. A: Immunofluorescence assay images of *Tg*ACS-HA-iKO strain with or without ATc. *Tg*ACS-HA fluorescent signal is shown in green. DAPI, as a marker for nucleus, is shown in blue. IMC1 and TOM40 are markers of the inner membrane complex and the parasite mitochondria, respectively, and both are shown in red. *Tg*ACS-HA localizes in the cytosol and this signal is lost after the addition of ATc. **B**: Western blotting image of *Tg*ACS-HA-iKO strain. *Tg*ACS-HA protein is detected at the predicted molecular weight, 79.8 kDa. The addition of ATc causes complete protein loss after 3 days. **C**: Plaque assay were used to evaluate the growh of the *Tg*ACS-HA_iKO strains with or without ATc in comparison to *T. gondii* reference strain, Tati-Ku80. **D**: Statistical analysis of plaque assay was performed to show that there was no difference in the presence or absence of *Tg*ACS protein. All scale bars, 5μm.

FIGURE 4

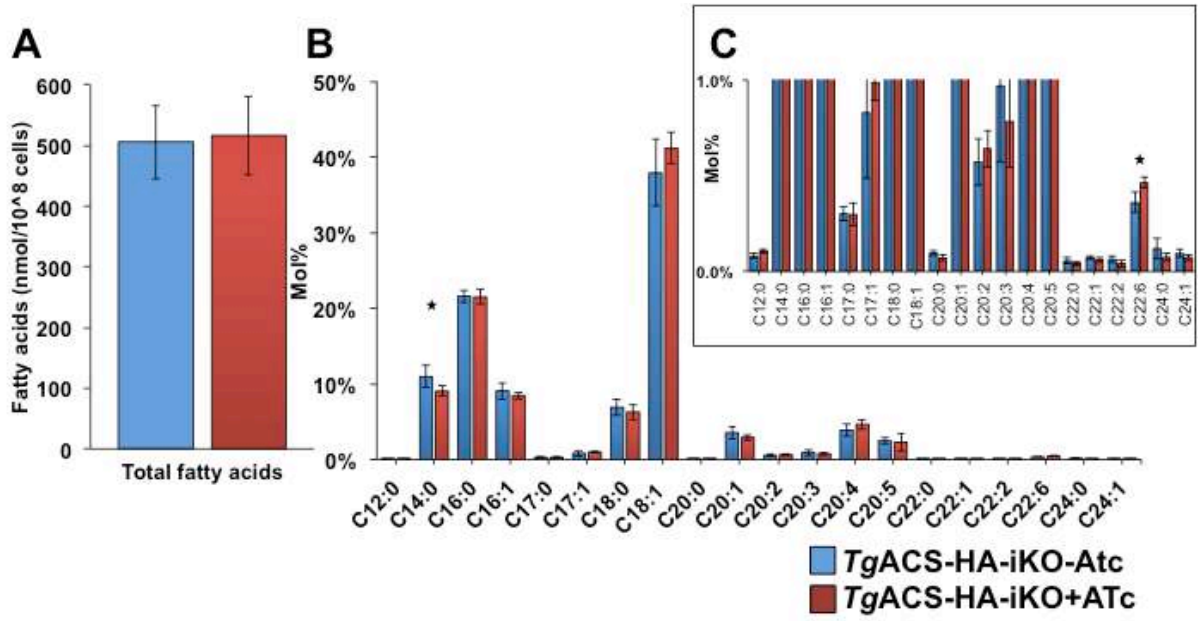

Fig. 4 Total fatty acid composition in *Tg*ACS-HA-iKO. A: Total lipids extracted from were *Tg*ACS-HA-iKO grown with or without ATc for 4 days. Then total lipid was derivatised with MethprepII to give fatty acid methyl ester and their amount was quantified by GC-MS following normalization according to internal standards (C14:0) and cell numbers. **B**: Relative abundance of fatty acids **C**: Magnified view of (B). *Tg*ACS-HA-iKO-ATc (blue) and *Tg*ACS-HA-iKO+ATc. (n=6) Star indicates significance ($P<0.05$).

FIGURE 5

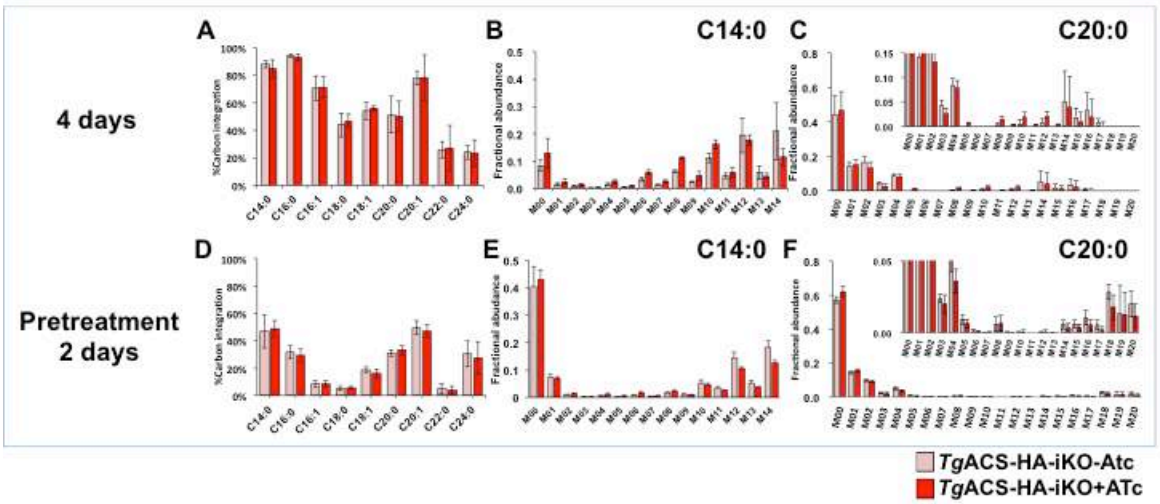

Fig. 5 Determination of the *Tg*ACS putative role in *de novo* fatty acid synthesis via the apicoplast FASII. (A, B, C) *Tg*ACS-HA-iKO was grown in the presence of U-^{13}C-glucose simultaneously with or without ATc for 4 days. **A**: %^{13}C carbon integration to each fatty acid species. **B**: Mass isotopomer distribution (MID) of C14:0. **C**: MID for C20:0 (n=4). **(D, E, F)** *Tg*ACS-HA_iKO was grown with or wihtout ATc for 2 days in prior to the addition of U-13-C-glucose and grown for a further 2 days **D**:%^{13}C carbon integration to each fatty acid species. **E**: MID for C14:0 **F**: MID for C20:0. *Tg*ACS-HA-iKO-ATc, pale red and *Tg*ACS-HA-iKO+ATc, dark red. (n=7).

FIGURE 6

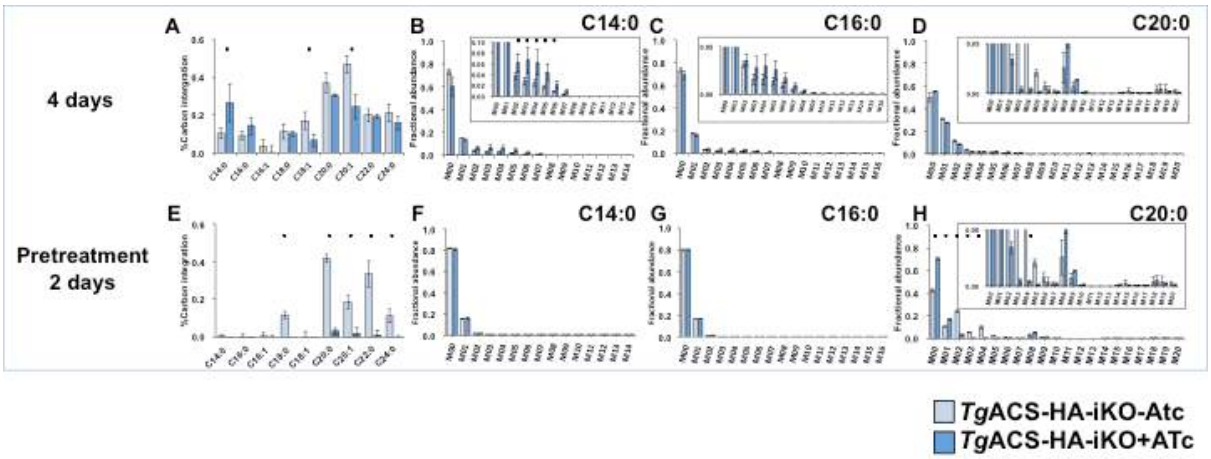

Fig.6 Determination of *Tg*ACS putative role for fatty acid elongation. (A, B, C, D) *Tg*ACS-HA-iKO was grown in the presence of U-^{13}C-acetate simultaneously with or without ATc for 4 days. **A**: %^{13}C carbon integration to each fatty acid species **B**: Mass isotopomer distribution (MID) of **C**14:0. C: MID for C16:0. **D**: MID for C20:0. (n=3) **(E, F, G, H)** *Tg*ACS-HA-iKO was grown with or wihtout ATc for 2 days in prior to the addition of U-^{13}C-acetate to grow further 2 days **E**: %^{13}C carbon integration to each fatty acid species. **F**: MID for C14:0 **G**: MID for C16:0. **H**: MID for C20:0. *Tg*ACS-HA-iKO-ATc, pale red and *Tg*ACS-HA-iKO+ATc, dark red. (n=5). Star indicates significance (P<0.05)

FIGURE 7

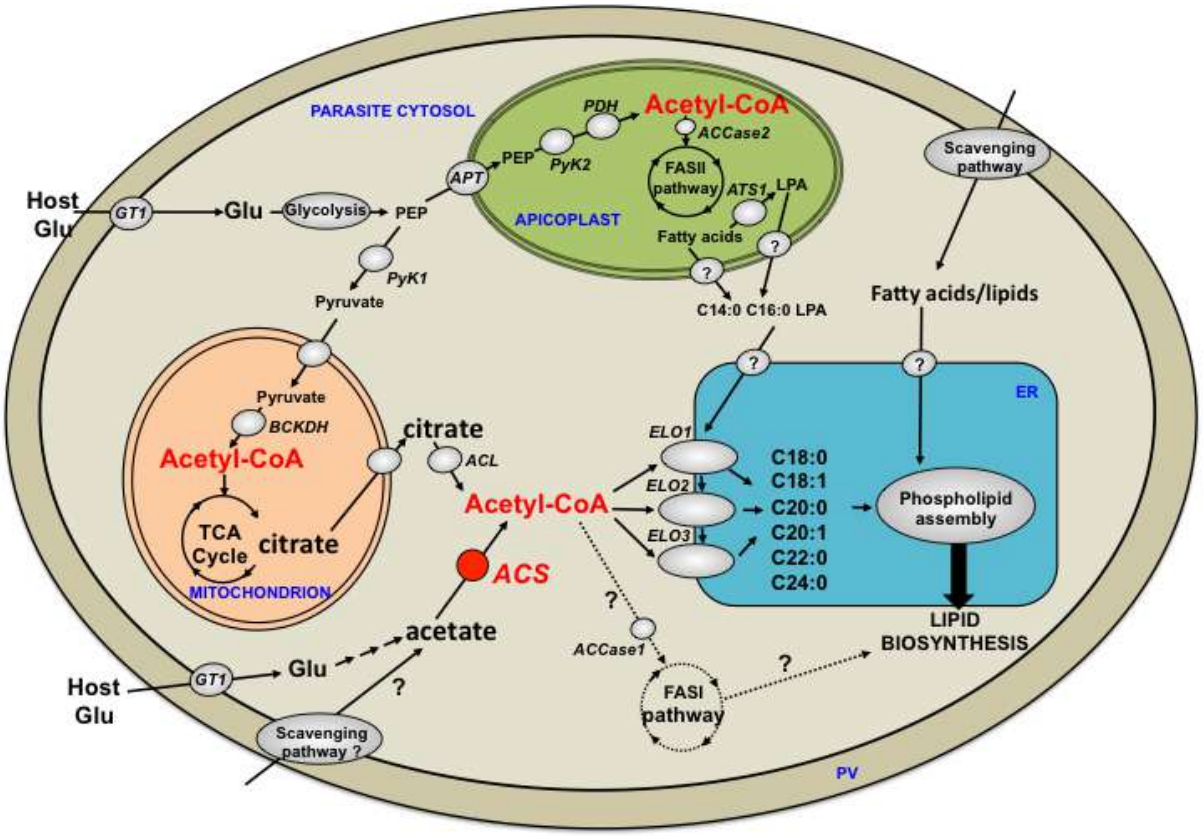

Fig. 7 Proposed role of *Tg*ACS and acetyl-CoA in the lipid biosynthetic pathway of *T. gondii* tachyzoite. Acetyl-CoA can be generated by the cytosolic ACS using acetate as a substrate. This pool of acetyl-CoA is used as a substrate for the parasite elongases (ELO1, 2, 3) in the endoplasmic reticulum to form C18:0, C18:1, C20:0, C20:1, C22:0, C24:0. These elongated fatty acids are used to generate phospholipids for the bulk lipid biosynthetic pathways along with the FASII derived fatty acid and lipid precursor (LPA) made in the apicoplast and the fatty acids and lipids scavenged from the host. The origin of acetate used by ACS partially derives from metabolized glucose whilst another fraction is likely scavenged from the host environment. Acetyl-CoA can also be generated via cytosolic ACL, which uses citrate made by the mitochondrial TCA cycle and that is exported into the cytosol. This pool of acetyl-CoA can most likely be used by the elongation pathway as a possible redundant route to ACS function in elongation. Fatty acids generated by the apicoplast FASII are the major substrates for the ER elongases. Acetyl-CoA is also made from glycolitic intermediates PEP and pyruvate by the apicoplast PDH and the mitochondrial BCKDH for the FASII pathway and the mitochondrial TCA cycle, respectively. Theoritically, acetyl-CoA generated by ACS and ACL could fuel the cytosolic FASI pathway but our current results suggest that this is not the case during tachyzoite life stages. Abbreviations: ACCase: Acetyl carboxylase, ACL: ATP citrate lyase, ACS: acetyl-CoA synthetase, APT: apicoplast phosphate transporter, ATS1: apicoplast glycerol-3phosphate acyltransferase, BCKDH: Branched chain keto acid dehydrogenase, ELO; elongase, ER: Endoplasmic reticulum, Glu: Glucose, GT1: Glucose transporter, LPA; lysophosphatidic acid, PDH: pyruvate dehydrogenase, PEP: Phosphoenol pyruvate, PV: parasitophorous vacuole, PyK: pyruvate kinase.

International Journal of
Molecular Sciences

MDPI

Article

Specific Targeting of Plant and Apicomplexa Parasite Tubulin through Differential Screening Using In Silico and Assay-Based Approaches

Emmanuelle Soleilhac [1], Loraine Brillet-Guéguen [1,2], Véronique Roussel [1,3], Renaud Prudent [4], Bastien Touquet [5], Sheena Dass [6], Samia Aci-Sèche [7], Vinod Kasam [8], Caroline Barette [1], Anne Imberty [9], Vincent Breton [8], Marylin Vantard [3,10], Dragos Horvath [11], Cyrille Botté [6], Isabelle Tardieux [5], Sylvaine Roy [1,3], Eric Maréchal [3,*] and Laurence Lafanechère [4,*]

1 Institut de Biosciences et Biotechnologies de Grenoble (BIG), Université Grenoble Alpes, CEA, INSERM, BGE U1038, CEA-Grenoble, 17 rue des Martyrs, 38000 Grenoble, France; emmanuelle.soleilhac@cea.fr (E.S.); loraine.gueguen@sb-roscoff.fr (L.B.-G.); veronique.roussel@uparc.fr (V.R.); caroline.barette@cea.fr (C.B.); sylvaine.roy@cea.fr (S.R.)
2 Sorbonne Université, CNRS, Integrative Biology of Marine Models (LBI2M), Station Biologique de Roscoff (SBR), 29680 Roscoff, France
3 Laboratoire de Physiologie Cellulaire Végétale, Unité Mixte de Recherches 5168 CNRS, CEA, INRA, Institut de Biosciences et Biotechnologies de Grenoble (BIG), Université Grenoble Alpes, CEA-Grenoble, 17 rue des Martyrs, 38000 Grenoble, France; marylin.vantard@univ-grenoble-alpes.fr
4 Institute for Advanced Biosciences (IAB), Team Regulation and Pharmacology of the Cytoskeleton, INSERM U1209, CNRS UMR5309, Université Grenoble Alpes, 38000 Grenoble, France; renaud_prudent@yahoo.fr
5 Institute for Advanced Biosciences (IAB), Team Membrane and Cell Dynamics of Host Parasite Interactions, INSERM U1209, CNRS UMR5309, Université Grenoble Alpes, 38000 Grenoble, France; bastien.touquet@univ-grenoble-alpes.fr (B.T.); isabelle.tardieux@inserm.fr (I.T.)
6 Institute for Advanced Biosciences (IAB), Team ApicoLipid, CNRS UMR5309, Université Grenoble Alpes, INSERM U1209, 38000 Grenoble, France; Sheena.dass@univ-grenoble-alpes.fr (S.D.); cyrille.botte@gmail.com (C.B.)
7 Institut de Chimie Organique et Analytique (ICOA), UMR7311 CNRS-Université d'Orléans, Université d'Orléans, 45067 Orléans CEDEX 2, France; samia.aci-seche@univ-orleans.fr
8 Laboratoire de Physique de Clermont, Université Clermont Auvergne, CNRS/IN2P3, UMR6533, 4 Avenue Blaise Pascal TSA 60026, CS 60026 63178 Aubière CEDEX, France; vinodkasam@gmail.com (V.K.); Vincent.Breton@clermont.in2p3.fr (V.B.)
9 Centre de Recherche sur les Macromolécules Végétales, Université Grenoble Alpes, CNRS, 38000 Grenoble, France; anne.imberty@cermav.cnrs.fr
10 Grenoble Institut des Neurosciences; Inserm U1216; Université Grenoble Alpes, 38000 Grenoble, France
11 Laboratoire de Chemoinformatique, UMR7140 CNRS—Université de Strasbourg, 4 rue Blaise Pascal, 67000 Strasbourg, France; dhorvath@unistra.fr
* Correspondence: eric.marechal@cea.fr (E.M.); laurence.lafanechere@univ-grenoble-alpes.fr (L.L.); Tel.: +33(0)476-54-95-71 (E.M.); +33(0)438-78-49-85 (L.L.); Fax: +33(0)438-78-50-91 (E.M.); +33(0)476-54-95-95 (L.L.)

Received: 6 September 2018; Accepted: 4 October 2018; Published: 9 October 2018

Abstract: Dinitroanilines are chemical compounds with high selectivity for plant cell α-tubulin in which they promote microtubule depolymerization. They target α-tubulin regions that have diverged over evolution and show no effect on non-photosynthetic eukaryotes. Hence, they have been used as herbicides over decades. Interestingly, dinitroanilines proved active on microtubules of eukaryotes deriving from photosynthetic ancestors such as *Toxoplasma gondii* and *Plasmodium falciparum*, which are responsible for toxoplasmosis and malaria, respectively. By combining differential in silico screening of virtual chemical libraries on *Arabidopsis thaliana* and mammal tubulin structural models together with cell-based screening of chemical libraries, we have identified dinitroaniline related and non-related compounds. They inhibit plant, but not mammalian tubulin assembly in vitro,

and accordingly arrest *A. thaliana* development. In addition, these compounds exhibit a moderate cytotoxic activity towards *T. gondii* and *P. falciparum*. These results highlight the potential of novel herbicidal scaffolds in the design of urgently needed anti-parasitic drugs.

Keywords: Tubulin; dinitroanilines; plant cells; *Toxoplasma gondii*; *Plasmodium falciparum*; virtual screening; small molecules; cell-based assays

1. Introduction

Microtubules (MTs) are hollow cylindrical polymers composed of α-β tubulin heterodimers. These highly dynamic assemblies organize the cytoplasm during interphase and form the mitotic spindle to segregate condensed chromosomes during mitosis. Microtubule organization shows a remarkable diversity in eukaryotes, with striking differences in clades deriving from photosynthetic ancestors. Animal microtubules are anchored on a structured microtubule-organizing center such as the centrosome, or in many differentiated animal cells they are arranged in non-centrosomal arrays that are non-radial [1]. In contrast, in vascular plant cells that lack a structurally defined microtubule-organizing center, interphase MTs are always organized into linear bundles that assume different configurations depending on the cell type [2,3]. In Apicomplexa single-celled eukaryotes, deriving from photosynthetic ancestors, although now lacking photosynthesis [4], such as *Toxoplasma gondii*, microtubule organization varies during the parasite life cycle. At the tachyzoite replicative stage, a corset of 22 evenly spaced sub-pellicular microtubules, anchored to the apical polar ring, critically directs the polarized and elongated shape of the zoite. In addition, this parasite builds an unusual microtubule-containing structure at the apical tip, which is named conoid [5]. In *Plasmodium falciparum*, a longitudinally oriented array of two–three sub-pellicular microtubules contributes to the shape and integrity of the parasite [6].

While α and β-tubulin are highly conserved proteins, the effects of microtubule-binding drugs vary in organisms belonging to distinct evolutionary groups. For example, plant tubulin and Apicomplexan tubulins have a much lower affinity for colchicine than animal tubulin [7]. In contrast, small synthetic molecules such as dinitroanilines (oryzalin, ethafluralin or trifluralin) bind specifically plant and Apicomplexa tubulins but not vertebrate or fungi ones [8–11]. Due to their selectivity towards plant tubulin, dinitroanilines have been used as herbicides for more than 40 years [7] and represent promising leads for the design of antiparasite drug candidates in particular in the case of *P. falciparum* and *T. gondii* [9,12].

Computational methods have provided evidences that the dinitroaniline binding site of *T. gondii* α-tubulin is located beneath the H1-S2 loop [13]. Such a location predicts the disruption of protofilament interactions in the microtubule lattice upon dinitroaniline binding.

Besides dinitroanilines and their derivatives, no chemical entities that selectively target tubulin of plants and parasites have yet been described. This is not the case for mammalian tubulin, which is the target of numerous diverse chemical compounds [14–16]. Therefore, to identify new chemical scaffolds that could be used as template for novel anti-parasitic drugs or herbicide, we have designed an integrated multi-step strategy. First, a differential in silico screen of small molecules from chemical libraries, docking to the α-tubulin dinitroaniline-binding site, was performed to select compounds that bind selectively to plant/parasite tubulins. The selected compounds were then screened on plant cells using a miniaturized assay. The compounds active on the plant cell MT cytoskeleton were further tested on plantlets viability and counter screened for their effect on the human cell cytoskeleton. A few residual molecules, active on the plant cell cytoskeleton and plantlets, but showing no detectable effect on human cells, were finally tested for their effect on in vitro tubulin assembly of plant versus mammalian tubulin. The combination of these approaches picked out three active molecules that are selectively active on plant tubulin. Remarkably, two of them are structurally different from

dinitroanilines, and therefore represent novel scaffolds that serve as leads for the design of new generation herbicides. Additionally, we checked whether any of the retained candidates affect *T. gondii* and *P. falciparum* growth and survival within their relevant human host cells. One of these compounds showed a low but selective toxicity on the proliferative stages of *T. gondii* and *P. falciparum*, as compared to human cells, highlighting the usefulness of such a multidisciplinary approach to discover new classes of herbicidal molecules with potential anti-*Plasmodium* and anti-*Toxoplasma* properties.

2. Results

2.1. Determination of 3D Discriminating Conformations of P. falciparum α-Tubulin for In Silico Screening

α-Tubulin is a highly conserved protein (Figure S1). While tubulin structures have been obtained in multiple organisms and are available in the PDB database, the resolution level was not sufficient to be directly used as templates for the present differential in silico docking experiments. To perform a virtual screening on a domain conserved only in the photosynthetic lineage, in broad sense, we first selected a representative tubulin structural model in an Apicomplexa, well known to be non-photosynthetic today but deriving initially from a photosynthetic ancestor [17,18]. The sequence of *P. falciparum* α-tubulin (Uniprot accession: CAA34101) was thus used, focusing on regions conserved in plants. *P. falciparum* α-tubulin structure was determined by homology modeling [19] using bovine (AAX09051) and porcine (P02550) α-tubulin crystal structures as templates (Figure S2, step1). In the predicted structure, the H1-S2 loop (residues 35–60) locked the oryzalin-binding site, preventing molecules from penetrating inside. An early version of the conformational sampling tool S4MPLE [20] specifically operating on the torsional degrees of freedom only [21] was used to explore alternative putative poses of that loop. Main chains and side chains of the loop aminoacids, as well as side chains of residues putatively in contact with loop residues were declared mobile, while freezing the rest of the protein to its initial geometry. In order to sample a protein loop anchored to a rigid protein core at both ends, S4MPLE (Sampler for Multiple Protein-Ligand Entities, an algorithm designed for the conformational sampling of small molecules and in-silico docking experiments) needs an input of a user-chosen identifier of an existing main chain bond (here, the N-C α of the loop-central aminoacid, i.e., between residues 28 and 47), which will be formally considered as “broken”. This allows free movement of the formally disjoined loop moieties in S4MPLE, while accounting for the complete molecular Hamiltonian (based, in that version of S4MPLE, on the CVFF force field [22]), i.e., including the concerned bond stretching and associated valence angle bending terms. This “trick” ensures a full sampling of possible loop geometries, while selecting only those that are properly closing the artificial "gap" and providing consistent geometries for the covalent elements. Since all other bond length and valence angle values were not subjected to changes (and remained set to their input values), the chirality of the C α involved in the formally broken bond was implicitly conserved. Several independent simulations of the system were run, using a genetic algorithm-based sampling strategy, for 1,000 generations each, until it was observed that, for 10 successive simulations, no absolutely lower energy value could be attained. We selected 100 conformers among the more stable ones according to a criterion of diversity, measured mainly on torsional axes (Figure S2, step 2). As shown in Figure 1, these conformers (Figure 1B, lower panel) present a well-formed “dockable” cleft as compared to the initial homology-modeled geometry (Figure 1B, upper panel).

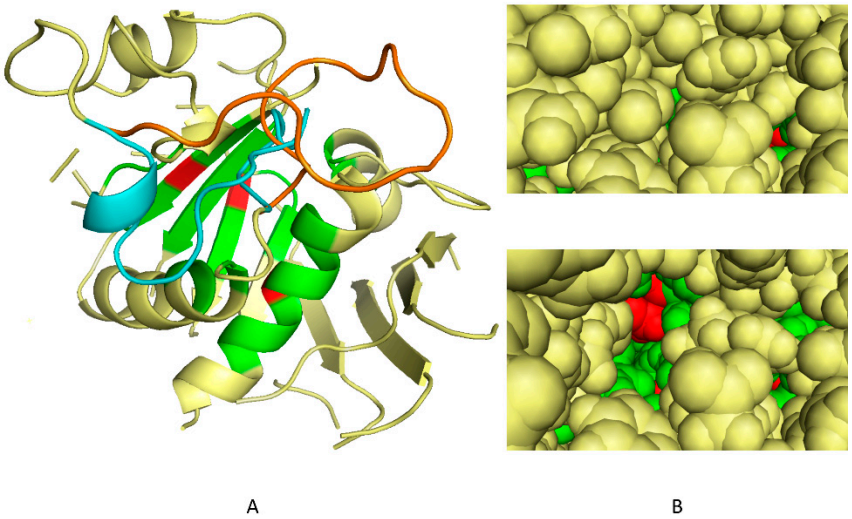

Figure 1. Determination of the best *P. falciparum*. α-tubulin conformations for in-silico screening. (**A**) Conformations of the H1-S2 loop (residues 35–60) of *P. falciparum* α-tubulin, showing the overlap of the initial homology model based on homology predictions to mammalian tubulin (cyan) and lowest-energy S4MPLE (Sampler for Multiple Protein-Ligand Entities)-generated open-site geometry model, which takes into account the dinitroaniline binding ability (orange). The residues Ser6, Ile235 and Leu167 in the dinitroaniline binding site of the *P. falciparum* tubulin that were found involved in interactions for every conformation and used as criteria for selection are coloured in red, and their immediate neighbourhood (within 4Å) is in green. The loop in the homology model—in cyan—is seen to block access to the site. When displaced to allow dinitroaniline binding ability the predicted new position (in orange) opens access to the three key residues. (**B**) View of the "red" key residues in a protein surface model, showing that they (and their immediate neighborhood, in green) are buried in the homology model (upper panel) but accessible in the sampled conformer model (lower panel).

To select the more likely conformations, we then docked on these 100 conformers a reference set of 37 molecules comprising 10 dinitroaniline derivatives known to target the dinitroaniline-binding site [13] and 27 compounds never reported for binding tubulin, to our knowledge. By ranking the conformers according to their ability to discriminate between the active/non active molecules we could select the five more likely conformations of the H1-S2 loop (Figure S2, step 3).

These five conformations as well as the mammalian and the original *Plasmodium* tubulin conformations were the final targets for the in silico differential screening.

2.2. In Silico Selection of Compounds that Bind to the Dinitroaniline Site of α-Tubulin from the Photosynthetic Lineage

Using the five most promising conformations, a virtual library of more than 300,000 chemical compounds was screened for its ability to dock into the identified cleft. We first analyzed the FlexX scores in the whole docked database to evaluate the possibility to rank conformations based on these scores. This analysis showed that the active compounds previously reported in the literature were close to the average value in the score distribution and not among the best scores. The use of FlexX scores was thus considered as not discriminant enough to select molecules. Post-processing of docking outputs through analyses of the three dimensional protein-ligand binding interactions has been reported to be a powerful alternative strategy [23–25]. A thorough analysis of the interaction data obtained for known active compounds on the 100 conformers described above revealed that numerous residues involved in the interactions were located at the pocket entrance, whereas the residues located in the depth of the pocket were more rarely involved. Among them, three residues (Ser6, Ile235 and Leu167, Figure S1) were involved in interactions for every conformation (Figure 1B). We decided to use them as a criterion for selection.

Based on the protein molecule interactions, 3,023 molecules that, in one or more of the five "open" protein conformations, had one or more docking poses in interaction with Ser6, Ile235 or Leu167 were selected. We checked that, among these compounds, none had been selected for their effect on mammalian cell microtubules, in previous screening campaigns [15,16]. This was never the case, therefore validating the proposed specificity of the binding pocket for the photosynthetic lineage. Among these 3,023 compounds, 82 molecules were readily available in the laboratory and therefore picked for further in vitro analysis.

2.3. Selection of Compounds Active only on Plant Cell Microtubules

The selected compounds were tested for their effect on tobacco BY-2 cell microtubules using immunofluorescence. Image-based screening is frequently performed on adherent mammalian cells [16,26] but has never yet been achieved on plant cells. We thus developed an optimized immunostaining procedure in 96-well plates, as described in the Material and Methods section and captured images using an automated fluorescent microscope.

The effect of a two-hour incubation with each of the 82 molecules (50 µM) was compared to those of dinitroaniline (25 µM) that depolymerizes plant MTs, and colchicine (2 µM) that has low affinity for the plant tubulin. As expected, MT depolymerization was observed upon dinitroaniline treatment whereas colchicine did not affect the plant-cell microtubule network (Figure 2). Eleven compounds, out of the 82 compounds tested, were found to have an effect on cortical MTs (Figure 2). This indicates that these compounds could be able to cross the BY-2 cell membrane to impact cellular microtubules. Their effect on mammalian cell microtubules was then tested by immunofluorescence using HeLa cells. When applied at concentrations ranging from 3 to 50 µM for 2 h at 37 °C none of the compound, except compound CM872, induced detectable effects on microtubules. Compound CM872 showed a toxic effect that was detected at the higher concentration tested only, i.e., 50 µM (Figure 3). Overall, 10 compounds were found to be active only on BY-2 cell MTs with no detectable effect on HeLa cell MTs.

In order to know if these compounds could penetrate into a whole plant organism and be active, they were finally tested for their effect on *Arabidopsis thaliana* growth. As shown in , three compounds, i.e., compounds CM571, CM094, and CM852 inhibited plant growth. In addition, severe symptoms of chlorosis could be detected for compounds CM571 and CM852, indicating that they circulated in plant vascular tissues and induced a systemic response (Figure S3).

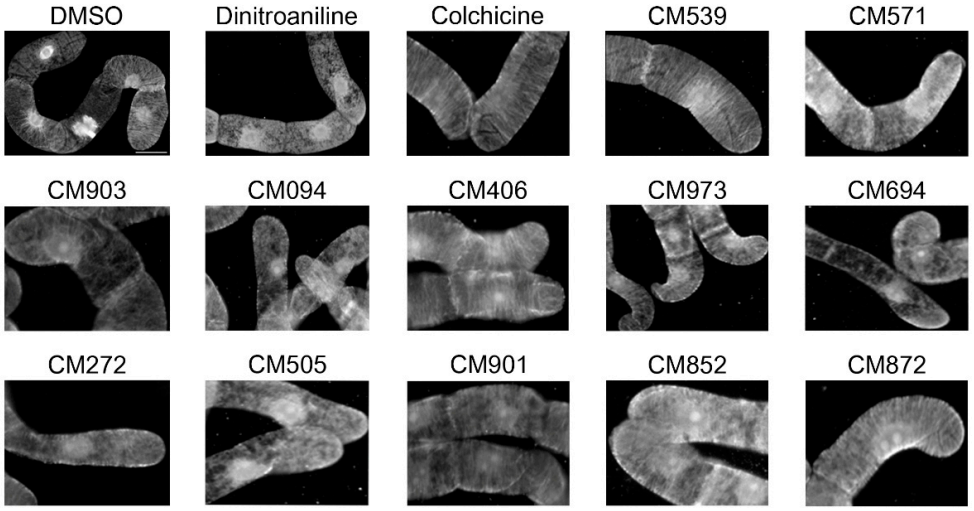

Figure 2. Effect of selected compounds on plant cell microtubule network organization. BY2 cells were incubated for 2 h with 0.25% DMSO (vehicle control); 25 µM dinitroaniline, 2 µM colchicine and 50 µM of the indicated compounds. Cells were then processed for tubulin immunofluorescence as described in Material and Methods. CM539 is an example of a compound that was found inactive. Bar = 20 µm.

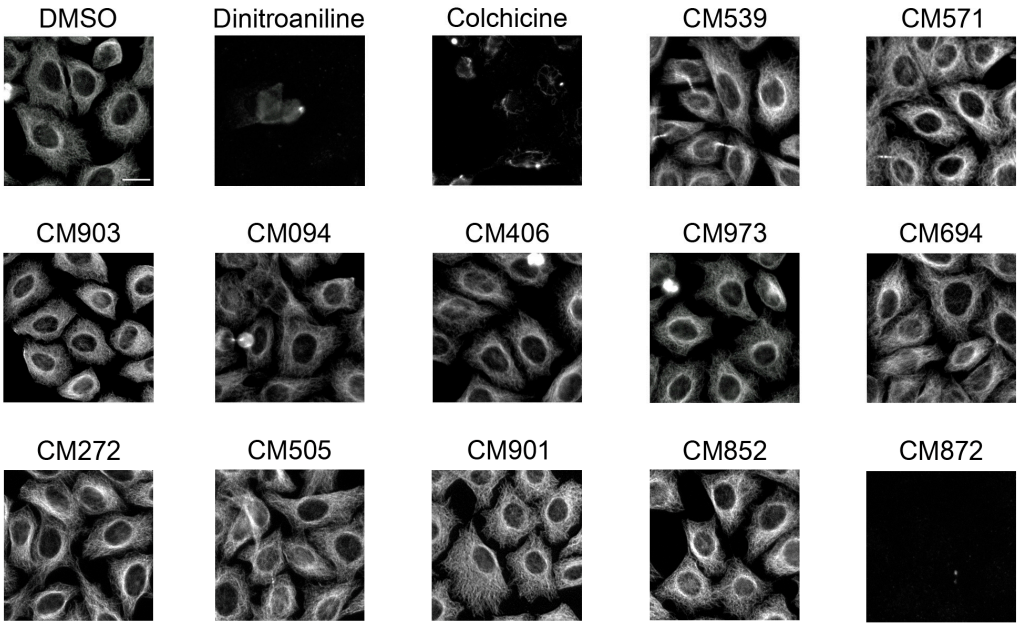

Figure 3. Effect of selected compounds on mammalian cell microtubule network organization. HeLa cells were incubated for 2 h with 0.25% DMSO (vehicle control); 25 μM dinitroaniline, 2 μM colchicine and 50 μM of the indicated compounds. Cells were then processed for tubulin immunofluorescence as described in Material and Methods. Bar = 20 μm.

2.4. Selected Compounds Target Plant but not Mammalian Tubulin

We next focused on these three compounds and evaluated at the molecular level whether they targeted plant tubulin but not mammalian tubulin. We thus compared their effect, at concentrations ranging from 0.1 to 50 μM on the in vitro assembly of tubulin purified from soybean or bovine brain. In contrast to colchicine and nocodazole, CM571, and CM852 even at high concentration (50 μM) did not show any significant effect on the assembly kinetics of bovine brain tubulin, in agreement with the lack of detectable changes in the cellular microtubule network of intact HeLa cells (Figure 4A). Of note CM094 induced a slight depolymerizing effect at 50 μM but had no effect at lower concentrations [27] While soybean tubulin was less assembly competent, we observed tubulin polymerization reaction under control conditions that was no longer detected in presence of dinitroaniline (Figure 4B). All three compounds impaired soybean tubulin assembly (Figure 4C–E). After dose-response analysis [27], the drug inhibitory profile is estimated as follows: dinitroaniline > CM852 > CM571 > CM094.

The comparison of the chemical structure of the compounds (Figure 5) showed that the three compounds belong to different classes of chemicals. No biological effects of CM571 have so far been described. Interestingly, CM094 shares common features with dinitroaniline, namely a nitro-phenyl-sulfonamide moiety, which may mediate the observed effect on plant tubulin assembly. Likewise, CM852 is a pyridasinone (n-chloridazon) that is currently used as a selective systemic herbicide [28]. Among other properties such as DNA intercalation and interference with the synthesis of fatty acids [29], n-chloridazon is primarily known to inhibit photosynthesis and thus to induce chlorosis, a symptom we observed in *A. thaliana* plantlets.

We concluded from these experiments that CM852, CM571, and CM094, originally selected by a virtual screen to bind to the dinitroaniline binding site of *P. falciparum* tubulin, were indeed able to target plant tubulin with no detectable effect on mammalian tubulin.

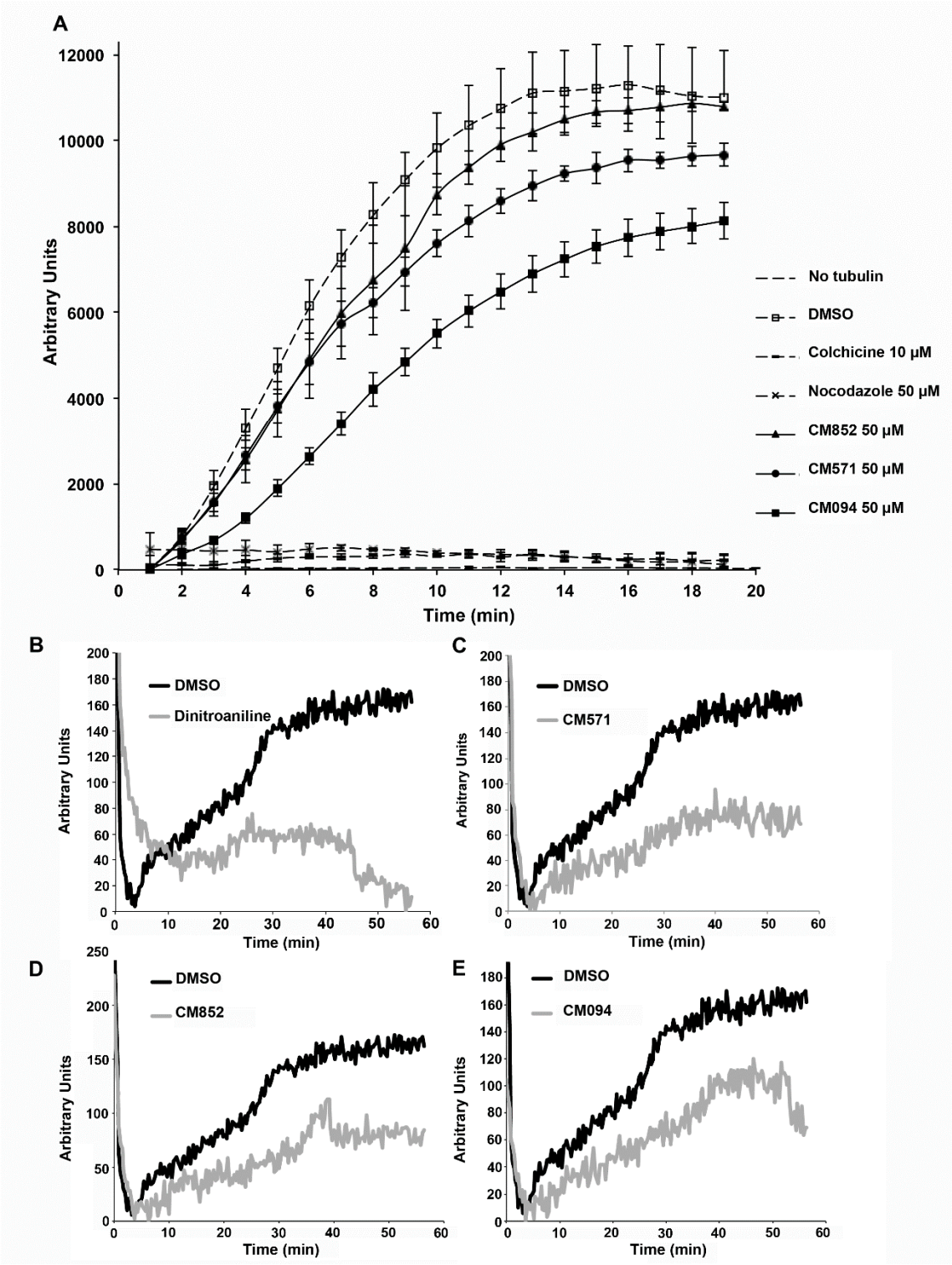

Figure 4. Comparison of the effects of CM094, CM571 and CM852 on mammalian and plant microtubule polymerization in vitro. (**A**) Pure bovine brain tubulin polymerization assay. Tubulin was allowed to polymerize at 37 °C. Fluorescence of DAPI bound to microtubules was measured to monitor microtubule polymerization, as described in the Material and Methods section. Experiments were performed in triplicate, in the presence of the indicated compounds. Results are presented as mean ± standard error of the mean (SEM). Effect of dinitroaniline (**B**), CM571 (**C**), CM852 (**D**), and CM094 (**E**) on soybean tubulin assembly. Recombinant soybean tubulin was polymerized as described in the Material and Methods section, in the presence of DMSO (control) or the indicated compounds.

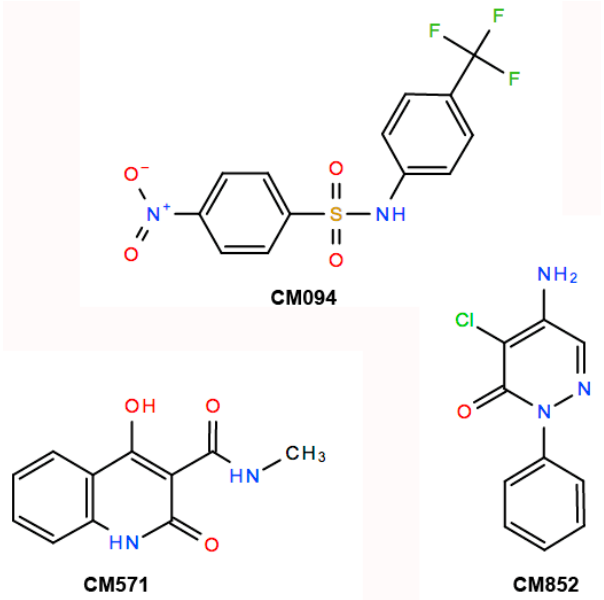

Figure 5. Structure of the selected compounds.

2.5. Analysis of the Effects of the Compounds on Apicomplexan Parasites

Due to the sensitivity of *T. gondii* to dinitroanilines that has already been reported with IC50 values for commercially available dinitroanilines ranging from 45 nM to 6.7 µM, we tested whether the selected compounds could impact *T. gondii* and *P. falciparum* intracellular development within their respective host cells. Taking into account that the subpellicular MTs of extracellular parasites are non-dynamic and notoriously insensitive to MT pharmacological disruptors, we had to perform the assays on intracellular multiplying parasites. This experimental requirement implies that the compounds of interest could access not only the host cell cytosol, but also pass the membrane of the parasitophorous vacuoles, within which the tachyzoite multiplies and ultimately reach the parasite cytosol. Using fluorescent *T. gondii* tachyzoite and High Content Imaging that allowed quantitative detection of individual progeny within intracellular parasitophorous vacuoles post infection, we found, as expected, that the dinitroaniline analog oryzalin was highly and selectively potent on parasites, with an IC_{50} of 0.8 µM (Figure 6A, blue line). Oryzalin IC_{50} reached 99 µM for the human host fibroblasts (HFF). Accordingly the selectivity index, defined as the ratio of IC_{50} human fibroblasts/ IC_{50} *T. gondii*, reached 123.7. We found that compounds CM094 and CM571 moderately impacted parasite growth with an IC50 of 35 and 130 µM, respectively (Figure 6A, red and green lines), whereas compound CM852 had no detectable effect (Figure 6A, purple line). CM094 and CM571 showed no significant effect on human fibroblasts, with IC50 of 240 and 237 µM, respectively [30], resulting, however, in lower selectivity indexes than oryzalin (i.e., 6.8 and 1.8, respectively). The compound effectiveness towards its target, the dynamic MTs, is significantly challenged by the need of successive translocations across three biochemically different membranes. Thus, we next tested for a longer time period the activity of the most potent compound on *T. gondii* tachyzoite proliferation, defined with the IC_{50}, i.e., CM094. To this end, we incubated 200 invasive tachyzoites on HFF monolayer in a six-well plate (9.61 cm^2/well) and added the drug immediately after one hour of invasion. The time window was adjusted to allow a single parasite to multiply and the progeny to undergo several rounds of infection or "lytic cycles". Under these conditions, we observed a significant difference in the size of HFF cleared areas between cells exposed to CM094 or to the vehicle alone. The effect was already observed after four days and drastically increased with time (Figure 6B,C). Assuming a conserved rate of infection between each sample, these assays document a significant loss of parasite fitness in presence of 15 µM of the compound and attest to the integrity of the HFF monolayer under drug treatment.

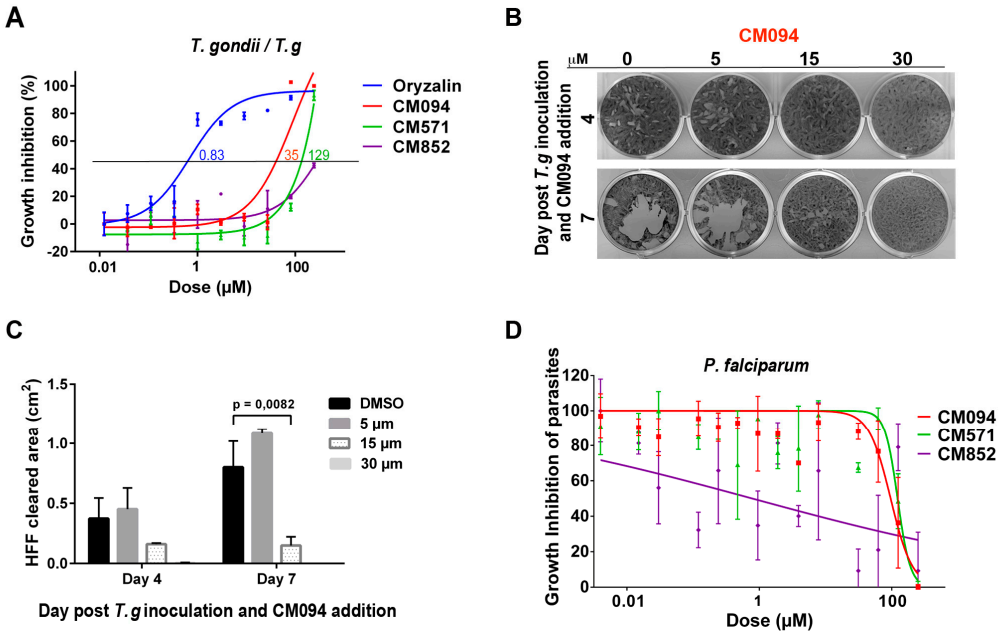

Figure 6. Effect of selected compounds on *T. gondii* and *P. falciparum*. (**A**) The effect of the compounds on *T. gondii* replication within human fibroblasts was tested. The graph presents *T. gondii* growth inhibition curves for each treatment at concentrations ranging from 0.01 to 100 µM, in triplicates. The quantity of individual parasites within intracellular vacuoles exposed or not to the drug for 30 h post-invasion was automatically scored. The calculated IC_{50} is indicated for each compound. (**B**) Plaque assays showing at 4 and 7 days the expansion of HFF cleared zones due to successive rounds of lytic cycle that were initiated by a single parasite. HFF monolayers plated on a 6-well plate were inoculated with 200 invasive tachyzoites per well for 1 h. The non-invading tachyzoites were washed away and cells were incubated with medium containing the vehicle (DMSO, 0) or different concentrations of CM094. After fixation and Crystal violet staining, cells were air dried and scanned before image processing and plaque area measurement. At day 7, post-inoculation, a highly significant reduction of parasite expansion was observed for the cultures exposed to 15 µM of CM094 and no plaque was detected at 30 µM while the HFF monolayer was well preserved. (**C**) Histograms showing the cumulated area of HFF cleared zones. *p* value = 0.0082. (**D**) The effect of selected compounds on *P. falciparum* intra-erythrocytic growth was tested. The growth of parasites within human red blood cells is determined using a classical SYBR Green assay followed by quantification of parasite DNA fluorescence. The graph presents growth curves for concentrations of each compounds ranging from 0 to 250 µM, in triplicates.

We then decided to investigate whether the compounds had an effect on the proliferation of *P. falciparum* (the most lethal agent of human malaria) during the intra-erythrocytic life stages, which are the symptomatic stages of the malaria infection. We thus incubated a tightly synchronized 3D7 ring wild-type population (i.e., initial intracellular developmental stage of the blood phase, 0.5% parasitaemia) in a 96-well plate (2% hematocrit) in the presence of different concentrations of the compounds ranging from 4 nM to 250 µM. Parasites were left in culture to undergo the intra-erythrocytic life cycle of 48h, which usually allows the 3D7 strain to increase its population of about 10-fold. Parasitaemia after drug treatment was determined by a typical SYBR Green assay [31]. Compound CM852 (Figure 6D, purple line) showed highly variable effects on the parasite growth whereas both compounds CM094 (Figure 6D, red line) and CM571 (Figure 6D, green line) slowed down the intracellular proliferation of *P. falciparum* at high concentrations. The IC_{50} values of CM094 and CM571 were determined to be 94.7 and 122.4 µM, respectively. Notably, no cytotoxic effect could be observed on the human host erythrocytes [32], thus suggesting a specific effect on the parasite itself.

These results identified CM094, the compound most closely related to dinitroanilines as the only one to significantly impact the *T. gondii* tachyzoite lytic cycle. Both CM094 and CM571 were found to impact the trophozoite intra-erythrocytic development in *P. falciparum*.

3. Discussion

By integrating in silico and assay-based approaches we were able to explore the diversity of chemical space to find agents able to bind to the dinitroaniline tubulin-binding site. These compounds were assayed on evolutionary close and distant organisms, which allowed the identification of drugs with new chemical scaffolds that target plants and to a moderate extent, Apicomplexa parasites, while sparing animal cells.

Eleven compounds, out of the 82 in vitro-assayed compounds, were found active on the plant BY-2 microtubule cytoskeleton. This unusual high ratio points out the efficiency of the docking step strategy likely resulting from the combination of the following factors. First, a great number of ligands (300,000) have been docked thanks to the grid computational power, increasing the probability to select active compounds. Second, the S4MPLE algorithm and the access to the grid allowed an exploration of the possible conformations of the targeted site. Using a pre-docking step with known active and putative inactive ligands allowed the selection of the five most probable conformations. The docking on these five conformations was thus conducted on judiciously restricted but flexible targets. Finally, the docking poses and the important amount of interaction data have been scrutinized both manually and with homemade scripts. This in-depth analysis allowed the definition of a subset of criteria that were subsequently proven to be relevant.

While numerous compounds targeting mammalian tubulin are described, much less is known regarding drugs acting on plant tubulin. One reason is that the systematic research of compounds that selectively affect plant tubulin assembly is hampered by the poor availability of purified assembly competent plant tubulin. High content screening methods, based on the visualization of the compound effect on plant cell microtubule networks, could represent a convenient alternative. Here, we did not use computer-based methods for the analysis of the high content screening experiments, which allowed the evaluation of compound effects on BY-2 cell microtubules, but care has been taken to develop a standardized protocol that could be readily automated. BY-2 cells have proven to be a good cell model for this screening but other plant cells could also be valuably used in similar screens. We anticipate that high throughput screens of the effect of large sets of compounds on plant proteins in the cellular context will be easily implemented and benefit of our methodological developments. Such a method could also be used in a chemical genetics approach to identify chemically targetable microtubule regulators [33,34].

Biochemical experiments confirmed that plant tubulin is the in vitro target of the three selected compounds and that their binding to tubulin is likely responsible for MT depolymerization. Their toxic effect on plant cells and their effect on plant growth can therefore most probably be attributed to their effect on tubulin dynamics. It has been shown, however, that oryzalin also induces changes in the morphology of the endoplasmic reticulum (ER) and Golgi apparatus, which could contribute to its herbicide properties [35]. Such additional effects could also be responsible of the observed herbicide activity of the compounds we have selected, especially CM094, which shares some structural similarities with dinitroaniline.

Interestingly compound CM852 (pyrazon [5-amino-4-chloro-2-phenyl-3(2*H*)-pyridazinone]) is already described as an herbicide that works by blocking electron transport in photosystem II in green plants, thereby inhibiting photosynthesis. Its inhibitory effect on tubulin assembly, uncovered in this work, is likely reinforcing its toxic effect on plants. Available toxicity data on this compound indicate that it is of low toxicity without highly specific responses in mammals. This study confirms the selectivity of CM852 and the other two selected compounds for plant cells since none of them affected human fibroblastic and epithelial cell viability, in full consistency with the fact that they do not target mammalian tubulin. Moreover, the absence of their toxicity indicates that these compounds

are not highly reactive and that they do not target proteins important for cell viability. Notably, since at least the CM094 compound has proven some activity on *T. gondii* intracellular growth and to a lesser extent on *P. falciparum*. This argues that CM094 can cross multiple biological barriers, and remain active. Remarkably, to target MTs dynamics that occur during apicomplexan zoites multiplication (i.e., *T. gondii* tachyzoites and *P. falciparum* trophozoite), the drug has to successfully translocate across the host cell plasma membrane, the membrane of the vacuole which houses the replicating tachyzoites and the plasma membrane of the tachyzoite itself. Whether the anti-tachyzoite MT activity of CM094 is reduced due the multistep obligate trafficking of the drug to reach its target once delivered into the culture medium remains to be evaluated. Previous work on the effect of dinitroanilines on *P. falciparum* corroborate our results showing a moderate activity on *P. falciparum*, but a very low mammalian cytotoxicity of the compounds [36]. This work also concluded that due to their hydrophobic nature, dinitroaniline derivatives largely accumulate in the parasite membranes. This reduces the amount of molecules having access to their microtubular target, likely explaining the modest effect observed on *P. falciparum*. Synthesis of chemical derivatives of CM094 may overcome this limitation and gain in anti-malarial activity.

The development of new herbicides, with no negative impact on humans and on the wild fauna, would have important consequences at the ecological and economical levels. While the compounds we have described act in the micromolar range, their chemical structure is simple. These molecules thus provide a useful platform for compound optimization. They also exhibit a selective effect on *T. gondii* and *P. falciparum* proliferation and could thus represent alternative scaffolds to the dinitroaniline analogs, in particular the meta-amino derivatives that have been already characterized as potent anti-*T. gondii* reagents [37]. Considering the urgent need for the development of therapeutic agents against malaria and other parasitic diseases, uncovering new scaffolds as leads for the future design of selective anti-parasitic drugs remains a priority.

4. Materials and Methods

4.1. Chemical Reagents, Recombinant and Purified Protein

Reagents used include DMSO (Sigma, D5879, Saint-Quentin Fallavier, France); oryzalin (Sigma, 36182); paclitaxel (Sigma, T1912); colchicine (Sigma, C9754); nocodazole (Sigma, M1404); phosphate buffer saline (PBS, Sigma P4417); foetal bovine serum (FBS, Sigma); formaldehyde (Sigma, F1635); glutaraldehyde (Polysciences, Inc, Warrington, PA, USA); Tween 20 (Sigma, P9416); sodium azide (Merck, Lyon, France, 6688); piperazine-*N*,*N*′-bis(2-ethanesulfonic acid (PIPES, Sigma, P6757); ethylene glycol-bis(β-aminoethyl ether)-*N*,*N*,*N*′,*N*′-tetraacetic acid (EGTA, Sigma, E4378); $MgCl_2$ (Sigma, M1028); Triton X100 (Sigma, T8787); Glycerol (Sigma); phenylmethylsulfonyl fluoride (PMSF, Sigma); 2-(*N*-morpholino)ethanesulfonic acid (MES, Sigma, M3671); 4′,6-diamidino-2-phénylindole (DAPI, Sigma, D8417); $CaCl_2$ (Sigma, C5670); mannitol (Sigma, M4125); pectolyase Y23 (Seishin Pharmaceutical, Tokyo, Japan); macerozyme R-10 (Serva, Heidelberg, Germany); caylase 345 (Cayla, Toulouse, France); Hoechst 33342 reagent (Sigma, B2261); protease cocktail inhibitors (Sigma, P8340); phosphatase cocktail inhibitors (Sigma, P5726); bovine serum albumin (BSA, Sigma, A3059); normal goat serum (Interchim, Montluçon, France); 3-[4,5-Dimethylthiazol-2-yl]-2,5-diphenyltetrazolium bromide (MTT); Thiazolyl blue (Sigma, M5655). Tubulin was prepared from fresh bovine brains as described in Paturle-Lafanechère et al. [38]. Soybean tubulin was purchased from Cytoskeleton, Inc. (Denver, CO, USA). Compounds screened were from ChemBridge Corporation (San Diego, CA, USA).

4.2. Antibodies

The α-tubulin antibody used was from clone α3a [39]. Anti-mouse IgG secondary antibodies conjugated with cyanine 3 were from Jackson ImmunoResearch Laboratories (Cambridgeshire, UK).

4.3. Mammalian, Plant and Apicomplexan Cell Lines

Mammalian cells: HeLa cells were originally purchased from the American Type Culture Collection (ATCC, Middlesex, UK), and maintained in Roswell Park Memorial Institute 1640 (RPMI-1640) medium supplemented with 10% (*v*/*v*) FBS and 1% penicillin/streptomycin, instead of DMEM, because the assayed compounds were more soluble in RPMI. MES-SA cells and MES-SA-DX5, from ATCC, were first grown in McCoy's 5A (ATCC) with 10% (*v*/*v*) FBS and 1% penicillin/streptomycin and further adapted to grow in RPMI-1640 with 10% (*v*/*v*) FBS and antibiotics. These mammalian cell lines were maintained at 37 °C with 5% CO_2 and 3% O_2. Cells were treated with the compounds for 2 h unless otherwise stated. Plant cells: Tobacco BY-2 cells (*Nicotiana tabacum* L. Bright-Yellow 2, Riken) were grown in suspension according to Nagata et al. [40]. Primary human foreskin fibroblasts (ATCC CRL-1634) were seeded at about 70–80% of confluence in P96 and P6 well plates in high glucose Dulbecco's Modified Eagle's Medium (DMEM), supplemented with 10% (*v*/*v*) heat-inactivated fetal bovine serum (FBS) and 10 mM HEPES pH 7.0 (i.e. complete medium) and used 48–72 h later when confluent. Apicomplexan cell lines: The *T. gondii* RH strain expressing cytosolic GFP was maintained by serial passage in Human Foreskin Fibroblats (HFF) monolayers maintained in complete medium and as previously described [41]. *P. falciparum* 3D7 cultures were grown, as previously described [42] in 2% hematocrit (obtained from Etablissement du Sang Français, Grenoble, France) in RPMI medium (Thermo Fisher Scientific, Waltham, MA, USA) complemented with 10% Albumax (Thermo Fisher Scientific), Gentamycin (Merck Sigma Aldrich, Lyon, France) and hypoxanthine at 37 °C with a beta gas mix (1% O_2, 5% CO_2, 96% N_2).

4.4. In Silico Screening on Alpha-Tubulin 3D-Model: Virtual Library of Compounds, Molecular Docking and Processing Methods

The dinitroaniline binding site of α-tubulin has been described in previous studies, located beneath the H1-S2 loop [13]. A sub-library of compounds, comprising 307,802 molecules available at ChemBridge Corporation was retrieved from the ZINC database (http://zinc15.docking.org/) in mol2 format with the hydrogen atoms and the atomic partial charges. The virtual library was massively docked on the EGEE (Enabling Grids for E-sciencE) European grid infrastructure [43] with the FlexX software [44] at the level of the putative dinitroaniline/oryzalin site. FlexX docking results contained several groups of data: (1) for each compound docked on each protein conformation, the 10 best poses were returned in mol2-format output files; (2) associated to each pose, the software returned also files giving the FlexX score value and the interactions between the protein residues and the ligand. The amount of information associated with 10 poses of 307,802 molecules docked on 7 active sites represented about 300 GB of textual data. To process this huge amount of data, analysis scripts were developed in Unix Shell, Unix Awk, or Perl languages; in order to visualize and sort the interesting values, the R programming language and the Kyplot package were used for statistics. To visualize, align ligands and to inspect, manually, their interactions with the dinitroaniline/oryzalin active site, the following software were used: Visual molecular dynamics VMD [45] Chimera [46], Ligplot [47]), MOE (Molecular Operating Environment, Chemical Computing Group–1010 Sherbrooke Street West, Montreal, Canada H3A2R7) and Hermes, the graphical interface of Gold [48].

4.5. Microtubule-Interference Assay in BY-2 Tobacco Cells

Samples of 90 µL of BY-2 cells, grown for 2.5 to 6.5 days, were transferred into 96-well polystyrene plates (Masterblock 2 mL, Greiner, Courtaboeuf, France) and supplemented with 10 µL of the chemical compounds (final concentration 50 µM). The cells were then incubated for 2 h at 27°C in the dark and under gentle agitation. Cells were further fixed by the addition in each well of 900 µL of MBS buffer (50 mM PIPES, 5 mM EGTA, 1 mM $MgCl_2$, 2% Glycerol, pH 6.9) containing 3.7% formaldehyde, 1% glutaraldehyde, 1% DMSO, 0.5% Triton X-100 and 200 µM phenylmethane sulfonyl fluoride (PMSF), for 15 min under gentle agitation. The fixation buffer was then removed after sedimentation of the cells under centrifugation (2 min, 100× *g*) and replaced by 500 µL of MBS buffer for 10 min. This washing

step was repeated 4 times. A volume of 50 µL of cell suspension was then transferred from Masterblock plates to Microclear 96-well flat bottom polypropylene plates (Greiner Bio-One #655090) coated with poly-D-Lysine. After a 15 min sedimentation period, cell walls were permeabilized for 2 min with 25 mM MES, 8 mM $CaCl_2$, 600 mM Mannitol, 0.02% Pectolyase, 0.1% Macerozyme, 0.3% Caylase at pH 5.6, at room temperature. They were then washed with 50 µL of MBS buffer, and incubated with 5% of normal goat serum for 2 h. After 5 washes with MBS buffer, 45 µL of anti-tubulin antibodies at 1/5000 dilution were added in each well and incubated overnight. After 5 washes with MBS buffer, cells were incubated with Cy3 secondary antibodies (dilution 1/2000) and Hoechst (dilution 1/1000) for nuclei staining for 2 h. Finally, after 5 washes in PBS, the BY-2 cells were stocked in 50 µL of PBS/glycerol (50/50) at 4 °C before automated imaging. Compounds found to be active were systematically tested again from freshly made solutions.

4.6. Microtubule-Interference Assay in Hela Cells

The effect of compounds on microtubules was assayed in HeLa cells in 96 well-microplates using immunofluorescence, after permeabilization, and fixation of the cells, as previously described [16].

4.7. Drug Effect on Toxoplasma gondii and Plasmodium falciparum Parasite In Vitro

The activity of compounds against *T. gondii* in vitro was tested by (i) automatic scoring of GFP-expressing parasites within intracellular vacuoles over 30 h post invasion and in presence of a wide range of compound concentration. These assays allowed assessing the growth potential over about 4 to 5 replication cycles (ii) analysis of clear zones developing in a host fibroblast monolayer over 4 and 7 days as a result of the cell lysis induced by tachyzoite multiplication following infection by a single parasite. The so-called comparative plaque assay therefore revealed the additive defects on growth, motile, invasive and egress capabilities caused by the compound under study over numerous cycles of infection. To first monitor parasite multiplication over the 30 h period, we applied high content screening using fluorescence microscopy on 96 well plates with 20 fields of acquisition for each well and performed in triplicates for each condition. Images were further processed with Scanˆ R software (Olympus Life Science, Rungis, France). In the plaque assay, area of clear zones in the HFF monolayer were defined by image segmentation and measured following ethanol fixation and Crystal violet (0.05% in distilled water) staining with ImageJ software (https://imagej.nih.gov/ij/, [49]) and for all assays the datasets were analyzed using GraphPad Prism 6 software (La Jolla, CA, USA) and organized using Adobe Photoshop CS6 software (Paris, France).

Activity of compounds on *P. falciparum* intra-erythocytic life stages was assayed on tightly synchronized cultures of 3D7 ring culture using a classical SYBR Green assay, as previously described [31]. Briefly, populations of infected red blood cells with 0.5% 3D7 *P. falciparum* rings were allowed to grow in culture medium containing various concentrations of compounds (ranging from 4 nM to 250 µM) for an entire intra-erythrocytic life cycle of 48 h in 96-well plates (Thermo Fischer Scientific). Parasites (i.e., infected red blood cells) were quantified using SYBR Green II (Merck Sigma Aldrich), which gives a green fluorescence upon its contact with *P. falciparum* DNA (erythrocyte lacking nuclei and DNA, fluorescence is specific to the parasite presence). Fluorescence quantification was measured using a CLARIOstar 96-well-plate reader (BMG Labtech, Champigny s/Marne, France) and data was analyzed using GraphPad Prism 6 software.

4.8. Automated Imaging

Automated imaging of cells seeded in 96-well clear-bottom plate (Greiner, #655090) was performed on INCell Analyzer 1000 (GE-Healthcare, Cardiff, UK) using an 20x air objective. Eight images/well were acquired in the center of the well. Excitation and emission filters pairs used for nuclei, A488 and Cy3 staining were 360 nm/460 nm, 475 nm/535 nm and 535 nm/620 nm, respectively. Acquisition parameters such as exposure time and Z-plane focus were specifically fixed for each immunofluorescence assay.

4.9. Arabidopsis Thaliana Growth Assay

Arabidopsis seeds were obtained from Lehle seeds Inc. (Round Rock, TX, USA). Plants were grown on solid agar medium containing Murashige and Skoog (Caisson Labs, Smithfield, USA; MSP09) growth medium complemented with molecules supplied as described, in 24-well microplates, for 3 days in a humid chamber. Plants were then transferred in a growth chamber for 2 weeks at 20 °C with white light (100 mmol $m^{-2} \cdot s^{-1}$) and a 16/8-h photoperiod. Observations were realized 7 days after transfer.

4.10. Tubulin Polymerization Assay

Microtubule polymerization assay was described in Prudent et al. [34], with final tubulin concentration of 25 μM for bovine tubulin or soybean tubulin.

4.11. Analysis of Cell Viability Using 3-(4,5-Dimethylthiazol-2-yl)-2,5-diphenyl-tetrazolium bromide (MTT)

Cytotoxicity was evaluated with a 3-(4,5-dimethylthiazol-2-yl)-2,5-diphenyl-tetrazolium bromide (MTT) colorimetric assay, performed in 96-well microplates as described in Martinez et al. [16].

Supplementary Materials: Supplementary materials can be found at http://www.mdpi.com/1422-0067/19/10/3085/s1.

Author Contributions: Conceptualization: L.L. and E.M.; Methodology: E.S., L.B.G. and D.H.; Software: D.H.; Data Curation: S.A.S., L.B.G., S.R., D.H. and C.B. (Caroline Barette); Resources: V.K., C.B. (Caroline Barette) and V.B.; Formal analysis: L.B.G.; Investigation: E.S., L.B.G., V.R., R.P., B.T., S.D. and E.M.; Visualization: D.H., S.R., E.S., R.P., B.T., S.D., E.M. and L.L.; Supervision: E.S., S.R., M.V., A.I., V.B., C.B. (Cyrille Botté), I.T. and L.L.; Validation: E.S., R.P., L.L., E.M., I.T. and C.B. (Cyrille Botté); Original Draft Preparation: L.L., E.M., M.V., S.R., D.H., E.S., I.T. and C.B. (Cyrille Botté); Writing: L.L. and E.M. Writing—Review & Editing: L.L., E.M., E.S., C.B. (Caroline Barette), A.I., D.H., C.B. (Cyrille Botté), I.T. and S.R. Funding acquisition: L.L., S.R. and C.B. (Cyrille Botté); Project Administration: L.L. and E.M.

Funding: S.R. and D.H. were supported by Agence Nationale de la Recherche, France (ANR-05-CIGC-008 DOCK). C.Bo. and S.D. were also supported by Agence Nationale de la Recherche, France (Grant ANR-12-PDOC-0028-Project Apicolipid), the Atip-Avenir and Finovi programs (CNRS-INSERM-Finovi Atip-Avenir Apicolipid projects), and the Laboratoire d' Excellence Parafrap, France (grant number ANR-11-LABX-0024).

Acknowledgments: The authors thank Magali Audry for her input in the initial steps of modelisation, Didier Rognan and Esther Kellenberger for having trained Loraine Brillet-Guéguen in molecular docking, Gilles Bisson for the scoring function which allowed to select the 5 tubulin conformations for docking, Aline Thomas for help on several molecular modeling softwares, Olivier Bastien for introduction on R scripting, the ChemAxon company (http://www.chemaxon.com) for having allowed academics to freely use their software, especially the Standardizer (version of 2006) for structure canonicalization and transformation of the ligands before the docking steps, Boris Striepen (Univ. Pensylvania, PA, USA) for providing the *T. gondii* RH strain expressing GFP, Karin Sadoul for critical reading of the manuscript. Part of this work has been performed at the CMBA molecular screening platform (Grenoble, France) which is a member of the GIS-IBiSA and the infrastructure ChemBioFrance.

Conflicts of Interest: The authors declare no conflict of interest. The funding sponsors had no role in the design of the study; in the collection, analyses, or interpretation of data; in the writing of the manuscript, and in the decision to publish the results.

References and Notes

1. Bartolini, F.; Gundersen, G.G. Generation of noncentrosomal microtubule arrays. *J. Cell Sci.* **2006**, *119*, 4155–4163. [CrossRef] [PubMed]
2. Wasteneys, G.O.; Ambrose, J.C. Spatial organization of plant cortical microtubules: Close encounters of the 2D kind. *Trends Cell Biol.* **2009**, *19*, 62–71. [CrossRef] [PubMed]
3. Portran, D.; Zoccoler, M.; Gaillard, J.; Stoppin-Mellet, V.; Neumann, E.; Arnal, I.; Martiel, J.L.; Vantard, M. MAP65/Ase1 promote microtubule flexibility. *Mol. Biol. Cell* **2013**, *24*, 1964–1973. [CrossRef] [PubMed]
4. Botté, C.Y.; Yamaryo-Botté, Y.; Janouskovec, J.; Rupasinghe, T.; Keeling, P.J.; Crellin, P.; Coppel, R.L.; Maréchal, E.; McConville, M.J.; McFadden, G.I. Identification of plant-like galactolipids in *Chromera velia*, a photosynthetic relative of malaria parasites. *J. Biol. Chem.* **2011**, *286*, 29893–29903. [CrossRef] [PubMed]

5. Morrissette, N. Targeting Toxoplasma Tubules: Tubulin, Microtubules, and Associated Proteins in a Human Pathogen. *Eukaryot. Cell* **2015**, *14*, 2–12. [CrossRef] [PubMed]
6. Aikawa, M.; Carter, R.; Ito, Y.; Nijhout, M.M. New observations on gametogenesis, fertilization, and zygote transformation in Plasmodium gallinaceum. *J. Protozool.* **1984**, *31*, 403–413. [CrossRef] [PubMed]
7. Morejohn, L.C.; Fosket, D.E. The biochemistry of compounds with anti-microtubule activity in plant cells. *Pharmacol. Ther.* **1991**, *51*, 217–230. [CrossRef]
8. Lyons-Abbott, S.; Sackett, D.L.; Wloga, D.; Gaertig, J.; Morgan, R.E.; Werbovetz, K.A.; Morrissette, N.S. α-Tubulin Mutations Alter Oryzalin Affinity and Microtubule Assembly Properties to Confer Dinitroaniline Resistance. *Eukaryot. Cell* **2010**, *9*, 1825–1834. [CrossRef] [PubMed]
9. Fennell, B.; Naughton, J.; Barlow, J.; Brennan, G.; Fairweather, I.; Hoey, E.; McFerran, N.; Trudgett, A.; Bell, A. Microtubules as antiparasitic drug targets. *Expert Opin. Drug Discov.* **2008**, *3*, 501–518. [CrossRef] [PubMed]
10. Morejohn, L.C.; Bureau, T.E.; Molé-Bajer, J.; Bajer, A.S.; Fosket, D.E. Oryzalin, a dinitroaniline herbicide, binds to plant tubulin and inhibits microtubule polymerization in vitro. *Planta* **1987**, *172*, 252–264. [CrossRef] [PubMed]
11. Hugdahl, J.D.; Morejohn, L.C. Rapid and Reversible High-Affinity Binding of the Dinitroaniline Herbicide Oryzalin to Tubulin from Zea mays L. *Plant Physiol.* **1993**, *102*, 725–740. [CrossRef] [PubMed]
12. Stokkermans, T.J.W.; Schwartzman, J.D.; Keenan, K.; Morrissette, N.S.; Tilney, L.G.; Roos, D.S. Inhibition of *Toxoplasma gondii* Replication by Dinitroaniline Herbicides. *Exp. Parasitol.* **1996**, *84*, 355–370. [CrossRef] [PubMed]
13. Mitra, A.; Sept, D. Binding and Interaction of Dinitroanilines with Apicomplexan and Kinetoplastid α-Tubulin. *J. Med. Chem.* **2006**, *49*, 5226–5231. [CrossRef] [PubMed]
14. Dumontet, C.; Jordan, M.A. Microtubule-binding agents: a dynamic field of cancer therapeutics. *Nat. Rev. Drug Discov.* **2010**, *9*, 790–803. [CrossRef] [PubMed]
15. Prudent, R.; Vassal-Stermann, É.; Nguyen, C.-H.; Mollaret, M.; Viallet, J.; Desroches-Castan, A.; Martinez, A.; Barette, C.; Pillet, C.; Valdameri, G.; et al. Azaindole derivatives are inhibitors of microtubule dynamics, with anti-cancer and anti-angiogenic activities. *Br. J. Pharmacol.* **2013**, *168*, 673–685. [CrossRef] [PubMed]
16. Martinez, A.; Soleilhac, E.; Barette, C.; Prudent, R.; Gozzi, G.J.; Vassal-Stermann, E.; Pillet, C.; di Pietro, A.; Fauvarque, M.-O.; Lafanechère, L.; et al. Novel Synthetic Pharmacophores Inducing a Stabilization of Cellular Microtubules. *Curr. Cancer Drug Targets* **2014**, *15*, 2–13. [CrossRef]
17. Botté, C.Y.; Maréchal, E. Plastids with or without galactoglycerolipids. *Trends Plant Sci.* **2014**, *19*, 71–78. [CrossRef] [PubMed]
18. Botté, C.Y.; Dubar, F.; McFadden, G.I.; Maréchal, E.; Biot, C. Plasmodium falciparum Apicoplast Drugs: Targets or Off-Targets? *Chem. Rev.* **2012**, *112*, 1269–1283. [CrossRef] [PubMed]
19. Sali, A.; Blundell, T.L. Comparative protein modelling by satisfaction of spatial restraints. *J. Mol. Biol.* **1993**, *234*, 779–815. [CrossRef] [PubMed]
20. Hoffer, L.; Chira, C.; Marcou, G.; Varnek, A.; Horvath, D. S4MPLE—Sampler for Multiple Protein-Ligand Entities: Methodology and Rigid-Site Docking Benchmarking. *Molecules* **2015**, *20*, 8997–9028. [CrossRef] [PubMed]
21. Tantar, A.-A.; Conilleau, S.; Parent, B.; Melab, N.; Brillet, L.; Roy, S.; Talbi, E.-G.; Horvath, D. Docking and Biomolecular Simulations on Computer Grids: Status and Trends. *Curr. Comput. Aided-Drug Des.* **2008**, *4*, 235–249. [CrossRef]
22. Dauber-Osguthorpe, P.; Roberts, V.A.; Osguthorpe, D.J.; Wolff, J.; Genest, M.; Hagler, A.T. Structure and energetics of ligand binding to proteins: *Escherichia coli* dihydrofolate reductase-trimethoprim, a drug-receptor system. *Proteins* **1988**, *4*, 31–47. [CrossRef] [PubMed]
23. Marcou, G.; Rognan, D. Optimizing fragment and scaffold docking by use of molecular interaction fingerprints. *J. Chem. Inf. Model.* **2007**, *47*, 195–207. [CrossRef] [PubMed]
24. Mpamhanga, C.P.; Chen, B.; McLay, I.M.; Willett, P. Knowledge-based interaction fingerprint scoring: A simple method for improving the effectiveness of fast scoring functions. *J. Chem. Inf. Model.* **2006**, *46*, 686–698. [CrossRef] [PubMed]
25. Deng, Z.; Chuaqui, C.; Singh, J. Structural Interaction Fingerprint (SIFt): A Novel Method for Analyzing Three-Dimensional Protein−Ligand Binding Interactions. *J. Med. Chem.* **2004**, *47*, 337–344. [CrossRef] [PubMed]

26. Perlman, Z.E.; Mitchison, T.J.; Mayer, T.U. High-content screening and profiling of drug activity in an automated centrosome-duplication assay. *ChemBioChem* **2005**, *6*, 145–151. [CrossRef] [PubMed]
27. Prudent, R.; Lafanechère, L. Institute for Advanced Biosciences (IAB), Team Regulation and Pharmacology of the Cytoskeleton, Grenoble, France. Analysis of the effect of selected molecules on the polymerization and depolymerization of tubulin, compared with dinitroaniline used as a positive control. Effects were studied at increasing doses of molecules up to 50 µM. Not intended for publication. 2011.
28. Buttiglieri, G.; Peschka, M.; Frömel, T.; Müller, J.; Malpei, F.; Seel, P.; Knepper, T.P. Environmental occurrence and degradation of the herbicide n-chloridazon. *Water Res.* **2009**, *43*, 2865–2873. [CrossRef] [PubMed]
29. Pokora, W.; Tukaj, Z. Induction time of Fe-SOD synthesis and activity determine different tolerance of two Desmodesmus (green algae) strains to chloridazon: A study with synchronized cultures. *Pestic. Biochem. Physiol.* **2013**, *107*, 68–77. [CrossRef] [PubMed]
30. Touquet, B.; Tardieux, I. Institute for Advanced Biosciences (IAB), Team Membrane and Cell Dynamics of Host Parasite Interactions, Grenoble, France. Analysis of the effect of increasing doses of the selected molecules on the growth of human fibroblasts. Not intended for publication. 2017.
31. Smilkstein, M.; Sriwilaijaroen, N.; Kelly, J.X.; Wilairat, P.; Riscoe, M. Simple and inexpensive fluorescence-based technique for high-throughput antimalarial drug screening. *Antimicrob. Agents Chemother.* **2004**, *48*, 1803–1806. [CrossRef] [PubMed]
32. Dass, S.; Botté, C. Institute for Advanced Biosciences (IAB), Team ApicoLipid, Grenoble, France, Analysis of the cytotoxic effect of the selected compounds on human erythrocytes. Not intended for publication. 2017.
33. Dejonghe, W.; Russinova, E. Plant Chemical Genetics: From Phenotype-Based Screens to Synthetic Biology. *Plant Physiol.* **2017**, *174*, 5–20. [CrossRef] [PubMed]
34. Prudent, R.; Vassal-Stermann, E.; Nguyen, C.-H.; Pillet, C.; Martinez, A.; Prunier, C.; Barette, C.; Soleilhac, E.; Filhol, O.; Beghin, A.; et al. Pharmacological inhibition of LIM kinase stabilizes microtubules and inhibits neoplastic growth. *Cancer Res.* **2012**, *72*, 4429–4439. [CrossRef] [PubMed]
35. Langhans, M.; Niemes, S.; Pimpl, P.; Robinson, D.G. Oryzalin bodies: in addition to its anti-microtubule properties, the dinitroaniline herbicide oryzalin causes nodulation of the endoplasmic reticulum. *Protoplasma* **2009**, *236*, 73–84. [CrossRef] [PubMed]
36. Naughton, J.A.; Hughes, R.; Bray, P.; Bell, A. Accumulation of the antimalarial microtubule inhibitors trifluralin and vinblastine by Plasmodium falciparum. *Biochem. Pharmacol.* **2008**, *75*, 1580–1587. [CrossRef] [PubMed]
37. Endeshaw, M.M.; Li, C.; de Leon, J.; Yao, N.; Latibeaudiere, K.; Premalatha, K.; Morrissette, N.; Werbovetz, K.A. Synthesis and evaluation of oryzalin analogs against *Toxoplasma gondii*. *Bioorg. Med. Chem. Lett.* **2010**, *20*, 5179–5183. [CrossRef] [PubMed]
38. Paturle-Lafanechere, L.; Edde, B.; Denoulet, P.; van Dorsselaer, A.; Mazarguil, H.; le Caer, J.P.; Wehland, J.; Job, D. Characterization of a major brain tubulin variant which cannot be tyrosinated. *Biochemistry* **1991**, *30*, 10523–10528. [CrossRef] [PubMed]
39. Peris, L.; Thery, M.; Faure, J.; Saoudi, Y.; Lafanechere, L.; Chilton, J.K.; Gordon-Weeks, P.; Galjart, N.; Bornens, M.; Wordeman, L.; et al. Tubulin tyrosination is a major factor affecting the recruitment of CAP-Gly proteins at microtubule plus ends. *J. Cell Biol.* **2006**, *174*, 839–849. [CrossRef] [PubMed]
40. Nagata, T.; Nemoto, Y.; Hasezawa, S. Tobacco BY-2 Cell Line as the "HeLa" Cell in the Cell Biology of Higher Plants. *Int. Rev. Cytol.* **1992**, *132*, 1–30. [CrossRef]
41. Roos, D.S.; Donald, R.G.; Morrissette, N.S.; Moulton, A.L. Molecular tools for genetic dissection of the protozoan parasite *Toxoplasma gondii*. *Methods Cell Biol.* **1994**, *45*, 27–63. [PubMed]
42. Shears, M.J.; MacRae, J.I.; Mollard, V.; Goodman, C.D.; Sturm, A.; Orchard, L.M.; Llinás, M.; McConville, M.J.; Botté, C.Y.; McFadden, G.I. Characterization of the Plasmodium falciparum and *P. berghei* glycerol 3-phosphate acyltransferase involved in FASII fatty acid utilization in the malaria parasite apicoplast. *Cell. Microbiol.* **2017**, *19*, e12633. [CrossRef] [PubMed]
43. Breton, V.; Jacq, N.; Kasam, V.; Hofmann-Apitius, M. Grid-Added Value to Address Malaria. *IEEE Trans. Inf. Technol. Biomed.* **2008**, *12*, 173–181. [CrossRef] [PubMed]
44. Rarey, M.; Kramer, B.; Lengauer, T.; Klebe, G. A fast flexible docking method using an incremental construction algorithm. *J. Mol. Biol.* **1996**, *261*, 470–489. [CrossRef] [PubMed]
45. Humphrey, W.; Dalke, A.; Schulten, K. VMD: Visual molecular dynamics. *J. Mol. Graph.* **1996**, *14*, 33–38. [CrossRef]

46. Pettersen, E.F.; Goddard, T.D.; Huang, C.C.; Couch, G.S.; Greenblatt, D.M.; Meng, E.C.; Ferrin, T.E. UCSF Chimera—A visualization system for exploratory research and analysis. *J. Comput. Chem.* **2004**, *25*, 1605–1612. [CrossRef] [PubMed]
47. Wallace, A.C.; Laskowski, R.A.; Thornton, J.M. LIGPLOT: a program to generate schematic diagrams of protein–ligand interactions. *Protein Eng.* **1995**, *8*, 127–134. [CrossRef] [PubMed]
48. Jones, G.; Willett, P.; Glen, R.C.; Leach, A.R.; Taylor, R. Development and validation of a genetic algorithm for flexible docking. *J. Mol. Biol.* **1997**, *267*, 727–748. [CrossRef] [PubMed]
49. Schneider, C.A.; Rasband, W.S.; Eliceiri, K.W. NIH Image to ImageJ: 25 years of image analysis. *Nat. Methods* **2012**, *9*, 671–675. [CrossRef] [PubMed]